TOUGHREACT User's Guide: A Simulation Program for Non-isothermal Multiphase Reactive Transport in Variably Saturated Geologic Media, Version 2.0

Tianfu Xu, Nicolas Spycher, Eric Sonnenthal, Liange Zheng, and Karsten Pruess

Earth Sciences Division, Lawrence Berkeley National Laboratory
University of California, Berkeley, CA 94720

October 2012 - Draft

The documentation of this version of the code was supported in part by the Zero Emission Research and Technology Project (ZERT) of the U.S. Department of Energy, under Contract No. DE-AC02-05CH11231.

TABLE OF CONTENTS

LIST OF FIGURES

LIST OF TABLES

1 Introduction

Coupled modeling of subsurface multiphase fluid and heat flow, solute transport, and chemical reactions can be applied to many geologic systems and environmental problems, including carbon geological storage, nuclear waste geological disposal, geothermal systems, diagenetic and weathering processes, acid mine drainage remediation, contaminant transport, and groundwater quality. To investigate these and other problems, TOUGHREACT has been developed by introducing reactive transport into the existing framework of a non-isothermal multi-component fluid and heat flow simulator TOUGH2 (Pruess et al., 1999). A number of subsurface thermo-physical-chemical processes are considered under various thermohydrological and geochemical conditions of pressure, temperature, water saturation, and ionic strength. TOUGHREACT can be applied to one-, two- or three-dimensional porous and fractured media with physical and chemical heterogeneity. The code can accommodate any number of chemical species present in liquid, gas and solid phases.

The first version of the TOUGHREACT code was released to the public through the US Department of Energy's Energy Science and Technology Software Center (ESTSC) in August 2004. It is among the most frequently requested of ESTSC's codes. The code has been widely used for studies in CO_2 geological sequestration, geothermal energy development, nuclear waste isolation, environmental remediation, and increasingly for petroleum applications. Over the last several years, many new capabilities have been developed within different research projects at Lawrence Berkeley National Laboratory. To effectively serve our in-house projects and to share with the user community, we incorporated these new capabilities into Version 2 of TOUGHREACT (V2). Major additions and improvements in Version 2 include:

- Intra-aqueous reaction kinetics and biodegradation
- Surface complexation models
- Multi-site exchange
- Improvements on the reactive surface area algorithm for mineral-water reactions, and fugacity coefficient corrections for gas-water reactions
- Improvements on coupling between chemistry and physics (such as with porosity and permeability changes)
- Improvement on the ideal mineral solid-solution modelImprovement on functionalities such as printout of mineral reaction rates, and output of aqueous and surface complexes concentrations with time
- More flexible input formats for chemical parameters
- Singnificant increase in computational efficiency

TOUGHREACT has been applied to a wide variety of problems, some of which are included as examples in this manual, such as:

- Supergene copper enrichment (Xu et al., 2001)
- Coupled thermal, hydrological, and chemical processes for nuclear waste disposal (Spycher et al., 2003a and b; Sonnenthal et al., 2003, 2005; Mukhopadhyay et al., 2009, Dobson et al., 2003)

- Mineral alteration in hydrothermal and geothermal systems (Xu and Pruess, 2001a; Xu et al., 2004a and 2006; Dobson et al., 2004; Todaka et al., 2004; Xu et al., 2009a)
- Mineral trapping for CO_2 disposal in deep saline aquifers (Audigane et al., 2007; Gherardi et al., 2007; Xu et al., 2004b, 2006, 2007; Zhang et al., 2009)
- Reactive transport and biogeochemical nitrogen cycling in vadose zone systems (Singleton et al., 2004; Xu, 2008; Gu et al., 2008, Maggi et al., 2008)

The TOUGHREACT program makes use of "self-documenting" features. It is distributed with a number of input data files for sample problems. Besides providing benchmarks for proper code installation, these can serve as a self-teaching tutorial in the use of TOUGHREACT, and they provide templates to help jump-start new applications. The fluid and heat flow part of TOUGHREACT is derived from TOUGH2 V2, so in addition to the current manual, users will need the manual of TOUGH2 V2 (Pruess et al., 1999) to set up hydrological inputs.

The present version of TOUGHREACT provides the following TOUGH2 fluid property or "EOS" (equation-of-state) modules:

- EOS1 for water, or two waters with typical applications to hydrothermal problems
- EOS2 for multiphase mixtures of water and CO_2 also with typical applications to hydrothermal problems
- EOS3 for multiphase mixtures of water and air with typical applications to vadose zone and nuclear waste disposal problems
- EOS4 that has the same capabilities as EOS3 but with vapor pressure lowering effects due to capillary pressure
- EOS7 for multiphase mixtures of water, brine, and air with density and viscosity effects of salinity as an extension of EOS3
- EOS9 for single phase water (Richards' equation) with typical applications to ambient temperature and pressure reactive geochemical transport problems, and
- ECO2N for multiphase mixtures of water, CO_2 and NaCl with typical applications to CO_2 geological storage (sequestration) in deep saline aquifers.

2 Requirements

2.1 Computer Requirements and Code Installation

TOUGHREACT V2.0 is written in FORTRAN 77 with some Fortran-90 extensions. It has been tested on various computer platforms, including Microsoft Windows- and Linux-based PCs, Apple Macintosh G4, G5, and Intel-based computers, and multiple core multiprocessor Linux clusters. An effort was made for the TOUGHREACT source code to comply with the ANSIX3.9-1978 (FORTRAN 77) standard, and on most machines the code should compile using Fortran 95, Fortran 90, and some Fortran 77 compilers, and run without modification. TOUGHREACT (like TOUGH2 V2) requires 64-bit arithmetic (8 byte word length for floating point numbers) for successful execution. The TOUGHREACT (V2.0) source program contains IMPLICIT DOUBLE PRECISION (A-H, O-Z) and IMPLICIT INTEGER*8 (I-N) statements that will automatically generate 64-bit arithmetic on 32 bit processors. The distribution files folders include documentation (this manual), test problems, source files and/or executable files (depending on the license) generated with compilers described in accompanying README files. Several MAKEFILEs for different unix/linux computer platforms are also included for compilation and linking.

2.2 Memory Requirements

The computer memory required by TOUGHREACT depends on the problem size. PARAMETER statements are used in three INCLUDE files: flowpar_v2.inc (for fluid and heat flow dimension parameters), perm_v2.inc for permeability-porosity coupling parameters, and chempar_v2.inc file (for reactive chemistry dimension parameters). All major arrays in the problem are automatically adjusted according to these dimension parameters. Different size problems can be modeled by changing the dimensions in the parameter statements, compiling all source files, and linking them to create an executable file. At the beginning of a simulation, the program automatically checks the array dimensions related to reactive geochemistry. If the dimensions are insufficient for the specific problem, it provides the user a message to change the parameter statements. The memory requirement for these dimensions is typically about 1 Gbyte.

2.3 User Knowledge Requirements

The correct implementation, setup, problem formulation, and interpretation of the results of TOUGHREACT requires knowledge of the basic equations of multiphase non-isothermal fluid flow and transport in geologic media and a basic understanding of the numerical solution of the equations that are used to describe these processes. In addition, the formulation of the geochemical problem requires familiarity with geochemical modeling and an in-depth understanding of the system that is being modeled and of the data used for input to the model. The model boundary conditions, time step length, convergence criteria, and grid properties are crucial elements for a realistic and accurate solution to a problem. The input files for flow parameters are based on TOUGH2 V2, with some extensions. However, TOUGH2 V2 input files can be used without modification. A comprehensive reference of TOUGH2 input formats along with illustrative sample problems are provided in the TOUGH2 user's guide,

Version 2.0 (Pruess et al., 1999). This information is essential for successful application of TOUGHREACT; it is not duplicated in the current manual.

3 Model Description

3.1 Main Scope of the Model

TOUGHREACT (Xu et al., 1998; Xu et al., 2006; Xu et al., 2011) is applicable to one-, two-, or three-dimensional geologic domains with physical and chemical heterogeneity and can be applied to a wide range of subsurface conditions. The temperature (T) and pressure (P) ranges are controlled by the applicable range of the chemical thermodynamic database, and the range of the EOS module employed. Thermodynamic databases from external sources are included with the distribution files. Typically, these thermodynamic databases are available for temperatures between 0 and 300°C, at 1 bar below 100°C, and water saturation pressure above 100°C. The temperature and pressure range of thermodynamic data can be extended by changing the thermodynamic database without code modifications. It is the user's responsibility to ensure that the thermodynamic data used with this software is appropriate for the temperature and pressure range of the simulated systems. Water saturation can vary from completely dry to fully water-saturated. The model can deal with ionic strengths from dilute to moderately saline water (up to ionic strengths in the 2–4 molal range, for an NaCl-dominant solution, depending on the system being modeled; see Appendix H for details).

TOUGHREACT is applicable to a variety of reactive fluid and geochemical transport problems, including (a) contaminant transport with linear Kd adsorption and radioactive decay (Sample problem 1), (b) natural groundwater chemistry evolution under ambient conditions (Sample 2), (c) assessment of nuclear waste disposal sites (Samples 3, 4, and 11), (d**)** CO_2 geological storage in deep formations (Samples 5 and 6), (e) mineral deposition such as supergene copper enrichment (Sample 7), and (f) mineral alteration and silica scaling in hydrothermal systems under natural and production conditions (Sample 8), and biogeochemical transport and environmental remediation (Samples 9 and 10).

3.2 Major Processes

The major processes for fluid and heat flow are: (1) fluid flow in both liquid and gas phases occurs under pressure, viscous, and gravity forces; (2) interactions between flowing phases are represented by characteristic curves (relative permeability and capillary pressure); (3) heat flow by conduction and convection, and (4) diffusion of water vapor and air. Thermophysical and geochemical properties are calculated as a function of temperature, such as fluid (gas and liquid) density and viscosity, and thermodynamic and kinetic data for mineral-water-gas reactions. Transport of aqueous and gaseous species by advection and molecular diffusion are considered in both liquid and gas phases. Depending on the computer memory and CPU performance, any number of chemical species in the liquid, gas and solid phases can be accommodated. Aqueous and surface complexation, acid-base, redox, gas

dissolution/exsolution, and multi-site cation exchange are considered under the local equilibrium assumption. Mineral dissolution and precipitation proceed under either equilibrium or kinetic constraints (Xu et al., 1999b). Intra-aqueous kinetics and biodegradation (Xu, 2008; Xu et al., 2009b; Spycher et al., 2009) and surface complexation using non-electrostatic, constant capacity and double layer electrostatic models (Zheng et al., 2009), have been incorporated into Version 2 of TOUGHREACT. Mineral dissolution and precipitation can proceed either subject to local equilibrium or kinetic conditions. Linear adsorption and decay can be also included.

3.3 Governing Equations

The primary governing equations for multiphase fluid and heat flow, and chemical transport have the same structure, derived from the principle of mass (or energy) conservation. These equations are presented in Appendix A. Expressions for non-isothermal multiphase flow are given in Pruess (1987) and Pruess et al. (1999). The transport equations are written in terms of total dissolved concentrations of chemical components, which are concentrations of the basis species plus their associated aqueous secondary species (Yeh and Tripathi, 1991; Steefel and Lasaga, 1994; Walter et al., 1994; Lichtner, 1996; and Xu and Pruess, 2001b). If kinetically-controlled reactions occur between aqueous species, then additional ordinary differential equations need to be solved to link the total concentrations of the primary species with the evolving concentrations of the secondary species (Steefel and MacQuarrie, 1996). Kinetically-controlled reactions between aqueous species are considered in the present version. Slow aqueous phase reactions are common in the case of redox reactions. Advection and diffusion processes are considered for both the aqueous and gaseous species. Aqueous species diffusion coefficients are assumed to be the same. Gaseous species, having a neutral valence, can have differing diffusion coefficients calculated as a function of T, P, molecular weight, and molecular diameter. The local chemical interactions in the transport equations are represented by reaction source/sink terms.

The primary governing equations must be complemented with constitutive local relationships that express all parameters as functions of fundamental thermophysical and chemical variables. The equations for chemical reactions are presented in Appendix B. Mass conservation in the closed chemical system is written in terms of basis (component) species. The species distribution must be governed by the total concentrations of the components. The oxygen is used for formulating redox reactions by attributing the oxidizing potential to the dissolved oxygen (Nordstrom and Muñoz, 1986; Wolery, 1992). In contrast to the free electron in the hypothetical electron approach (Yeh and Tripathi, 1991), oxygen can be present and can be transported in natural subsurface flow systems. The formulation for cation exchange is similar to that of Appelo and Postma (1993). For intra-aqueous kinetic reactions, sorption kinetic reactions, and biodegradation, a general-rate law that can deal with multiple mechanisms and multiple products, Monod, and inhibition terms (Xu et al., 2008), is used (Appendix B). For kinetically-controlled mineral dissolution and precipitation, a general form of the rate law (Lasaga, 1984; Steefel and Lasaga, 1994; Palandri and Kharaka, 2004) is used (Appendix B). Thermodynamic and kinetic data are functions of temperature.

Temporal changes in porosity, permeability, and unsaturated hydrologic properties owing to mineral dissolution and precipitation can modify fluid flow. This feedback between transport and chemistry can be important

(e.g., Raffensperger, 1996), and can be treated by TOUGHREACT. Changes in porosity during the simulation are calculated from changes in mineral volume fractions. The porosity-permeability correlation in geologic media can be complex, depending on several factors, such as pore size distribution, pore shapes, connectivity (Verma and Pruess, 1988), and crystal morphology. Several porosity-permeability and fracture aperture-permeability relationships are included in the model (Appendix F). The code can also be set to monitor changes in porosity and permeability during the simulation without considering their effects on fluid flow. In unsaturated systems, capillary pressure can be modified via permeability and porosity changes using Leverett scaling (based on Slider, 1976).

3.4 Simplifying Approximations

Hydrodynamic dispersion is an important solute transport phenomenon that arises from an interplay between non-uniform advection and molecular diffusion. This process in not currently explicitely implemented in TOUGHREACT for various reasons, one of which being that typical representations of this process (such as Fickian dispersion models) have fundamental flaws and limitations, as demonstrated in numerous studies in the hydrogeology literature over the last twenty years. As necessary, hydrodynamic dispersion can be modeled through appropriate spatial resolution on multiple scales, using multiple continua (or multi-region) models (Pruess and Narasimhan, 1985; Gwo et al., 1996) to describe interactions between fluid regions with different velocities.

We currently neglect deformation of the porous skeleton, and fluid pressure effects owing to porosity changes. Heat effects from chemical reactions are neglected, as are changes in thermophysical properties of fluid phases (such as viscosity, surface tension, and density) owing to changes in chemical composition.

Finally, the pressure effect on chemical equilibrium constants is typically neglected, unless molar volume data for specific reactions are introduced in the thermodynamic database (Section 6.4).

Figure 4—1 Flow chart of the TOUGHREACT program

This figure shows the flow chart for solving coupled non-isothermal multiphase fluid flow, solute transport, and reactive geochemistry in TOUGHREACT.

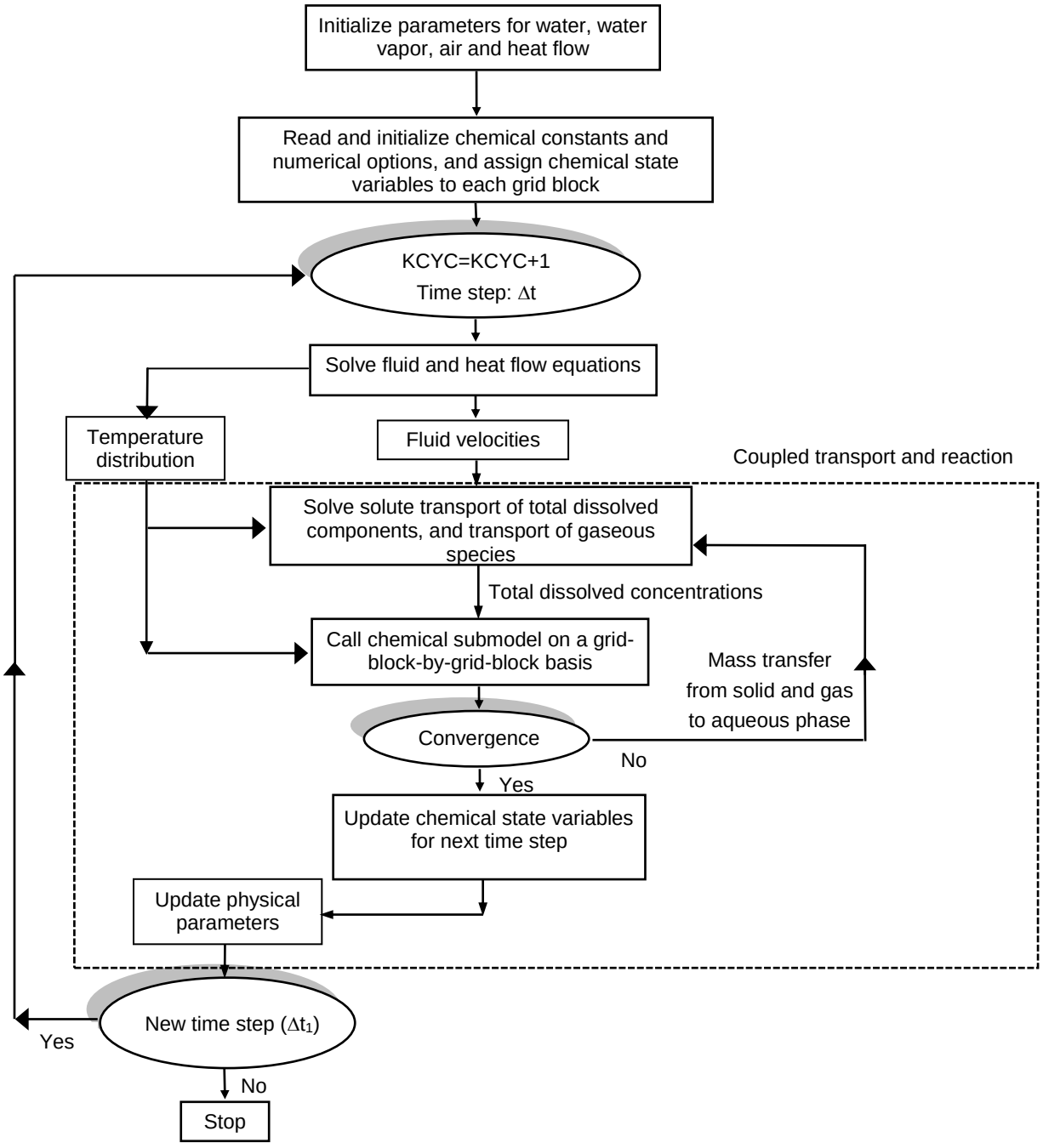

The numerical solution of multi-phase fluid and heat flow proceeds as in TOUGH2. Space discretization is employed by means of integral finite differences (IFD; Narasimhan and Witherspoon, 1976). Because chemical transport equations (derived from mass conservation) have the same structure as fluid and heat flow equations, the transport equations can be solved by the same numerical method. The discretization approach used in the IFD method and the definition of the geometric parameters are illustrated in Figure 4-2. The basic mass- (for water, air, and chemical components) and energy- (for heat) balance equations are written in integral form for an arbitrary domain V_n

$$V_n \frac{\Delta M_n}{\Delta t} = \sum_m A_{nm} F_{nm} + V_n q_n \qquad (4.1)$$

where subscript n labels a grid block, subscript m labels grid blocks connected to grid block n, Δt is time step size, and M_n is the average mass or energy density in grid block n. Surface integrals are approximated as a discrete sum of averages over surface segments A_{nm}, F_{nm} is the average flux (of mass or energy) over the surface segment A_{nm} between volume elements n and m, and q_n is the average source/sink rate in grid block n per unit volume. Time is discretized fully implicitly as a first-order finite difference to achieve unconditional stability. More detail on the numerical discretization is given in Pruess et al. (1999). The IFD method gives a flexible discretization for geologic media that allows the use of irregular unstructured grids, which is well suited for simulation of flow, transport, and fluid-rock interaction in multi-region heterogeneous and fractured rock systems. For systems with regular grids, IFD is equivalent to conventional finite differences.

Figure 4—2 Space discretization and geometric data for the integral finite difference method

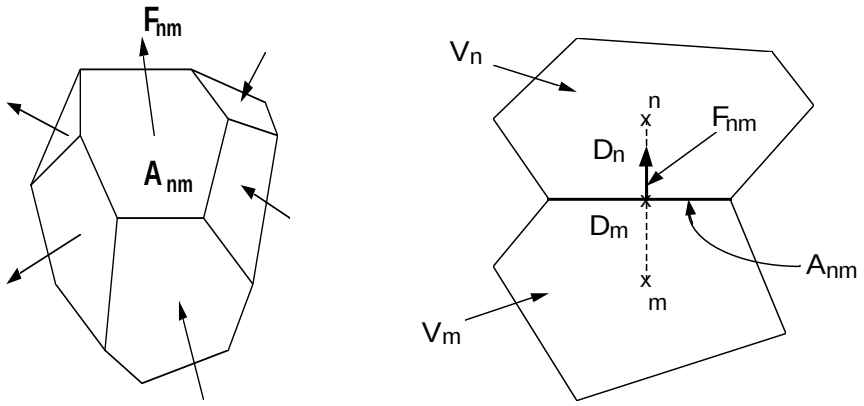

The time discretization of fluid and heat flow equations results in a set of coupled non-linear algebraic equations for the unknown thermodynamic state variables in all grid blocks. These equations are solved by Newton-Raphson iteration as implemented in the original TOUGH2 simulator (Pruess, 1991). The set of coupled linear

equations arising at each iteration step is solved iteratively by means of preconditioned conjugate gradient methods (Moridis and Pruess, 1998).

TOUGHREACT uses a sequential iteration approach (SIA) similar to Yeh and Tripathi (1991), Engesgaard and Kipp (1992), Simunek and Suares (1994), and Walter et al. (1994). After solution of the flow equations, the fluid velocities and phase saturations are used for chemical transport simulation. The chemical transport is solved on a component-by-component basis (details on the solution method are given in Appendix C). The resulting concentrations obtained from solving transport equations are substituted into the chemical reaction model. The system of mixed equilibrium-kinetic chemical reaction equations is solved on a grid block by grid block basis by Newton-Raphson iteration (details are given in Appendix D). Optionally, the chemical transport and reactions are solved iteratively until convergence. An automatic time stepping scheme is implemented in TOUGHREACT, which includes an option to recognize "quasi-stationary states" (QSS; Lichtner, 1988) and perform a “large” time step towards the end of a QSS.

As an alternative to the sequential iterative approach, a sequential non-iterative approach (SNIA) may be used, in which the sequence of transport and reaction equations is solved only once (Walter et al., 1994; Steefel and MacQuarrie, 1996; and Xu et al., 1999a). Xu et al. (1999a) analyzed the accuracy of SIA and SNIA using several test cases. They concluded that the accuracy of SNIA depends mainly on the Courant number, which is defined as $C = v\Delta t/\Delta x$, where v is fluid velocity and Δx is grid spacing. For small Courant numbers, satisfying the stability condition $C \leq 1$, the differences between SNIA and SIA are generally small. The accuracy of SNIA also depends on the type of chemical process. Therefore, the applicability of the decoupling of chemical reactions from transport will depend on time and space discretization parameters, the nature of the chemical reactions and the desired accuracy. When SNIA is used, the Courant number condition $C \leq 1$ can be automatically enforced during the simulation.

When analyzing water flow through partially saturated porous media, the gas phase may often be considered a passive by stander and not be represented explicitly (Richards, 1931). This means that for the purpose of solving for water flow, the entire gas phase is at the same pressure (usually the atmospheric pressure). TOUGHREACT allows a choice of considering saturated-unsaturated liquid phase flow in which case only molecular diffusion is considered for gaseous species transport. Alternatively, the full non-isothermal multiphase flow equations (liquid, gas, and heat) may be solved. To test the passive gas phase approach under ambient conditions, Xu et al. (2000) performed numerical simulation experiments on pyrite oxidation in a variably saturated porous medium. They found that under ambient conditions the effects of partial pressure reduction due to oxygen consumption on the fluid flow is not significant, and oxygen diffusion is the dominant gas phase transport process. However, when fluid flow and chemical reactions are strongly coupled, as e.g. in boiling hydrothermal reservoirs, gas phase advection could be essential (White, 1995).

5 General Description of Input and Output Files

5.1 Input Files

Three user-specified input files are required. The input file names have been fixed in the program (i.e., names cannot be specified by the user). Descriptions of these input files are given below. Details on input formats and contents are given in Chapter 6.

flow.inp – Flow input. This file mainly includes rock properties, time-stepping information, geometric grid information, initial and boundary conditions, and data related to a multi-phase fluid and heat flow simulation. The flow input is the same as the original TOUGH2 V2 (see the manual; Pruess et al., 1999), with an additional data block REACT (see Section 6.1), and a few other extensions. This is a "fixed" format file.

solute.inp – Transport and other run parameters. This file contains various flags and input parameters for calculations of reactive transport, such as diffusion coefficients, tolerance limits for convergence of transport and chemical iterations, printout flags for mineral and aqueousspecies, and the configuration of model zones with different chemical composition (the composition of each zone, however, is defined in file chemical.inp described below). This is a "free" format file.

chemical.inp – Chemical parameters and properties. This file is used to define the chemical system (i.e. the type and number of aqueous component species, minerals, gases, and sorbed species considered in the simulation). It also includes the initial compositions of water, minerals, and gases in zones that are assigned to grid blocks in file solute.inp, and kinetic data for intra-aqueous reactions and minerals (rate constants, surface areas, etc.) This is "free" format file.

In addition to the above-mentioned three input files, the program requires a thermodynamic database file with a file name specified in the solute.inp file. This file contains reaction stoichiometries, dissociation constants (log(K)), and regression coefficients of log(K) as a function of temperature and pressure (see Section 6.4 for details). The thermodynamic database is also a "free" format file.

5.2 Output Files

Two types of output files are generated from TOUGHREACT: (1) fixed file names, and (2) user-specified file names.

5.2.1 Fixed name output files

flow.out – Flow output. This file is identical to the TOUGH2 V2 output file, including data on temperature, pressure, liquid saturation, mass flux, and phase velocities for all grid blocks of the model.

solute.out – Echo of input file solute.inp. This file lists data that was read from input file solute.inp, including all transport parameters, chemical zone configuration, and other run-specific parameters.

chemical.out – Echo of input file chemical.inp. This file lists data that was read from input files chemical.inp and the thermodynamic database, including initial water, rock, and gas compositions, equilibrium constants and stoichiometries of chemical reactions, kinetic data, and linear adsorption Kd values and decay constants for certain species.

runlog.out – Log of the simulation progress. This file is updated throughout the simulation. It lists some run input parameters and all run-related messages, including error messages (Chapter 7).

chdump.out – chemical speciation data. This file contains results of geochemical speciation calculations for each initial water composition input into the model, including a printout of chemical mass balances (total mass balance and aqueous species mass balance). It also lists these data for grid blocks where chemical convergence fails (not reaching the specified convergence criteria). For debugging purposes, or for small number of grids, the flag ICHDUMP in the solute.inp input file allows geochemical speciation results to be output in the *chdump.out* file for every grid block, or certain specific grid blocks, at time step intervals. As a precaution to avoid filling up disk space, results of speciation calculations are output only for the first thousand grid blocks and/or time steps, after which output in this file is suspended.

savechem – save of geochemical data for restart. This file can be used to restart a TOUGHREACT run from the end of a previous run. Geochemical conditions obtained in one run are written to disk file *savechem*, and can be used as initial conditions in a subsequent run. The restart run for reactive geochemical transport simulation must be used together with a restart of the flow simulation (see p. 61 of the TOUGH2 V2 manual; Pruess et al., 1999). For a restart run, the name of file *savechem* must be changed to *inchem*, and the name of file *SAVE* to *INCON* (same as in the original TOUGH2).

In addition, TOUGHREACT creates the following optional fixed-name output files:

mbalance.out – chemical mass balance information
min_SI.out – mineral saturation indices
rct_area.out – mineral reactive surface areas
rctn_rate.out – mineral reaction rates

Printing of these files is controlled by parameter MOPR(8) in the *flow.inp* file, which is described in Section 6.1.

5.2.2 User-specified output files

The names of these files must be specified in the input file *solute.inp*, and cannot be left blank. The output files are described below:

Iteration data (e.g., *iter.dat*): This file lists the number of flow, transport, and chemical iterations used to reach convergence at some time steps.

Aqueous species data (e.g., *tec_conc.dat*): This file contains times, grid block coordinates (m), gas and liquid saturations, temperature (°C), pH, and aqueous species concentrations at all grid blocks for times specified in the flow.inp file. The number and types of species output are specified by flags in the input file solute.inp. This file has a TECPLOT-compatible format.

Solid phase data (e.g., *tec_min.dat*): This file contains time, grid point coordinates (m), temperature (°C), mineral abundance, and exchanged species concentrations at all grid blocks for time printout intervals specified in the flow.inp file. This file has a TECPLOT-compatible format.

Gas phase data (e.g., *tec_gas.dat*): This file contains time, grid point coordinates (m), temperature (°C), and gas partial pressures for all grid blocks at times specified in the flow.inp file. This file has a TECPLOT-compatible format.

Plot data at specified grid blocks (time evolution) (e.g., *time.dat*): This file contains the grid block identifier, time, gas and liquid saturations, temperature, pH, aqueous species concentrations, mineral abundances, gas pressures, and exchanged species concentrations for specific grid blocks and time intervals, as specified in the input file solute.inp.

6 Input File Formats and Contents

6.1 Flow Input (flow.inp)

Input formats for multiphase flow are similar to TOUGH2 Version 2.0 (Pruess et al. 1999), with some enhancements and the addition of keyword block 'REACT' for invoking a reactive transport simulation. The REACT block has one record that specifies option parameters related to reactive transport. Without this data block, the program runs a multiphase flow simulation only. In TOUGHREACT, keyword blocks 'PARAM' and 'INCON' from TOUGH2 V2.0 were extended. Inputs for these options are discussed below. Also note that the TOUGH2 capability of defining an "inactive" grid block with a zero or negative volume in the input block 'ELEME' (used for a constant boundary condition), is not operational in TOUGHREACT. Instead, constant chemical boundary conditions are set in TOUGHREACT by input of a very large volume ($\geq 10^{20}$ m^3) for boundary grid blocks. Chemical concentrations in these grid blocks will not undergo speciation or mineral-gas-water-reactions, and pressure and temperature will also remain constant. In TOUGH2 V2.0, setting the volume to greater than 10^{50} will also remove the boundary grid blocks from mass balance calculations.

TOUGHREACT also incorporates some options of other TOUGH2 versions that were developed specifically for unsaturated flow and boiling in fractured rock. The addition to the flow input file is given below.

REACT Parameter choices for reactive transport simulation

Variable: MOPR(20)

Format: 20I1

MOPR(1) = 0 perform reactive transport

= 1 no reactive transport, but input files with chemical data are read

= 2 no reactive transport, no chemical data files are read

= 3 solves flow and transport without chemical reaction

= 4 solves transport and chemical reactions using constant velocity field (flow calculated at first time step only)

= 5 solves transport (no chemical reactions) using constant velocity field (flow calculated at first time step only)

MOPR(2) > 0 writes the transport coefficient matrix, Darcy velocities, porosities, and other transport data in the runlog.out file during calculations of aqueous species and gas transport. Primarily used for debugging (very large output!).

MOPR(3) > 0 writes source terms, old and new aqueous concentrations, and various other parameters in the *runlog.out* file during transport calculations. Also outputs the permeability, porosity, and

capillary pressure correction factor at each grid block in the *runlog.out* file. Primarily used for debugging (very large output!).

MOPR(4) ≠ 1 Force at least one fluid flow step to be calculated (MOPR(4) =2 is normally suggested)

= 1 does not force at least one fluid flow step to be calculated. This option can be useful to compute chemical reactions in single-grid block problems. When the chemical quasi-stationary states (QSS) option is considered, MOPR(4) must be set equal to one.

MOPR(5) = 0 Results in printout of time step iteration information for the flow calculations, as in the original TOUGH2 V2. The use of this option is normally suggested unless the file *flow.out* becomes too big. In the latter case, use =1 option.

= 1 No printout

MOPR(6) = 0 No Leverett scaling of capillary pressure

= 1 Leverett scaling (Eq. F.9 in Appendix F) of capillary pressure for heterogeneous porosity and permeability fields and/or from porosity-permeability changes owing to mineral dissolution and precipitation.

MOPR(7) ≥0 This option allows the specification of the # number of digits past the decimal in tecplot-format output files (up to 8 digits). Zero or blank gives the default of 4 digits.

MOPR(8) = 0 No printout of extra output files.

≥ 1 Outputs mineral saturation indices, for each grid block, in file *min_SI.dat*. This information is output at the same intervals as specified in *flow.inp* for the flow (and chemistry) information.

≥ 2 Creates an additional output file (at same time intervals as above) with mineral reaction rates at all grid blocks. The file name is fixed as *rctn_rate.out*.

≥ 3 Creates an additional output file (at same time intervals as above) with mineral reactive surface areas. The file name is fixed as *rct_area.out*.

≥ 4 Outputs mass balance information in file *mbalance.out*.

MOPR(9): Not currently used. Leave blank.

MOPR(10) ≥ 1 The time step length will NOT be shortened if chemical convergence is slow (i.e., no time-step control by chemistry)

MOPR(11) =1 Enables approximating sedimentation/compaction processes by forward explicit advection of solids and aqueous species. If enabled, a sedimentation velocity (constant in time but optionally variable with depth) must be entered in record 11 and 12 of file *solute.inp* (Section 6.2). This option works only for a vertical 1D column with grid blocks and connections ordered sequentially from top to bottom (this option is only beta-tested !).

MOPR(12)-MOPR(14): Not currently used. Leave them blank.

MOPR(15) =1, the permeability will be modified according to the domain "SEED" specified in file *flow.inp* (see the TOUGH2 V2 manual).

MOPR(16) Enables reading a heterogeneous field of mineral volume fractions. If =1, an ascii input file with name *min_volf.inp* must be provided in addition to the other input files. This file must contain a

header in record 1, immediately followed (starting in record 2) with one record per mesh gridblock (for all gridblocks in the mesh) in the same gridblock order as specified in file *flow.inp* (or *MESH*). Each of these records must include, separated by blanks: gridblock ID (format A5); dry initial volume fraction of each mineral (free format), in the same mineral order as specified in the input file *chemical.inp*.

MOPR(17)-MOPR(20): Not currently used. Leave them blank.

PARAM The meaning of variable MCYC (maximum number of time steps to be calculated) in Record PARAM.1 was extended slightly from the original TOUGH2. In TOUGHREACT, if MCYC = 9999, the number of time steps is not controlled by MCYC, and therefore the maximum simulation time is only controlled by TIMAX in Record PARAM.2. IF MCYC ≤ 9998, it is the same as in TOUGH2 V2.

Variable ELST in record PARAM.2 was also modified so that if the keyword "wdata" is used the program will look for a line after PARAM.2 giving the number of grid blocks to write out specific flow data. Following the integer variable, the 5 character identifiers for the grid blocks must be listed sequentially in column format. The name of the output file is fixed as GASOBS.DAT. The records PARAM.3 and PARAM.4 should follow immediately after the last grid block name. An example is shown below.

```
PARAM           1234567890123456789012345
   29999    99990000000001200000471005000   2.14e-5     2.334
 0.00000  0.157785e8    1.e+006.0480e+05wdata      -9.806650
3
wp001
dr357
d2357
 1.0000e-4
 0.0000000000000D+00 0.0000000000000D+00 0.0000000000000D+00
```

Also note a minor format difference for Record PARAM.4 for default initial conditions (inconsequential change from E20.14 to E20.13):

Format (4E20.13)

DEP(I), I = 1, NKIN+1

INCON Three variables for three components of permeability were added to Record INCON.1 after porosity PORX (…, PORX, *PER1*, *PER2*, *PER3* with format …, E15.9, *3E15.9*). Like porosity, if zero or blank, three values of permeability will be taken as specified in block 'ROCKS' if option START is used. If the values of porosity and/or permeability are different in INCON and ROCKS then the ratios will be used for calculation of modified capillary pressures if the Leverett scaling option is selected (MOPR(6)=1). If zero or blank, temperature will be taken as default value specified in block 'ROCKS'. The SAVE file will also include the updated porosity and permeability values resulting from mineral precipitation or dissolution.

A minor format difference is present in Record INCON.2 (inconsequential change from E20.14 to E20.13):

Format (4E20.13)

X1, X2, X3, X4

For use of the EOS9 flow module, in Record INCON.2 the second primary variable X2 is used for specifying grid block dependent temperature (in ^{o}C). This allows for variable gas species diffusion coefficients and chemical calculations to be performed assuming a fixed temperature field.

As explained in the TOUGH2 manual for restarts (Pruess et al., 1999, p. 61–62, 169), when record INCON.3 starts with the string '+++', the code will look for time stepping information in one additional record. This record is generated by the code and is output in file SAVE. This additional record has the following format:

Format (2I10, I5, 2E15.8)

KCYCX, INTERCX, NMX, TSTX, TIMINX

where KCYCX is the total (cumulative) number of time steps at the current time, INTERCX is the total (cumulative) number of iterations at the current time, NMX is the total number of rock types in the present simulation, TSTX is the prior starting simulated time, and TIMINX is the current simulated time (i.e. when the SAVE file was generated).

ROCKS The following hydrological property options were added to those in TOUGH2 V2 (Pruess et al., 1999) within the ROCKS input records.

ROCKS 1.1

Format (9E10.4) (TORTX was modified and PTORT and PHICRIT were added)

COM, EXPAN, CDRY, **TORTX**, GK, XKD3, XKD4, **PTORT**, **PHICRIT**

TORTX < 0 Generalized power law (Burnol and Claret, 2012; Lagneau, 2002) with saturation-dependence added. For direct porosity or saturation-porosity dependence, set TORTX = -1.0. If TORTX < 0, then PTORT and PHICRIT must be set. For TORTX = 0.0, the option reverts to the Millington-Quirk formulation as in TOUGH2 V2. If TORTX > 0.0 then tortuosity is a fixed value, as in TOUGH2 V2.

PTORT Exponent for generalized power law. Required for TORTX < 0, and is an added parameter in the ROCKS 1.1 line (entries 71-80).

PHICRIT Critical porosity for generalized power law. Required for TORTX < 0, and is an added parameter in the ROCKS 1.1 line (entries 81-90).

ROCKS 1.2

RP(5) > 0.0 This option, with IRP = 7 and RP(4) = 0.0, enables the modified Brooks-Corey for gas relative permeability, as implemented by Wu et al. (1999). Note that RP(4) must be smaller than or equal to zero if this option (RP(5) > 0.0 is used.

ROCKS 1.3

ICP = 10 Capillary pressure linearization at small liquid saturations, as implemented in Wu and Mishra (1998). With this option, the input parameters CP(I) are the same as for the Van Genuchten function option (ICP = 7), except that CP(4) is set to parameter *epsilon* instead of P_{max}. In this case, the capillary pressure is linearly extrapolated from $S_l = S_r + epsilon$ (with S_l and S_r being the current and residual liquid saturations, respectively) down towards $S_l = 0$. The slope of the linear extrapolation corresponds to the slope of the capillary-pressure/liquid-saturation function at $S_l = S_r + epsilon$.

CP(6) > 0.0 This option, with either ICP = 7 or ICP = 10, and together with flag ISOT = –10 in the CONNE first input record, enables the active fracture model (Liu et al., 1998) as implemented by Wu et al. (1999). In this option, CP(6) is used to input the active fracture parameter γ.

GENER An option was added for time-dependent thermal conductivity. For this option, one more parameter, KTAB, was added at the end of record GENER.1:

Format (A3, I2, A3, I2, 4I5, 5X, A4, A1, 3E10.4, I2)

EL, NE, SL, NS, NSEQ, NADD, NADS, LTAB, TYPE, ITAB, GX, EX, HX, KTAB

KTAB is the number of points (number of time values and same number of factors) to read in following records for time-dependent thermal conductivities (variables before KTAB are unchanged from Pruess et al., 1999, p. 174).

If KTAB > 0, the following sets of time values and factors are read:

Record GENER.1.4 (format unchanged from GENER.1.1):

Format (4E14.7)

TIMKTH (1:KTAB)

TIMEKTH (1:KTAB) are the time values ("generation times") at which thermal conductivity values change

Record GENER.1.5:

Format (4E14.7)

FACKTH (1:KTAB)

FACKTH (1:KTAB) are the values of the time-dependent factors corresponding to the list of time values given in GENER.1.4. At each time values specified in record GENER.1.4, the thermal conductivity (determined from wet and dry conductivity values input in records ROCKS.1 and ROCKS.2) is multiplied by these factors.

6.2 Transport Input (solute.inp)

Except for non-numeric variables (title, grid block names, and names of species and minerals), data from this file are read in free format. The first input record to be read in this file is the title. It is followed by 14 main data records. "Skip" records (see below) can be included anywhere in the file, as long as not within a sequence of array inputs of the same variable (e.g., list of species, or list of gridblocks). Some records can be omitted in certain conditions. Some variables in data records are not required under certain conditions. In such cases, one should input them as zero values. Each record is described below, including the description of each input variable and its corresponding FORTRAN format for appropriate reading.

"Skip" records:

One or more heading (comment) line can precede each record described below (see inputs of the sample problems, such as in Figure 8.1-3). The comment line is indicated by beginning with "#" followed by one blank (without quotes), or any blank record. These records will be skipped on input, and can be inserted anywhere in the file. These "skip" records can be also used for data source references, or other purpose.

Record_1. Title

Variable: TITLE

Format: A82

```
TITLE:      title and comments.
```

Record_2. Options for reactive geochemical transport (1)

Variable: ISPIA INIBOUND ISOLVC NGAMM NGAS1 ICHDUMP KCPL

ICO2H2O iTDS_REACT

Format: 9I (integer free format)

ISPIA : flag for iteration scheme between transport and reaction. ISPIA = 2 is much faster and more commonly used, but ISPIA = 0 gives a more accurate result at each time step.

0 Sequential iteration between transport and chemistry
2 No sequential iteration (fully explicit reaction source terms)

INIBOUND : not currently used, place a value of '0'

ISOLVC : flag for the linear equation solver for transport. The solvers are the same as in TOUGH2 V2 (see p. 73 of the manual, Pruess et al., 1999), except for the removal of MA28. ISOLVC = 3 or 5 are often used, and in some cases DLUSTB (5) converges where other solvers fail

2 - DSLUBC, a bi-conjugate gradient solver
3 - DSLUCS, a Lanczos-type bi-conjugate gradient solver
4 - DSLUGM, a general minimum residual solver
5 - DLUSTB, a stabilized bi-conjugate gradient solver

NGAMM : flag for sub-iteration between calculation of activity coefficients and secondary species concentrations at the beginning of each chemical Newton-Raphson iteration. NGAMM is the number of subiterations. For most problems this should be set to zero (use a default value of 2). If convergence of the Newton-Raphson iterations for the chemical system fails, increase NGAMM up to a maximum of about 4. Note that increasing this parameter significantly increases computation time.

NGAS1 : Number of gaseous species (excluding H_2O) to include in transport calculations.

=0 Gases (other than H_2O) are not transported, and their partial pressure (as input or calculated as part of the initial chemical speciation) remains constant.
≥1 Number of gas species included in transport calculations (besides H_2O)

ICHDUMP : flag to enable detailed printout of chemical speciation results (typically enabled only for debugging chemical convergence problems).

0 Disabled
1 Printout of chemical speciation at each grid block and each time step
2 Printout of chemical speciation at time intervals specified by NWTI in the following Record_7 and grid blocks specified in Record_8.

If this option is enabled, the program will abort after the output of speciation results for the first 1000 grid blocks and/or time steps, to avoid accidentally filling up disk space.

KCPL : flag to consider feedback effects of changes of porosity, permeability, and capillary pressure due to mineral dissolution and precipitation on flow.

0 Disabled
1 Enabled
2 Only monitor changes in output files, without feedback on flow.

(To consider porosity changes from sedimentation, with option MOPR(11)=1, this flag must be set ≥ 1)

ICO2H2O : flag to consider effects of CO_2 and H_2O reaction source/sink terms on fluid flow calculations. ICO2H2O is only used for the EOS2 and ECO2N flow modules. For other flow modules, set ICO2H2O = 0.

0 Effects ignored
1 Only effects of CO_2 reaction source/sink terms
2 Effects of both CO_2 and H_2O reaction source/sink terms

iTDS_REACT : Must be set to zero in this version (not used)

Record_3. Options for reactive geochemical transport (2)

Variable: SL1MIN, RCOUR, STIMAX, CNFACT

Format: Real (free format)

SL1MIN: Geochemical calculations are skipped at grid blocks where the liquid saturation is less than SL1MIN. For typical boiling simulations, use SL1MIN less than or equal to 10-3.

RCOUR : both a variable and a flag to limit the time step size. RCOUR $\neq$ 0.0 limits the maximum time step size to |RCOUR| $\times$ Courant Number. Positive RCOUR values limit the time step by the velocity of the gas or liquid phase, whichever is highest. Negative RCOUR values limit the time step by the velocity of the liquid phase only. This option is disabled if RCOUR = 0.0.

STIMAX : Geochemical calculations are skipped at grid blocks where the stoichiometric ionic strength is more than STIMAX. STIMAX can be up to 6 mol/kg H_2O for NaCl-dominant solutions. For other solutions, STIMAX can be up to a value between 2.0 and 4.0 regarding the calculation of activity coefficients at elevated ionic strengths (see Appendix H for details).

CNFACT : Weighting factor for mineral and gas reaction source terms in the transport equations (1.0 = fully implicit source terms, 0.0 = fully explicit source terms). This parameter has an effect only if sequential iterations are enabled (ISPIA = 0). In this program version, CNFACT always defaults to 1.0 if a non-zero value is input (implicit only). Simulations with CNFACT = 0.0 using sequential iterations will produce the same results as simulations without sequential iterations (explicit source terms) but requires increased computing time and therefore should be avoided.

Record_4.1 through 4.6. Names of input thermodynamic database and output files regarding chemical data and numerical iterations

Variable: THERMO_in , OUTiter, OUTplot, OUTsolid, OUTgas, OUTtime

Format: A20, each file name occupies one line.

THERMO_in : name of thermodynamic data input file.

OUTiter : name of file (e.g., iter.out) to output iteration information.

OUTplot : name of file (e.g., tec_conc.out) to output aqueous concentrations in tecplot format for all grid blocks at specified printout times defined in flow.inp.

OUTsolid : name of file (e.g., tec_min.out) to output mineral abundances and exchanged species concentrations in tecplot format for all grid blocks at specified printout times defined in flow.inp.

OUTgas : name of file (e.g., tec_gas.out) to output gas pressures in tecplot format for all grid blocks at specified times defined in flow.inp.

OUTtime : name of file (e.g., time.out) to output aqueous concentrations, mineral/gas abundances, and adsorbed/exchanged species concentrations versus time, in tecplot format, for specific grid blocks input in Record_8, at time step intervals (NWTI) input in Record_7.

Record_5. Weighting parameters and diffusion coefficients

Variable: WTIME, WUPC, DIFUN, DIFUNG

Format: 4F (real free format)

WTIME : time weighting factor, ranging from 0.0 to 1.0. WTIME = 1.0 (implicit) is recommended.

WUPC : upstream weighting factor, ranging from 0.0 to 1.0. WUPC = 1.0 (fully upstream) is recommended.

DIFUN : diffusion coefficient (m^2/s) for aqueous species. DIFUN is multiplied by the tortuosity (τ) (defined in the ROCKS block of the flow input file, flow.inp), porosity, and liquid saturation. Notice that if τ in flow input is zero, the program computes τ from $\tau_\beta = \phi^{1/3} S_\beta^{7/3}$ (Millington and Quirk, 1961), where ϕ is porosity, S is phase saturation, and β is the fluid phase index.

DIFUNG : diffusion coefficients (m^2/s) of the medium for gaseous species other than H_2O. If DIFUNG < 0.0, TOUGHREACT computes gaseous diffusion coefficients as function of molecular weight and diameter, temperature, and pressure according to Eq. A.1 (Appendix A). DIFUNG is multiplied by the tortuosity (τ), defined in the ROCKS block of the flow input (flow.inp), porosity, and gas saturation, or if τ=0.0, the Millington-Quirk formulation is used as described for aqueous diffusion coefficients.

Record_6. Data related to convergence criteria

Variable: MAXITPTR, TOLTR, MAXITPCH, TOLCH, MAXITPAD, TOLAD, TOLDC, TOLDR

Format: I, E, I, E, I, E, E, E (All are free format)

MAXITPTR: maximum number of sequential iterations between transport and chemistry. If MAXITPTR=1, a sequential non-iterative approach is used where transport and chemistry are sequentially solved without iteration. Note that the value of MAXITPTR has no effect if ISPIA in Record_2 is set to 2 (non-iterative approach). Computing performance will significantly decrease as MAXITPTR increases.

TOLTR: convergence criterion (as relative change of aqueous concentrations) for the sequential iterative (transport/chemistry) scheme; a value between 1.0E-03 to 1.0E-06 is suggested. This convergence criterion is used only when MAXITPTR > 1 and ISPIA=0.

MAXITPCH: maximum number of iterations allowed for solving chemical speciation. Most often, a value of 200 is appropriate.

TOLCH: convergence criterion (as relative change of aqueous concentrations) for chemical speciation computations; a value between 1.0E-05 to 1.0E-07 is suggested. For simulations with a large number of time steps (> 10,000), values larger than 1.0E-6 should be avoided to minimize the potential for cumulative mass balance errors.

MAXITPAD: not currently used.

TOLAD: not currently used.

TOLDC: relative concentration change (between two consecutive time steps) tolerance for quasi-stationary state (QSS); a value between 1.0E-03 to 1.0E-06 is suggested; if not using the QSS option, set equal to zero. MOPR(4) (in flow.inp) must be set to 1 to enable this option. When KCPL>0 or ICO2H2O>0 or iTDS_REACT in Record_2, no QSS can be attained and this option is not available, set equal to zero.

TOLDR: relative dissolution and/or precipitation rate change tolerance for the quasi-stationary state option (QSS) (i.e., if TOLDC $\neq$ 0); a value between 1.0E-03 to 1.0E-06 is suggested; if not using QSS approximation set equal to zero. When KCPL>0 or ICO2H2O>0 or iTDS_REACT in Record_2, set equal to zero.

Record_7. Output control variables

Variable: NWTI, NWNOD, NWCOM, NWMIN, NWAQ, NWADS, NWEXC, ICONFLAG, MINFLAG

Format: 9I (integer free format)

NWTI : printout frequency (i.e., every NWTI time steps) of model output for selected grid blocks (NWNOD≠0). These data will be output in the file specified on Record_4.6.

NWNOD : number of grid blocks for time evolution printout. NWNOD grid blocks (with names EL) will be read below on Record_8. NWNOD can be set to a negative value as a flag for line-by-line input starting on Record_8.

NWCOM : number of chemical components (species) for which to output total concentrations in files specified on Record_4.3 and Record_4.6. NWCOM primary species (with indices IWCOM) will be read below on Record_9. NWCOM can be set to a negative value, in which case species names (instead of indices) will be read line-by-line starting on Record_9.

NWMIN : number of minerals for which to output abundances in files specified on Record_4.4 and Record_4.6. NWMIN minerals (with indices IWMIN) will be read below in Record_10. NWMIN can be set to a negative value, in which case mineral names (instead of indices) will be read line-by-line starting on Record_10.

NWAQ : number of individual aqueous species for which to output concentrations in files specified on Record_4.3 and Record_4.6. NWAQ species (with indices IWAQ) will be read below in Record_11. NWAQ can be set to a negative value, in which case species names (instead of indices) will be read line-by-line starting on Record_11.

NWADS : number of surface complexes for which to output concentrations in files specified on Record_4.3 and Record_4.6. NWADS surface complexes (with indices IWADS) will be read below in Record_12. NWADS can be set to a negative value, in which case names of surface complexes (instead of indices) will be read line-by-line starting on Record_12.

NWEXC : number of exchange species for which to output concentrations in files specified on Record_4.3 and Record_4.6. NWEXC exchange species (with indices IWEXC) will be read below in Record_13. NWEXC can be set to a negative value, in which case names of exchange species (instead of indices) will be read line-by-line starting on Record_13.

ICONFLAG: flag to specify the aqueous concentration units in output files specified on Record_4.3 and Record_4.6.

=0 mol/kg H_2O (molal)
=1 mol/L liquid (molar – concentrations will change as water density changes with temperature!)
=2 g/L liquid (concentrations will change as water density changes with temperature!)
=3 mg/L (~ppm if water density remains close to 1 g/cc; concentrations will change as water density changes with temperature!)

MINFLAG: flag for units of mineral abundances output in files specified on Record_4.4 and Record_4.6.

=0 Change (relative to t = 0) of mineral abundance in mol/m3 medium
=1 Change (relative to t = 0) of mineral abundance in volume fraction (dimensionless)
=2 Current mineral abundance (total amount) in volume fraction (dimensionless)
=3 Change (relative to t = 0) of mineral abundance in volume %

Record_8. List of grid blocks for printout of time evolution results

If NWNOD (on Record_7) > 0:

Variable: EL(I), I=1,NWNOD

Format: 15A5

Description: five-character code name of a grid block (up to 200 names, 15 per record). NWNOD names will be read. Each name must match one of those specified in the flow.inp input file or MESH file. No blank line follows the list!

If NWNOD (on Record_7) < 0:

Variable: EL(I), I=1,N

Format: A5

Description: Five-character code name of a grid block (up to 200, one name per record). The list of names must end with a blank record. Each name must match one of those specified in the flow.inp input file or MESH file.

If NWNOD (on Record_7) =0: leave a blank record.

Record_9. Indices or names of component species for which to output total concentrations

If NWCOM (on Record_7) > 0:

Variable: IWCOM(I), I=1,NWCOM

Format: Integer (free format). One record up to 200 characters long. NWCOM indices will be read, up to total number of primary species. No blank line follows this record!

Description: indices of component species.

If NWCOM (on Record_7) <0:

Variable: PRT_COM(I), I=1,N

Format: A20 (one name per record, without quotes, up to total number of primary species). The list of names must end with a blank record. Each name must match one of those specified in the thermodynamic database and included in the simulation (e.g. in file chemical.inp).

Description: names of component species

If NWCOM (on Record_7) =0: leave a blank record.

Record_10. Indices or names of minerals for which to output amounts

If NWMIN (on Record_7) > 0:

Variable: (IWMIN(I), I=1, NWMIN)

Format: Integer (free format). One record up to 200 characters long. NWMIN indices will be read, up to total number of minerals. No blank line follows this record!

Description: indices of minerals (which correspond to order entered in chemical.inp)

If NWMIN (on Record_7) <0:

Variable: PRT_MIN(I), I=1,N

Format: A20 (one name per record, without quotes, up to total number of minerals). The list of names must end with a blank record. Each name must match one of those specified in the thermodynamic database and included in the simulation (e.g. in file chemical.inp).

Description: names of minerals

If NWMIN=0 (on Record_7): leave a blank record.

Record_11. Indices or names of individual aqueous species for which to output concentrations

If NWAQ (on Record_7) > 0:

Variable: (IWAQ(I), I=1, NWAQ)

Format: Integer (free format). One record, up to 200 characters long. NWAQ indices will be read, up to total number of individual species. No blank line follows this record!

Description: indices of aqueous species (e.g., as shown in chemical.inpt)

If NWAQ (on Record_7) <0:

Variable: PRT_AQ(I), I=1,N

Format: A20 (one name per record, without quotes, up to total number of individual species). The list of names must end with a blank record. Each name must match one of those specified in the thermodynamic database and included in the simulation (e.g. in file chemical.inp).

Description: names of aqueous species

If NWAQ=0 (on Record_7): leave a blank record.

Record_12. Indices or names of surface complexes for which to output concentrations

If NWADS (on Record_7) > 0:

Variable: (IWADS(I), I=1, NWADS)

Format: Integer (free format). One record up to 200 characters long. NWADS indices will be read, up to total number of surface complexes. No blank line follows this record!

Description: indices of surface complexes (e.g., as shown in chemical.inp)

If NWADS (on Record_7) <0:

Variable: PRT_ADS(I), I=1,N

Format: A20 (one name per record, without quotes, up to total number of surface complexes). The list of names must end with a blank record. Each name must match one of those specified in the thermodynamic database and included in the simulation (e.g. in file chemical.inp).

Description: names of surface complexes

If NWADS=0 (on Record_7): leave a blank record.

Record_13. Indices or names of exchange species for which to output concentrations

If NWEXC (on Record_7) > 0:

Variable: (IWEXC(I), I=1, NWEXC)

Format: Integer (free format). One record up to 200 characters long. NWEXC indices will be read, up to total number of exchange species. No blank line follows this record!

Description: indices of exchange species (e.g., as shown in chemical.inp)

If NWEXC (on Record_7) <0:

Variable: PRT_EXC(I), I=1,N

Format: A20 (one name per record, without quotes, up to total number of exchange species). The list of names must end with a blank record. Each name must match one of those specified in the simulation (e.g. in file chemical.inp).

Description: names of exchange species

If NWEXC=0 (on Record_7): leave a blank record.

Record_14. Default indices for all chemical property zones

If MOPR(11) ≠ 1 (in flow.inp)

Variable: IZIWDF, IZBWDF, IZMIDF, IZGSDF, IZADDF, IZEXDF, IZPPDF, IZKDDF

Format: 8I (integer free format)

Description: IZIWDF, IZBWDF, IZMIDF, IZGSDF, IZADDF, IZEXDF, IZPPDF, and IZKDDF are default values of IZIW, IZBW, IZMI, IZGS, IZAD, IZEX, IZPP, and IZKD, respectively, as described for Record_15.

If MOPR(11) = 1 (in flow.inp)

Variable: IZIWDF, IZBWDF, IZMIDF, IZGSDF, IZADDF, IZEXDF, IZPPDF, IZKDDF, VSED

Format: 8I, F (free format)

Description: Same as above, except for the last variable, VSED, which is the sedimentation velocity (m/s). This option will only work for a vertical 1D column with grid blocks and connections sequentially ordered from top to bottom.

Record_15. Chemical property zone indices for specific grid blocks

If MOPR(11) ≠ 1 (in flow.inp)

Variable: EL, NSEQ, NADD, IZIW, IZBW, IZMI, IZGS, IZAD, IZEX, IZPP, IZKD

Format: A5, 10I (integer free format), one record per grid block, up to the total number of grid blocks. The list of records must end with a blank record.

EL: grid block name

NSEQ: number of additional grid blocks having the same chemical properties

NADD: increment between the code numbers of two successive grid blocks

Indices of the various zones (for different waters, mineralogies, gas compositions, sorption characteristics, etc.) defined in file chemical.inp:

IZIW: initial water zone number

IZBW: boundary inflow (and pumping/injection grid blocks) water zone number

IZMI: mineral zone number

IZGS: gas zone number

IZAD: adsorption zone number

IZEX: ion exchange zone number

IZPP: zone number for porosity-permeability relation

IZKD: linear adsorption Kd zone number

If MOPR(11) = 1 (in flow.inp)

Variable: EL, NSEQ, NADD, IZIW, IZBW, IZMI, IZGS, IZAD, IZEX, IZPP, IZKD, VSED

Format: A5, 10I, F (free integer and real format) one record per grid block, up to the total number of grid blocks. The list of records must end with a blank record.

Description: Same as above, except for the last variable, VSED, which is the sedimentation velocity (m/s). This option will only work for a vertical 1D column with grid blocks and connections sequentially ordered from top to bottom. By specifying decreasing velocities with depth, the effect of compaction can be approximated (set KCPL > 0 in Record_2 to capture resulting porosity changes).

6.3 Geochemical Input (chemical.inp)

All variables in this file are input in free format. Input character variables must be enclosed in quotes, and variables that are not used must be entered as zero values and cannot be left blank, unless specifically indicated otherwise.

Inputs are organized in groups (e.g., records Akin for aqueous kinetics, Aque for aqueous species, Mine for minerals, etc.). These groups are always preceded by a header record, and always end with a trailing record starting with '*' (or a blank record). Entries for any group can be skipped altogether (e.g., if no minerals are present),

however one or more "skip" records followed by a trailing ('*') record must always be entered in the file for all groups. The order in which input groups are entered cannot be changed from that shown below.

Names of all aqueous species, gases, and minerals input in this file are internally converted to lower case characters. The electronic charge in the names of cations and anions are also internally converted to display the charge sign followed by the number of charges (for example, 'CO3--' is converted to 'co3-2' and 'Al+++' is converted to 'al+3'. This allows for input flexibility and maintains internal consistency. Examples of chemical.inp are given in Figure 8.1-4, 8.2-2, 8.9-4 and 8.10-5.

"Skip" records:

One or more heading (comment) line can precede each record described below (see inputs of the sample problems, such as in Figure 8.2-2). The comment line is indicated by beginning with "#" followed by one blank (without quotes), or any blank record, and will be skipped on input. These "skip" records can be inserted anywhere in the file, except within input blocks that end with '*'. These "skip" records can be also used for data source references, or other purpose.

Record-1. Title

Variable: TITLE

Format: A (free format)

TITLE: title and comments in one line.

Record-2. Label (a "Skip" record)

Variable: LABEL

Format: A (free format)

LABEL: comments to appear in the output file.

6.3.1 Definition of the geochemical system

These records contain the information on aqueous species, minerals, gases, surface complexes, species with linear adsorption Kd and radioactive decay, and exchangeable cations. Their names must match exactly those in the thermodynamic database file (it's not case sensitive).

Record-3. Label (a "Skip" record)

Variable: LABEL

Format: A (free format)

LABEL: comments to appear in the output file.

Primary species (Prim)

Prim-1. Header for Prim records (a "Skip" record)

Variable: LABEL

Format: A (free format)

LABEL: header describing Prim records.

Prim-2. Primary aqueous species

Variable: NAPRI, NOTRANS, NAADS_MIN, SDENS, IMOD, CAPAC

Format: A, I, A, F, I, F (free format, one record per primary species)

NAPRI: name of the primary species, enclosed in quotes (truncated after 20 characters). It must match exactly that in the thermodynamic database file. A record starting with '*' is needed to indicate the end of the list of the primary species.

NOTRANS: flag for transport and surface complexation options.

=0 species (component) will be transported

=1 no transport for this species (component)

All species specified with NOTRANS ≥2 must be listed at the end of the list of species.

=2 flag to indicate this is a surface (primary) species, with molality-based surface complexation constants in the thermodynamic database.

=3 flag to indicate this is a surface (primary) species, with mole-fraction based surface complexation constants in the thermodynamic database.

=4 flag to indicate this is a surface (primary) species, with equivalent-fraction based surface complexation constants in the thermodynamic database (e.g., as with phreeqc v2).

The remaining variables on record Prim-2 are required only if NOTRANS=2

NAADS_MIN: name of mineral associated with this surface species (in quotes, up to 20 characters). More than one surface species (NAPRI) can be associated with the same mineral. NAADS_MIN can be either:

A name (in quotes) matching the name of one of the minerals included in the simulation (on record Mine-1), or

'no_mineral' (including quotes), in this case sorption is not tied to a specific mineral, and a constant sorption surface area is entered in $cm^2/g_{mineral}$ on record Zads-6, or

'surface.....' (including quotes; the first 7 characters after the initial quote must spell *surface*): in this case adsorption is tied to a generic surface with a constant sorption surface area input in m^2/kg_{H2O} on record Zads-6.

SDENS: sorption site density in $mol_{sites}/m^2_{mineral}$ for this surface species

IMOD: adsorption model type.

=0 surface complexation without electrostatic terms

=1 constant capacitance model

=2 double diffuse layer model, linear

=3 double diffuse layer model, Gouy-Chapman (most common)

CAPAC: this variable must be entered only if IMOD=1. Capacitance in F m^{-2} (these units are identical to C V^{-1} m^{-2})

Prim-3. Trailer for Prim records

Variable: LABEL

Format: A (free format)

LABEL: character string starting with '*' (including quotes) or blank record

Aqueous Kinetics (Akin)

Akin-1: Header for Akin records (a "Skip" record)

Variable: LABEL

Format: A (free format)

LABEL : character string starting with 'AQUEOUS KINETICS' (including quotes; upper or lower case.

Akin-2:

Variable: NTRX

Format: I (free format)

NTRX : Total number of kinetic reactions among aqueous species

The following records, from Akin-3 through Akin-9, are repeated NTRX times. The format of this input block is given below.

Akin-3:

Variable: IRX

Format: I (free format)

IRX : Index of kinetic reaction, from 1 to NTRX.

Akin-4:

Variable: NCP, (S(i), NAM(i), I = 1, NCP), irkaq_typ, rkaq_logK, rkaq_cf

Format: I, NCP(F, A), I, 2F (free format)

NCP : number of aqueous species involved in each reaction

S : stoichiometric coefficients of primary species NAM included in the reaction. Negative values are for reactants, positive values for products. The stoichiometric coefficients must be in terms of moles for the species involving in other reactions such as aqueous complexation, cation exchange and mineral dissolution and precipitation (undergoing mass-action calculations). Otherwise, they can be input in any units such as mg and g. Details are illustrated in the related sample problems (in Sections 8.9 and 8.10).

The last three entries below are optional and are used to define a reaction affinity term to limit, stop, and potentially reverse the rate of the reaction as it reaches and potentially crosses the equilibrium point. The affinity term is based on the reaction ion activity product Q and the reaction equilibrium constant K. Note that Q/K is always positive and equals 1 at equilibrium. When Q/K is < 1 and the specified reaction rate (RKAQ) is positive, the reaction proceeds from left to right (the "normal" case). If Q/K > 1 (with a positive RKAQ), the reaction can reverse and proceeds from right to left.

irkaq_typ: if not zero nor blank, this flag enables limiting the reaction rate by an affinity term (fG) that multiplies the reaction rate and drops to zero at equilibrium. The form of the affinity term depends on the value of irkaq_typ, as shown below.

=0 $f_G = 1$ (no limit – beware, the equilibrium point may be overshot!)

=1 Function based on transition state theory (TST):

$f_G = (1 - Q/K)^{rkaq\_cf}$ (f_G varies from +1 to 0 when reaction is from left to right)
(f_G varies from 0 to large numbers when reaction is from right to left)

Note that primary species defined with NOTRANS=1 in record Prim-2 (see Section 6.3.1) are not included in the calculation of *Q*. When $Q/K \leq 1$, the reaction proceeds from left to right, and f_G varies from 1 away from equilibrium to 0 at equilibrium (positive rate). When $Q/K > 1$, the reaction reverses (proceeds from right to left, i.e., negative rate) and f_G can become very large. Note that setting the coefficient *rkaq_cf* to a small value limits the upper value of f_G and can help convergence.

=2 Symmetric TST form with f_G varying between +1 and –1:
$f_G = (1 - Q/K)^{rkaq\_cf}$ when $Q/K \leq 1$ (f_G varies from +1 to 0; reaction from left to right)
$f_G = -(1 - K/Q)^{rkaq\_cf}$ when $Q/K \geq 1$ (f_G varies from 0 to – 1; reaction from right to left)

This option is useful in limiting the rate by the same amount on each side of the equilibrium point. It has no real theoretical basis.

=3 Similar effect as with irkaq_typ=2, with f_G varying between +1 and –1, but using a different function shape:

$$f_G = \frac{\log\left(\frac{Q}{K}\right)}{\left|\log\left(\frac{Q}{K}\right)\right| + rkaq\_cf}$$

Here the value of *rkaq_cf* is the value of $\log(Q/K)$ at which the rate is cut in half (i.e., at which $f_G = \pm 0.5$). This function has no real theoretical basis.

=4 Same effect as irkaq=1 in the forward direction (TST affinity term when reaction operates from left to right), but reversal of the reaction is not allowed (i.e., $f_G = 0$ in the reverse direction).

rkaq_cf: value of coefficient *c* in the affinity functions described above.

rkaq_logK: log of the equilibrium constant *K* of the reaction.

Akin-5:

Variable: I_MOD, N_MECH

Format: 2I (free format)

I_MOD : Type-index of kinetic rate model.

=1 Main model currently implemented (Eq. B.2 in Appendix B)

=2 Not used (do not use as it may create an input error)

=3 Special case: Monod and inhibition limiters in Eq. B.2 are suppressed when the reaction operates in a reverse direction (i.e., when f_G becomes negative, the rate is not multiplied by Monod and inhibition terms).

I_MECH : Number of mechanisms (pathways) to include in the rate expression.

Akin-6:

Variable: RKAQ

Format: F (free format)

RKAQ : forward rate constant or maximum specific growth rate (mass/L/s). If RKAQ = -1.0, the rate constant will be temperature-dependent, and dynamically calculated according to the following equation:

$$k = k_{25} \exp\left[\frac{-E_a}{R}\left(\frac{1}{T} - \frac{1}{298.15}\right)\right]$$

Where E_{25} is a rate constant (1/s) at 25^{o}C, and E_a is activation energy (KJ/mol), and T is the absolute temperature. E_{25} and E_a need to read from additional record AKIN-6-1

Akin-6-1:

Variable: RK_a, RK_b

Format: F, F (free format)

RK_a : is k_{25} of the above equation (1/s).

RK_b : is E_a of the above equation (KJ/mol).

Akin-7:

Variable: NCP_rx1, (NAM_rx1(i), ia1(i), S_rx1(i), i=1,NCP_rx1)

Format: F, NCP_rx1(A, I, F) (free format)

NCP_rx1 : Number of species (primary or secondary) involved in product terms, see Eq. B.2 in Appendix B

NAM_rx1 : chemical formula of the species.

ia1: flag for using activity (ia1 = 1) or concentration (ia1 = 2) of the species for calculations of the product term

S_rx1 : value of power term applied to activity or concentration of the species

Akin-8:

Variable: NCP_rx2, (NAM_rx2(i), ia2(i), S_rx2(i), i=1,NCP_rx2)

Format: F, NCP_rx2(A, I, F) (free format)

NCP_rx2 : Number of species (primary or secondary) involved in Monod terms, see Eq. B.2 in Appendix B

NAM_rx2 : chemical formula of the species.

Ia2: flag for using activity (ia1 = 1) or concentration (ia1 = 2) or total concentration (ia1 = 3, only for primary species) of the species for calculations of the Monod term

S_rx2 : value of half-saturation constant for the species

Akin-9:

Variable: NCP_rx3, (NAM_rx3(i), ia3(i), S_rx3(i), i=1,NCP_rx3)

Format: F, NCP_rx3(A, I, F) (free format)

NCP_rx3 : Number of species (primary or secondary) involved in Inhibition terms, see Eq. B.2 in Appendix B

NAM_rx3 : chemical formula of the species.

Ia3: flag for using activity (ia1 = 1) or concentration (ia1 = 2) or total concentration (ia1 = 3, only for primary species) of the species for calculations of the inhibition term

S_rx3 : value of inhibition constant for the species

Akin-10: Trailer for Akin records

Variable: LABEL

Format: A (free format)

LABEL: character string starting with '*' (including quotes) or blank record

Secondary aqueous species (Aque)

Aque-1. Header for Aque records (a "Skip" record)

Variable: LABEL

Format: A (free format)

LABEL: header describing Aque records.

Aque-2. Secondary aqueous species

This input block can be omitted. In this case, all possible secondary aqueous species found in the input thermodynamic database will be automatically selected.

Variable: NAAQX

Format: A (free format, one record per secondary species)

NAAQX: name of secondary aqueous species, in quotes (truncated after 20 characters). The name must match exactly that in the thermodynamic database file.

Aque-3. Trailer for Aque records

Variable: LABEL

Format: A (free format)

LABEL: character string starting with '*' (including quotes) or blank record

Minerals (Miner)

Miner-1. Header for Miner records (a "Skip" record)

Variable: LABEL

Format: A (free format)

LABEL: header describing Aque records.

The following two main records (Miner-2 and Miner-3) are repeated as many times as the number of minerals. Minerals can be entered in any order as long as the minerals at equilibrium precede those under kinetic constraints. The specified minerals consist of reactants and any possible products. Their names must match exactly the names of minerals in the database. Minerals with identical stoichiometries (i.e. quartz and cristobalite) cannot both be specified at equilibrium, but can be specified to react under kinetic constraints. Minerals under kinetic constraints require more records (per mineral) than minerals under equilibrium constrains.

Miner-2.

Variable: NAMIN, IKIN, IDISPRE, ISS, M1

Format: A, 4I (free format)

NAMIN: name of the mineral phase, in quotes (truncated after 20 characters). It must be consistent with that in the thermodynamic database. Omit NAMIN if no minerals are required. However, the trailer record starting with '*' (or blank) is always needed to indicate the end of the list.

IKIN: flag for the type of mineral: 0 for minerals at equilibrium, and 1 for those under kinetic constraints.

IDISPRE: flag for the type of kinetic constraint: 1 for dissolution only, 2 for precipitation only, and 3 for both (mineral can either precipitate or dissolve). Always set IDISPRE = 0 if IKIN = 0; and IDISPRE > 0 if IKIN = 1.

ISS: index for a solid solution mineral endmember. All endmembers for a specified phase are given the same ISS value: ISS = 1 for each endmember of the first solid solution, ISS = 2 for each endmember of the second solid solution, and so on (numbers cannot be skipped). Records for each member can appear in any order in the mineral records.

M1: flag to indicate that the mineral may precipitate in a dry grid block as a result of complete evaporation (when liquid saturation < sl1min specified in the solute.inp file), or if there is water flux into the grid block that dries out during the flow step (and therefore liquid saturation is zero). The mineral with M1 = 1 precipitates first, with M1 = 2 second, and so on. If this flag is set to zero, then the mineral will not be formed in the dry grid block.

If IKIN = 1 and IDSPRE = 1 or 3, one or more additional records (Miner-2.1) are required to define dissolution rate law parameters.

If IKIN = 1 and IDSPRE = 2 or 3, one or more additional records (Miner-2.2) are required to define precipitation rate law parameters.

Miner-2.1.

Variable: RKF, IDEP, CK1, CK2, EA, ACFDISS, BCFDISS, CCFDISS

Format: F, I, 6F (free format)

RKF: coefficient k_{25} in the expression (B.7) given in Appendix B, where k_{25} is the rate constant (in mol/m^2/sec) at 25°C, EA is the activation energy in kJ/mol. The form of the rate law is given in Eq. (B.6).

IDEP: flag for rate constant dependence on pH (see Figure B.4-1 in Appendix B) or multiple mechanisms (see Eq. B.13 in Appendix B). If IDEP = 0, pH (species) dependent rate constants and multiple mechanisms are not considered. If IDEP = 1, and additional record (Miner-2.1.1) must be entered to include information on the rate dependence on pH. If IDEP = 2, additional records Miner-2.1.2 and Miner-2.1.2.1 must be entered to include information on the rate constants contributed from additional mechanisms.

CK1 and CK2: the exponents η and θ, respectively in Eq. (B.6).

EA: the activation energy (kJ/mol).

ACFDISS, BCFDISS, and CCFDISS: should be set to zero, unless a different form of rate constant dependence with temperature is desired. This alternate form is: $\log_{10}(k) = a + b \cdot T + c/T$, where T is absolute temperature in K. To enable this option, RFK must be set to 1.0, EA must be set to 0.0, CK1 and CK2 can be set to any value, and ACFDISS, BCFDISS, and CCFDISS must be specified as the coefficients *a*, *b*, and *c*, respectively, in the above expression.

Miner-2.1.1 (only if IDEP = 1)

Variable: PH1, SLOPE1, PH2, SLOPE2

Format: 4F (free format)

See Figure B.4-1 (in Appendix B) for the meaning of these parameters.

Miner-2.1.2 (only if IDEP = 2)

Variable: NDIS

Format: I (free format)

NDIS is the number of additional mechanisms contributed to the rate constant (see Eq. B. 13 in Appendix B) (maximum allowed is 5). An example of the multiple mechanisms can be found in the CO_2 disposal sample problem (Section 8.5).

Miner-2.1.2.1 (repeat NDIS times after Miner-2.1.2, only if IDEP=2)

Variable: RKDS, EADS, NSPDS, NADIS, EXPDSP

Format: 2F, I, A, F (free format)

RKDS is k_i in Eq. (B. 13) where i is the additional mechanism index.

EADS: is the activation energy (kJ/mol) for each additional mechanism.

NSPDS: is the number of species involved in each mechanism (a maximum of five species can be considered).

NADIS is the name of species involved in the mechanism that must be in the list of primary or secondary species. NADIS and the following variable EXPDSP must be repeated as many as NSPDS times.

EXPDSP is the power term n_j in Eq. (B. 13).

Miner-2.2.

Variable: RKPREC, IDEPREC, CK1PREC, CK2PREC, EAPREC, ACFPREC, BCFPREC, CCFPREC, RNUCL, NPLAW

Format: F, I, 7F, I (free formats)

The first 8 input parameters are listed in the same order and have the same functions as those described above for mineral dissolution, except that the parameters apply to mineral precipitation instead of dissolution. Therefore if IDEPREC = 1, an additional record identical to Miner-2.1.1 needs to include information on the rate dependence on pH; if IDEPREC = 2, additional records identical to Miner-2.1.2 and Miner-2.1.2.1 need to be inserted with information on the rate constants contributed from additional mechanisms.

RNUCL: the initial volume fraction ($V_{mineral}/V_{solid}$) to be assumed for calculating initial effective surface area if the mineral is not present at the start of a simulation but precipitates as a new reaction product. If zero, RNUCL is assumed to be 10^{-10}.

NPLAW: precipitation law index. NPLAW = 0 for Eq. (B.6 and B.13) in Appendix B; NPLAW = 1 for Eq. (B.9).

Miner-3.

This record is required for all minerals reacting at equilibrium, but only for those minerals reacting under kinetic constraints that are allowed to precipitate (IDSPRE = 2 or 3).

Variable: SSQK0, SSTK1, SSTK2

Format: 3F (free format)

SSQK0: log (Q/K) gap (supersaturation window, see Eq, B.14 in Appendix B). A zero value represents no gap.

SSTK1: temperature (in °C) at which to begin reducing gap.

SSTK2: temperature (in °C) endpoint at which the gap has diminished to nearly zero (1% of original value). The gap decreases exponentially from the first (SSTK1) to the second (SSTK2) temperature, and SSTK2 must always be greater than SSTK1.

Miner-4. Trailer for Mine records

Variable: LABEL

Format: A (free format)

Gaseous species (Gas)

Note that H_2O gas is not entered in the list of gases here, because its transport and thermodynamics are treated by the TOUGH2 EOS module selected for any given simulation.

Gas-1. Header for Gas records (a "Skip" record)

Variable: LABEL

Format: A (free format)

LABEL: header describing Gas records.

Gas-2. Gases

Variable: NAGAS

Format: A (free format, one record per gas)

NAGAS: name of a gaseous species, in quotes (truncated after 20 characters). It must match exactly that in the thermodynamic database file. Omit NAGAS if no gaseous species are required. However, the trailer record starting with '*' (or blank) is always needed to indicate the end of the list.

Gas-3. Trailer for Gas records

Variable: LABEL

Format: A (free format)

LABEL: character string starting with '*' (including quotes) or blank record

Surface complexes (Surx)

Surx-1. Header for Surx records (a "Skip" record)

Variable: LABEL

Format: A (free format)

LABEL: header describing Surx records.

Surx-2. Surface complexes

This input block can be omitted. In this case, all possible surface complexes found in the input thermodynamic database will be automatically selected.

Variable: NAADS

Format: A (free format, one record per surface complex)

NAADS: name of surface complex, in quotes (truncated after 20 characters). Omit NAADS if no surface complexes are required. However, the trailing record starting with '*' (or blank) is always needed to indicate the end of the list.

Surx-3. Trailer for Surx records

Variable: LABEL

Format: A (free format)

LABEL: header describing Kdde records.

Aqueous species (primary) with Kd and decay (Kdde)

Kdde-1. Header for Kdde records (a "Skip" record)

Variable: LABEL

Format: A (free format)

LABEL: header describing Kdde records.

Kdde-2. Species with Kd and decay

Variable: NAKDD, DECAYC, a_TDecay, b_TDecay

Format: A, F, F, F (free format, one species per record)

NAKDD: name of the aqueous primary species with Kd and/or decay, in quotes (truncated after 20 characters). These names must appear in the above mentioned primary species records (Prim records). Omit these records if no primary species with Kd and/or decay are required. However, the trailing record starting with '*' (or blank) is always needed to indicate the end of the list.

DECAYC: a positive value is radioactive decay constant (in 1/s). For species with only Kd adsorption and without decay, set DECAYC equal to 0.0. For DECAYC greater than or equals to zero (0.0), set the following two parameters (a_TDecay and b_TDecay) to zero. If DECAYC=-1.0, the decay constant is temperature-dependent according to ln(k) = a – b/T (ln stands for natural logarithm), where k is the decay constant (in **1/day**), a and b are two parameters that will read from the following two variables, and T is absolute temperature in K.

a_TDecay: parameter a in the above equation.

b_TDecay: parameter b in the above equation.

Kdde-3. Trailer for Kdde records

Variable: LABEL

Format: A (free format)

LABEL: character string starting with '*' (including quotes) or blank record

Exchanged species (Exch)

Exch-1. Header for Exch records (a "Skip" record)

Variable: LABEL

Format: A (free format)

LABEL: header describing Exch records.

Exch-2. Number of exchange sites

Variable: NXsites, Mod_Xsl

Format: 2I (free format)

NXsites: number of exchange sites

Mod_Xsl: Models for dependence of exchange sites on water saturation. Mod_Xsl = 1 for ideal-wetting condition; Mod_Xsl = 2 for considers multiplying a (correction) factor f that depends on liquid saturation, $f(S_l)$. Details can be found in Appendix K.

Exch-3. Label (a "Skip" record)

Variable: LABEL

Format: A (free format)

LABEL: sub-header describing the data that follows.

Exch-4. Exchanged species

Variable: NAEXC IMS IEX (EKX(i), i=1,NXsites)

Format: A, 2I, NXsites(F) (free format, one record per exchanged species)

NAEXC: name of exchangeable species, in quotes (truncated after 20 characters). Omit NAEXC if no exchangeable cations are required. However, a record starting with '*' is always needed to indicate the end of the list.

IMS: If IMS = 1, the cation is used as reference for the exchange reactions (normally Na^+). For the remaining cations, IMS must be 0.

IEX: exchange convention type used in the calculations: 1= Gaines-Thomas; 2= Vanselow; 3= Gapon (see Section B.6 of Appendix B for definition)). The value of IEX must be the same for all the exchanged cations.

EKX: exchange coefficient of the cation with respect to the reference cation. If IMS = 1, then EKX = 1.0. Note, for example, if Na^+ is selected as the reference cation, using Gaines-Thomas convention (commonly used), for Na-Ca exchange Ca^{2+} selectivity must be specified according to the following reaction, $Na^+ + 0.5Ca\text{-}X_2 = 0.5Ca^{2+} + Na\text{-}X$ where X represents cation exchange site (see Section B.6 of Appendix B and Table 8.2-2 of Sample 2 for details). Note also that there are NXsites values, exch for one exchange site)

Exch-5. Trailer for Exch records

Variable: LABEL

Format: A (free format)

LABEL: character string starting with '*' (including quotes) or blank record

6.3.2 Composition of initial and boundary waters (Water)

This section describes the different water zones initially assigned to various parts of the modeled system. These zones are mapped to the numerical grid through variables defined on Record_14 and Record_15, respectively, in file solute.inp, as described further below.

Water-1. Label (a "Skip" record)

Variable: LABEL

Format: A (free format)

LABEL: comments or blank line.

Water-2. Header for Water records (a "Skip" record)

Variable: LABEL

Format: A (free format)

LABEL: header describing Water records.

Water-3. Total number of different water compositions in the system

Variable: NIWTYPE NBWTYPE

Format: 2 I (free format)

NIWTYPE: total number of aqueous solutions initially present in the system, excluding waters at boundaries and pumping/injection grid blocks. These are referred to as "initial waters".

NBWTYPE: total number of aqueous solutions at boundaries and pumping/ injection grid blocks. These are referred to as "boundary waters".

Aqueous solution compositions

This part describes the input of "initial" and "boundary" water compositions. Records Water-4, Water-5, Water-6, and Water-7 form the ensemble of records necessary to input one water composition. These records must be repeated NIWTYPE times for initial waters, followed by NBWTYPE times for boundary waters. Note that "boundary water" records must always follow "initial water" records. Each water composition is given a specific index, which is then mapped onto the numerical grid through variables IZIWDF and IZIW (for initial waters) and IZIBDF and IZIB (for boundary waters) on Record_14 and Record_15, respectively, in file solute.inp.

For boundary waters, the flux of each chemical component at the boundary is calculated from the given composition (Water-6) multiplied by the water flux given under keyword block 'GENER' in the *flow.inp* file (or in the separate GENER file). For a negative water flux (such as pumping and discharge), the boundary solution composition is not required.

Each "initial" and "boundary" water composition defined here undergoes initial speciation computations, with results output in file chdump.out.

Water-4. Identification of the aqueous solution

Variable: IWTYPE TC2 PT

Format: I, F, F (free format)

IWTYPE: Index of the solution. This index must correspond to one of the water zone indices specified on Record_14 and Record_15 in file solute.inp. The value of IWTYPE must start at 1 for the first initial water, then sequentially increase up to NIWTYPE; it is then set again to 1 for the first boundary water, then increases again sequentially up to NBWTYPE.

TC2: temperature of the solution (°C). Note that this temperature is used only for initial speciation calculations for this water, before the water composition is assigned to different grid blocks. The initial temperatures and pressures of grid blocks assigned to this water composition are defined in the INCON block of the flow.inp file, and are not necessarily the same as TC2.

PT: pressure of the solution (bar). This value can be omitted, in which case PT is assumed 1 bar. As for TC2, this pressure is used only for initial speciation calculations for this water, before the water composition is assigned to different grid blocks. If PT is zero, or is below the water-saturation pressure, it is recalculated as the water saturation pressure at temperature TC2.

Water-5. Label (a "Skip" record)

Variable: LABEL

Format: A (free format)

LABEL: sub-header describing the data that follows.

Water-6. Composition of aqueous solution

Variable: NAPRI ICON CGUESS CTOT NAMEQ QKSAT

Format: A, I, F, F, A, F (free format, one per primary species)

NAPRI: name of the primary aqueous species, in quotes (truncated after 20 characters). The name of the species must match exactly those previously listed as primary species in the definition of the system, although the order may change. The trailing record (Water-7) must end the list of species.

ICON: flag indicating the type of constraint controlling the input concentration of the aqueous species:

ICON=1: input values of CTOT represent total amounts (in moles) for aqueous species, and total kilograms for liquid H_2O. Thus, to input total molalities, set CTOT = 1 for H_2O.

ICON=2: the total concentration of the species will be computed such that the saturation index (log(Q/K)) of mineral or gas NAMEQ equals QKSAT at temperature and pressure TC2

and PT, respectively. Therefore, for equilibrium with a mineral, use this option with QKSAT = 0.0, and for equilibrium with a gas at a given fugacity, use this option with QKSAT = log(fugacity). With this option, input CTOT values are irrelevant and discarded.

ICON =3: input values of CTOT represent the known activity of the specific species (i.e., not total concentration) at temperature and pressure TC2 and PT, respectively. For example, to input a known pH value, use this option and set CTOT = 10^{-pH} for H^+ activity.

ICON=4: the total concentration of the species is adjusted to yield charge balance. Use only with a charged species. If convergence occurs, choose a species with an opposite charge. With this option, input CTOT values are irrelevant and discarded.

CGUESS: initial guess (trial) value for the concentration of the individual primary species (not total concentration), in moles/kg H_2O (molal) for species other than H_2O and in kg for H_2O. Input values of CGUESS do not affect results of speciation calculations, but could affect the number of chemical iterations required during initial speciation computations.

CTOT: if ICON=1, CTOT is total moles of aqueous species, and total amount (in kg) of liquid water for H_2O. Molalities are then internally computed as $CTOT_{i \neq H2O}/CTOT_{H2O.}$ If ICON > 1, refer to the discussion of ICON above for the meaning of CTOT.

NAMEQ: name of mineral or gas (in quotes) to use with option ICON=2. Names must match exactly those previously listed as minerals or gases in the definition of the chemical system. If ICON≠2, this entry is ignored, but cannot be omitted and should be entered as one of more characters between single quotes (suggested ' ' or '*').

QKSAT: desired value of mineral log(Q/K) or gas log(fugacity) when option ICON=2 is used. For equilibrium with mineral NAMEQ use QKSAT=0.0, and for equilibrium with gas NAMEQ at a given fugacity use QKSAT = log(fugacity). If ICON≠2, this entry is ignored, but cannot be omitted and should be entered as a real number (suggested 0.0).

Water-7. Trailer for Water records (one record after each water)

Variable: LABEL

Format: A (free format)

LABEL: character string starting with '*' (including quotes) or blank record

6.3.3 Initial mineral zones (Imin)

This section describes the mineral zones initially present in the system. These zones are mapped to the numerical grid through variables IZMIDF and IZMI on Record_14 and Record_15, respectively, in file solute.inp.

Imin-1. Label (a "Skip" record)

Variable: LABEL

Format: A (free format)

LABEL: comments or blank line.

Imin-2. Header for Imin records (a "Skip" record)

Variable: LABEL

Format: A (free format)

LABEL: header describing Imin records.

Imin-3.

Variable: NMTYPE

Format: I (free format)

NMTYPE: Total number of mineral zones in the system.

The following records (Imin-4, Imin-5 and Imin-6, and Imin-7) define each mineral zone, and must be repeated NMTYPE times.

Imin-4.

Variable: IMTYPE

Format: I (free format)

IMTYPE: Index of the mineral zone. It must be 1 for the first zone, increasing sequentially thereafter. This index must correspond to one of the mineral zone indices specified on Record_14 and Record_15 in file solute.inp.

Imin-5. Label (a "Skip" record)

Variable: LABEL

Format: A (free format)

LABEL: sub-header describing the data that follow.

Imin-6. Composition of the mineral zone

Variable: NAMIN VOL IKIN

Format: A, F, I (free format, one record per mineral)

NAMIN: name of the mineral present in the system, in quotes. The name of the mineral must be included among those previously listed in the definition of the system (Miner records), although the order may change, and it is not needed to repeat the complete list. However, names of minerals specified to react under equilibrium constraints all (and always) must precede the names of minerals reacting under kinetic constraints. Minerals defined for the system (Miner records) but excluded from the list are assumed to take zero values for all input parameters specified below. A trailing record (Imin-7) must end the list of minerals (for each given zone).

VOL: initial volume fraction of the mineral, excluding liquid (mineral volume divided by total volume of solids). The sum of VOL's need not add up to 1. If the sum is less than 1, the remaining solid volume fraction is considered nonreactive.

IKIN: flag for the mineral type:

IKIN = 0 for minerals at equilibrium.

IKIN = 1 for minerals under kinetic constraints. For minerals under kinetic constraints, an additional record (Imin-6.1, below) is always required.

IKIN = 2 to suppress reaction for either kinetic and/or equilibrium minerals.

Imin-6.1.

Variable: RAD, AMIN, IMFLG

Format: 2F, I (free format)

RAD: radius of mineral grain (in m) used to calculate surface area. RAD is used in conjunction with RNUCL (Miner-6) for precipitation of minerals not initially present, and in conjunction with current amounts for minerals initially present, as long as the calculated surface area from RAD is larger than the AMIN value specified below. Suggested values are RAD=1.0E-8 with RNUCL=1.0E-6. Using this option, surface areas will decrease as the mineral initially precipitates and grain size increases, down to the AMIN value specified below. If RAD = 0.0, this option is turned off, and surface areas are calculated using the AMIN value below.

AMIN: specific reactive surface area. If a mineral is not initially present, and the option to use mineral grain size is turned off (RAD = 0.0), its surface area will be computed from the value of RNUCL specified on record Miner-6, as long the surface area computed in this way remains below AMIN. The units of AMIN depend on the value of flag IMFLG below.

IMFLG: A flag to specify the units of input AMIN values (IMFLG = 0 is mostly used) (see Appendix G)

IMFLG = 0 for $cm^2_{mineral}/g_{mineral}$

IMFLG = 1 for $m^2_{mineral}/m^3_{mineral}$

IMFLG = 2 for $m^2_{rock}/m^3_{medium\ (total)}$

IMFLG = 3 for $m^2_{rock}/m^3_{medium\ (solids)}$

If IMFLG=3 and RAD=0, the input surface area will remain constant

IMFLG = 4 (constant rate is input in mol/sec; surface area is not used)

Imin-7. Trailer for Imin records (one record after each zone)

Variable: LABEL

Format: A (free format)

LABEL: character string starting with '*' (including quotes) or blank record

6.3.4 Initial gas zones (Igas)

This section describes the initial gas zones present in the system. These zones are mapped to the numerical grid through variables IZGSDF and IZGF on Record_14 and Record_15, respectively, in file solute.inp. Note that H_2O gas is not entered in the list of gases here, because its transport and thermodynamics are treated by the TOUGH2 EOS module selected for any given simulation.

Igas-1. Label (a "Skip" record)

Variable: LABEL

Format: A (free format)

LABEL: comments or blank line.

Igas-2. Header for Igas records (a "Skip" record)

Variable: LABEL

Format: A (free format)

LABEL: header describing Igas records.

Igas-3.

Variable: NGTYPE

Format: I (free format)

NGTYPE: total number of gas zones in the system.

The following records Igas-4, Igas-5, Igas-6 and Igas-7 define each gas zone, and must be repeated NGTYPE times.

Igas-4.

Variable: IGTYPE

Format: I (free format)

IGTYPE: Index of the gas zone. It must be 1 for the first zone, increasing sequentially thereafter. This index must correspond to one of the gas zone indices specified on Record_14 and Record_15 in file solute.inp.

Igas-5. Label

Variable: LABEL (a "Skip" record)

Format: A (free format)

LABEL: sub-heading describing the data that follow.

Igas-6. Composition of the gas zone

Variable: NAGAS VOLG

Format: A, F (free format)

NAGAS: name of the gaseous species present in the system (in quotes). The name of the gas must be included among those previously listed in the definition of the system (Gas records), although the order may change, and it is not needed to repeat the complete list. Gases defined for the system (Gas records) but excluded from the list are assumed to take zero values for VOLG below. A trailing record (Igas-7) must end the list of gases (for each given zone).

VOLG: initial partial pressure of the gaseous species (in bars). If zero, grid blocks corresponding to this zone will be given a partial pressure equal to the fugacity of the gas at equilibrium with the aqueous solution in these blocks, as computed for initial and boundary waters (records Water) during initialization.

Igas-7. Trailer for Igas records (one record after each zone)

Variable: LABEL

Format: A (free format)

LABEL: character string starting with '*' (including quotes) or blank record

6.3.5 Zones for permeability-porosity relationship (Zppr)

This section describes zones where different correlations can be applied to compute the coupling of porosity with permeability. These zones are mapped to the numerical grid through variables IZPPDF and IZPP on Record_14 and Record_15, respectively, in file solute.inp.

Zppr-1. Label (a "Skip" record)

Variable: LABEL

Format: A (free format)

LABEL: comments or blank line.

Zppr-2. Header for Zppr-2 records (a "Skip" record)

Variable: LABEL

Format: A (free format)

LABEL: header describing Igas records

Zppr-3.

Variable: NPPZON

Format: I (free format)

NPPZON: Total number of permeability zones defined for the system.

The following records, Zppr-4, Zppr-5, and Zppr-6 define each permeability zone, and must be repeated NPPZON times. Note, in this case, the trailer record (Zppr-7) is required only once at the end of the list of all permeability zones.

Zppr-4.

Variable: IPPZON

Format: I (free format)

IPPZON: index of the permeability zone. It must be 1 for the first zone, increasing sequentially thereafter. This index must correspond to one of the permeability-porosity zone indices specified on Record_14 and Record_15 in file solute.inp.

Zppr-5. Label

Variable: LABEL (a "Skip" record)

Format: A (free format)

LABEL: sub-heading describing the data that follow.

Zppr-6. Data related to zone for permeability-porosity relationship

Variable: ipptyp, aparpp, bparpp

Format: I, 2F (free format)

Ipptyp: the index for the permeability law. Details on permeability-porosity relationships are described in Appendix F.

Ipptyp = 0: no change in permeability. Can be used to turn off permeability changes in specific zones.

Ipptyp = 1: simplified Carman-Kozeny (Eq. F.7 in Appendix F). The parameter values (aparpp and bparpp) are not used and may be set to 0.0 or any real number.

Ipptyp=2: Modified Hagen-Poiseulle Model. Permeability calculated from pore throat diameter, number of throats per pore, and number of pores per area using the Hagen-Poiseulle equation (modified from Ehrlich et al. 1991). Cubic packed spheres used to calculate pore throat diameters. The parameters are: (a) number of effective throats per pore (typically about 2 to 3). (b) number of pores per m^2 area.

Ipptyp = 3: cubic law (Eq. F.2). The parameter values (aparpp and bparpp) are not used and may be set to 0.0 or any real number.

Ipptyp = 4: modified Cubic Law (Eqs. F.3-F.6). The parameters are: (a) *fracture porosity / fracture-matrix area* (analogous to fracture aperture) (m^3/m^2) and (b) fracture spacing (m)

Ipptyp = 5: Verma-Pruess permeability-porosity relation (Eq. F.8). The parameters are: (a) the value of "critical" porosity at which permeability goes to zero and (b) a power law exponent

Zppr-7. Trailer for Zppr records (one record only, at end zone list)

Variable: LABEL

Format: A (free format)

LABEL: character string starting with '*' (including quotes) or blank record

6.3.6 Surface adsorption zones (Zads)

This part is used to input zones with specific surface areas for surface complexation (adsorption). These zones are mapped to the numerical grid through variables IZADDF and IZAD on Record_14 and Record_15, respectively, in file solute.inp.

Zads-1. Label (a "Skip" record)

Variable: LABEL

Format: A (free format)

LABEL: comments or blank line.

Zads-2. Header for Zads records (a "Skip" record)

Variable: LABEL

Format: A (free format)

LABEL: header describing Zads records.

Zads-3.

Variable: NDTYPE

Format: I (free format)

NDTYPE: total number of surface adsorption zones defined for the system.

Zads-4. Label (a "Skip" record)

Variable: LABEL

Format: A (free format)

LABEL: sub-heading describing the data that follow.

The following records, Zads-4, Zads-5, and Zads-6 define each adsorption zone, and must be repeated NDTYPE times. Note, in this case, the trailer record (Zads-6) is required only once at the end of the list of all adsorption zones.

Zads-5. Adsorption zone index and type

Variable: IDZONE IEQUIL

Format: 2 I (free format)

IDZONE: index of the surface adsorption zone. It must be 1 for the first zone, increasing sequentially thereafter. This index must correspond to one of the adsorption zone indices specified on Record_14 and Record_15 in file solute.inp.

IEQUIL: flag for type of initialization.

=0 do not equilibrate the surface with initial aqueous solutions

=1 equilibrate the surface with initial aqueous solutions at each model grid block prior to starting flow/transport calculations. In such case, initial sorbed amounts are computed at each grid block, and for each surface, such that initial water compositions remain unchanged after sorption. Results of this initial surface equilibration can be output in file chdump.out if ichdump is set to 1 or 2 in solute.inp (on Record_2).

Zads-6. Adsorption surface area

Variable: NAME IFLAG S_AREA

Format: A, I, F (free format)

NAME: name of primary surface species, in quotes. The name must match one of the primary surface complex species entered at the end of the list of primary species at the top of the file (Prim records, species defined with NOTRANS=2).

IFLAG: flag to specify the units of the sorption surface area.

=0 $cm^2_{mineral}/g_{mineral}$. If NAADS_MIN = 'no_mineral' (on record Prim-2), internal conversions will assume a generic mineral density of 2.65 g/cm^3 for this surface.

=1 $m^2_{mineral}/m^3_{mineral}$

=2 $m^2_{mineral}/m^3_{medium\_solids}$

If NAADS_MIN starts with 'surface' (on record Prim-2), a constant surface area entered in units of m^2/kg_{H2O} will be assumed.

S_AREA: surface area for sorption, in units as defined by the value of IFLAG and/or NAADS_MIN (on record Prim-2).

Zads-7. Trailer for Zads records (one record only, at end of zone list)

Variable: LABEL

Format: A (free format)

LABEL: character string starting with '*' (including quotes) or blank record

6.3.7 Linear Kd zones (Zlkd)

This section describes the linear adsorption Kd zones initially present in the system. These zones are mapped to the numerical grid through variables IZKDDF and IZKD on Record_14 and Record_15, respectively, in file solute.inp.

Zlkd-1. Label (a "Skip" record)

Variable: LABEL

Format: A (free format)

LABEL: comments or blank line.

Zlkd-2. Header for Zlkd records (a "Skip" record)

Variable: LABEL

Format: A (free format)

LABEL: header describing Zads records

Zlkd-3.

Variable: KDTYPE

Format: I (free format)

KDTYPE: total number of Kd zones in the system.

The following records, Zlkd-4, Zlkd-5 and Zlkd-6, define each linear Kd zone, and must be repeated KDTYPE times.

Zlkd-4.

Variable: IDTYPE

Format: I (free format)

IDTYPE: index of the Kd zone. It must be 1 for the first zone, increasing sequentially thereafter. This index must correspond to one of the Kd zone indices specified on Record_14 and Record_15 in file solute.inp.

Zlkd-5. Label

Variable: LABEL (a "Skip" record)

Format: A (free format)

LABEL: sub-heading describing the data that follow.

Zlkd-6. Data related to the Kd zone

Variable: NAME, SDEN2, VKD2

Format: A, F, F (free format)

NAME : the name of primary aqueous species with Kd (in quotes), which can be listed in any order. The species spelling must be the same as defined previously.

SDEN2: the solid density (in kg/dm^3).

VKD2 is value of Kd (in kg^{-1} which is mass/kg solid divided by mass/l solution). If SDEN2=0.0, VKD2 automatically represents retardation factor (≥ 1).

Zlkd-7. Trailer for Zlkd records (one record only, at end of zone list)

Variable: LABEL

Format: A (free format)

LABEL: character string starting with '*' (including quotes) or blank record

6.3.8 Cation exchange zones (Zexc)

This section describes the characteristics of the cation exchange capacity zones present in the system. These zones are mapped to the numerical grid through variables IZEXDF and IZEX on Record_14 and Record_15, respectively, in file solute.inp.

Zexc-1. Label (a "Skip" record)

Variable: LABEL

Format: A (free format)

LABEL: comments or blank line.

Zexc-2. Header for Zexc records (a "Skip" record)

Variable: LABEL

Format: A (free format)

LABEL: header describing Zexc records.

Zexc-3.

Variable: NXTYPE

Format: I (free format)

NXTYPE: total number of cation exchange zones.

Zexc-4. Label

Variable: LABEL

Format: A (free format)

LABEL: sub-heading describing the data that follow.

Zexc-5. Data related to the cation exchange zone
Zexc-5 must be repeated NXTYPE times. If NXTYPE is zero omit this card.

Variable: IXTYPE NXsites(CEC)

Format: I, NXsites(F) (free format)

IXTYPE: index of the cation exchange zone. It must be 1 for the first zone, increasing sequentially thereafter. This index must correspond to one of the exchange zone indices specified on Record_14 and Record_15 in file solute.inp.

CEC: cation exchange capacity (meq/100 g of solid). Note also that there are NXsites values, exch for one exchange site

Zexc-7. Trailer for Zexc records (one record only, at end of zone list)

Variable: LABEL

Format: A (free format)

LABEL: character string starting with '*' (including quotes) or blank record

6.4 Thermodynamic Database

Aqueous species, minerals, and gases read in file chemical.inp must be found in the thermodynamic database file. The name of the database file is specified in file solute.inp. The format of the database file is free, and values for all input data (even if zero) must be supplied, unless specifically indicated otherwise. If any aqueous species, mineral, or gas is not in the supplied database or one desires to use different thermodynamic data, users must add these data to the database. An example of a chemical database file is given in Figure 6.4-1. The distribution files include a utility program for converting databases from other codes (such as EQ3/6 and PHREEQC) to the TOUGHREACT database format. The description of the conversion program is given in Appendix L. Appendix L also gives descriptions of other utility programs for switching basis (primary) species and regressing log(K) data.

Spelling convention for reactants/products names

Names of all reactants and products must be input within quotes. On input, these strings are all converted to lower case characters. In addition, any multiple electronic charge incorporated into the names of cations and anions are converted to one charge sign followed by the number of charges. For example, 'CO3--' is converted to 'co3-2' and 'Al+++' is converted to 'al+3'. All names must be no more than 20 characters long. Longer names will be truncated. The use of a consistent spelling in the database is recommended, although the internal conversion to lower case characters and unique style for charge allow for input flexibility.

The following aqueous and gas species require specific spelling for proper internal handling of special functions with some EOS modules:

water	'H2O' or 'h2o'
hydrogen ion	'H+' or 'h+'
hydroxide anion	'OH-' or 'oh-'
carbon dioxide gas	'CO2(g)' or 'co2(g)'
hydrogen gas	'H2(g)' or 'h2(g)'
methane gas	'CH4(g)' or 'ch4(g)'
hydrogen sulfide gas	'H2S(g)' or 'h2s(g)'
sulfur dioxide gas	'SO2(g)' or 'so2(g)'
oxygen gas	'O2(g)' or 'o2(g)'
carbonic acid	'CO2(aq)' or 'co2(aq)'
bicarbonate	'HCO3-' or 'hco3-'
carbonate	'CO3-2' or 'co3-2'
methane (dissolved)	'CH4(aq)' or 'ch4(aq)'
hydrogen sulfide (dissolved)	'H2S(aq)' or 'h2s(aq)'
sulfur dioxide (dissolved)	'SO2(aq)' or 'so2(aq)'
oxygen (dissolved)	'O2(aq)' or 'o2(aq)'

End-of-header record (first record):

Variable: 'DUMMY'

Format: A

DUMMY: a label used to indicate the start of the database. This label must start with '!end-of-header', without quotes. All inputs prior to this record are skipped. All records after this record must follow the formatting and record order described below.

Temperature record:

Variable: 'DUMMY', NTEMP, (TEMPC(i), i=1,NTEMP)

Format: A, I, NTEMP(F)

DUMMY: a label (in quotes) used to describe the data for this record.

NTEMP : the number of TEMPC values to read.

TEMPC : temperatures (ºC) at which the log(K) data are listed in this file, at a given reference pressure P^0 (for databases distributed with TOUGHREACT, P^0=1 bar at T<100°C, and the saturation pressure of pure water at T≥100°C). TEMPC values must be listed in order of increasing temperature. These values are used to constrain log(K) extrapolation within this temperature range. Log(K)'s are not extrapolated outside this temperature range. For example, if the maximum TEMPC is 150ºC but the computed system temperature is 250ºC, log(K)'s will be extrapolated only to 150ºC (i.e. the geochemical speciation will be computed at 150ºC, not 250ºC). *Therefore, users must make sure that simulation temperatures are within the range of thermodynamic data temperatures.*

Basis (primary species) records:

Basis-1.

Variable: 'NAME', A0, Z, MWT

Format: A, 3F (one record per primary species)

NAME : name or chemical formula of aqueous basis species, in quotes (truncated after 20 characters).

A0 : Ion effective or hydrated radius used to compute the Debye-Hückel a0 parameter (see Appendix H for details). For neutral species other than typical dissolved gases (see Section H.3 of Appendix H), if A0 > 100, the value of A0 is used to compute a salting-out coefficient K_i equal to A0 – 100 (i.e., salting-out coefficients for neutral species can be entered as values of A0 equal to 100+K_i; see Equation H.9 for the definition of K_i).

Z : the ion electric charge

MWT : Molecular weight of the aqueous species (g/mol).

This record is repeated as many times as the number of primary species.

Trailer record after Basis records:

Variable: 'DUMMY'

Format: A

DUMMY: must spell 'end' or 'null', including quotes. This record indicates the end of the list of basis species, and must appear directly after the last basis species.

"Skip" records:

Starting from this point, any record beginning with either # (without quotes), or * followed by one blank (without quotes), or any blank record will be skipped on input. These "skip" records can be inserted anywhere in the database (after the first trailer record closing the list of basis species), as long as they are not inserted within records pertaining to the same reaction (i.e., these records can be inserted only between sets of records that pertain to one reaction). These "skip" records can be used for comments, data source references, or simply to clear the appearance of the database.

Secondary (derived) species records:

The data for each secondary species are input as a set of 3 records, as follows:

Sec-1.

Variable: 'NAME', Xmwt, A0, Z, NCPS, (STQS(i), 'NAM(i)', i=1,NCPS)

Format: A, 3F, I, NCPS(F, A)

NAME : chemical formula of secondary species, in quotes (truncated after 20 characters).

Xmwt : molecular weight of the aqueous species (g/mol).

A0 : ion effective or hydrated radius (Angstrom) used to compute the Debye-Hückel a0 parameter (see Appendix H for details). For neutral species other than typical dissolved gases (see Section H.3 of Appendix H), if A0 > 100, the value of A0 is used to compute a salting-out coefficient K_i equal to A0 – 100 (i.e., salting-out coefficients for neutral species can be entered as values of A0 equal to 100+K_i; see Equation H.9 for the definition of K_i).

Z : ion electric charge.

NCPS : number of basis species defining the secondary species.

STQS: stoichiometric coefficients of component (basis) species NAM included in the dissociation reaction of the derived species (negative and positive values for reactants and products, respectively). The derived species is always assumed to have a stoichiometric coefficient of -1.0, which is not included in STQS.

NAM: name of the reactant or product, in quotes (truncated after 20 characters; must match one of the basis species).

Sec-2.

Variable: 'NAME', (AKLOG(i), i=1,ntemp)

Format: A, ntemp(F)

NAME : name or chemical formula of secondary species, as in Sec-1.

AKLOG : contains the equilibrium constants (log(K) in base 10) for the given reaction at each discrete temperature listed in record Temp-1 above (at a reference pressure P^0). These data are generally skipped on input if log(K) regression coefficients as a function of temperature are entered on record Sec-3 (the discrete log(K) values should, however, always be included in the file to provide for easy reference to the data). If no regression coefficients are given on record Sec-3, AKLOG values are used to internally regress log(K) as a function of temperature on input. Note that AKLOG values equal to 500 are interpreted as "no data".

Sec-3.

Variable: 'NAME', (AKCOES(i), i=1,5), (AKCOP(i), i=1,5)

Format: A, 5(E), 5(E)

NAME : name or chemical formula of secondary species, as in Sec-1.

AKCOES : contains regression coefficients a, b, c, d, and e to calculate $\log_{10}(K)$ as a function of temperature (at a reference pressure P^0) with $\log_{10}(K)_{T,P0} = a*\ln(T_k) + b + c*T_k + d/T_k + e/T_k^2$, where T_k is absolute temperature (K), and *ln* stands for natural logarithm. Values must be entered for all coefficients. If all coefficient values are omitted, the coefficients will be internally computed from AKLOG values input on record Sec-2.

AKCOP : (optional) contains regression coefficients a, b, c, d, and e to calculate the volume change ΔV (in cm^3/mol) for the reaction as a function of temperature (average ΔV over the pressure interval P^0 to P), with $\Delta V = a + b*T_k + c*T_k^2 + d/T_k + e/T_k^2$. This option is enabled with a $\neq 0$, in which case all coefficients must be entered. These coefficients are used to correct log(K) values as a function of pressure, with $\log_{10}(K)_{T,P} = \log_{10}(K)_{T,P0} - \Delta V*(P-P^0)/(2.303RT_k)$, where R is the gas constant.

Records Sec-1, Sec-2, and Sec-3 are repeated as sets of triplets, as many times as the number of secondary species. Each set can be spaced by as many "skip" records as desired.

Trailer record after secondary species records:

Variable: 'DUMMY'

Format: A

DUMMY: must spell 'end' or 'null', including quotes. This record indicates the end of the list of secondary species, and must appear anywhere between the last secondary species and first mineral.

Mineral Records:

The data for each mineral are input as a set of 3 records, as follows:

Mineral-1.

Variable: 'NAME', MOLWT, VMIN, NCPM, (STQM(i), 'NAM(i)', i=1,NCPM)

Format: A, 2F, I, NCPM(F, A)

NAME : name or chemical formula of a mineral, in quotes (truncated after 20 characters).

MOLWT : molecular weight (g/mol).

VMIN : molar volume (cm3/mole).

NCPM : the number of component species defining the mineral.

STQM : contains the stoichiometric coefficient of basis species NAM in the dissociation (hydrolysis) reaction of the mineral (negative and positive values for reactants and products, respectively). The mineral species is always assumed to have a stoichiometric coefficient of -1.0, which is not included in STQM.

NAM: name of the reactant or product, in quotes (truncated after 20 characters; must match one of the basis species).

Mineral-2.

Variable: 'NAME', (AKLOG(i), i=1,ntemp)

Format: A, ntemp(F)

NAME : name or chemical formula of the mineral, as in Mineral-1.

AKLOG : contains the equilibrium constants (log(K) in base 10) for the reaction at various temperatures. See record Sec-2 for formatting and other details.

Mineral-3.

Variable: 'NAME', (AKCOEM(i), i=1,5), (AKCOP(i), i=1,5)

Format: A, 5(E)

NAME : name or chemical formula of the mineral, as in Mineral-1.

AKCOEM : contains regression coefficients a, b, c, d, and e to calculate $\log_{10}(K)$ as a function of temperature. See record Sec-3 for formatting and details.

AKCOP : (optional) contains regression coefficients a, b, c, d, and e to calculate ΔV for the reaction (in cm^3/mol) as a function of temperature. See record Sec-3 for formatting and details.

Records Mineral-1, Mineral-2, and Mineral-3 are repeated as sets of triplets, as many times as the number of secondary species. Each set can be spaced by as many "skip" records as desired.

Trailer record after Mineral records:

Variable: 'DUMMY'

Format: A

DUMMY: must spell 'end' or 'null', including quotes. This record indicates the end of the list of minerals, and must appear anywhere between the last mineral and first gas.

Gas records:

The data for each gas species are input as a set of 3 records, as follows:

Gas-1.

Variable: 'NAME', DMOLWT, DMDIAM, NCPG, (STQG(i), 'NAM(i)', i=1,NCPG)

Format: A, 2F, I, NCPG(F, A)

NAME : name or chemical formula of a gas species, in quotes (truncated after 20 characters).

DMOLWT : molecular weight (g/mol)

DMDIAM: molecular diameter (m) used to calculate gas diffusion coefficient (see Eq. (A.1) in Appendix A)

NCPG : the number of basis species defining the gas.

STQG : contains the stoichiometric coefficient of component species NAM in the dissociation reaction of the gas (negative and positive values for reactants and products, respectively). The gas is always assumed to have a stoichiometric coefficient of -1.0, which is not included in STQG.

NAM: name of the reactant or product, in quotes (truncated after 20 characters; must match one of the basis species).

Gas-2.

Variable: 'NAME', (AKLOG(i), i=1,ntemp)

Format: A, ntemp(F)

NAME : name or chemical formula of the gas, as in Gas-1.

AKLOG : contains the equilibrium constants (log(K) in base 10) for the reaction at various temperatures. See record Sec-2 for formatting and other details.

Gas-3.

Variable: 'NAME', (AKCOEG(i), i=1,5), (AKCOPG(i), i=1,5)

Format: A, 5(E)

NAME : name or chemical formula of the gas, as in Gas-1.

AKCOEG : contains regression coefficients a, b, c, d, and e to calculate $\log_{10}(K)$ as a function of temperature. See record Sec-3 for formatting and details.

AKCOPG : (optional) contains regression coefficients a, b, c, d, and e to calculate ΔV for the reaction (in cm^3/mol) as a function of temperature. See record Sec-3 for formatting and details.

Records Gas-1, Gas-2, and Gas-3 are repeated as sets of triplets, as many times as the number of secondary species. Each set can be spaced by as many "skip" records as desired.

Trailer record after Gas records:

Variable: 'DUMMY'

Format: A

DUMMY: must spell 'end' or 'null', including quotes. This record indicates the end of the list of gases, and must appear anywhere between the last gas and first surface complex.

Surface complexes records:

The data for each surface complex are input as a set of 3 records, as follows:

Surface-1.

Variable: 'NAME', Z, NCPS, (STQS(i), 'NAM(i)', i=1,NCPS)

Format: A, F, I, NCPS(F, A)

NAME : chemical formula of surface complex, in quotes (truncated after 20 characters).

Z : electric charge of surface complex.

NCPS : number of basis species defining the surface complex.

STQS: stoichiometric coefficients of component species NAM included in the dissociation reaction of the surface complex (negative and positive values for reactants and products, respectively). The surface complex is always assumed to have a stoichiometric coefficient of -1.0, which is not included in STQS.

NAM: name of the reactant or product, in quotes (truncated after 20 characters; must match one of the basis species).

Surface-2.

Variable: 'NAME', (AKLOG(i), i=1,ntemp)

Format: A, ntemp(F)

NAME : name or chemical formula of the surface complex, as in Surface-1.

AKLOG : contains the equilibrium constants (log(K) in base 10) for the reaction at various temperatures. See record Sec-2 for formatting and other details.

Surface-3.

Variable: 'NAME', (AKCOE(i), i=1,5)

Format: A, 5(E)

NAME : name or chemical formula of the surface complex, as in Surface-1.

AKCOE : contains regression coefficients a, b, c, d, and e to calculate $\log_{10}(K)$ as a function of temperature. See record Sec-3 for formatting and details.

Records Surface-1, Surface-2, and Surface-3 are repeated as sets of triplets, as many times as the number of surface complexes. Each set can be spaced by as many "skip" records as desired.

Trailer record after Surface records:

Variable: 'DUMMY'

Format: A

DUMMY: must spell 'end' or 'null', including quotes. This record indicates the end of the list of secondary species, and must appear anywhere after the last surface complex.

Figure 6.4—1 An example of chemical database file.

```
Any text here, for any number of records

!end-of-header     Do not remove this record!
'Temperature points:' 8 0.01 25.0 60.0 100.0 150.0 200.0 250.0 300.0
'H2O'                                0.00  0.00     18.015
'Ca++'                               2.87  2.00     40.078
'Cl-'                                1.81 -1.00     35.453
'Fe++'                               2.62  2.00     55.845
'H+'                                 3.08  1.00      1.008
'HCO3-'                              2.10 -1.00     61.017
'K+'                                 2.27  1.00     39.098
'Na+'                                1.91  1.00     22.990
'Hfo_sOH'                            0.00  0.00      0.000
'null'

####################
# Aqueous species #
####################
'CO2(aq)'       44.010  0.00  0.00    3  -1.00000 'H2O'  1.00000 'H+'  1.00000 'HCO3-'
'CO2(aq)' -6.5804   -6.3447   -6.2684   -6.3882   -6.7235   -7.1969   -7.7868   -8.5280
'CO2(aq)' 0.10476478E+03 -0.67138541E+03 -0.10862163E+00 0.38868294E+05 -0.26528340E+07
#  Data source:     EQ3/6 database data0.ymp.R5 YM Project SN0612T0502404.14

'NaSO4-'        119.053  1.81 -1.00    2   1.00000 'Na+'  1.00000 'SO4--'
'NaSO4-'  -0.6765   -0.7000   -0.8416   -1.0629   -1.3893   -1.7724   -2.2416   -2.8730
'NaSO4-' 0.15443167E+03 -0.98620007E+03 -0.14872193E+00 0.56350439E+05 -0.34707590E+07
#  Data source:     EQ3/6 database data0.ymp.R5 YM Project SN0612T0502404.14

'null'

####################
#   Minerals      #
####################

'Calcite'  100.087    36.934    3  -1.00000 'H+'  1.00000 'Ca++'  1.00000 'HCO3-'
'Calcite'  2.2257    1.8487    1.3330    0.7743    0.0999   -0.5838   -1.3262   -2.2154
'Calcite' 0.14237876E+03 -0.90313945E+03 -0.14436024E+00 0.50619704E+05 -0.29300495E+07
#  Data source:     EQ3/6 database data0.ymp.R5 YM Project SN0612T0502404.14

'Carnallite' 277.853 172.580 4 1.00000 'K+' 1.00000 'Mg++' 3.00000 'Cl-'  6.00000 'H2O'
'Carnallite' 500.0000 4.2721 500.0000  500.0000  500.0000  500.0000  500.0000  500.0000
'Carnallite' 0.00000000E+00 0.42721000E+01 0.00000000E+00 0.00000000E+00 0.00000000E+00
#  Data source:     EQ3/6 database data0.ymp.R5 YM Project SN0612T0502404.14
```

```
'null'
###################
#   Gases         #
###################

'CO2(g)' 44.010 2.5e-10 3 -1.00000 'H2O' 1.00000 'H+' 1.00000 'HCO3-'
'CO2(g)'  -7.7695 -7.8257 -8.0437 -8.3390 -8.7356 -9.2136 -9.7552 -10.3962
'CO2(g)' 9.833583157 -59.02305875 -0.026997768 950.3210943 0.0 -30.76062599 0.126305497 -
5.45461E-05 9039.990466 0.0
#  Data source:     Regressed from Spycher and Pruess (2009)
#  The coefficients for P correction correspond to dV=-32.6 cm3 up to 100C, then
#   increase to -39.4 at 300C
#  Note, these values are for the CO2(g)=>CO2(aq) reaction, so dV must be zero
#   for CO2(aq)=>HCO3- reaction
'null'



########################
#   Surface complexes  #
########################

'Hfo_sOH2+' 1.000  2  1.00000 'Hfo_sOH'  1.00000 'H+'
'Hfo_sOH2+'500.0000 -7.2900 500.0000  500.0000  500.0000  500.0000  500.0000  500.0000
'Hfo_sOH2+' 0.00000000E+00 -0.72900000E+01 0.00000000E+00 0.00000000E+00 0.00000000E+00
# source:  (phreeqc) minteq.v4.dat 85 2005-02-02

'null'
```

7 Anticipated Error Messages

All execution stops built into TOUGHREACT are accompanied by a message indicating why the execution was aborted. These messages are written to file runlog.out. Other error messages do not lead to a program interruption. Only messages related to the reactive transport part of the program are reviewed below. Error messages originating from fluid and heat flow calculations are the same as for TOUGH2 V2 (Pruess et al., 1999).

7.1 From Routine: INIT (reads the CHEMICAL.INP file)

Most of these messages are self-explanatory and refer to exceeded array dimensions or other errors encountered when reading the chemical.inp file. Array dimension problems can be corrected by reducing the problem size or changing array dimensions in the source file chempar23.inc and recompiling the program. Some examples are given as follows:

Error: maximum number of component species (MPRI) was exceeded. Current max=(MPRI)
Execution stop: yes. Self-explanatory.

Error: maximum number of minerals (MMIN) was exceeded. Current max= (MMIN)
Execution stop: yes. Self-explanatory.

error reading aqueous species of the system
Execution stop: yes. Self-explanatory.

error reading minerals of the system
Execution stop: yes. Self-explanatory.

error reading gases of the system
Execution stop: yes. Self-explanatory.

error reading initial water zone= ___ (iwtype)
Execution stop: yes. Self-explanatory.

error reading initial mineral zone= ____ (imtype)
Execution stop: yes. Self-explanatory.

error reading initial gas zone= ___ (imtype)
Execution stop: yes. Self-explanatory.

7.2 From Routine: NRINIT (initial Newton-Raphson iterations)

ERROR (convergence problem in initialization of water composition)
Please adjust convergence criteria regarding chemical iteration
and initial guess of concentration of primary species
Execution stop: yes. Self-explanatory. This error results in calling routine chdump for troubleshooting (i.e. the last chemical speciation data are output in the chdump.out file). This error occurs during the initial geochemical speciation of waters specified in chemical.inp (no minerals, before the first time step). Check the *chdump.out* file for clues, and also check that water temperatures specified in chemical.inp data are not too different than the initial condition of temperature specified in the flow.inp file.

7.3 From Routine: READTHERM (reads thermodynamic database file)

All these messages occur while reading the thermodynamic database and are self-explanatory. These indicate improperly formatted records in the database file. All errors result in a program execution stop. Some examples are:

Error reading temperature data: stop
Error reading primary species: stop
Error reading secondary species: stop (followed by the species name)
Error reading minerals: stop (followed by the mineral name)
Error reading gases: stop (followed by the gas name)
Error reading adsorbed species: stop (followed by the species name)
Error in opening database file: stop

7.4 From Routine: READSOLU (reads the file solute.inp)

There are currently no specific error messages generated while reading the file solute.inp. The unit number of this file is 31. System error messages relating to this I/O number originate while reading this file. Make sure the fixed formats of this file are respected.

7.5 From Routine: CR_CP (kinetic data calculations)

error in data option for mineral (kinetic)= ____
Execution stop: yes. This message occurs if the flag IDEP for any of the kinetic minerals is not set to either 0 or 1. With this program version, IDEP must always be zero (this flag is specified in the mineral section of the chemical.inp file).

7.6 From Routine: NEWTONEQ (Newton-Raphson iterations after 1st time step)

ERROR: chemistry did not converge at node ____ (routine NEWTONEQ)

Species: ____ Error=____ Error limit= ____ relative

Node temperature (C): ____

Program execution was not aborted. Check results!
Execution stop: only if this error occurs at more than fifty grid blocks at any given time step. This error also calls routine chdump for troubleshooting (i.e., the last chemistry calculation data are output in the *chdump.out* file). This error occurs during the block-by-block geochemical speciation computations after the first time step (complete system, with minerals and gases if any). Check the *chdump.out* file for clues on why convergence was not reached. You may need to increase the loop limit (MAXITCH) and/or tolerance (TOLCH) in the solute.inp file. If boiling occurs, you may try increasing ST1MIN or decreasing STIMAX (specified in *solute.inp*). Chemical convergence may also fail because of errors during transport, resulting in erroneous system compositions that cannot yield a solution to geochemical speciation calculations. In this case, the time step may be decreased and/or the Courant number option enabled (RCOUR in *solute.inp* input file). Depending on the type of problem, chemical speciation in closely spaced grid blocks can be skipped by setting D1MAX > 0 (last resort).

Error: Negative concentration for species ____
Execution stop: no. Self-explanatory. A concentration may temporarily become negative during the chemical Newton-Raphson iterations, but should not remain negative. This error may indicate problems to come. It is rarely encountered.

8 Sample Problems

In this section we present applications of TOUGHREACT to problems in geothermal reservoir behavior, groundwater quality, nuclear waste isolation, supergene copper enrichment, and geologic disposal of greenhouse gases. The test problems serve as checks and benchmarks to verify proper code installation. The input files can be used as templates to facilitate preparation of input data for new problems. To assist with checking on code performance, the distribution files include output files generated for each of the sample problems. These problems were run on a Dell workstation running 64-bit MS Windows with the code compiled using the Intel Visual Fortran XE Composer v12.1. Differences in results may occur on different platforms or with different compilers. Our tests have shown essentially identical results with those obtained on Linux platforms using the Intel V11.1 (and above) Fortran compilers.

8.1 Problem 1 – Aqueous Transport with Adsorption (Linear Kd) and Decay (EOS9)

A 1-D homogeneous fully water-saturated porous medium is considered (Figure 8.1-1), using the following parameters: a porosity of 0.1, a pore velocity v of 0.1 m/day, a solid density of 2600 kg/m^3, a distribution coefficient (Kd) of 0.042735 l/kg, which corresponds to a retardation factor R of 2 (Equation C.8 in Appendix C),

and a half-life $t_{1/2}$ of 20 days. The flow system is a cylindrical, horizontal porous medium with cross-sectional area of 1 m^2 and 12 m length, divided into 60 grid blocks of 0.2 m thickness. Parameters for water flow are specified in file flow.inp (Fig. 8.1.2). Water chemical compositions are assigned through data in files solute.inp (Figure 8.1-3) and chemical.inp (Fig. 8.1.4). In chemical.inp, the record starting with "(1 1)" following the record 'INITIAL AND BOUNDARY WATER TYPES' specify that one initial water composition will be read, as well as one boundary water composition. The data entered in solute.inp under "default values of chemical zone codes for grid blocks" assign the first (and only) initial water type to all grid blocks in the problem, as well as assigning the first (only) boundary water composition to all injection grid blocks. Injection occurs only in block "F 1" (GENER block in file flow.inp), and with the boundary water chemical composition.

Figure 8.1—1 Simplified conceptual model for 1-D transport with linear Kd and decay

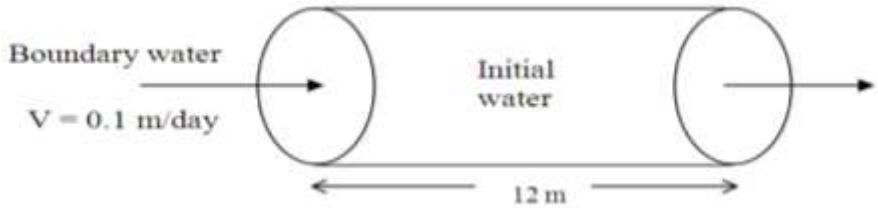

The EOS9 flow module is used. Part of the concentration output file is given in Figure 8.1-5. The complete input and output files are provided with the distribution files.

A total of four species are simulated in a single run. Species 1 is not subject to adsorption (R = 1) and decay ($t_{1/2}$ = infinite), and is denoted by 'na$^+$' in chemical input file 'chemical.inp'. Species 2 has R = 2 and $t_{1/2}$ = infinite, and is denoted by 'skdd1' in the chemical input file 'chemical.inp'. Species 3 has a R = 1 and a $t_{1/2}$ = 20 days, and is denoted by 'skdd2' in the input file. Species 4 has R = 2 and $t_{1/2}$ = 20 days, and is denoted by 'skdd3' in the input file. Species skdd1, skdd2, and skdd3 are artificial tracer species. The species names must appear in the primary species block of the thermodynamic database. Initial concentrations for all four species are set equal to a very small value of 10^{-10} mol/l (practically zero, because TOUGHREACT uses log10 calculations for concentrations in order to avoid convergence problems). The inlet concentrations are set equal to 10^{-4} mol/l for all four species. An analytical solution for this problem is given in Javandel et al. (1984). In the numerical simulation, we give a diffusion coefficient of zero. Dispersion is not considered in this code. However, the upstream weighting scheme used in the code results in a numerical dispersivity $\alpha_n = \Delta x/2 = 0.1$ m (where Δx is the grid size, 0.2 m is used in the simulation). In the analytical calculations, we use a dispersion coefficient $D = \alpha_n v = 0.01$ m^2/day to account for the numerical dispersion in the simulation. The numerical results together with analytical solution are presented in Figure 8.1-6.

Figure 8.1—2 Flow input file (flow.inp) for Problem 1, transport with Kd and decay

```
# aqueous transport with line Kd adsorption and decay
# EOS9 flow input
ROCKS----1----*----2----*----3----*----4----*----5----*----6----*----7----*----8
rock1    1     2600.       0.1  6.51E-12  6.51E-12  6.51E-12  2.50E+00     952.9
                                    0.00
REFCO         1.0E05       4.0

START----1----*----2----*----3----*----4----*----5----*----6----*----7----*----8
REACT----1MOPR(20)-2----*----3----*----4----*----5----*----6----*----7----*----8
0002
PARAM----1----*-123456789012345678901234----*----5----*----6----*----7----*----8
   21000     500000000000000020571005000
 0.00000E0  8.6400E6    1.e+01  8.64E+03F   1      -9.806650
    1.E-06
          1.001E+05                4.0

RPCAP----1----*----2----*----3----*----4----*----5----*----6----*----7----*----8
    1           .333       -.1        1.        0.
    1      9.79020E3      .333        1.
TIMES----1----*----2----*----3----*----4----*----5----*----6----*----7----*----8
    2
   4.32e+6  8.6400E6
ELEME----1----*----2----*----3----*----4----*----5----*----6----*----7----*----8
F   1   59    1rock1   2.00E-1

CONNE----1----*----2----*----3----*----4----*----5----*----6----*----7----*----8
F   1F   2   58    1    1    1       0.1       0.1       1.0       0.0

GENER----1----*----2----*----3----*----4----*----5----*----6----*----7----*----8
F   1    0                   1     WATE  1.1576E-4          0.
F  60    0                   1     WATE -1.1576E-4          0.

INCON----1----*----2----*----3----*----4----*----5----*----6----*----7----*----8

ENDCY
```

Figure 8.1—3 Solute transport input file (solute.inp) for Problem 1, transport with Kd adsorption and decay

```
# Title
'Aqueous transport with Kd and decay'
#options for reactive chemical transport: ISPIA,INIBOUND,ISOLVC,ngamm,NGAS1,...
    2    1    5    0    0    0    2    0    0
#constraints for reactive chemical transport:  sl1min, rcour, stimax, cnfact
   1.00e-4       0.9       4.0       1.0
#Read input and output file names:
TherAkin10.dat                ! thermodynamic database
iter.dat                      ! iteration information
#Read input and output file names:
kdd_conc.dat                  ! aqueous concentrations in tecplot form
kdd_min.dat                   ! mineral data  in tecplot form
kdd_gas.dat                   ! gas data  in tecplot form
kdd_tim.dat                   ! concentrations at specific elements over time
#Weighting parameters
       1.0       1.0    0.d-10   0.0d-05           ! itime wupc,dffun,dffung
#data to convergence criteria:
    1 0.100E-03  300 0.100E-04   30 0.100E-05  0.00E-05  0.00E-05    !  TOLDC,TOLDR
#writing control variables: NWTI NWNOD NWCOM NWMIN NWAQ NWADS NWEXC, …
   40    1    4    0    0    0    0    1    1
#pointer of nodes for writing in time:
F   1
#pointer of components for writing:
    3    4    5    6
#pointer of minerals for writing:

#Individual species for which to output concentrations in time and plot files:
```

```
#Adsorption species for which to output concentrations in time and plot files:

#Exchange species for which to output concentrations in time and plot files:

#default values of chemical zone codes for grid blocks:
    1    1    1    1    0    0    1    0
#chemical zone codes for nodes:

# this "end" record is needed now
end
```

Figure 8.1—4 Chemical input file (chemical.inp) for Problem 1, transport with Kd adsorption and decay

```
# Title
'Aqueous transport with Kd and decay'
# '-------------------------------------------------------------------------------'
# 'DEFINITION OF THE GEOCHEMICAL SYSTEM'
# 'PRIMARY AQUEOUS SPECIES'
'h2o'       0
'h+'        0
'na+'       0
'skdd1'     0           ! species with Kd/decay
'skdd2'     0
'skdd3'     0
'*'
# 'AQUEOUS KINETICS'
'*'
# 'AQUEOUS COMPLEXES'
'oh-'
'*'
# 'MINERALS'
'*'
# 'GASES'
'*'
# 'SURFACE COMPLEXES'
'*'
# 'species with Kd and decay    decay constant(1/s)'
'skdd1'                 0.0d0        0.0  0.0     ! with only Kd
'skdd2'                 4.0113d-07   0.0  0.0     ! with only decay  t(1/2)=20 days
'skdd3'                 4.0113d-07   0.0  0.0     ! with both Kd and decay
'*'
# 'EXCHANGEABLE CATIONS'
'*'
#'-------------------------------------------------------------------------------'
# 'INITIAL AND BOUDARY WATER TYPES'
1   1        !niwtype, nbwtype = number of initial and boundary waters
# Index  Speciation T(C)  P(bar)
1               25.0      1.0
#'        icon        guess         ctot         '
'h2o'      1        1.000d+0       1.000d+0       ,  ,   0.
'h+'       1        1.0000d-7      1.000d-7       ,  ,   0.
'na+'      1        1.000d-10      1.000d-10      ,  ,   0.
'skdd1'    1        1.000d-10      1.000d-10      ,  ,   0.
'skdd2'    1        1.000d-10      1.000d-10      ,  ,   0.
'skdd3'    1        1.000d-10      1.000d-10      ,  ,   0.
'*'
# Index  Speciation T(C)  P(bar)
1               25.0      1.0
#'       icon        guess         ctot         '
'h2o'      1        1.000d+0       1.000d+0       ,  ,   0.
'h+'       1        1.0000d-7      1.000d-7       ,  ,   0.
'na+'      1        1.000d-04      1.000d-04      ,  ,   0.
'skdd1'    1        1.000d-04      1.000d-04      ,  ,   0.
'skdd2'    1        1.000d-04      1.000d-04      ,  ,   0.
'skdd3'    1        1.000d-04      1.000d-04      ,  ,   0.
'*'
#'-------------------------------------------------------------------------------'
#'INITIAL MINERAL ZONES'
'*'
#'-------------------------------------------------------------------------------'
#'INITIAL gas ZONES'
'*'
#'-------------------------------------------------------------------------------'
#'Permeability-Porosity Zones'
'*'
#'-------------------------------------------------------------------------------'
#'INITIAL SURFACE ADSORPTION ZONES'
'*'
#'-------------------------------------------------------------------------------'
#'INITIAL LINEAR EQUILIBRIUM Kd ZONE'
```

```
1                              !kdtpye=number of Kd zones
1                              !idtype
#'species   solid-density(Sden,kg/dm**3)  Kd(l/kg=mass/kg solid / mass/l'
'skdd1'            0.0                  2.0
'skdd3'            0.0                  2.0
'*'
#'--------------------------------------if Sden=0 Kd store retardation factor'
#'INITIAL ZONES OF CATION EXCHANGE'
'*'
#'-------------------------------------------------------------------------'
#'end'
```

Figure 8.1—5 **Part of aqueous concentrations output file (kdd_conc.dat) for Problem 1, transport with Kd adsorption and decay after 50 days (0.136896 yr)**

X	Sl	T(C)	pH	t_na+	t_skdd1	t_skdd2	t_skdd3
0.100	0.1000E+01	4.000	6.9427	0.1000E-03	0.9996E-04	0.9352E-04	0.8782E-04
0.300	0.1000E+01	4.000	6.9427	0.1000E-03	0.9992E-04	0.8746E-04	0.7712E-04
0.500	0.1000E+01	4.000	6.9427	0.1000E-03	0.9988E-04	0.8180E-04	0.6773E-04
0.700	0.1000E+01	4.000	6.9427	0.1000E-03	0.9978E-04	0.7650E-04	0.5947E-04
0.900	0.1000E+01	4.000	6.9427	0.1000E-03	0.9940E-04	0.7154E-04	0.5217E-04
1.100	0.1000E+01	4.000	6.9427	0.1000E-03	0.9842E-04	0.6690E-04	0.4567E-04
1.300	0.1000E+01	4.000	6.9427	0.1000E-03	0.9639E-04	0.6257E-04	0.3979E-04
1.500	0.1000E+01	4.000	6.9427	0.1000E-03	0.9280E-04	0.5852E-04	0.3437E-04
1.700	0.1000E+01	4.000	6.9427	0.9999E-04	0.8723E-04	0.5472E-04	0.2931E-04
1.900	0.1000E+01	4.000	6.9427	0.9997E-04	0.7957E-04	0.5117E-04	0.2454E-04
2.100	0.1000E+01	4.000	6.9427	0.9993E-04	0.7006E-04	0.4785E-04	0.2006E-04
2.300	0.1000E+01	4.000	6.9427	0.9983E-04	0.5929E-04	0.4473E-04	0.1593E-04
2.500	0.1000E+01	4.000	6.9427	0.9963E-04	0.4810E-04	0.4180E-04	0.1225E-04
2.700	0.1000E+01	4.000	6.9427	0.9926E-04	0.3735E-04	0.3903E-04	0.9085E-05
2.900	0.1000E+01	4.000	6.9427	0.9860E-04	0.2774E-04	0.3639E-04	0.6490E-05
3.100	0.1000E+01	4.000	6.9428	0.9753E-04	0.1970E-04	0.3385E-04	0.4458E-05

Figure 8.1—6 **Relative concentrations at 50 days for 1-D aqueous solute transport with adsorption (linear Kd) and decay (concentrations are normalized to the inlet concentration of 10-4 mol/l).**

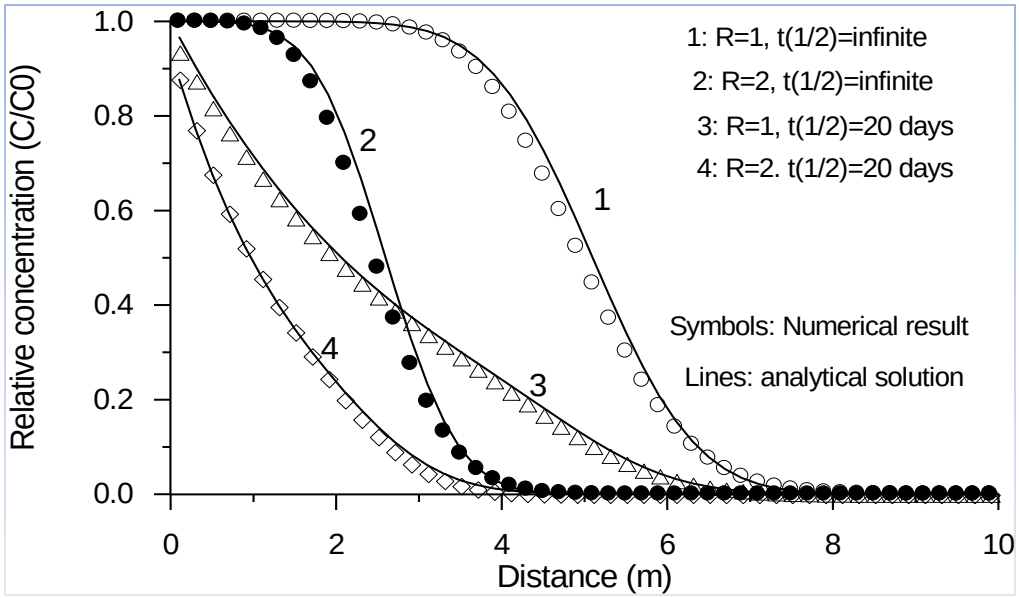

8.2 Problem 2 – Water Quality in the Aquia Aquifer, Maryland (EOS9)

$NaHCO_3$ type waters in coastal plain aquifers of the eastern United States have been related to freshening of the aquifer (Chapelle and Knobel, 1983). These investigators depict major cation concentration patterns as a function of flow length in the Aquia aquifer (Maryland). The water composition in this aquifer shows zonal bands with changes in concentrations of major cations that have been attributed to cation exchange and calcite dissolution/precipitation.

The observed water compositional pattern has been simulated previously using PHREEQM (Appelo, 1994). For the TOUGHREACT simulation, hydrological conditions and all input data are the same as those used in Appelo (1994). The aim is to validate our model applicability to field-scale ambient problems. Figure 8.2-1 shows a schematic cross section along a flow path. The aquifer is bounded to the east by a change in facies. The prepumping hydraulic head distribution suggests a confined aquifer in the upstream half and gradual loss of water in the downstream part of the aquifer (Chapelle and Drummond, 1983). Leakage probably occurs via Pleistocene channels that cut through the confining beds. The hydrological conditions have been modeled assuming a one-dimensional flow tube with recharge at x = 0, and with seepage into the confining layers evenly distributed over the second half of the flow tube.

Figure 8.2—1 **Schematic cross section of the Aquia aquifer (Maryland) adapted from Appelo (1994). Recharge occurs in the outcrop of the formation: discharge is assumed to take place evenly in the downstream half. (1 foot equals 0.3048 m; 1 mile equals 1.609 km).**

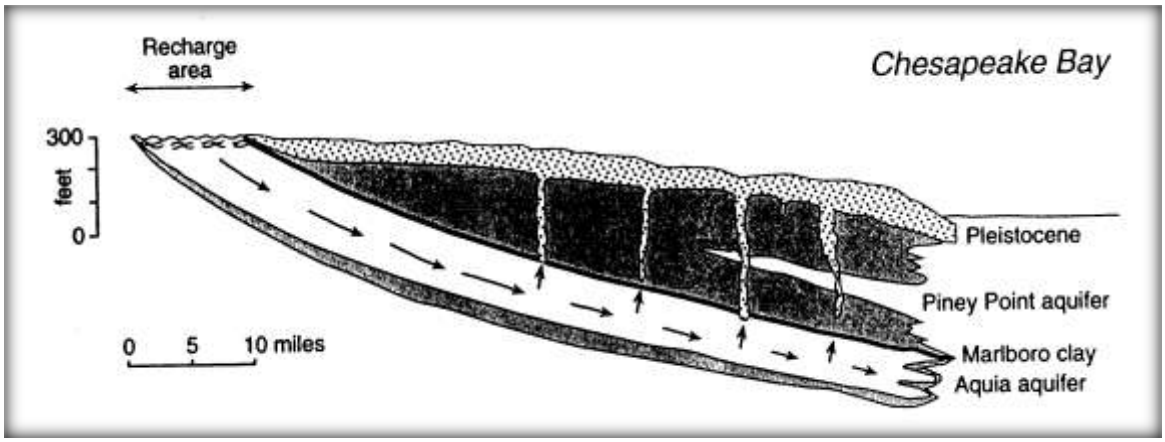

It was assumed that the initial water composition was brackish as a result of mixing of seawater with fresh water during deposition of the overlying Marlboro clay, a brackish water clay. The recharge water composition is presumed to be unchanged from that analyzed in the upstream reaches of the aquifer. The initial and recharge water compositions are presented in Table 8.2-1. These data are inferred from observations and paleohydrochemical conditions. A detailed analysis of this problem is presented in Appelo (1994). To obtain the recharge water composition in the first 10 miles (16 km) of the flow path, the exchange capacity for the first 10 miles was set to zero.

Table 8.2—1 **Initial and recharge water composition (concentrations are given in mmol/l) for modeling the water quality patterns in the Aquia aquifer. X^- represents cation exchange sites. Data are from Appelo (1994).**

	pH	Na^+	K^+	Mg^{2+}	Ca^{2+}	Cl^-	HCO_3^-	SO_4^{2-}	X^-
Initial	6.80	87.4	1.9	9.92	4.38	101.8	15.5	0.27	200
Recharge	7.57	0.1	0.05	0.0	1.40	0.1	2.8	0.0	

The EOS9 flow module is used. The flow and solute transport input files are similar to the previous example. Here we only present the chemical input file in Figure 8.2-2. The complete input and output files are provided with the distribution files. The thermodynamic data used for aqueous species and mineral (calcite) can be found in the database file ThermAkin10.dat. Part of the output file for aqueous chemical concentrations is given in Figure 8.2-3. Parameters for water flow are specified in file flow.inp. A pore velocity of 2.42 mile/ka (1.2347×10^{-10} m/s) was used in the upper part of the aquifer. A porosity of 0.3 was used throughout. A dispersivity of 2.0 miles (3.2 km) was used by Appelo (1994). Dispersion is not treated in TOUGHREACT, and therefore it was approximated by setting the diffusion coefficient $D = \alpha v = 3.951\times10^{-7}$ m^2/s (entered in solute.inp) and setting the tortuosity to 1.0 in flow.inp.

Aqueous species chemical compositions are assigned in files solute.inp and chemical.inp. In chemical.inp, the record with "(1 1)" following the record 'INITIAL AND BOUNDARY WATER TYPES' specifies that one initial water composition as well as one boundary water composition will be read. The data entered in solute.inp under "default values of chemical zone codes for nodes" assign the first (and only) initial water type to all grid blocks in the problem, as well as assigning the first (only) boundary (recharge) water composition to all injection grid blocks. Recharge takes place only in grid block "F 1" using the boundary water chemical composition. The cation exchange reactions and their selectivities are listed in Table 8.2-2 (from Appelo, 1993). The Gaines-Thomas convention (Appelo, 1993) was used for cation exchange. In this convention, selectivities are calculated by using the equivalent fraction of the exchanged cations for the activity of the exchanged cations. It should be pointed out that selectivity is a relative concept. Na^+ was chosen as the reference. Therefore, Na^+ selectivity is equal to one. According to this definition, a lower selectivity corresponds to a higher exchange capacity. A divalent cation, in general, is more strongly exchanged than a monovalent cation. Usually, Ca^{2+} has a higher affinity for the exchange complex, usually in the following exchange order: $Ca^{2+} > Mg^{2+} > K^+ > Na^+$ (Appelo, 1993). Selectivity of H^+ is very sensitive in the simulation, because it affects pH and thus calcite dissolution and the availability of Ca^{2+}. To obtain a better pH fit with the observations, the original H^+ selectivity (1.3092×10^{-6}) was adjusted to 3.1×10^{-6} (Figure 8.2-4).

Table 8.2—2 **List of cation exchange reactions considered for modeling the water quality patterns in the Aquia aquifer (–X represents cation exchange sites). The cation selectivity listed is based on Appelo (1994).**

Cation exchange	Selectivity (in terms of Na^+)
$Na^+ + 0.5Ca\text{-}X_2 = 0.5Ca^{2+} + Na\text{-}X$	0.3981
$Na^+ + 0.5Mg\text{-}X_2 = 0.5Mg^{2+} + Na\text{-}X$	0.5012
$Na^+ + K\text{-}X = K^+ + Na\text{-}X$	0.1995
$Na^+ + H\text{-}X = H^+ + Na\text{-}X$	1.3092×10^{-6}

Figure 8.2—2 Chemical input file (chemical.inp) for Problem 2.

```
# Title
'Water quality in the Aquia aquifer'
# '-------------------------------------------------------------------------------'
# 'DEFINITION OF THE GEOCHEMICAL SYSTEM'
# 'PRIMARY AQUEOUS SPECIES'
'h2o'      0
'h+'       0
'ca+2'     0
'mg+2'     0
'na+'      0
'k+'       0
'hco3-'    0
'so4-2'    0
'cl-'      0
'*'
# 'AQUEOUS KINETICS'
'*'
# 'AQUEOUS COMPLEXES'
'oh-'
'nahco3(aq)'
'cahco3+'
'mghco3+'
'co2(aq)'
'co3-2'
'caco3(aq)'
'mgso4(aq)'
'naso4-'
'kso4-'
'naco3-'
'*'
# 'MINERALS'         ! equilibrium mineral goes first
'calcite'          0    0     0    0
0.0   0.    0.00
'*'
# 'GASES'
'*'
# 'SURFACE COMPLEXES'
'*'
# 'species with Kd and decay    decay constant(1/s)'
'*'
# 'EXCHANGEABLE CATIONS'
1     1
# '                master     convention     ex. coef.'
'na+'              1            1            1.0000
'k+'               0            1            0.1995
'ca+2'             0            1            0.3981
'mg+2'             0            1            0.5012
'h+'               0            1            3.1E-6      !initial:1.3092E-6
'*'
# '-------------------------------------------------------------------------------'
# 'INITIAL AND BOUDARY WATER TYPES'
1   1        !niwtype, nbwtype = number of initial and boundary waters
# Index  Speciation T(C)  P(bar)
1     25.0   1.0
# '        icon        guess         ctot          '
'h2o'      1        1.000d+0       1.000d+0   '   '    0.
'h+'       3        1.585d-7       1.585d-7   '   '    0.       !pH=6.8
'ca2+'     1        2.000d-3       4.380d-3   '   '    0.
'mg+2'     1        5.000d-3       9.920d-3   '   '    0.
'na+'      1        8.000d-2       8.740d-2   '   '    0.
'k+'       1        1.000d-3       1.900d-3   '   '    0.
'hco3-'    1        1.000d-2       1.550d-2   '   '    0.
'so4-2'    1        1.500d-4       2.700d-4   '   '    0.
'cl-'      1        1.000d-1       1.018d-1   '   '    0.
'*'
# Index  Speciation T(C)  P(bar)
1     25.0   1.0
# '        icon        guess         ctot        '
```

```
'h2o'      1        1.000d+0       1.000d+0    '   '    0.
'h+'       3        2.692d-7       2.692d-7    '   '    0.      !pH=7.57
'ca+2'     1        1.000d-3       1.400d-3    '   '    0.
'mg+2'     1        0.600d-6       1.000d-6    '   '    0.
'na+'      1        0.800d-4       1.000d-4    '   '    0.
'k+'       1        3.000d-5       5.000d-5    '   '    0.
'hco3-'    1        1.000d-3       2.800d-3    '   '    0.
'so4-2'    1        0.500d-6       1.000d-6    '   '    0.
'cl-'      1        0.900d-4       1.000d-4    '   '    0.
'*'
# '--------------------------------------------------------------------------------'
#  'INITIAL MINERAL ZONES'
 1                                      !nmtype= number of mineral zones
 1                            !imtype
#  'mineral         vol.frac.'
 'calcite'            0.3     0
 '*'
# '--------------------------------------------------------------------------------'
# 'INITIAL gas ZONES'
'*'
# '--------------------------------------------------------------------------------'
# 'Permeability-Porosity Zones'
'*'
# '--------------------------------------------------------------------------------'
# 'INITIAL SURFACE ADSORPTION ZONES'
'*'
# '---------------------------------------if Sden=0 Kd store retardation factor'
# 'INITIAL LINEAR EQUILIBRIUM Kd ZONE
'*'
# '---------------------------------------if Sden=0 Kd store retardation factor'
# 'INITIAL ZONES OF CATION EXCHANGE'
1                !nxtype= number of exchange zones
# 'zone             ex. capacity(meq/100 g solid)'
1                   3.2345
# '--------------------------------------------------------------------------------'
# 'end'
```

Figure 8.2—3 Part of aqueous concentrations output file (aqui_con.dat) for Problem 2, water quality in Aquia aquifer after 144×10^6 years.

X	pH	t_ca+2	t_mg+2	t_na+	t_k+	t_hco3-
6.000	7.5695	0.1913E-02	0.1871E-03	0.1027E-03	0.6555E-04	0.3483E-02
10.000	7.6173	0.1712E-02	0.3772E-03	0.1068E-03	0.8558E-04	0.3458E-02
14.000	7.6809	0.1479E-02	0.5899E-03	0.1155E-03	0.1201E-03	0.3427E-02
18.000	7.7471	0.1271E-02	0.7584E-03	0.1338E-03	0.1740E-03	0.3391E-02
22.000	7.8051	0.1117E-02	0.8446E-03	0.1719E-03	0.2504E-03	0.3346E-02
26.000	7.8560	0.1003E-02	0.8494E-03	0.2498E-03	0.3491E-03	0.3284E-02
30.000	7.9119	0.8954E-03	0.7864E-03	0.4075E-03	0.4625E-03	0.3195E-02
34.000	7.9925	0.7602E-03	0.6624E-03	0.7202E-03	0.5680E-03	0.3071E-02
38.000	8.1329	0.5650E-03	0.4749E-03	0.1320E-02	0.6149E-03	0.2920E-02
42.000	8.4233	0.2960E-03	0.2323E-03	0.2377E-02	0.5036E-03	0.2799E-02
46.000	8.7950	0.1259E-03	0.9092E-04	0.3343E-02	0.2829E-03	0.2867E-02
50.000	8.9168	0.9132E-04	0.6409E-04	0.3808E-02	0.1902E-03	0.3088E-02
54.000	8.8670	0.9270E-04	0.6558E-04	0.4191E-02	0.1728E-03	0.3459E-02
58.000	8.7568	0.1046E-03	0.7518E-04	0.4672E-02	0.1806E-03	0.4001E-02
62.000	8.6466	0.1185E-03	0.8662E-04	0.5218E-02	0.1956E-03	0.4626E-02
66.000	8.5777	0.1279E-03	0.9467E-04	0.5624E-02	0.2074E-03	0.5088E-02

The results after a simulation time of 144 ka are compared to observations of major cations and alkalinity (Figure 8.2-4). The agreement between numerical results and observations is reasonably satisfactory. The fit for Mg^{2+} can be further improved by adjusting Mg^{2+} selectivity. The sequential appearance of Mg^{2+} and K^+ is attributed to chromatographic separation and can be varied in the model only by varying the Mg^{2+}/K^+ selectivity. An apparent dip in alkalinity is observed just before Na^+ concentrations increase, which is matched by the simulation. The upstream increase of Ca^{2+} concentrations in the region where K^+ and Mg^{2+} are at a peak indicates an increased concentration of $Ca\text{-}X_2$ (X represents cation exchange sites). The increase occurred during flushing of Na^+ and is due to dissolution of calcite. The increase of Na^+ and alkalinity at the downstream end agrees with earlier conclusions about the development of $NaHCO_3$ water quality in a freshening aquifer (Chapelle and Knobel, 1983).

Figure 8.2—4 **Concentrations of Na+, K+, Mg2+, Ca2+, alkalinity, and pH along a flow path in the Aquia aquifer (Maryland). Symbols indicate observations provided by Appelo (1994) and originally from Chapelle and Knobel (1983); solid lines represent simulated concentrations using TOUGHREACT.**

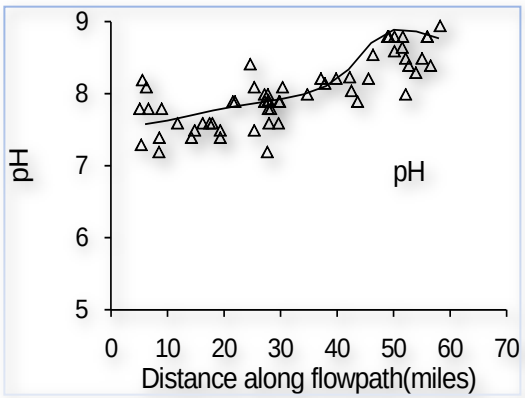

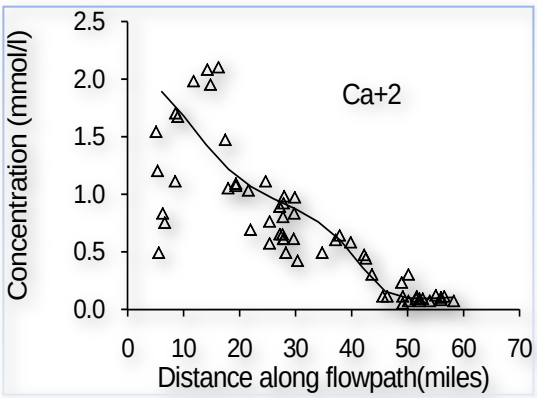

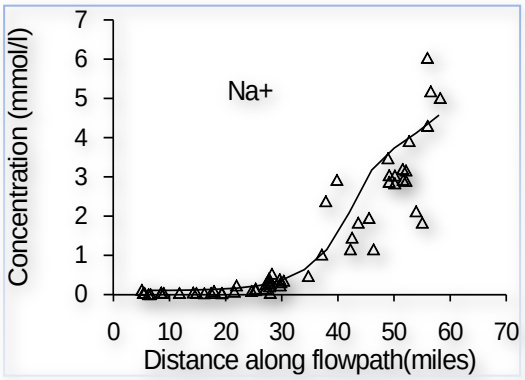

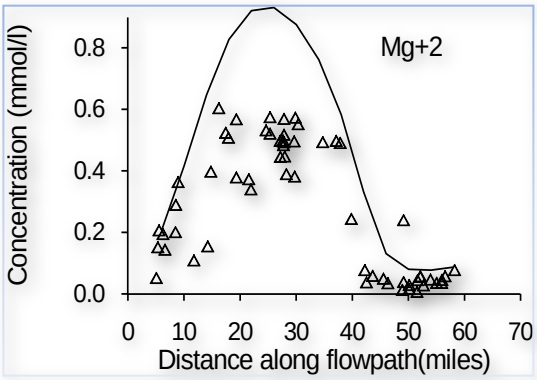

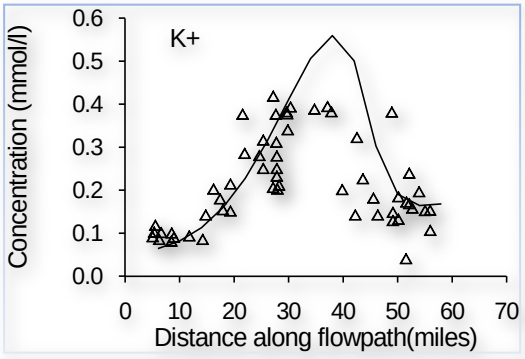

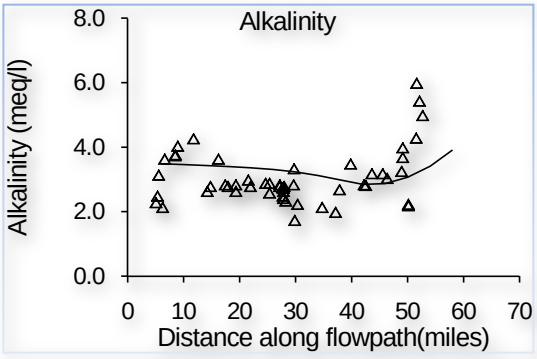

8.3 Problem 3 – Infiltration and Calcite Deposition at Yucca Mountain, Nevada (EOS3)

8.3.1 Problem statement

Yucca Mountain in southern Nevada (USA) is being investigated as a possible site for an underground nuclear waste repository. The semiarid environment and a thick (500 to 700 m) unsaturated zone (UZ) are considered to be favorable for long-term isolation of radioactive waste (Montazer and Wilson, 1984). The percolation flux in the UZ is an important parameter addressed in site characterization and hydrological modeling of Yucca Mountain, because it controls seepage into drifts that may contact waste packages. Hydrogenic calcite deposits in fractures and lithophysal cavities at Yucca Mountain were studied to estimate past percolation fluxes (Carlos et al., 1995; Vaniman and Chipera, 1996; Paces et al., 1998; Marshall et al., 1998; Marshall et al., 1999). These deposits provide evidence of water flow in the past and may improve an understanding of current and future UZ percolation rates, because direct measurements of infiltration fluxes over thousands of years are not possible.

An objective of these prior studies was to investigate the relationship between percolation flux and measured calcite abundances. The U.S. Geological Survey determined calcite abundances from a deep surface-based borehole (WT-24) (Paces et al., 2001) by measuring the CO_2 given off by heating of the rock. Geochronology work performed by the Geological Survey (Paces et al., 1998; Neymark et al., 2001) indicates that calcite formed over approximately 10 million years. Hydrogenic mineral coatings in the UZ are non-uniformly distributed and located almost entirely on fracture footwalls and cavity floors, in contrast to saturated environments, in which vein and cavity deposits usually coat all surfaces (Paces et al., 1998).

Here, we present some results of a reaction-transport numerical model for calcite deposition under different infiltration conditions using TOUGHREACT. The model considers a complete set of hydrological and geochemical processes, including the following essential factors affecting calcite precipitation: (1) infiltration, (2) the ambient geothermal gradient, (3) gaseous CO_2 diffusive transport and partitioning in liquid and gas phases, (4) fracture-matrix interaction for water flow and chemical constituents (dual permeability), and (5) water-rock interaction. In addition, any effects of water-rock interaction (e.g., pH modification) also affects the calcite solubility and hence its abundance in each rock unit. The dual permeability model allows us to address not only the abundances of calcite with depth, but also their relative abundances in fractures and in the rock matrix as a function of the hydrological/geochemical processes. More details on problem setup and results are given in Xu et al. (2003a).

8.3.2 Calcite precipitation mechanisms

Rainfall, along with wind-blown dust, carries much of the calcium to the surface (Vaniman et al., 2001). In the soil zone, strong evapotranspiration along with some water-rock interaction and root-zone biological processes leads to saturation with respect to calcite. The depth to reach calcite equilibrium depends on climate and infiltration variations over time and episodic water flow, as well as on near-surface biogeochemical conditions. During more typical smaller infiltration events, calcite may reach equilibrium close to the surface. However, large infiltration

pulses of calcite-undersaturated water can dissolve near-surface calcite and reach equilibrium at a greater depth. Because we are primarily interested in calcite deposition in a deep geological unit, the Topopah Spring welded tuff (TSw), where the potential repository may be located, uncertainties in the infiltrating water composition near the surface are not significant because calcite reaches saturation well above this unit. In addition, the constant infiltration rate and steady-state water flow conditions over geological time used in our simulations are also justified by evidence that calcite growth in the UZ has remained approximately constant over at least the past 8 million years, as indicated by radiocarbon, ^{230}Th/U, and U-Pb ages (Paces et al., 1998).

The primary driving force for calcite precipitation from percolating waters in the UZ is its decreasing solubility with increasing temperature. Therefore, consideration of the ambient geothermal gradient is very important for calcite precipitation. The temperature distribution is a function of the crustal heat flow and the effect of infiltration, which has been evaluated in Sonnenthal and Bodvarsson (1998). The modeled temperature distributions in borehole WT-24 are discussed later. Pore waters extracted from deep locations of the Yucca Mountain rock matrix are close to equilibrium with respect to calcite (Paces et al., 2001), and no measurements of aqueous concentrations are available from fractures because they generally have low liquid saturations. Previous models for calcite precipitation, under conditions of local equilibrium (Marshall et al., 1999), have indicated that increased infiltration-percolation fluxes result in greater abundances of calcite precipitated over time. These models have not considered, however, effects such as water-rock interaction, changes to the geothermal gradient, and fracture-matrix interaction. They have also assumed a fixed partial pressure of CO_2.

The Ca concentration and CO_2 partial pressure in percolating water are major controlling factors for the abundance of calcite and its stability. This is a result of the decreasing solubility of CO_2 gas in water with increasing temperature, which in turn causes the following degassing process: $HCO_3^- + H^+ \rightarrow CO_2\,(g) + H_2O$. Gaseous CO_2 is also redistributed by gas phase diffusive transport. Degassing increases the pH, and then contributes to calcite precipitation: $Ca^{2+} + HCO_3^- \rightarrow CaCO_3$ (calcite) $+ H^+$. Water and gas flow between fractures and the adjacent matrix governs the resulting calcite distribution within each medium. Calcite precipitation is also affected by other factors such as the dissolution and precipitation of aluminosilicate minerals (mainly through modifying the pH and the CO_2 partial pressure).

8.3.3 Hydrogeological and geochemical conditions

Hydrogeological Conditions

The Yucca Mountain UZ consists of layers of welded and non-welded volcanic tuffs. The welded and non-welded tuffs have vastly different hydrologic properties. The welded units are characterized by relatively low porosity, low matrix permeability, and high fracture density, whereas the nonwelded tuffs have higher matrix porosity and permeability, and lower fracture density (Liu et al., 1998; Sonnenthal and Bodvarsson, 1999). Montazer and Wilson (1984) developed a conceptual model for the UZ at Yucca Mountain that identified five main hydrogeological units based on the degree of welding and on the associated relationship to fracture intensity. This

conceptual model has formed the basis for modeling flow in the UZ at Yucca Mountain. A schematic East-West cross-section through Yucca Mountain illustrating the major hydrogeological units in the UZ at Yucca Mountain is shown in Figure 8.3-1. Table 8.3-1 provides a description of the units, each of which is further divided into a number of model layers with different hydrogeological and geochemical properties (Ahlers and Liu, 2000; Sonnenthal and Spycher, 2001; Spycher et al., 2003a). The Calico Hills nonwelded (CHn) unit is comprised of zeolitic and vitric nonwelded tuffs underlying the basal vitrophyre of the Topopah Spring Tuff. Below the CHn are the Crater Flat undifferentiated (CFu) units, consisting of the lower Bullfrog and Tram Tuffs of the Crater Flat Group. The hydrogeological units below the TSw were not considered in the geochemical transport simulations, so details regarding these units are not given in Table 8.3-1. This is based on: (1) the lateral flow that may occur in these units, (2) they have a more complex mineral assemblage (zeolites, glass, and clays) which has a less well-constrained effect on calcite reactions, and (3) we are primarily interested in calcite deposition within the TSw unit, where the potential repository is located (TSw4 and TSw5 model layers in Table 8.3-1). The exclusion of the underlying hydrogeological units does not affect the results in the TSw unit because flow is predominantly gravity driven, and upward chemical diffusion is subordinate to downward advective transport.

Figure 8.3—1 **Schematic East-West cross-section through Yucca Mountain depicting the major hydrogeological units in the unsaturated zone and the approximate location of the potential repository horizon (Xu et al., 2001; Sonnenthal and Bodvarsson, 1999).**

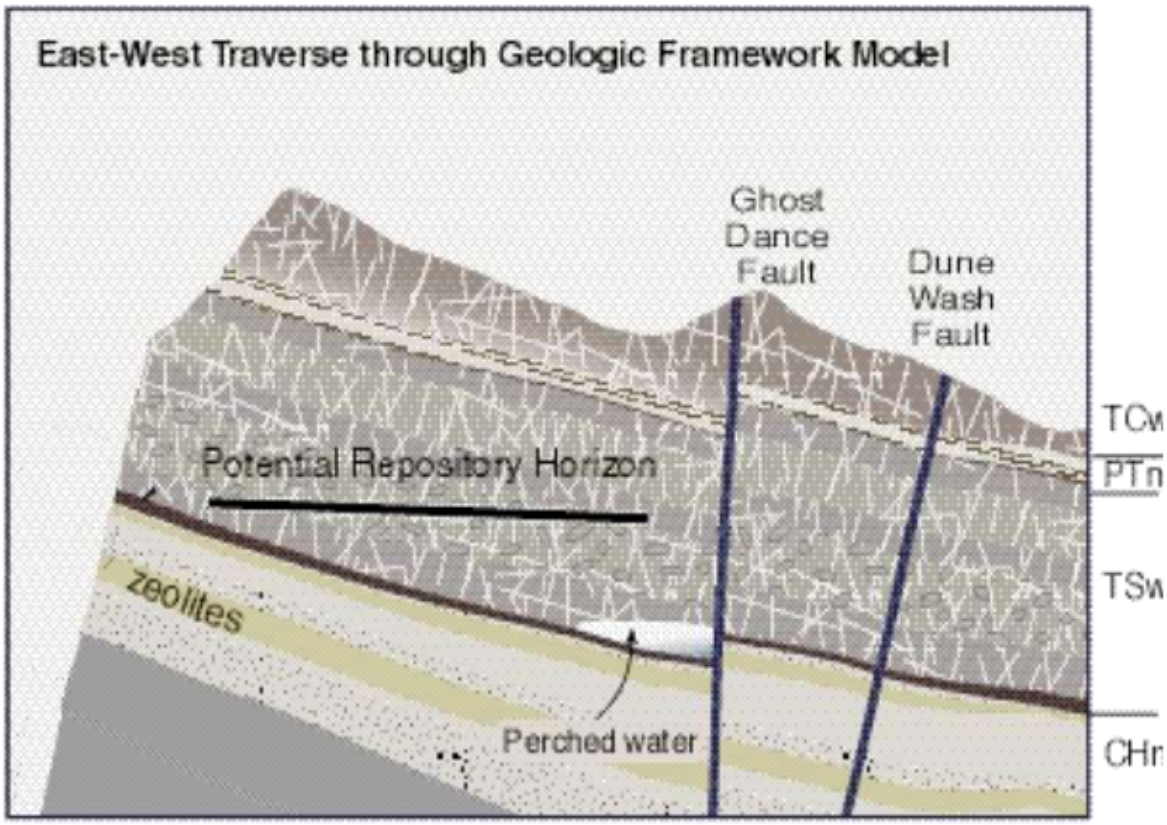

Table 8.3—1 Hydrogeologic units, model layers, and hydrogeological properties for the Yucca Mountain Unsaturated Zone Flow and Transport Model as given by the property calibration model (Ahlers and Liu, 2000).

Hydrogeologic unit	Description	Model layer	Fracture		Matrix	
			Permeability (m2)	Porosity	Permeability (m2)	Porosity
TCw: Tiva Canyon Welded unit	Moderately to densely welded portions of the Tiva Canyon Tuff of the Paintbrush Group	TCw1	2.41×10-12	3.7×10-2	3.86×10-15	0.253
		TCw2	1.00×10-10	2.6×10-2	2.74×10-19	0.082
		TCw3	5.42×10-12	1.9×10-2	9.23×10-17	0.203
PTn: Paintbrush Nonwelded unit	Variably welded Paintbrush Tuff and its associated bedded tuffs, including those located at the bottom of the Tiva Canyon and top of the Topopah Spring Tuffs	PTn1	1.86×10-12	1.4×10-2	9.90×10-13	0.387
		PTn2	2.00×10-11	1.5×10-2	2.65×10-12	0.439
		PTn3	2.60×10-13	3.2×10-3	1.23×10-13	0.254
		PTn4	4.67×10-13	1.5×10-2	7.86×10-14	0.411
		PTn5	7.03×10-13	7.9×10-3	7.00×10-14	0.499
		PTn6	4.44×10-13	4.6×10-3	2.21×10-13	0.492
TSw: Topopah Spring welded unit	Moderately to densely welded portions of the Topopah Spring Tuff down to and including the densely welded basal vitrophyre	TSw1	3.21×10-11	7.1×10-3	6.32×10-17	0.053
		TSw2	3.56×10-11	1.2×10-2	5.83×10-16	0.157
		TSw3	3.86×10-11	8.4×10-3	3.08×10-17	0.154
		TSw4	1.70×10-11	1.0×10-2	4.07×10-18	0.110
		TSw5	4.51×10-11	1.5×10-2	3.04×10-17	0.131
		TSw6	7.01×10-11	2.0×10-2	5.71×10-18	0.112
		TSw7	7.01×10-11	2.0×10-2	4.49×10-18	0.094
		TSw8	5.92×10-13	1.6×10-2	4.53×10-18	0.037
		TSw9	4.57×10-13	5.9×10-3	5.46×10-17	0.173

A one-dimensional vertical column corresponding to the location of a deep borehole (WT-24) was chosen for modeling calcite deposition because measured calcite abundances (Paces et al., 2001) were available for comparison. The model grid, hydrogeological parameters and flow conditions were adopted from the hydrological property calibration work performed by Ahlers and Liu (2000).

Geochemical Model

Initial mineral abundances, potential secondary minerals, reactive surface areas, kinetic and thermodynamic data were taken from the modeling work of coupled thermal, hydrological, and chemical (THC) processes for the potential high-level nuclear waste repository at Yucca Mountain (Sonnenthal and Spycher, 2001; Spycher et al., 2003a). Minerals considered in the simulations are calcite, gypsum, goethite, tridymite, cristobalite-α, quartz,

amorphous silica, hematite, fluorite, albite, K-feldspar, anorthite, Ca-smectite, Mg-smectite, Na-smectite, illite, kaolinite, opal-CT, stellerite, heulandite, mordenite, clinoptilolite, and volcanic glass. This full assemblage of minerals and the corresponding aqueous species are hereafter termed the extended-case geochemical system, because it has more complexities and uncertainties in terms of thermodynamics and kinetics of mineral solid solutions (clays, zeolites and feldspars), effects on pH, and the partial pressure of CO_2. A simpler set of minerals and aqueous species (base-case geochemical system) disregards all aluminosilicates, Fe- and Mg-bearing minerals.

Calcite and gypsum dissolution and precipitation were assumed to take place under geochemical equilibrium, whereas dissolution and precipitation of the other minerals was treated under kinetic constraints. Initial mineral abundances were derived from X-ray diffraction measurements on cores and studies of fracture surfaces (Carey et al., 1998; S. Levy, unpublished data). Potential secondary minerals (i.e., those allowed to precipitate but which may not necessarily form) were determined from field and experimental observations of water-rock interaction and from equilibrium geochemical model calculations. Reactive surface areas of minerals on fracture walls were calculated from the fracture-matrix interface area/volume ratio, the fracture porosity, and the derived mineral volume fractions. These areas were based on the fracture densities, fracture porosities, and mean fracture diameter. Mineral surface areas in the rock matrix were calculated using the geometric area of a cubic array of truncated spheres that make up the framework of the rock and reductions to those areas owing to the presence of alteration phases such as clays and zeolites. Full details are given in Sonnenthal and Spycher (2001).

Initial pore water chemical concentrations were based on analyses of ultracentrifuged water (L. DeLoach, unpublished data) and chemical speciation calculations (Sonnenthal and Spycher, 2001; Spycher et al., 2003a). Except for perched water that lies well below the potential repository horizon, water has not been observed in fractures in the UZ. Therefore, the initial composition of water in the fractures was assumed to be the same as the matrix pore water (Table 8.3-2). The same water composition, re-equilibrated at the temperature of the top model boundary, was assumed for infiltrating water. Oxidizing conditions were considered for this water, because the fracture permeability of the rock is high and the system is unsaturated (air phase is everywhere present). The CO_2 gas partial pressures used for initial and top boundary conditions of the gas transport are in equilibrium with the corresponding aqueous chemical composition. An elevated gas partial pressure (relative to an atmospheric value of 0.344×10^{-3} bar) at the upper boundary can be attributed to soil-zone CO_2 production.

Table 8.3—2 Water and gas chemistry used for initial and boundary conditions of the reaction-transport simulations (Sonnenthal and Spycher, 2001).

Component	Concentration	Unit
Ca^{2+}	101	mg/L
Mg^{2+}	17	mg/L
Na^{+}	61.3	mg/L
K^{+}	8	mg/L
SiO_2 (aq)	70.5	mg/L
Al^{3+}	1.67×10^{-5}	mg/L
HCO_3^{-}	200	mg/L
Cl^{-}	117	mg/L
SO_4^{2-}	116	mg/L
F^{-}	0.86	mg/L
Fe^{3+}	6.46×10^{-8}	mg/L
pH	8.32 (at 25 ºC) 7.75 (at 17ºC)	
PCO_2	2.726×10^{-3} at 17 ºC	bar

Simulation Setup

Simulations were performed using three infiltration rates, a base-case rate of 5.92 mm/yr (Ahlers and Liu, 2000), and bounding rates of 2 mm/yr and 20 mm/yr. The corresponding steady-state water flow conditions were used for geochemical transport simulations. Steady-state temperature distributions corresponding to the same three infiltration rates were obtained using a top temperature of 15.6ºC at the land surface and a bottom temperature of 28ºC at the water table (Figure 8.3-5). For the three infiltration rates, the same water and gas chemistry was used for the top boundary condition. The EOS3 flow module was used for these simulations.

For the reactive transport simulations of calcite precipitation, a simulation time of 10 million years was selected, based on the following inferences: (1) calcite growth has remained approximately constant over the past 8 million years, as indicated by radiocarbon, ^{230}Th/U, and U-Pb ages (Paces et al., 1998) (2) the tuff is 12.7 million years old (Paces et al., 1998), and (3) all dated surfaces indicated by ages of outer mineral surfaces are young compared to the age of the tuffs. Infiltration rates and temperatures were held constant throughout the simulation, and therefore the results can only be considered to reflect the average conditions over this period of time.

In this manual, we only present results for a base-case infiltration rate of 5.92 mm/yr. More results are given in Xu et al. (2003a). The corresponding input and output files are provided with the distribution files. To shorten the run time for testing, the simulation time in the PARAM input block of flow.inp is specified as 3.15576E09 s (100 years). For a simulation of ten million years, users can reset this variable to 3.15576E13. Parts of output files for fluid flow, aqueous chemical concentrations, and changes of mineral abundances are given in Figures 8.3-2, 8.3-3 and 8.3-4.

Figure 8.3—2 **Part of file flow.out for Problem 3 (calcite and infiltration).**

```
Fua18(     1,   1) ST = 0.100000E+01 DT = 0.100000E+01 DX1= 0.000000E+00
Fua18(     2,   1) ST = 0.300000E+01 DT = 0.200000E+01 DX1= 0.000000E+00
Fua18(     3,   1) ST = 0.700000E+01 DT = 0.400000E+01 DX1= 0.000000E+00
Fua18(     4,   1) ST = 0.150000E+02 DT = 0.800000E+01 DX1= 0.000000E+00
Fua18(     5,   1) ST = 0.310000E+02 DT = 0.160000E+02 DX1= 0.000000E+00

----------------------------

          OUTPUT DATA AFTER (  1022,  1)-2-TIME STEPS

@@@@@@@@@@@@@@@@@@@@@@@@@@@@@@@@@@@@@@@@@@@@@@@@@@@@@@@@@@@@@@@@@@@@@@@@@@@@@@@@@@@@

 TOTAL TIME     KCYC    ITER  ITERC    KON        DX1M         DX2M         DX3M
 0.31557E+10    1022       1  2088      2       0.00000E+00  0.00000E+00  0.00000E+00

@@@@@@@@@@@@@@@@@@@@@@@@@@@@@@@@@@@@@@@@@@@@@@@@@@@@@@@@@@@@@@@@@@@@@@@@@@@@@@@@@@@@

ELEM.  INDEX      P           T          SG           SL        XAIRG       XAIRL
                 (PA)       (DEG-C)

Faa18      1 0.84256E+05 0.15750E+02 0.96625E+00 0.33752E-01 0.98668E+00 0.13256E-04
Maa18      2 0.84256E+05 0.15750E+02 0.70350E+00 0.29650E+00 0.98668E+00 0.13256E-04
Fba18      3 0.84581E+05 0.16021E+02 0.98275E+00 0.17250E-01 0.98650E+00 0.13304E-04
Mba18      4 0.84581E+05 0.16021E+02 0.61598E-02 0.99384E+00 0.98650E+00 0.13304E-04
Fca18      5 0.84842E+05 0.16287E+02 0.96976E+00 0.30242E-01 0.98631E+00 0.13340E-04
```

Figure 8.3—3 **Part of file YMC_conc.dat for Problem 3 after t = 100 yr (SL is water saturation, T is temperature in °C, unit of concentrations is mol/l).**

```
   Z          Sl         pH      t_ca+2       t_na+       t_cl-      t_sio2(aq)

 1482.000  0.3375E-01  8.2121  0.2231E-02  0.2666E-02  0.3304E-02  0.1233E-02
 1482.000  0.2965E+00  8.2128  0.2230E-02  0.2666E-02  0.3303E-02  0.1236E-02
 1449.000  0.1725E-01  8.1370  0.2385E-02  0.2667E-02  0.3301E-02  0.1403E-02
 1449.000  0.9938E+00  8.1380  0.2383E-02  0.2667E-02  0.3301E-02  0.1403E-02
 1422.000  0.3024E-01  8.1124  0.2402E-02  0.2667E-02  0.3301E-02  0.1293E-02
 1422.000  0.8104E+00  8.1124  0.2402E-02  0.2667E-02  0.3301E-02  0.1293E-02
 1413.000  0.4217E-01  8.1098  0.2405E-02  0.2667E-02  0.3301E-02  0.1197E-02
 1413.000  0.8338E+00  8.1097  0.2405E-02  0.2667E-02  0.3301E-02  0.1195E-02
 1404.000  0.2536E-01  8.1056  0.2392E-02  0.2667E-02  0.3301E-02  0.1182E-02
 1404.000  0.3328E+00  8.1056  0.2392E-02  0.2667E-02  0.3301E-02  0.1182E-02
 1396.000  0.3065E-01  8.1058  0.2395E-02  0.2667E-02  0.3301E-02  0.1186E-02
 1396.000  0.6580E+00  8.1057  0.2395E-02  0.2667E-02  0.3301E-02  0.1186E-02
 1370.000  0.2463E-01  8.1038  0.2398E-02  0.2667E-02  0.3300E-02  0.1182E-02
 1370.000  0.6159E+00  8.1037  0.2398E-02  0.2667E-02  0.3300E-02  0.1182E-02
 1344.000  0.2052E-01  8.1000  0.2390E-02  0.2666E-02  0.3300E-02  0.1181E-02
 1344.000  0.4469E+00  8.1000  0.2390E-02  0.2666E-02  0.3300E-02  0.1181E-02
```

Figure 8.3—4 **Part of file YMC_min.dat for Problem 3 after t = 100 yr, giving changes in mineral abundances (in volume fraction, positive values indicate precipitation and negative dissolution).**

```
Z       Porosity   calcite    ,glass        fluorite

 1482.000  0.99000  0.5215E-05  -0.6937E-11  0.0000E+00
 1482.000  0.25300  0.9256E-06  -0.1586E-06  0.0000E+00
 1449.000  0.99000  0.2815E-06  -0.2587E-11  0.0000E+00
 1449.000  0.08200  0.3220E-06  -0.5846E-06  0.0000E+00
 1422.000  0.99000  0.2767E-06  -0.6266E-11  0.0000E+00
 1422.000  0.20300  0.6945E-06  -0.4830E-06  0.0000E+00
```

1413.000	0.99000	0.3649E-06	-0.2132E-10	0.0000E+00
1413.000	0.38700	0.1355E-05	-0.5392E-07	0.0000E+00
1404.000	0.99000	0.2389E-06	-0.1301E-10	0.0000E+00
1404.000	0.43900	0.7408E-06	-0.2203E-07	0.0000E+00
1396.000	0.99000	0.2989E-06	-0.3547E-10	0.0000E+00
1396.000	0.25400	0.7384E-06	-0.6207E-07	0.0000E+00
1370.000	0.99000	0.2449E-06	-0.1265E-10	0.0000E+00
1370.000	0.41100	0.1133E-05	-0.5461E-07	0.0000E+00
1344.000	0.99000	0.2172E-06	-0.1451E-10	0.0000E+00
1344.000	0.49900	0.1084E-05	-0.4607E-07	0.0000E+00

Figure 8.3—5 Modeled temperature profiles in borehole WT-24 as a function of depth for three infiltration rates.

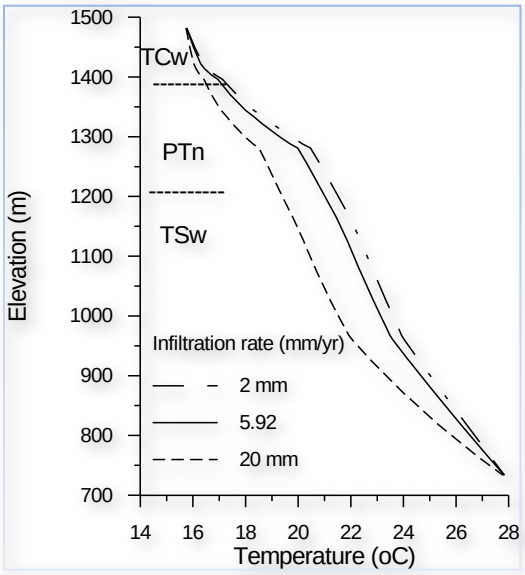

8.3.4 Results and discussion

The simulated total (fracture plus matrix) calcite abundances in the WT-24 column for three infiltration rates, together with USGS measured data, are presented in Figure 8.3-6. In general, the results obtained using the base-case infiltration rate (5.92 mm/yr) agree more closely with the measured WT-24 calcite abundances than those obtained using the other infiltration rates, especially for the PTn unit.

Figure 8.3—6 **Simulated total (fracture plus matrix) calcite abundances (volume fraction) in the WT-24 column for different infiltration rates after 10 million years (Extended geochemical system). Diamonds represent bulk rock calcite abundances measured by the U.S. Geological Survey (Paces et al., 2001).**

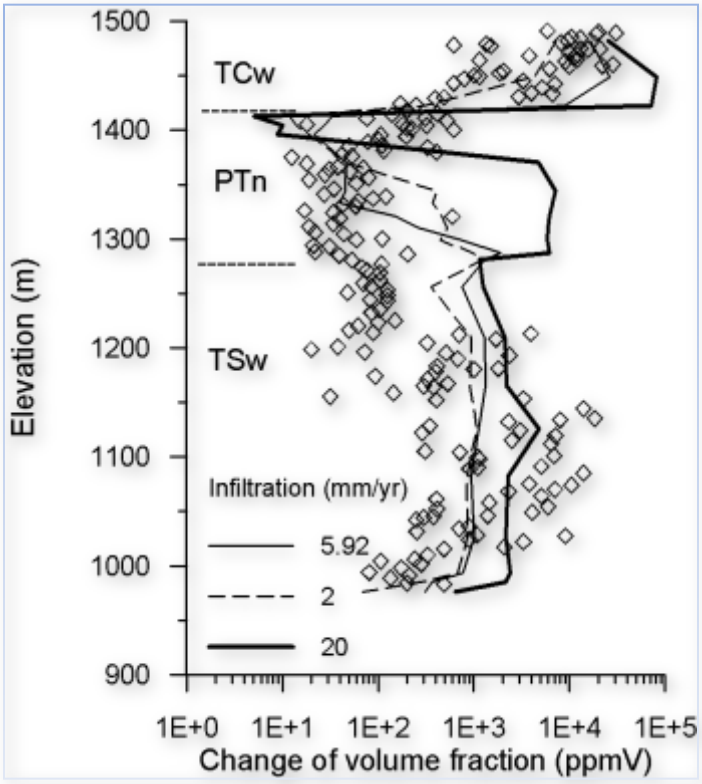

The simulated calcite abundances in the basal PTn layer for the three infiltration simulations are higher than those measured in WT-24. This is a result of an increase in the temperature gradient (Figure 8.3-5) resulting in a concomitant decrease in calcite solubility. Relatively greater calcite abundances in the bottom layer of the PTn have been observed at other locations such as in another deep borehole USW G-2 (Carey et al., 1998). The lower measured calcite abundances may also be a result of lateral flow that is not captured in the one-dimensional simulations.

Results for the welded TSw unit (a potential repository host rock unit) generally fall in the wide range of measured calcite data. Calcite abundances obtained using the highest infiltration rate (20 mm/yr) are closer to the high bound of measured values. Those values from the base-case (5.92 mm/yr) fall in the middle of the TSw measured data range. This may imply that 20 mm/yr is the high bound for the infiltration rate at the WT-24 location; whereas the base-case infiltration (5.92 mm/yr) from the flow property calibration (used for the flow model) may be close to the long-term mean infiltration rate for this location. More results are presented in Xu et al. (2003a)

8.4 Problem 4 – Bentonite Alteration due to Thermo-Hydro-Chemical (THC) Processes during the Early Thermal Period in a Nuclear Waste Repository (EOS4)

8.4.1 Problem statement

Simulating coupled thermal-hydrological-chemical (THC) processes in the backfill material and near-field environment of a heat-generating nuclear waste repository requires site-specific and detailed information to assess the coupled processes and their impact at any particular site, and to develop engineering designs. Before moving into site-specific investigations, we explore general features and issues representing characteristics that are common and essential for many such systems.

The present study is not related to any particular site. However, the geometric configuration and the hydraulic parameters and mineralogical composition of the clayey formation are abstracted from a nuclear waste repository concept considered in Switzerland (NAGRA, 2002). The reference design for canisters to be stored in a repository for spent fuel and high-level waste (SF/HLW) involves a cast steel canister with about 20 cm wall thickness. The canisters are about 1 m in diameter and are surrounded by a 0.75-m thick bentonite buffer in emplacement tunnels which are 2.5 m in diameter (Figure 8.4-1). The repository tunnel is assumed to be in the water-saturated zone at a depth of 650 m below the land surface in the host rock which is referred to as the Opalinus Clay.

The swelling process of bentonite and clay is not considered in this paper. The impact of clay swelling on porosity and related flow and transport properties could be important. No redox reactions are considered in the simulations. While the system evolves from an oxidizing to a reducing environment, we concentrate our modeling analyses on the early period of heat loading and water resaturation, when oxidizing conditions are expected to prevail. The problem has been presented in Xu et al. (2011).

8.4.2 Problem Setup

Thermal and hydrological conditions

The present study employed a simplified model, which was previously used by Senger et al. (2008) and Xu et al. (2008). The model is represented by a radially symmetric geometry, ignoring the lateral no-flow boundary and gravity effects (Figure 8.4-1). The repository is located 650 m below the land surface. The Opalinus clay host rock is assumed to be initially fully water-saturated with a background pressure of 65 bar. The outer boundary at a radial distance of 75 m was set at a constant pressure of 65 bar and a constant temperature of 38°C.

Figure 8.4—1 **Radially symmetric model, representing a single waste canister, canister hull, bentonite backfill, and the Opalinus clay host rock.**

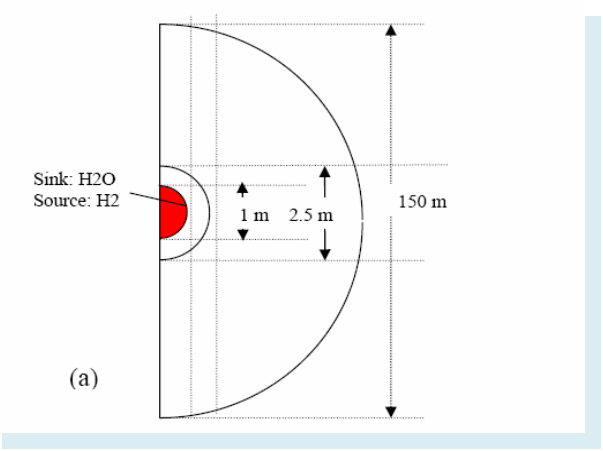

The thermo-physical properties for bentonite buffer and Opalinus clay are summarized in Table 8.4-1. The van Genuchten model (van Genuchten, 1980; Mualem, 1976) is used to describe the functional relationships between relative permeability and saturation, and capillary pressure and saturation for the different materials. The parameters were taken from Xu et al. (2008) and Senger and Ewing (2008). Senger and Ewing reported simulation results for a 3-D model of the thermo-hydrologic conditions in the vicinity of a backfilled SF emplacement tunnel. They quantified the coupled thermo-hydrologic evolution of temperature, saturation, and pressure to determine potential non-uniform resaturation of the bentonite buffer or potential localized accumulation of pore water in contact with the waste canister.

Table 8.4—1 **Thermo-physical parameters used for bentonite and Opalinus clay in the THC model.**

	Bentonite	Opalinus Clay
Porosity ϕ [-]	0.475	0.14
Permeability k [m^2]	1×10^{-19}	1×10^{-20}
Pore compressibility (c_ϕ) [Pa^{-1}]	3.58×10^{-9}	1.83×10^{-9}
Rock grain density ρ_R (kg/m^3)	2700	2670
Rock specific heat C_R (J/kg/^{o}C)	964	946.5
Thermal conductivity λ (W/m/^{o}C)	1.35	2.5
Two-Phase Constitutive Model	van Genuchten	van Genuchten
Residual liquid saturation S_{lr} [-]	0.3	0.5
Residual gas saturation S_{gr} [-]	0.02	0.02
van Genuchten parameter n [-]	1.82	1.67
Capillary strength pressure $1/\alpha$ [Pa]	1.8×10^7	1.8×10^7

A variable temperature inner boundary, representing heat generation due to decay from the waste package, was developed using successive fixed heat capacity at the canister grid block. This heat boundary was specified such that a rough correspondence was obtained to the temperatures at the canister surface computed in the simulation of Senger and Ewing (2008). The temperature was set initially at 150°C at this grid block, and allowed to decrease through conductive heat transport into the bentonite buffer and surrounding host rock. The temperatures decreased from the initial 150°C to about 55°C after 1,000 years (Figure 8.4-2). An initial temperature of 38°C was used for the remaining grid blocks of the model domain.

Figure 8.4—2 Temperature evolution at the canister surface

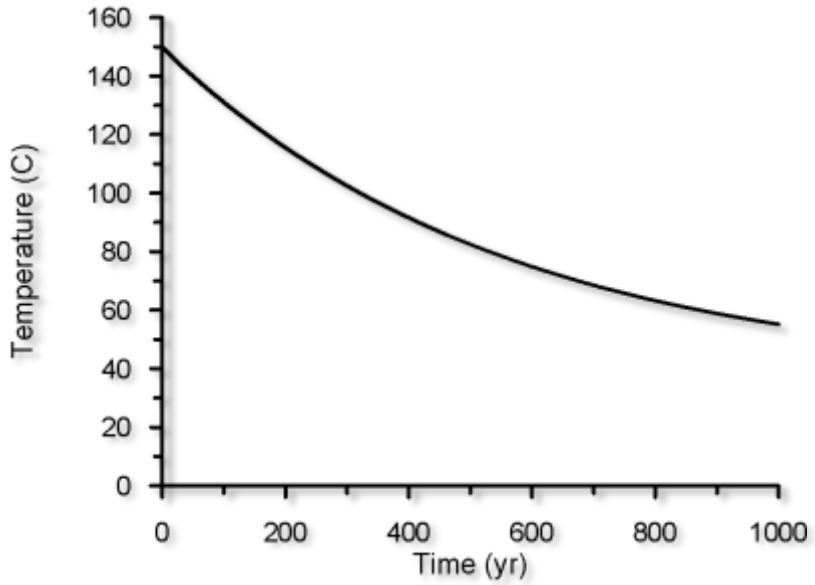

Geochemical conditions

The initial mineral composition of bentonite and Opalinus clay used in the present modeling is given in Table 8.4-2. The MX-80 type of bentonite is used for the buffer materials, containing 75% montmorillonite-Na, which is the dominant mineral. The mineral content of Opalinus clay was assigned based on that given in JNC (2000). Two initial water chemical compositions were used: (1) a dilute water composition, and (2) a composition measured for the BWS-A6 water extracted from the host rock (Fernández et al., 2006). Prior to simulating reactive transport, batch geochemical modeling of water-rock interaction for the two materials was conducted, equilibrating the initial water with the primary minerals listed in Table 8.4-2 at a temperature of 38°C. A reasonably short simulation time of 10 years is needed to obtain nearly steady-state aqueous solution compositions, which were then used as initial chemical conditions for reactive transport (THC) simulations.

Table 8.4—2 Initial mineral volume fractions and possible secondary mineral phases used in the simulations.

Mineral	Volume percent in term of solid	
	Bentonite	Opalinus clay
Calcite	1.4	15.0
Quartz	15.1	18.0
Kaolinite	1.0	10.0
Illite		20.0
K-feldspar	6.5	3.0
Montmorillonite-Na	75	10.0
Montmorillonite-Ca		10.0
Chlorite		10.0
Dolomite		1.0
Siderite		3.0
Ankerite		1.0
Annite	1.0	
Anhydrite		
Amorphous silica		

Kinetic parameters

Reactive chemical-transport modeling requires not only a conceptual understanding of the mechanisms involved in the nucleation, precipitation, and dissolution of the suite of participating minerals, but also quantitative estimates of relevant kinetic parameters. In this work, a general form of rate expression was used, which is based on transition state theory (TST; Lasaga, 1998).

The kinetic rate of mineraldissolution and precipitation includes a product of the rate constant and reactive surface area as represented by Eq. B.6 in Appendix B. The parameters used for the kinetic rate expression are given in Table 8.4-3. Calcite and anhydrite are assumed to react rapidly (relative to the time frame being modeled), and thus an equilibrium model can be used. In Table 8.4-3, we include separate rate constants (k^{25}), activation energies (E), and reaction order (n) for processes catalyzed by H^+ or OH^-. At any pH, the total rate is the sum of the rates from all three mechanisms. Catalysis by H^+ or OH^- is considered only for mineral dissolution. Parameters for the rate law were taken from Palandri and Kharaka (2004), who compiled and fitted experimental data reported by many investigators. Parameters for montmorillonite were set to those of smectite.

If the aqueous phase supersaturates with respect to a potential secondary mineral, a small volume faction of 1×10^{-6} is used for calculating the seed surface area for the new phase to grow. The precipitation of secondary minerals is represented using the same kinetic expression as that for dissolution. However, because precipitation rate

data for most minerals are unavailable, only the neutral mechanism with parameters given in Table 8.4-3 were employed to describe precipitation. Multiple kinetic precipitation mechanisms can be specified in an input file of the TOUGHREACT program, should such information become available.

Mineral reactive-surface areas (the second column of Table 8.4-3) are based on the work of Sonnenthal et al. (2005) and Mukhopadhyay et al. (2009), and were calculated assuming that the rock framework consists of a cubic array of truncated spheres. The larger surface areas for clay minerals are due to smaller grain sizes.

Table 8.4—3 **Parameters for calculating kinetic rate constants of minerals. Note that (1) all rate constants are listed for dissolution except opal-A; (2) *A* is specific surface area, k^{25} is kinetic constant at 25°C, *E* is activation energy, and *n* is the power term (Eq. B.12 in Appendix B); (3) the power terms *n* for both acid and base mechanisms are with respect to H^+.**

Mineral	A (cm^2/g)	Parameters for kinetic rate law								
		Neutral mechanism		Acid mechanism			Base mechanism		
		k^{25} ($mol/m^2/s$)	E (KJ /mol)	k^{25}	E	$n(H^+)$	k^{25}	E	$n(H^+)$
Calcite	Equilibrium								
Quartz	98	1.023×10^{-14}	87.7						
Kaolinite	1516	6.918×10^{-14}	22.2	4.898×10^{-12}	65.9	0.777	8.913×10^{-18}	17.9	-0.472
Illite	1516	1.660×10^{-13}	35	1.047×10^{-11}	23.6	0.34	3.020×10^{-17}	58.9	-0.4
K-feldspar	98	3.890×10^{-13}	38	8.710×10^{-11}	51.7	0.5	6.310×10^{-12}	94.1	-0.823
Montmorillonite-Na	1516	1.660×10^{-13}	35	1.047×10^{-11}	23.6	0.34	3.020×10^{-17}	58.9	-0.4
Montmorillonite-Ca	1516	1.660×10^{-13}	35	1.047×10^{-11}	23.6	0.34	3.020×10^{-17}	58.9	-0.4
Chlorite	1516	3.02×10^{-13}	88	7.762×10^{-12}	88	0.5			
Dolomite	98	2.951×10^{-8}	52.2	6.457×10^{-4}	36.1	0.5			
Siderite	98	1.260×10^{-9}	62.76	6.457×10^{-4}	36.1	0.5			
Ankerite	98	1.260×10^{-9}	62.76	6.457×10^{-4}	36.1	0.5			
Annite	98	2.818×10^{-14}	22.0	1.413×10^{-12}	22.0	0.37	2.818×10^{-15}	22.0	-0.22
Anhydrite	Equilibrium								
Amorphous silica	98	3.000×10^{-10}	49.8						

Simulations

Four simulations were performed. The first, base-case simulation used parameters given in Tables 8.4-1, 8.4.2, and 8.4.3. Mineral dissolution and precipitation rates are a product of the kinetic rate constant and reactive surface area, the magnitudes of which are highly uncertain and cover a wide range of values. Therefore, two sensitivity simulations (Simulations 2 and 3) were performed by decreasing and increasing the surface area by one order of magnitude from the base-case value. Simulation 4 includes cation exchange from the base-case.

The EOS4 fluid property module was used to calculate the thermo-physical properties of the fluid mixture. In the EOS4 module, provision is made for vapor pressure lowering effects (see Pruess et al., 1999). Vapor pressure is expressed by Kelvin's equation, which is a function not only of temperature, but depends also on capillary

pressure, which in turn is a function of saturation. Only the base-case simulation is presented here. The input and major output files are provided with the distribution files.

8.4.3 Results

After closure of an underground nuclear waste repository, the decay of radionuclides elevates temperature, and the bentonite buffer resaturates through water flow from the surrounding host rock. The perturbations from these thermal and resaturation processes induce mineral dissolution and precipitation. Consequently, the porosity of the bentonite buffer is changed. The simulated porosity distribution at different times for different cases is presented in Figure 8.4-3. For the first three cases without cation exchange, porosity decreases from the initial value of 0.475, indicating that precipitation dominates. Changes in porosity are larger close to the interface between the bentonite buffer and Opalinus Clay host rock, because resaturation processes carry chemical constituents from the host rock. Decreases in porosity are smaller close to the canister surface. Decreases in reactive surface area (rate) result in reductions in mineral alteration and porosity change (compare Figure 8.4-3b to 8.4-3a). Conversely, increases in reactive surface area cause increases in mineral alteration and porosity change (compare Figure 8.4-3c with 8.4-3a). Considering cation exchange (Figure 8.4-3d), porosity mostly increases, but slightly decreases close to the interface with the host rock; it does not change close to the canister surface. Overall, no significant changes in porosity occur during the first 1,000 years of thermal and resaturation processes.

Figure 8.4—3 Distribution of porosity in bentonite buffer: (a) base case, (b) reactive surface area decreased by one order of magnitude, (c) reactive surface area increased by one order of magnitude, and (d) including cation exchange.

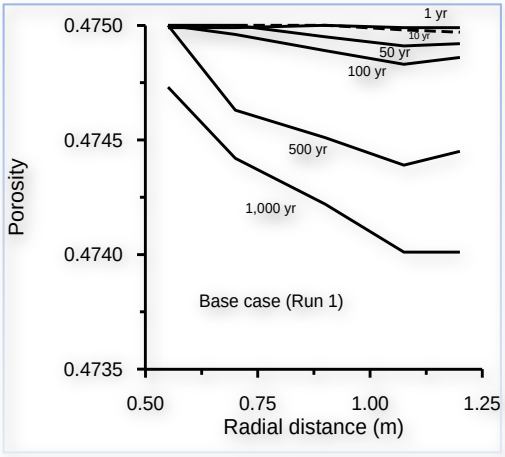

(a)

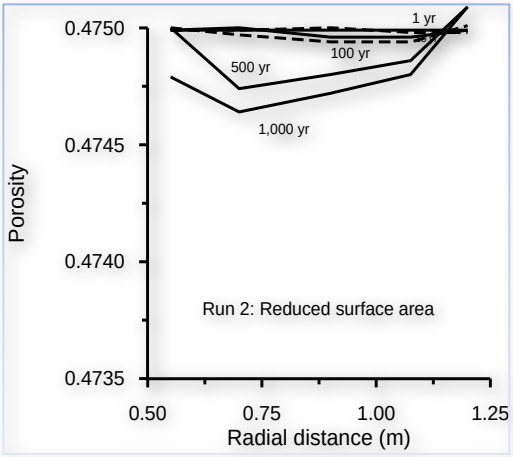

(b)

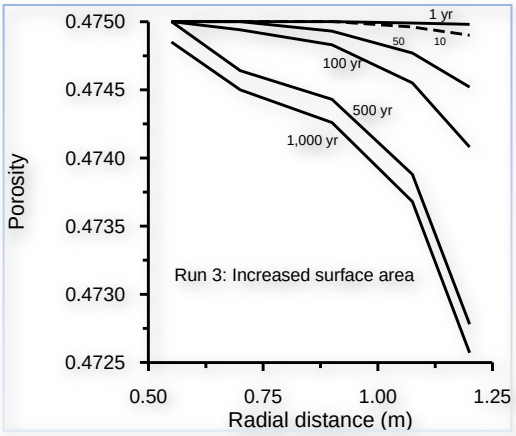

(c)

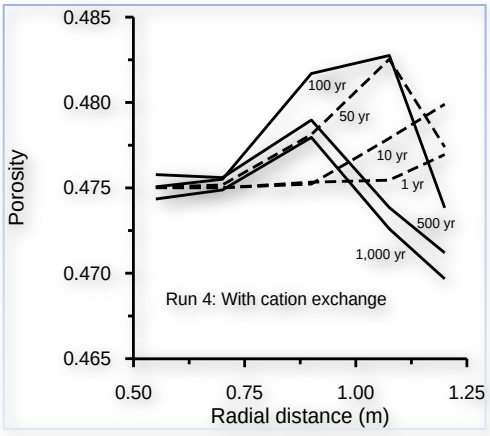

(d)

Montmorillonite-Na, the dominant mineral (with an initial volume fraction of 75%), dissolves in all four cases (Figure 8.4-4a). Decreases in reactive surface area (rate) results in reductions in montmorillonite-Na dissolution. Conversely, increases in reactive surface area cause increases in its dissolution. Considering cation exchange results in a reduction in Montmorillonite-Na dissolution. The pattern of annite dissolution is similar to that of montmorillonite-Na (Figure 8.4-4b). Calcite precipitates in most parts of the bentonite because its solubility decreases with temperature, but it dissolves close to the interface with the host rock supplying reactants for its precipitation close to the hot end of the canister surface (Figure 8.4-4c). Calcite dissolution and precipitation is not sensitive to changes in surface area. K-feldspar precipitation occurs over the entire radial distance, with more precipitation close to the interface with the host rock (Figure 8.4-4d). K-feldspar precipitation is proportional to changes in surface area. With cation exchange, less K-feldspar precipitates. Similar to K-feldspar, kaolinite precipitates over the entire thickness of the bentonite buffer, with more precipitation close to the interface with the host rock (Figure 8.4-4e). The pattern of chlorite precipitation is the same as kaolinite (Figure 8.4-4f).

Figure 8.4—4 **Change in volume fraction of montmorillonite-Na in bentonite buffer obtained for the base case.**

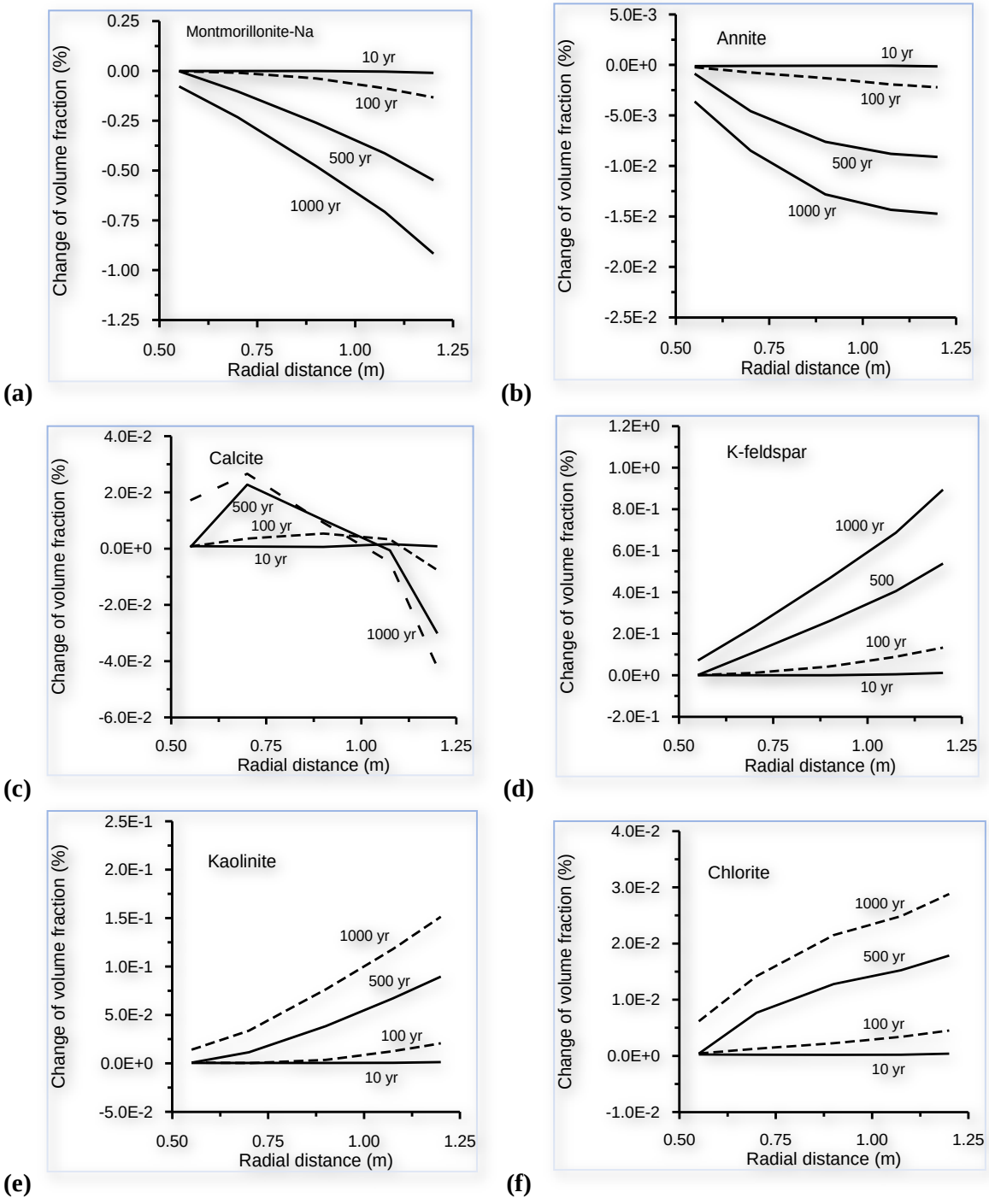

8.4.4 Summary

A 1D radially symmetric model of a SF waste canister emplaced with bentonite buffer in a deep underground repository in the Opalinus clay has been developed, representing the essential general features and issues related to a nuclear waste repository. Using this model, mineral alteration and changes in porosity for the early thermal and resaturation processes in a waste repository for SF waste canisters were examined for different cases. The following conclusions can be drawn from the modeling analyses:

The perturbations from these thermal and hydrological processes result in a decrease in porosity for cases without considering cation exchange, indicating precipitation dominates. Even though montmorillonite-Na with an initial volume fraction of 75% of the bentonite, dissolves for all simulation cases, the slight decrease in porosity is due to precipitation of K-feldspar, kaolonite, and chlorite. Decreases in porosity in the bentonite are larger close to the interface with the Opalinus clay host rock because resaturation processes carry chemical constituents from the host rock into the bentonite. Mineral alteration and changes in porosity are sensitive to reactive surface area, which strongly affects the kinetic reaction rates. Cation exchange indirectly affects mineral alteration, and thus has a second-order impact on porosity changes. Overall, mineral alteration and associated changes in porosity during the 1,000 year period of thermal and hydrological processes are relatively small and are expected to not significantly affect flow and transport properties.

The preliminary modeling presented here is for a simplified geometric configuration and abstracted hydraulic parameters and mineralogy of the clayey formation. However, this modeling and the sensitivity analyses were useful in identifying the role of some physical and chemical parameters in the alteration of the bentonite buffer materials. The developed model may provide a useful tool for gaining a better understanding of the coupled chemical and physical processes, as well as the controlling conditions and relevant parameters, for a site-specific repository system.

8.5 Problem 5 – 1-D Radial Model for CO_2 Sequestration in a Deep Saline Formation (ECO2N)

8.5.1 Problem statement

The feasibility of storing CO_2 in deep geologic formations has been discussed in the technical literature over the last decade. Studies include an evaluation of the feasibility of CO_2 aquifer storage in The Netherlands (Lohuis, 1993) and in the Alberta Basin, Canada (Gunter et al., 1993; Bachu et al., 1994; Law and Bachu 1996; Gunter et al., 1996 and 1997). Furthermore, large-scale CO_2 disposal in an aquifer is already being practiced in the Norwegian sector of the North Sea (Korbol and Kaddour, 1995).

Carbon dioxide is retained in geologic formations in three ways (Hitchon, 1996). First, CO_2 can be trapped as a gas or supercritical fluid under a low-permeability caprock. This process, commonly called hydrodynamic trapping, will likely be, in the short term, the most important mechanism of retention. Second, CO_2 can dissolve into

the groundwater, referred to as a solubility trapping. The dissolution of CO_2 in groundwater increases the acidity of water and affects the solubilities of minerals composing the host rock matrix. Third, CO_2 can react directly or indirectly with minerals and organic matter in the geologic formation leading to the precipitation of secondary carbonates. The latter process, so-called "mineral trapping", is attractive because it could immobilize CO_2 for long time scales, and prevent its easy return to the atmosphere. The interaction of CO_2 with alkaline aluminosilicate minerals will also result in the formation of dissolved alkali carbonates and bicarbonates, thereby enhancing "solubility trapping".

Numerical modeling of geochemical processes is a necessary tool for investigating the long-term consequences of CO_2 disposal in deep formations, because alteration of the predominant host rock aluminosilicate minerals is very slow and is not experimentally accessible under ambient deep-aquifer conditions. Johnson et al. (2001) simulated CO_2 injection at Statoil's North-Sea Sleipner facility and analyzed the coupled process mechanisms that lead to hydrodynamic, solubility, and mineral trapping, as well as the relative effectiveness of the distinct sequestration processes as a function of key reservoir properties. McPherson and Lichtner (2001) used a sedimentary basin model, including multiphase flow of CO_2, groundwater, and brine, to evaluate resident times in possible aquifer storage sites and migration patterns and rates away from such sites in the Powder River Basin of Wyoming. Xu et al. (2004a) performed batch geochemical modeling for three different formation mineralogies in the presence of CO_2 at high pressure. The modeling included (1) redox processes that could be important in deep subsurface environments, (2) the presence of organic matter, (3) the kinetics of chemical interactions between the host rock minerals and the aqueous phase, and (4) CO_2 solubility dependence on pressure, temperature and salinity of the system (see Eq. B.14 through B.17 in Appendix B).

During large-scale injection of CO_2 into deep formations, geochemical processes are strongly affected by physical processes such as multiphase fluid flow and solute transport. Fluid pressures will rise as CO_2 displaces formation water in which it partly dissolves. The dissolution of primary and precipitation of secondary minerals change formation porosity and permeability, and could alter fluid flow patterns. All coupled hydrologic and chemical processes affect the feasibility of CO_2 injection and storage in deep formations. Uncoupled batch geochemical modeling and flow simulation are inadequate to describe the complex subsurface physical and chemical interactions expected to occur. A systematic process-based understanding of the coupled physical and chemical phenomena is required.

8.5.2 Definition of test problem

The response of deep formations to CO_2 injection will depend on many factors, including formation permeability and porosity, the presence of heterogeneities such as faults and layers of high or low permeability, the physical and chemical characteristics of the brines, and the nature of the mineral phases that are present. A great deal of specific and detailed information will be required to assess the feasibility of disposing of CO_2 in a brine formation at any particular site, and to develop engineering designs for CO_2 disposal systems. A basic issue in geologic disposal of CO_2 is the physical and chemical behavior in the vicinity of a CO_2 injection well. Previous numerical

studies have investigated simple models of one- and two-dimensional radial flow to examine the displacement of formation waters by injected CO_2 (Pruess and Garcia, 2002; Pruess et al., 2005). These studies have provided initial insight into issues regarding volumetric sweep, CO_2 storage capacity, and pressurization processes that would arise from large-scale CO_2 injection. Exploratory studies of geochemical effects have also been conducted, using a zero-dimensional batch reaction approach to model the chemical reactions that would take place when different mineral assemblages are exposed to CO_2 at high pressures in the presence of brine (Perkins and Gunter, 1996; Gunter et al., 1997; Xu et al., 2004a). The present study combines the simple 1-D radial model previously investigated by Pruess et al. (2003) with the batch chemical reaction model of Xu et al. (2004a), to model the coupled processes of fluid flow and chemical reactions near a CO_2 injection well.

Geologic formation

The setup of the problem is similar to that of Xu et al. (2003b), except using the following (1) a porosity of 0.3 not 0.1, (2) a temperature of 75ºC (at about 2000 m depth) instead of 40ºC, (3) improved mineralogical composition, and kinetic rate law and parameters.

The geologic formation is assumed to be infinitely long and homogeneous with a thickness of 100 m, containing 1 M NaCl brine at a constant temperature of 75ºC. A 1-D radial model is used. This simplification does not consider non-uniform sweep that may occur due to formation heterogeneities, or due to buoyancy forces that would tend to drive CO_2 towards the top of the aquifer. Some justification for a 1-D approach can be derived from the slow rates and long time scales of geochemical changes, which will cause processes to play out over time that will make the distribution of CO_2 more uniform. Initially, injected CO_2 will tend to accumulate and spread out near the top of permeable intervals, partially dissolving in the aqueous phase. CO_2 dissolution causes the aqueous-phase density to increase by a few percent. This will give rise to buoyant convection where waters enriched in CO_2 will tend to migrate downward (Weir et al., 1995; Garcia, 2001). The process of CO_2 dissolution and subsequent aqueous phase convection will tend to mix aqueous CO_2 in the vertical direction. The time scale for significant convective mixing is likely to be slow (of the order of hundreds of years or more; Ennis-King and Paterson, 2003), and may be roughly comparable to time scales for significant geochemical interactions of CO_2.

The well field is modeled as a circular region of 10,000 m radius, at the center of which CO_2 is injected uniformly at a constant rate of 90 kg/s. A 1-D radial grid was used with a spacing gradually increasing away from the well. The CO_2 injection was assumed to continue for a period of 10 years. The fluid flow and geochemical transport simulation was run for a period of 1,000 years.

Table 8.5—1 Hydrogeologic parameters for Problem 5.

Aquifer thickness	100 m
Permeability	10-13 m2
Porosity	0.30
Compressibility	4.5×10-10 Pa-1
Temperature	75 0C
Pressure	200 bar
Salinity	0.06 (mass fraction)
CO_2 injection rate	90 kg/s
Relative permeability	
Liquid (van Genuchten, 1980): $k_{rl} = \sqrt{S^*}\left\{1-\left(1-\left[S^*\right]^{1/m}\right)^m\right\}^2$ irreducible water saturation exponent	$S^* = (S_l - S_{lr})/(1-S_{lr})$ $S_{lr} = 0.30$ $m = 0.457$
Gas (Corey, 1954):	
$k_{rg} = (1-\hat{S})^2(1-\hat{S}^2)$ irreducible gas saturation	$\hat{S} = \frac{(S_l - S_{lr})}{(S_l - S_{lr} - S_{gr})}$ $S_{gr} = 0.05$
Capillary pressure	
van Genuchten (1980) $P_{cap} = -P_0\left(\left[S^*\right]^{-1/m} - 1\right)^{1-m}$ irreducible water saturation exponent strength coefficient	$S^* = (S_l - S_{lr})/(1-S_{lr})$ $S_{lr} = 0.00$ $m = 0.457$ $P_0 = 19.61 kPa$

Geochemical system

A proxy for sediment from the United States Gulf Coast, modified from that originally presented by Apps (1996), was used for the reactive geochemical transport simulations. The mineralogy is similar to that commonly encountered in sedimentary basins. Apps (1996) presented a batch geochemical simulation of the evolution of Gulf Coast sediments as a basis for interpreting the chemical processes relating to the deep injection disposal of hazardous and industrial wastes.

The initial mineral abundances are shown in Table 8.5-2. The specification of formation mineralogy is determined in part by the availability of data. Most studies related to the Tertiary Gulf Coast sediments are

concentrated in the state of Texas. The principal reservoir-quality sandstones within that region are respectively, the Frio, the Vicksberg and the Wilcox formations, all of which are found within the lower Tertiary. Of the three formations, the Frio was chosen as a representative candidate for the sequestration of supercritical carbon dioxide. It is the shallowest of the three formations, but over much of its areal extent, it is located at depths between 5,000 and 20,000 ft, depths sufficient to ensure adequate CO_2 densities for effective storage.

Calcite was assumed to react with aqueous species at local equilibrium because its reaction rate is typically quite rapid. Dissolution and precipitation of other minerals are kinetically-controlled. Kinetic rates are a product of the rate constant and reactive surface area (Eq. B.5 in Appendix B). Multiple mechanisms (including neutral, acid and base) are used for dissolution of minerals (Eqs. B.11 and B.12 in Appendix B). Kinetic parameters: rate constant (k_{25}), the activation energy (E_a), and the power term (n) for each mechanism are listed in Table 8.5-2. At any pH the total rate is the sum of the rates via each mechanism. Most of these parameters were taken from Palandri and Kharaka (2004) who compiled and fitted many experimental data reported by a large number of investigators. Parameters for illite were set to those of smectite. Acid pH parameters for siderite, ankerite, and dawsonite were set to those of dolomite. Neutral pH parameters for siderite were taken from Steefel (2001). Neutral pH parameters for ankerite and dawsonite are set to those of siderite.

Precipitation rate data do not exist for most minerals. Several aspects regarding precipitation are different from dissolution, including nucleation, crystal growth and Ostwald ripening processes, as well as the calculation of the reactive surface area (Steefel and van Capellen, 1990). These processes for mineral precipitation are not considered. Parameters for neutral pH in Table 8.5-2 were used for precipitation of the corresponding minerals. Notice that different sets of parameters for precipitation can be specified in the chemical input file of TOUGHREACT code.

The evolution of surface area in natural geologic media is complex, especially for multi-mineralic systems, and is not quantitatively understood at present. Mineral reactive surface areas (the third column of Table 8.5-2) were taken from Sonnenthal and Spycher (2001), which were calculated using a cubic array of truncated spheres that make up the framework of the rock. For clay minerals kaolinite, illite, and smectite, increased surface areas were based on the smaller grain sizes of these sheet silicate minerals (Nagy, 1995). A reactive surface area calculated from grain size may be a poor estimate of the hydrologically accessible mineral surface area. To account for this effect, surface areas listed in Table 8.5-2 were reduced by one order of magnitude in the present simulations. The magnitudes of surface areas are highly uncertain and cover a wide range of values. Sensitivity regarding the kinetic rate constants and reactive surface areas should be addressed in the future.

Prior to CO_2 injection, a simulation of water-rock interaction was performed to obtain a nearly equilibrated water chemistry using a pure 1.0 M solution of sodium chloride reacting with the primary minerals listed in Table 8.5-2 at a temperature of 75 °C. The resulting water chemistry was used for the initial condition of reactive geochemical transport simulations under CO_2 injection.

Table 8.5—2 **Initial mineral volume fractions, possible secondary mineral phases, and their kinetic properties. Note that: (1) all rate constants are listed for dissolution; (2) A is the reactive surface area (Eq. B.5 in Appendix B), k_{25} is the kinetic constant at 25 °C, E_a is activation energy, and n is the power (Eq. B.11); (3) the power terms n for both acid and base mechanisms are with respect to H^+, (4) for pyrite, the neutral mechanism has a n with respect to O_2(aq), the acid mechanism has two species involved: one n with respect to H^+ and another n with respect to Fe^{3+} (see Eq. B.12); (5) dolomite, Ca-smectite, and pyrite were included in the list of possible secondary mineral phases in the input but they were not formed during the simulation.**

Mineral	Vol. % Of solid	A (cm^2/g)	Parameters for kinetic rate law							
			Neutral mechanism		Acid mechanism			Base mechanism		
			k_{25} ($mol/m^2/s$)	E_a (KJ /mol)	k_{25}	E_a	$n(H^+)$	k_{25}	E_a	$n(H^+)$
Primary:										
Quartz	57.888	9.8	1.023×10^{-14}	87.7						
Kaolinite	2.015	151.6	6.918×10^{-14}	22.2	4.898×10^{-12}	65.9	0.777	8.813×10^{-18}	17.9	-0.472
Calcite	1.929	Assumed at equilibrium								
Illite	0.954	151.6	1.660×10^{-13}	35	1.047×10^{-11}	23.6	0.34	3.020×10^{-17}	58.8	-0.4
Oligoclase	19.795	9.8	1.445×10^{-13}	69.8	2.138×10^{-11}	65	0.457			
K-feldspar	8.179	9.8	3.890×10^{-13}	38	8.710×10^{-11}	51.7	0.5	6.310×10^{-22}	94.1	-0.823
Na-smectite	3.897	151.6	1.660×10^{-13}	35	1.047×10^{-11}	23.6	0.34	3.020×10^{-17}	58.8	-0.4
Chlorite	4.556	9.8	3.02×10^{-13}	88	7.762×10^{-12}	88	0.5			
Hematite	0.497	12.9	2.512×10^{-15}	66.2	4.074×10^{-10}	66.2	1			
Secondary:										
Magnesite		9.8	4.571×10^{-10}	23.5	4.169×10^{-7}	14.4	1			
Dolomite		9.8	2.951×10^{-8}	52.2	6.457×10^{-4}	36.1	0.5			
Low-albite		9.8	2.754×10^{-13}	69.8	6.918×10^{-11}	65	0.457	2.512×10^{-16}	71	-0.572
Siderite		9.8	1.260×10^{-9}	62.76	6.457×10^{-4}	36.1	0.5			
Ankerite		9.8	1.260×10^{-9}	62.76	6.457×10^{-4}	36.1	0.5			
Dawsonite		9.8	1.260×10^{-9}	62.76	6.457×10^{-4}	36.1	0.5			
Ca-smectite		151.6	1.660×10^{-13}	35	1.047×10^{-11}	23.6	0.34	3.020×10^{-17}	58.8	-0.4
Pyrite		12.9	$k_{25}=2.818\times10^{-5}$ $E_a=56.9$ $n(O_2(aq))=0.5$		$k_{25}=3.02\times10^{-8}$ $E_a=56.9$ $n(H^+)=-0.5$, $n(Fe^{3+})=0.5$					

A new fluid property module, ECO2N, was used for this CO_2 disposal problem. ECO2N is based on work by Spycher and Pruess (2005), and provides an accurate description of the thermophysical properties of mixtures of water and CO_2 under conditions typically encountered in saline aquifers of interest for CO_2 disposal (10 $^oC \le T \le$ 110 ^oC; $P \le 600$ bars). Details on this new fluid property module can be found in the ECO2N manual.

As mentioned above, the reactive transport simulation was performed for a time period of 1,000 years. To demonstrate the RESTART feature, we performed a series of two TOUGHREACT runs. The first run was

performed for 10 years. The input and major output files for the first run are provided with the distribution files. For the continuation run (restart) to 1,000 yr, we create a new subdirectory ~/P5_ECO2N-1Dradial/restart, into which we copy the input files (flow.inp, solute.inp, chemical.inp, therakin10.dat), the CO_2 property file (CO_2TAB), and the files SAVE and savechem from the first run. File SAVE is renamed INCON, savechem is renamed inchem, and the following minor changes are made in flow.inp: delete the INCON input block, and change the final simulation time from 3.15576E08 (10 years) to 3.15576E10 (1,000 years) in the PARAM input block. Now we can perform the restart run. Major output files from the restart run are also in subdirectory: ~/ P5_ECO2N-1Dradial/restart. Changes in porosity and permeability are a result of mineral dissolution and precipitation, consumption of CO_2 due to formation of carbonate minerals, and consumption of H_2O due to hydration reactions affecting the multiphase fluid flow. For longer time simulation, these feedback effects should be coupled. This option can be used by specifying kcpl = 1 (porosity and permeability coupling) and Ico2h2o = 2 (CO_2 and H_2O coupling) in input file solute.inp. However, if the coupling options are used, the convergence for solving flow equations could be slower.

An important feature for ECO2N module (and also EOS2) from other modules is that partial pressures of CO_2 gas are calculated from fluid flow calculations and then fed to geochemistry. In contrast, with the EOS3 and EOS4 modules, CO_2 is assumed to be a trace gas and transported with the bulk gas phase by advection and diffusion. With EOS9, CO_2 is also assumed to be a trace gas but is transported only by diffusion because the bulk gas phase is not considered. With the ECO2N (or EOS2), if the CO_2 partial pressure in block 'INITIAL gas ZONES' of chemical.inp (see the file chemical.inp in the distribution files) is greater than zero, this partial pressure is taken as the background partial pressure (regions not flooded with the injected CO_2). If this value is set to zero, no background CO_2 partial pressure buffer is allowed.

8.5.3 Results and discussion

Figure 8.5-1a shows CO_2 gas (supercritical fluid) saturations along the radial distance (water saturations are complementary to gas saturations, or $S_l = 1- S_g$). After 10 years, the region close to the well in about 40 m radial distance is completely dryout. The CO_2 plume (two-phase region) extends to a radial distance of 1,250 m. Later, the gas saturation gradually decreases due to formation of secondary carbonate minerals (see Figures 8.5-1 and 8.5-2). In the CO_2 plume region, pH is mainly buffered by CO_2 gas dissolution and calcite dissolution, values close to 5 are maintained as long as both CO_2 gas and calcite mineral are present. pH gradually increases with time due to mineral alteration. After 1,000 years, a value close to 6 was attained.

Figure 8.5—1 **Distributions of CO_2 gas saturation (a) and pH at different times for Problem 5 (in the region close to the well in about 160 m distance, water is completely removed).**

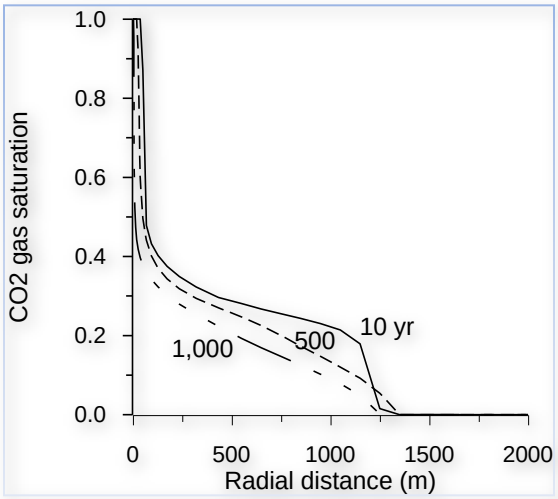

(a) CO_2 saturation

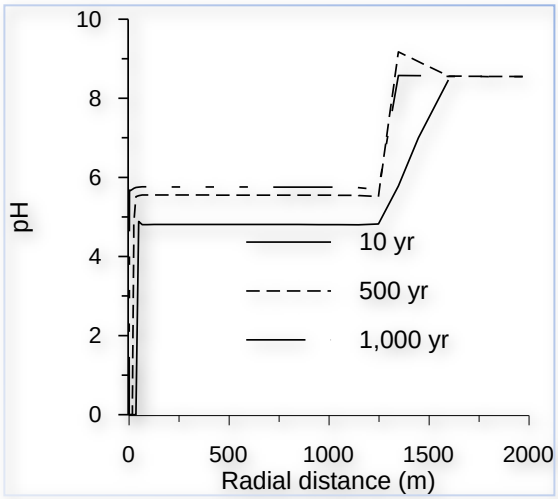

(b) pH

Significant ankerite precipitates due to CO_2 injection and dissolution of alumino-silicate minerals (Figure 8.5-2a). After 1,000 years, a maximum volume fraction of 0.02 (2%) formed at 1,250 m distance. Calcite dissolves rather than precipitates in the injected CO_2 plume region because a slightly low pH. Some dawsonite precipitates (Figure 8.5-2b) with a maximum volume fraction of 0.003 (0.3%). A small amount precipitation of magnesite and siderite occurs. No dolomite precipitation is observed in the simulation. The cumulative sequestration of CO_2 by carbonate mineral precipitation is given in Figure 8.5-3a. After 1,000 years, a maximum of 20 kg CO_2 per cubic meter medium could be sequestrated by carbonate precipitation. Addition of CO_2 mass to the solid matrix as secondary carbonate minerals decreases porosity (Figure 8.5-3b). More results on mineral alteration and on aqueous concentrations are given in the files, co2d_min.dat and co2d_conc.dat in the distribution files.

Figure 8.5—2 **Change in mineral abundance (in volume fraction, positive values indicate precipitation and negative dissolution) after different times for the 1-D radial flow problem.**

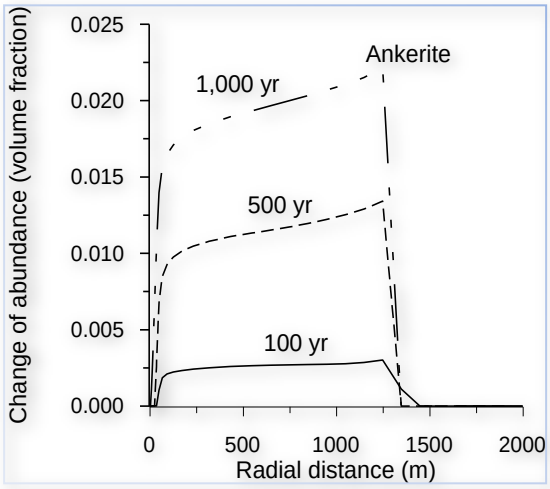

(a) Ankerite

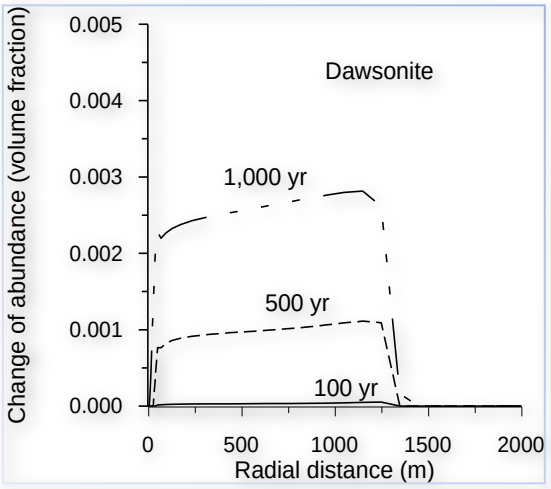

(b) Dawsonite

Figure 8.5—3 **Cumulative CO_2 sequestration by carbonate mineral precipitation for different times.**

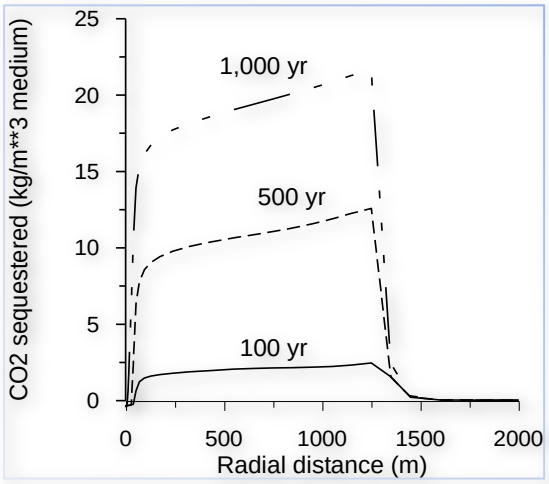

(a) CO_2 sequestered

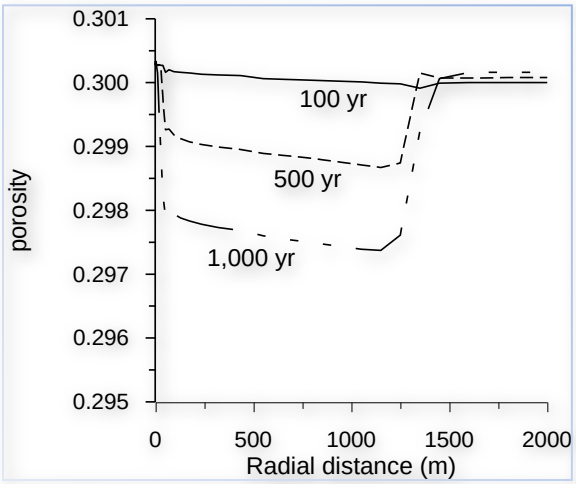

(b) Porosity

8.6 Problem 6 – 2-D Radial Model for CO_2 Sequestration in Deep Saline Formation

8.6.1 Problem Setup

The response of deep formations to CO_2 injection will depend on many factors, including formation permeability and porosity, the presence of heterogeneities such as faults and layers of high or low permeability, the physical and chemical characteristics of the brines, and the nature of the mineral phases that are present. A great deal

of specific and detailed information will be required to assess the feasibility of storing CO_2 in a brine formation at any particular site, and to develop engineering designs for CO_2 storage systems. Here, a generic two-dimensional (2-D) radial model was used to study the temporal evolution and spatial distribution of the injected CO_2 and the subsequent physical and chemical changes.

Fluid flow conditions

The 2-D radial model was a sandstone formation of 40 m thickness with a cylindrical geometrical configuration (Figure 8.6-1). The hydrogeological parameters used are essentially the same as the previous 1-D radial CO_2 sequestration problem (Table 8.5-1), except here using a porosity of 0.34, a horizontal permeability of 2.264×10^{-13} m^2, and a vertical permeability of 2.264×10^{-14} m^2. Temporal changes in porosity were calculated dynamically from changes in mineral volumes, and permeability calculated using cubic law (Eq. F.2 in Appendix F). A hydrostatic pressure distribution over the depth was specified initially. The shale caprock was assumed impermeable and non-reactive for the present study of coupled processes in the storage reservoir.

Figure 8.6—1 Schematic representation of the 2-D radial flow model for supercritical CO_2 injection into a sandstone formation.

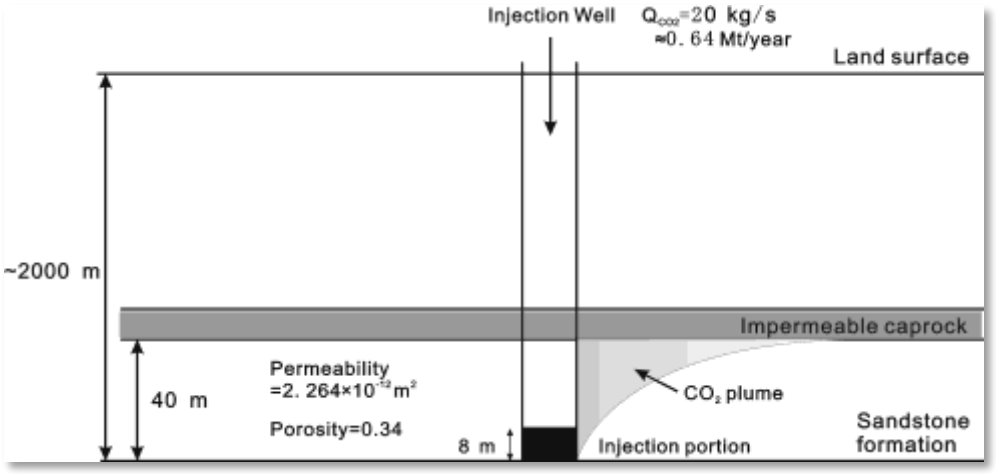

For numerical simulation, in the vertical direction a total of 20 model layers were used with a constant spacing of 2 m. In the horizontal direction, a radial distance of 100 km was modeled with a radial spacing that increases gradually away from the injection well. A total of 56 radial grid elements were used. The volume of the outer grid element is specified a large value of 10^{30} m^3, representing an infinite lateral boundary for constant pressure, temperature and concentrations. CO_2 injection was applied at the bottom portion over 8 m thickness with a constant rate of 20 kg/s (corresponding to 0.64 Mt/year) for a period of 10 years. The 2-D radial model of fluid flow and geochemical transport was simulated for a period for 1,000 years, which may be the interested time scale for CO_2 geological sequestration. We started a homogeneous field for the geological model, later heterogeneity resulted

from changes in porosity and permeability due to mineral alteration will seed the instability and motivate the convective mixing.

8.6.2 Geochemical system

The initial rock mineralogical composition was the same as the previous 1-D radial example, which may be representative of US Gulf Coast sandstone formations (Table 8.5-2). Calcite was assumed to react with aqueous species at local equilibrium because its reaction rate is typically quite rapid. Dissolution and precipitation of other minerals are kinetically-controlled. A multiple mechanism rate law is used. Kinetic parameters are the same as in the previous example. The initial water chemical composition, a NaCl-dominated brine, was also the same as the previous example. A temperature of 75°C was used throughout the domain and time, which may represent temperature at a depth of about 2 km, given a land surface temperature of 15°C and a geothermal gradient of 30°C/km.

8.6.3 Simulations

Same as the previous example, ECO2N fluid module was used for this 2-D radial flow CO_2 sequestration problem. As mentioned above, the reactive transport simulation was performed for a time period of 1,000 years. We performed a series of two TOUGHREACT runs. The first run was performed for 10 years (injection period). The input and major output files for the first run are provided with the distribution files. For the continuation run (restart) to 1,000 yr, create a new subdirectory into which copy the input files (flow.inp, solute.inp, chemical.inp, thermkin10.dat), the CO_2 property file (CO_2TAB), and the files SAVE and savechem from the first run. File SAVE is renamed INCON, savechem is renamed inchem, and the following minor changes are made in flow.inp: delete the INCON input block, and change the final simulation time from 3.15576E08 (10 years) to 3.15576E10 (1,000 years) in the PARAM input block. Now the restart run can be executed.

8.6.4 Results and discussion

Simulation results indicate that the supercritical CO_2 fluid injected at near the bottom of the storage formation migrates upward rapidly by buoyancy forces because the density of supercritical CO_2 phase is lower than that of aqueous phase (Figure 8.6-2). A small fraction of CO_2 gas is trapped in the porous rock as residual gas after injection. The residual gas trapping keeps CO_2 dissolving into brine and precipitating carbonate minerals, and gradually disappears at the bottom of the reservoir. With time most of the free CO_2 gas accumulates below the caprock, and then spreads laterally.

Figure 8.6—2 Distribution of supercritical CO_2 phase saturation at 10 and 1000 yr for the 2-D radial injection model.

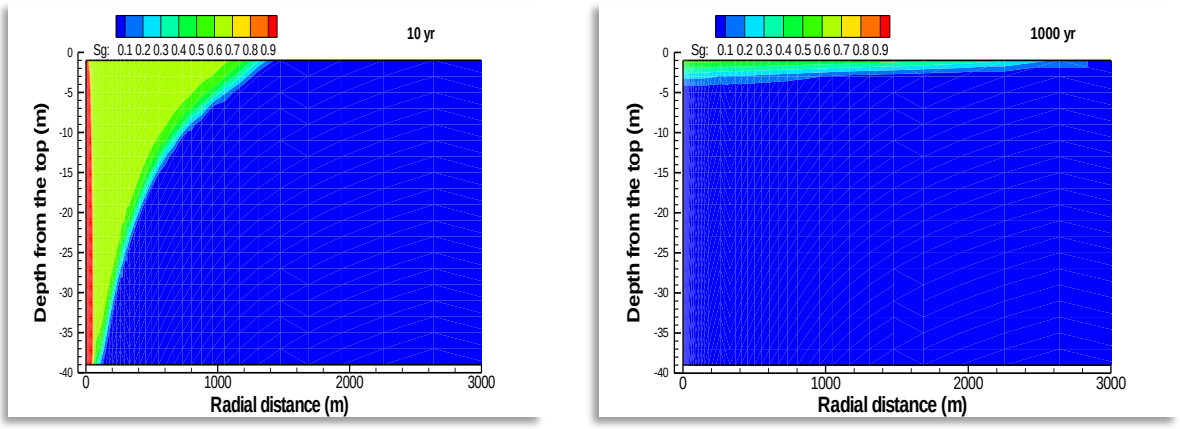

With the migration of CO_2 gas, the concentration of dissolved CO_2 rapidly increases to larger than 1 mol/kg H_2O in the two-phase region (Figure 8.6-3). The injected CO_2 dissolves in the surrounding formation water, forming H_2CO_3, HCO_3^-, and CO_3^{2-}, and decreasing pH. Then, the increased acidity induces dissolution of many of the primary host rock minerals (discussed later). The mineral dissolution increases concentrations of cations such as Na^+, Ca^{2+}, Mg^{2+}, and Fe^{2+}, which in turn form aqueous complexes with the bicarbonate ion such as $NaHCO_3$, $CaHCO_3^+$, $MgHCO_3^+$, and $FeHCO_3^+$. Over time they tend to increase dissolved CO_2 (solubility) and enhance solubility trapping.

Figure 8.6—3 Distribution of total dissolved CO_2 (mol/kg H_2O) at 10 and 1000 yr.

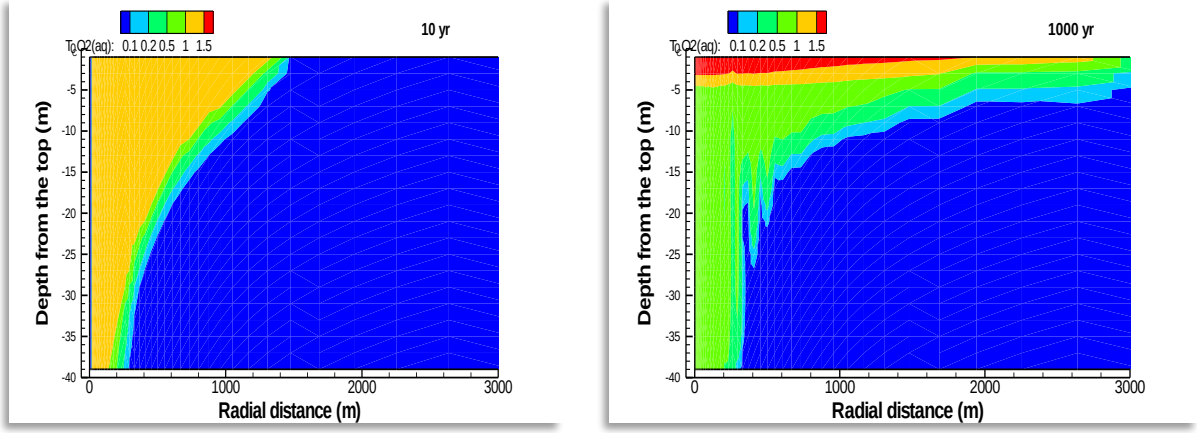

Minerals such as oligoclase and chlorite dissolve in the two-phase region and near the front of the single aqueous-phase zone, supplying reactants for carbonate mineral precipitation. Some amount of siderite and

dawsonite, and significant amount of ankerite precipitate (Figure 8.6-4), sequestering injected CO_2 (mineral trapping). At the same time, clay minerals such as smectite-Na precipitate. Changes in porosity are calculated from variations in mineral volume fractions (the bottom of Figure 8.6-5). Figures 8.6-3 and 8.6-4 show "finger" flow patterns near the bottom of the CO_2 plume. These are because of advection in the aqueous phase that is triggered by an increase in density due to CO_2 dissolution.

Figure 8.6—4 Distribution of siderite and ankerite precipitation at 1000 yr.

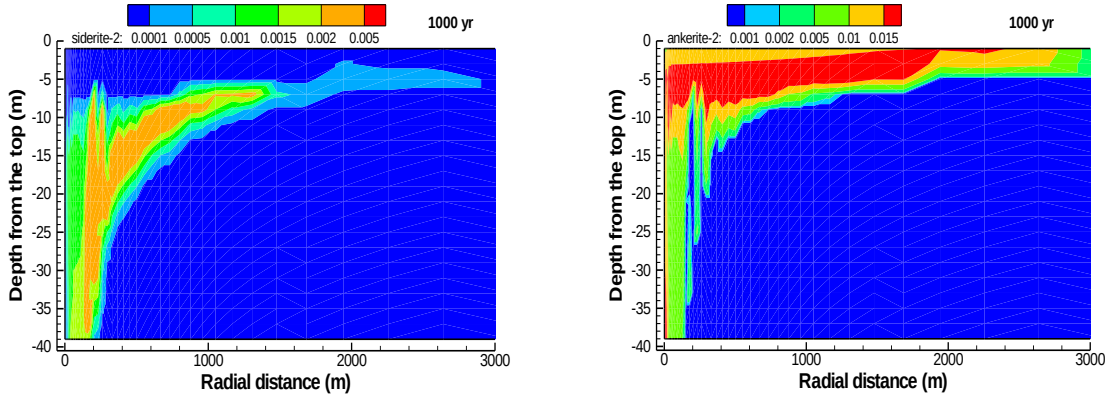

Figure 8.6—5 Distribution of porosity change at 1000 yr.

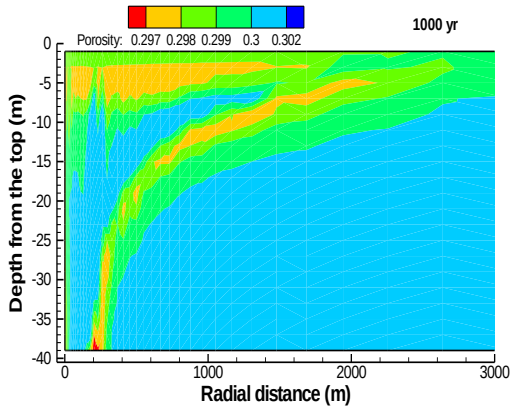

Mineral alteration and CO_2 trapping capability depends on the primary mineral composition. Precipitation of siderite and ankerite requires Fe^{2+}, which can be supplied by the dissolution of iron-bearing minerals, such as chlorite, or by reduction of Fe^{3+} in small amounts of hematite. Variation in Ca content in plagioclase significantly affects carbonate mineral precipitation, and thus CO_2 mineral trapping. The time required for mineral alteration and CO_2 sequestration depends on the rates of mineral dissolution and precipitation, which are products of the kinetic rate constant and reactive surface area. The current simulated mineral alteration pattern is generally consistent with available mineralogy observed at natural high-pressure CO_2 gas reservoirs.

8.7 Problem 7 – Supergene Copper Enrichment (EOS9)

8.7.1 Problem statement

This simulation problem was published in Xu et al. (2001). Supergene copper enrichment (SCE) involves hydrochemical differentiation by near-surface weathering processes in which water transports metals from a source region or leached zone (Brimhall et al., 1985; Brimhall and Dietrich, 1987; Ague and Brimhall, 1989) to an enrichment blanket zone where they are reprecipitated as secondary ore compounds conserving mass (Figure 8.7-1). The schematic system shown in Figure 8.7-1 captures, in a simplified manner, conditions of desertification in Northern Chile that led to oxidation and chemical enrichment of copper deposits at certain times in the past (of order 15 Ma) when a decline of the ground water table exposed sulfides to unsaturated conditions (Brimhall et al., 1985; Brimhall and Dietrich, 1987; Alpers and Brimhall, 1989; Ague and Brimhall, 1989).

Figure 8.7—1 A schematic representation of a supergene copper enrichment system according to Ague and Brimhall (1989).

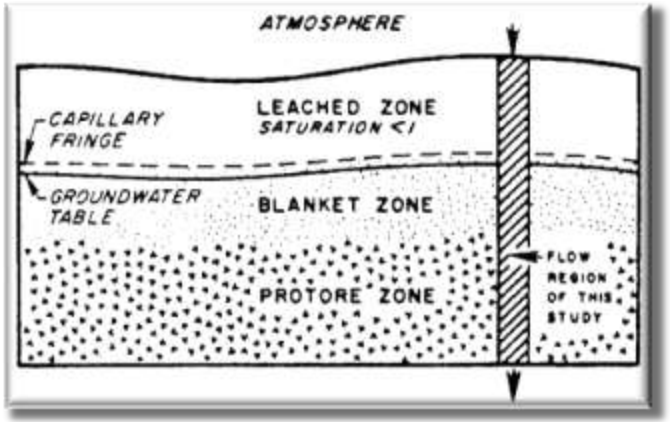

Oxidative weathering of pyrite (FeS_2) and chalcopyrite ($CuFeS_2$) causes acidification and mobilization of metals in the oxidizing zone and intense alteration of primary minerals, with subsequent formation of enriched secondary copper bearing sulfide mineral deposits (enrichment blanket) in the reducing conditions below the water table. Such oxidative weathering-driven processes have produced some of the world's largest copper deposits (Ague and Brimhall, 1989). The present investigation on geochemical transport in SCE systems is not specific to any field site, but the geochemistry for this work was based on field and laboratory studies of SCE systems as carried out by Brimhall et al. (1985), and Ague and Brimhall (1989). The coupled modeling study is intended to provide a better understanding of the complex interplay of oxygen diffusion, sulfide mineral oxidation, subsequent intense alteration of primary minerals and reprecipitation of secondary minerals. The SCE processes typically took place in a fractured porous medium such as at the El Salvador mine, Chile (Mote et al., 2001). To gain better insight into the processes involved, we first considered a problem in a one-dimensional unsaturated-saturated porous medium. Then we considered the case of SCE processes in a variably saturated fractured rock system using the "multiple interacting

continua" (MINC) method. Here we only present the case of SCE processes in a variably saturated fractured rock. The simple porous medium case is given in Xu et al. (2001)

8.7.2 Problem setup

The method of "multiple interacting continua" (MINC) is used to resolve "global" flow and diffusion of chemicals in the fractured rock and its interaction with "local" exchange between fractures and matrix rock. This method was developed by Pruess and Narasimhan (1985) for fluid and heat flow in fractured porous media. The extension of the MINC method to reactive geochemical transport is described in detail by Xu and Pruess (2001b). It is well-known that in the case of reactive chemistry diffusive fluxes may be controlled by reactions occurring near (within millimeters) the fracture walls. The resolution of concentration gradients in matrix blocks is achieved by appropriate subgridding. The MINC concept is based on the notion that changes in fluid pressures and chemical concentrations propagate rapidly through the fracture system, while invading the tight matrix blocks only slowly. Therefore, changes in matrix conditions will be (locally) controlled by the distance from the fractures and can then be modeled by means of one-dimensional strings of nested grid blocks (Figure 8.7-2).

In general it is not necessary to consider explicitly subgrids in all the matrix blocks separately. Within a certain subdomain (corresponding to a finite difference grid block), all fractures will be lumped into continuum # 1, all matrix material within a certain distance from the fractures will be lumped into continuum # 2, matrix material at larger distance becomes continuum # 3, and so on. Quantitatively, the subgridding is specified by means of a set of volume fractions VOL(j), j = 1, ..., J, into which the "primary" porous medium grid blocks are partitioned. The information on fracturing (spacing, number of sets, shape of matrix blocks) required for this is provided by a "proximity function" PROX(x) which expresses, for a given domain V_0 , the total fraction of matrix material within a distance x from the fractures (Pruess and Karasaki, 1982). If only two continua are specified (one for fractures, one for matrix), the MINC approach reduces to the conventional double-porosity or dual permeability methods.

We consider an idealized fractured porous medium with two perpendicular sets of plane, parallel, vertical fractures of equal aperture and spacing. Because of symmetry only one column of matrix blocks needs to be modeled. Figure 8.7-2 shows an areal view of a rock matrix column that is surrounded by vertical fractures with a spacing of 0.5 m, with subgridding of the matrix according to the MINC method. Subgrid 1 represents the fracture domain that is defined to include 50 percent by volume of wall rock. Subgrids 2 through 7 represent the rock matrix. In the vertical direction, a total of 10 model layers are used with a thickness of 2 m. A net rainwater infiltration rate of 0.015 m yr^{-1} over the entire area was applied to the fractures. Water pressure is held constant at 2 bars at the bottom (z = -20 m), so that the water table is located at a depth of approximately 10 m. In addition to global water flow and chemical transport in the fracture network, the model considers flow and transport between fractures and matrix, as well as vertical matrix-matrix water flow and chemical transport. The steady-state water saturations obtained without chemical reactions are used as initial conditions for the calculation of reactive geochemical transport. Hydrological parameters for the fracture and matrix are listed in Table 8.7-1.

Figure 8.7—2 **Subgridding of a rock matrix in the method of "multiple interacting continua" (MINC). The figure represents an areal view of a rock matrix column that is surrounded by vertical fractures.**

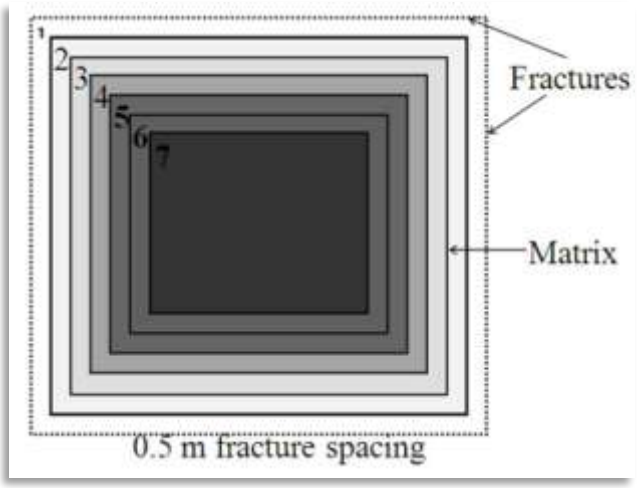

Table 8.7—1 **Hydrological parameters used for supergene copper enrichment in the fractured rock.**

Parameter	Matrix	Fracture
Permeability (m^2)	10^{-16}	10^{-12}
Fracture domain volume fraction, v *		0.01
Fracture spacing (m)		0.5
Porosity	0.08	0.5
Relative permeability and capillary pressure (van Genuchten, 1980):		
λ	0.457	0.457
S_{lr}	0.1	0.05
S_{ls}	1.0	1.0
P_0(pa)	2.17×10^5	6.2×10^3

* $v = V_f/(V_f + V_m)$ where V_f and V_m are fracture and matrix domain volumes.

The geochemical transport simulation considers unsaturated-saturated liquid phase flow and diffusive supply of oxygen to the protore. The domain modeled is initially filled entirely with a protore mineral assemblage as listed in Table 8.7-2. The dissolution of the primary minerals is considered to be kinetically-controlled. The kinetic rate constants and reactive surface areas are also given in Table 8.7-2. Precipitation of secondary minerals (Table 8.7-2 with initial $V_f = 0$ where V_f is mineral volume fraction) is represented using the same expression as dissolution. To simplify the description of precipitation kinetics, in the present study all secondary minerals are assigned the same kinetic rate constant (2.0×10^{-10} mol $m^{-2}s^{-1}$) and reactive surface areas (0.1 m^2 per dm^3 bulk medium). Because the rate constants assumed for precipitation reactions are larger than those for dissolution of primary minerals, formation of secondary minerals occurs effectively at conditions close to local equilibrium. The

kinetic rate of sulfide mineral oxidation can be strongly influenced by catalytic effects of bacteria (Singer and Stumm, 1970; Olson, 1991; Nordstrom and Alpers, 1997), which are not considered in the present study. Estimates of field oxidation rate cover a wide range of values (Nordstrom and Alpers, 1997). The rate determining process is commonly the transport of oxygen or other reactants to the reaction site. This process is the main focus of the simulation. Heat generation by pyrite oxidation may change temperature, but this effect is not considered in the simulations. Calculations are carried out at a constant temperature of 25°C. Thermodynamic data used in the simulations were taken from the EQ3/6 V8.2b database (Wolery, 1992), which were derived using SUPCRT92 (Johnson et al., 1992).

Table 8.7—2 **Initial protore mineral volume fractions (V_f) and possible secondary mineral phases (V_f = 0.0) considered in the supergene copper enrichment problem. Kinetic data for primary minerals are based on Ague and Brimhall (1989) and Gérard et al. (1997).**

Mineral	Composition	Volume fraction, V_f	Rate constant at 25°C (mol $m^{-2} s^{-1}$)	Surface area (m^2 dm^{-3} medium)
Primary:				
pyrite	FeS_2	0.090	$4.0x10^{-11}$	0.0587
chalcopyrite	$CuFeS_2$	0.045	$4.0x10^{-11}$	0.0587
magnetite	Fe_3O_4	0.045	$2.0x10^{-11}$	0.0787
k-feldspar	$KAlSi_3O_8$	0.180	$3.1x10^{-12}$	0.2710
albite	$NaAlSi_3O_8$	0.090	$3.1x10^{-12}$	0.1360
anorthite	$CaAl_2Si_2O_8$	0.090	$1.5x10^{-12}$	0.1420
annite	$KFe_3AlSi_3O_{10}(OH)_2$	0.045	$2.4x10^{-14}$	0.0587
muscovite	$KAl_3Si_3O_{10}(OH)_2$	0.090	$2.4x10^{-14}$	0.0123
quartz	SiO_2	0.180	$4.3x10^{-14}$	0.0850
anhydrite	$CaSO_4$	0.045	$1.5x10^{-12}$	0.0510
		total=0.9		
		porosity=0.1		
Secondary:				
covellite	CuS	0.0	$2.0x10^{-10}$	0.1
chalcocite	Cu_2S	0.0	$2.0x10^{-10}$	0.1
bornite	Cu_5FeS_4	0.0	$2.0x10^{-10}$	0.1
goethite	FeOOH	0.0	$2.0x10^{-10}$	0.1
hematite	Fe_2O_3	0.0	$2.0x10^{-10}$	0.1
kaolinite	$Al_2Si_2O_5(OH)_4$	0.0	$2.0x10^{-10}$	0.1
alunite	$KAl_3(OH)_6(SO_4)_2$	0.0	$2.0x10^{-10}$	0.1
amorphous silica	SiO_2	0.0	$2.0x10^{-10}$	0.1

Oxygen is treated as an ideal gas, and its interaction with the aqueous solution is assumed to be at equilibrium. The oxygen partial pressure at the land surface boundary is assumed to be constant at 0.2 bars. A dilute oxidized water that was equilibrated with an oxygen partial pressure of 0.2 bars is initially placed in the unsaturated zone, while a reducing water is assumed for the saturated zone. The infiltrating water composition is the same as the initial unsaturated water. The aqueous complexation is assumed at equilibrium, even though some aqueous redox

pairs such as sulfite and sulfide species may not be at equilibrium (Stumm and Morgan, 1981). Whether a particular reaction should be described as governed by the local equilibrium approximation (LEA) or by kinetic rates depends not only on the reaction itself but also on the rates of hydrodynamic transport processes (Domenico and Schwarz, 1990). The LEA is applicable when the characteristic time for transport of reactants is longer than the time required to reach chemical equilibrium. In the present simulations for reactive geochemical transport, the choice of equilibrium depends mainly on kinetic rate, infiltration rate, oxygen availability, and space discretization.

The EOS9 flow module was used for this ambient mineral deposition problem. The input and output files for the problem are provided with the distribution files. To shorten the run time for benchmarking purposes, the simulation time in the PARAM input block of flow.inp is specified as 3.15576E08 s (or 10 years). Users can reset this variable to their desired time. Parts of output files for fluid flow, aqueous chemical concentrations, and changes of mineral abundances are given in Figures 8.7-3, 8.7-4 and 8.7-5.

Figure 8.7—3 Part of file flow.out for Problem 7.

```
@@@@@@@@@@@@@@@@@@@@@@@@@@@@@@@@@@@@@@@@@@@@@@@@@@@@@@@@@@@@@@@@@@@@@@@@

 TOTAL TIME      KCYC    ITER  ITERC    KON         DX1M
 0.31557E+08    7330       2  14660      2       0.22258E-06

@@@@@@@@@@@@@@@@@@@@@@@@@@@@@@@@@@@@@@@@@@@@@@@@@@@@@@@@@@@@@@@@@@@@@@@@

ELEM.  INDEX    PRES        S(liq)       PCAP        K(rel)       DIFFUS.
                (PA)                     (PA)                     (m^2/s)

TOP 0      1 0.10000E+06 0.29322E-01 0.00000E+00 0.00000E+00 0.00000E+00
    1      2 0.10000E+06 0.26921E+00 -.28543E+05 0.14555E-04 0.43658E-08
2   1      3 0.10000E+06 0.97605E+00 -.44640E+05 0.51420E+00 0.75917E-06
3   1      4 0.10000E+06 0.97605E+00 -.44641E+05 0.51419E+00 0.75914E-06
4   1      5 0.10000E+06 0.97604E+00 -.44645E+05 0.51416E+00 0.75906E-06
5   1      6 0.10000E+06 0.97604E+00 -.44652E+05 0.51411E+00 0.75890E-06
6   1      7 0.10000E+06 0.97602E+00 -.44664E+05 0.51402E+00 0.75862E-06
7   1      8 0.10000E+06 0.97601E+00 -.44677E+05 0.51393E+00 0.75833E-06
    2      9 0.10000E+06 0.25775E+00 -.30146E+05 0.88783E-05 0.29217E-08
2   2     10 0.10000E+06 0.98320E+00 -.36590E+05 0.57672E+00 0.98343E-06
3   2     11 0.10000E+06 0.98320E+00 -.36591E+05 0.57672E+00 0.98342E-06
4   2     12 0.10000E+06 0.98320E+00 -.36591E+05 0.57671E+00 0.98339E-06
5   2     13 0.10000E+06 0.98319E+00 -.36593E+05 0.57670E+00 0.98334E-06
6   2     14 0.10000E+06 0.98319E+00 -.36596E+05 0.57668E+00 0.98325E-06
7   2     15 0.10000E+06 0.98319E+00 -.36598E+05 0.57665E+00 0.98315E-06
```

Figure 8.7—4 **Part of file Amic_aqu.dat for Problem 7 after t = 1 yr (Sl is water saturation, unit of concentrations is mol/l).**

X	Y	Sl	pH	t_so4-2	t_fe+2	t_cu+2	t_na+
0.000	0.000	0.2932E-06	7.0000	0.1037E-11	0.7326E-12	0.1030E-11	0.1007E-04
0.000	-1.000	0.2692E-05	3.7720	0.1449E-03	0.3642E-04	0.2163E-04	0.1209E-04
0.254	-1.000	0.9760E-05	3.7660	0.1470E-03	0.3698E-04	0.2194E-04	0.1212E-04
0.900	-1.000	0.9760E-05	3.7471	0.1540E-03	0.3880E-04	0.2298E-04	0.1222E-04
2.247	-1.000	0.9760E-05	3.7140	0.1668E-03	0.4217E-04	0.2490E-04	0.1240E-04
5.215	-1.000	0.9760E-05	3.6703	0.1856E-03	0.4703E-04	0.2770E-04	0.1266E-04
10.790	-1.000	0.9760E-05	3.6422	0.1988E-03	0.5041E-04	0.2967E-04	0.1284E-04
14.340	-1.000	0.9760E-05	3.6362	0.2017E-03	0.5116E-04	0.3011E-04	0.1288E-04
0.000	-3.000	0.2578E-05	3.6711	0.1849E-03	0.4648E-04	0.2760E-04	0.1265E-04
0.254	-3.000	0.9832E-05	3.6699	0.1855E-03	0.4665E-04	0.2768E-04	0.1266E-04
0.900	-3.000	0.9832E-05	3.6661	0.1873E-03	0.4718E-04	0.2795E-04	0.1268E-04
2.247	-3.000	0.9832E-05	3.6588	0.1907E-03	0.4819E-04	0.2847E-04	0.1273E-04
5.215	-3.000	0.9832E-05	3.6472	0.1963E-03	0.4973E-04	0.2930E-04	0.1281E-04
10.790	-3.000	0.9832E-05	3.6379	0.2009E-03	0.5094E-04	0.2998E-04	0.1287E-04
14.340	-3.000	0.9832E-05	3.6357	0.2020E-03	0.5122E-04	0.3015E-04	0.1289E-04

Figure 8.7—5 **Part of file Amic_sod.dat for Problem 7, showing changes in mineral abundances (in volume fraction, positive values indicate precipitation and negative dissolution) after t = 1 yr.**

X	Y	pyrite	chalcopyrit	magnetite	k-feldspar	albite
0.000	0.000	0.0000E+00	0.0000E+00	0.0000E+00	0.0000E+00	0.0000E+00
0.000	-1.000	-0.9909E-08	-0.7578E-08	-0.4777E-08	-0.3563E-08	-0.1678E-08
0.254	-1.000	-0.1322E-06	-0.1011E-06	-0.6373E-07	-0.4753E-07	-0.2239E-07
0.900	-1.000	-0.1322E-06	-0.1011E-06	-0.6373E-07	-0.4753E-07	-0.2239E-07
2.247	-1.000	-0.1322E-06	-0.1011E-06	-0.6372E-07	-0.4753E-07	-0.2239E-07
5.215	-1.000	-0.1322E-06	-0.1011E-06	-0.6372E-07	-0.4753E-07	-0.2239E-07
10.790	-1.000	-0.1322E-06	-0.1011E-06	-0.6372E-07	-0.4753E-07	-0.2239E-07
14.340	-1.000	-0.1322E-06	-0.1011E-06	-0.6372E-07	-0.4753E-07	-0.2239E-07
0.000	-3.000	-0.9488E-08	-0.7257E-08	-0.4574E-08	-0.3412E-08	-0.1607E-08
0.254	-3.000	-0.1332E-06	-0.1018E-06	-0.6419E-07	-0.4788E-07	-0.2255E-07
0.900	-3.000	-0.1332E-06	-0.1018E-06	-0.6419E-07	-0.4788E-07	-0.2255E-07
2.247	-3.000	-0.1332E-06	-0.1018E-06	-0.6419E-07	-0.4788E-07	-0.2255E-07
5.215	-3.000	-0.1332E-06	-0.1018E-06	-0.6419E-07	-0.4788E-07	-0.2255E-07
10.790	-3.000	-0.1332E-06	-0.1018E-06	-0.6419E-07	-0.4788E-07	-0.2255E-07
14.340	-3.000	-0.1332E-06	-0.1018E-06	-0.6419E-07	-0.4788E-07	-0.2255E-07

8.7.3 Results

Some selected plots of simulation results are presented in Figures 8.7-6, 8.7-7, and 8.7-8. More results and discussion are presented in Xu et al. (2001).

Figure 8.7—6 **Steady-state water saturation and water flux (relative to total infiltration) passed through the fractures**

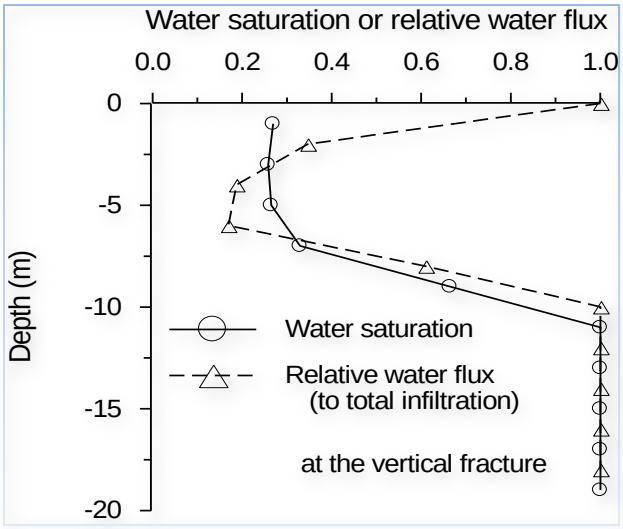

Figure 8.7—7 **Change of mineral abundance (positive values indicate precipitation and negative dissolution) after 20,000 yrs in the fractured rock.**

(A)

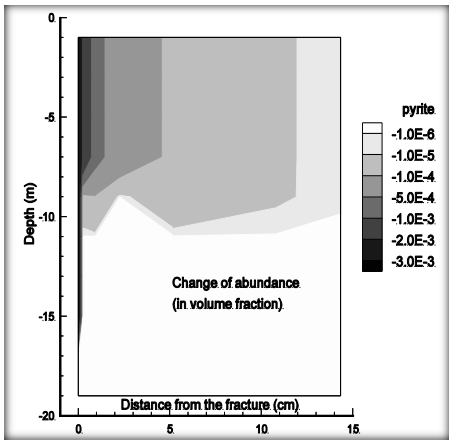

(B)

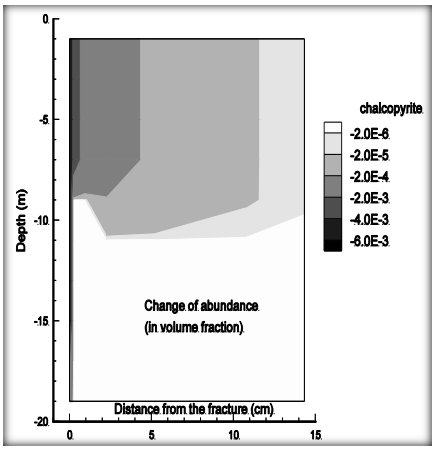

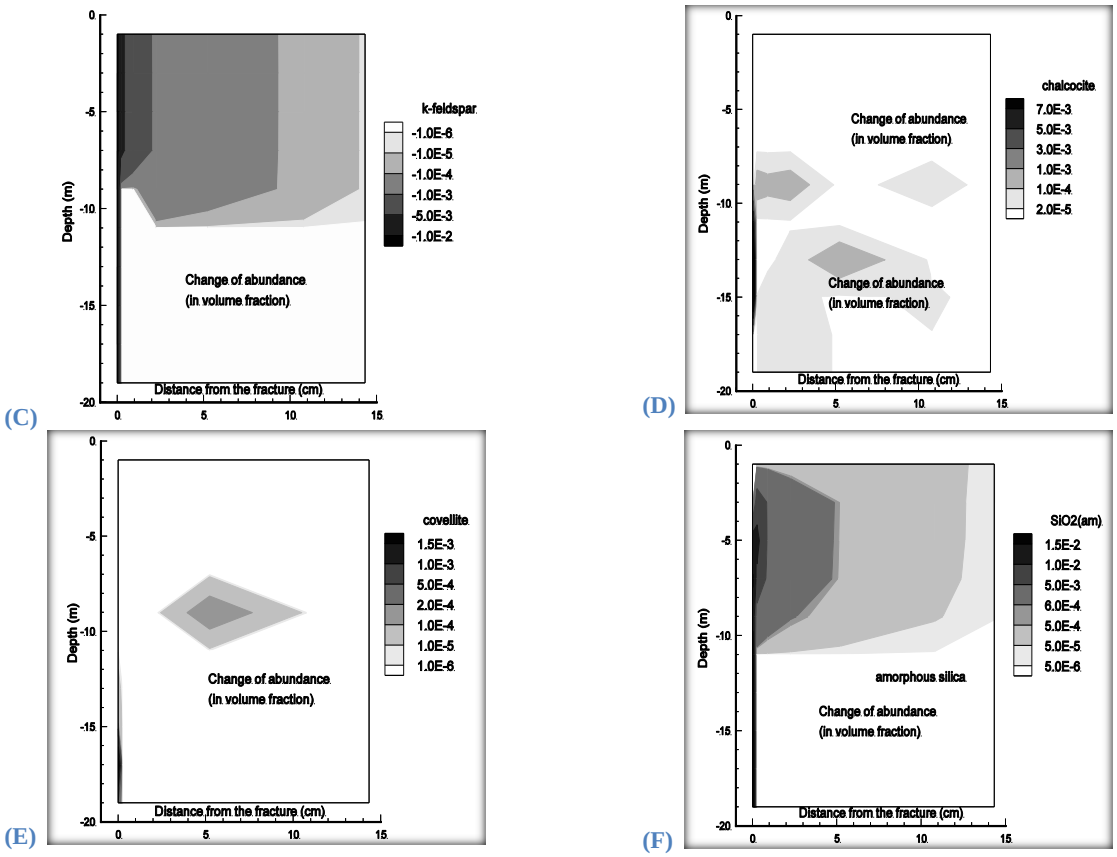

Figure 8.7—8 pH and dissolved copper concentration at 20,000 yrs in the fractured rock.

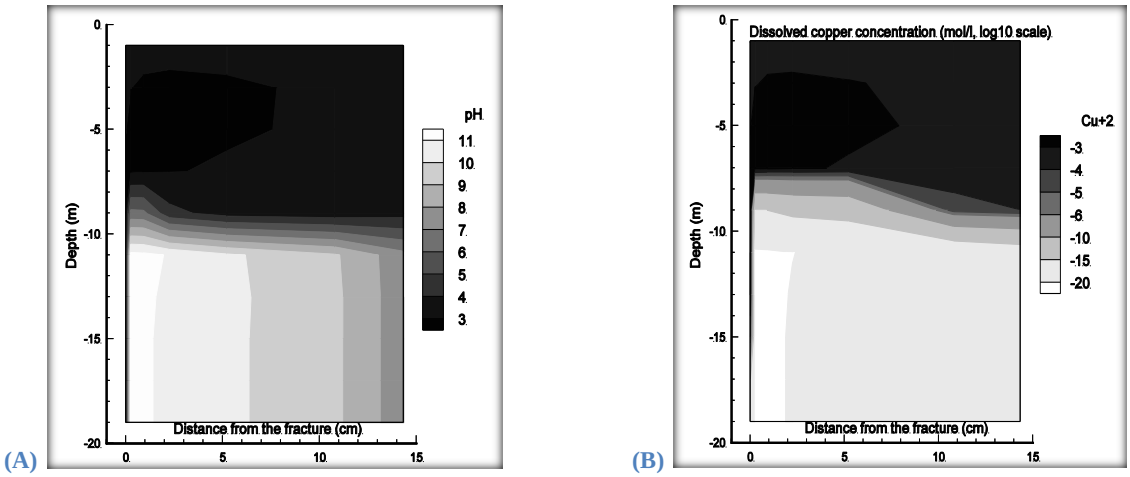

8.8 Problem 8 – Injection Well Scaling and Acidizing at Tiwi Field, Philippines (EOS1)

8.8.1 Problem statement

Nag-67 is one of the hot brine injectors located to the south-east of the Tiwi geothermal field, Philippines. The well was completed in March 1987. The injectivity of the well decreased significantly with time. The drop in injection capacity was attributed to scaling inside the wellbore as early as October 1992.

Records of injection history (Figure 8.8-1) and fluid chemistry for Nag-67 were reviewed to determine the nature of the deposited scale and to estimate the amount and location of the deposits. The well was acidized in January 1989 primarily to clear the near-wellbore formation of drilling mud damage and to improve its injectivity. Injection capacity of the well after the stimulation was 126 kg/s at a wellhead pressure of 1.38 MPa. In 1996, the well was found to accept only 38 kg/s at an injection wellhead pressure of about 1 MPa. In 1999, an injectivity test indicated that the capacity of the well had dropped to 17 kg/s at an injection wellhead pressure of 1.31 MPa. In March 2000, the recorded injection rate in Nag-67 suddenly decreased to 3. 8 kg/s.

In January 2001, the scale inside the Nag-67 wellbore was drilled-out, and the scale deposited in the near-well formation was dissolved by acid. Measurements after the scale drillout indicated that the capacity of the injector went up to 25.2 kg/s, and another test after the acid stimulation showed a further increase to 113.4 kg/s. These results strongly suggested that the decline in injectivity of the well was caused primarily by scale deposition in the near-well formation. Based on the chemistry of the brine injected and analysis of deposited scale, it was determined that most of the scale in Nag -67 was amorphous silica.

The silica concentration and pH of the brine being supplied to the Nag-67 injector were monitored between 1989 and 2000. Complete brine analyses were also available for every year except 1999 and were used to characterize the saturation state of the brine with respect to other minerals. From this historical chemical record, the degree of amorphous silica saturation in each analyzed water sample was determined.

Figure 8.8—1 Historical injection rates (kg/s) in Nag-67.

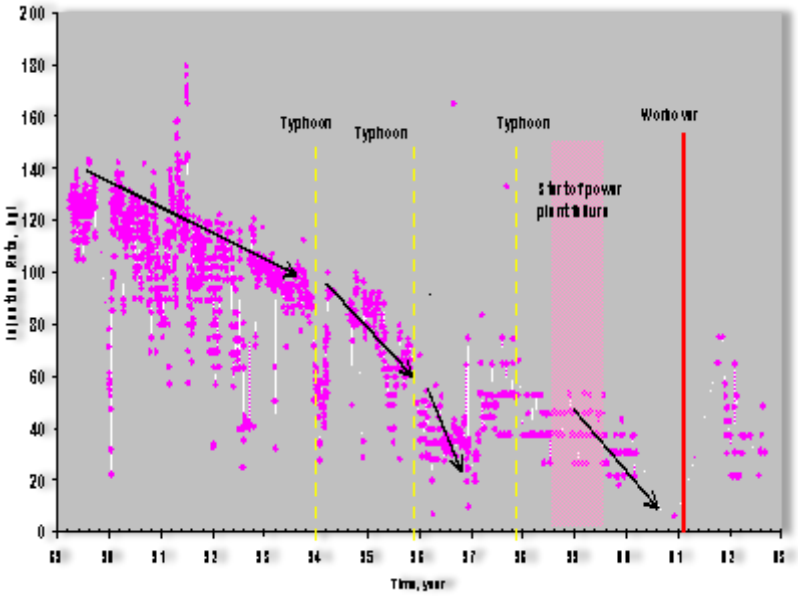

The estimated amount of silica (in the formation) dissolved by acid stimulation was calculated by assuming that the acid dissolved a stoichiometrically equivalent amount of silica. The silica scale volume calculated in this way was only 1.4 m^3. The dissolution of this seemingly small amount of amorphous silica nevertheless increased the injection capacity of the well to near original capacity. Therefore, it would appear that a significant part of the injectivity loss was related to silica deposition in the formation close to the wellbore, as opposed to in the wellbore itself.

To understand the scaling process and loss of injectivity in hot brine injectors, Ontoy et al. (2003) identified factors that cause the deposition of amorphous silica in the near-well formation and the extent of their effect using TOUGHREACT. These factors include the silica concentration in the hot brine injectate, the temperature of the injectate, the flowrate of the injectate, the pH of the injectate, and the temperature and pressure conditions of the reservoir in the vicinity of the injector.

Xu et al. (2004b) conducted a large number of numerical simulations to reproduce the loss of injectivity and its recovery by acid injection. A porosity-permeability relationship (Verma and Pruess, 1988; see Eq. F.8 in Appendix F) was calibrated by comparing predicted injection indexes with field observed data. Here we give brief description of the work of Xu et al. (2004b).

8.8.2 Problem setup

Grid and fluid flow parameters

A 120 m thick reservoir formation at the bottommost permeable zone of the injection well (Nag-67) was modeled. A simple one-dimensional radial flow model was used, consisting of 50 radial blocks with logarithmically increasing radii (Figure 8.8-2). The 50 blocks represent a distance of 1000 m from the wall of the drilled open hole. A fracture porosity of 1% (ratio of fracture volume over the total formation volume) was assumed. The initial bulk permeability has been estimated at 8.5×10^{-14} m^2, to be consistent with the observed initial injectivity index of the well. Conductive heat exchange with rocks of low permeability above and below this zone is an important process. The confining layers are modeled as semi-infinite half spaces, and heat exchange is treated with a semi-analytical technique due to Vinsome and Westerveld (1980).

Figure 8.8—2 Simplified conceptual model for injection well Nag-67.

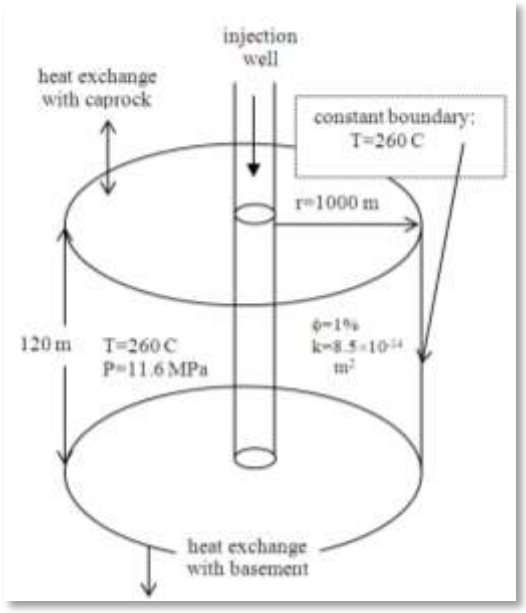

Only the fracture network is considered in the flow simulation, with the assumption that the fluid exchange with the surrounding low permeability matrix is insignificant. To allow for chemical reaction with the rock, 50% porosity was assigned to the blocks, and the total volume was accordingly doubled. The simulation zone was therefore "compressed" into a 2.4 m thick layer with 50% pore volume and 50% rock volume. A fracture permeability of 4.3×10^{-12} m^2 was used in the simulation (corresponding to a bulk fracture permeability value of 8.5×10^{-14} m^2 for the whole formation thickness with 1% fracture porosity). For consistency, bulk fracture porosity and permeability are reported here.

Initial reservoir temperature and pressure were assumed as 260°C and 11.6 MPa, respectively. The injection history of the well was used to define the amount of injected mass versus time (Figure 8.8-1): 50% of the total injection rate in Nag-67 was used because spinner surveys showed that the bottommost permeable zone accepted about 50% of the injectate. A constant injection temperature of 160°C was used because measured temperature fluctuations were generally small and with a relatively flat average trend (Figure 8.8-3).

Figure 8.8—3 Measured temperature of the injected water.

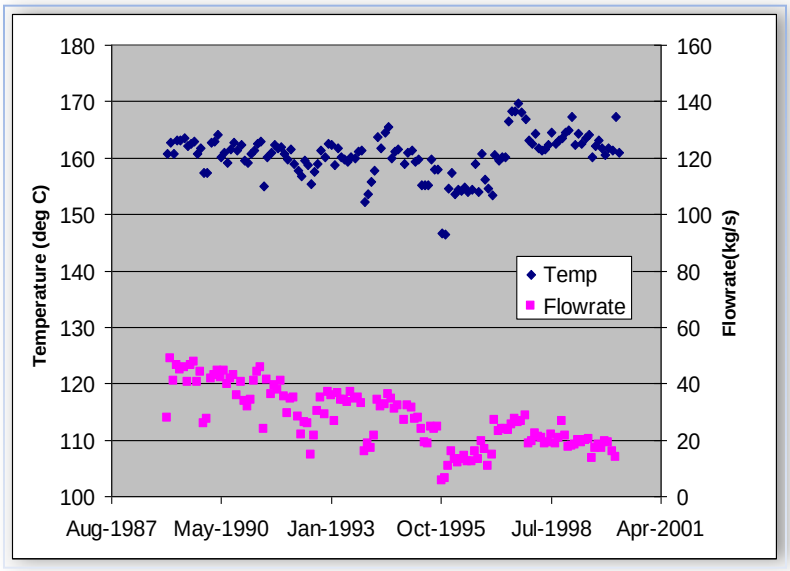

Geochemical data

The types and initial abundances of primary minerals were determined from the reported Nag-67 alteration mineralogy at the 1798-1920 m MD permeable zone (propylitic/phyllic rock). Secondary minerals were also determined from field observations (Table 8.8-1).

Table 8.8—1 List of minerals and aqueous species considered in the simulations

Mineral	Mineral Precipitation/ Dissolution	Mineral Initial Volume fraction	Primary Aqueous Components
Primary:			
albite-low	Kinetic	0.18	H_2O
anorthite	Kinetic	0.02	H^+
illite	Kinetic	0.05	Ca^{+2}
quartz	Kinetic	0.14	Mg^{+2}
muscovite	Kinetic	0.16	Na^+
clinochlore-7a	Kinetic	0.08	Cl^-
clinozoisite	Kinetic	0.01	$SiO_{2(aq)}$
calcite	Equilibrium	0.13	HCO_3^-
			SO_4^{-2}
Secondary:			K^+
amorphous silica	Kinetic		AlO_2
microcline	Kinetic		
kaolinite	Kinetic		
anhydrite	Equilibrium		

The composition of the injected brine was provided from historical analytical data. The formation water was reconstituted from the known brine composition as follows. First, the brine was diluted to yield saturation with quartz at the observed reservoir temperature of 260°C (thus reversing the concentrative effect of flashing). The resulting water was then equilibrated with minerals identified in the well mineralogy log (calculating the aluminum concentration using equilibrium with microcline, sodium using albite, pH using calcite, calcium using clinozoisite, and magnesium using clinochlore). Calcite and anhydrite were assumed to react at equilibrium because their reaction rate is typically quite rapid. Other minerals were set to react under kinetic constraints (Table 8.8-1). Thermodynamic and kinetic data for amorphous silica were taken from Carroll et al. (1998), and Gunnarsson and Arnorsson (2000). For other minerals, thermodynamic and kinetic data were taken from various other literature sources.

For all minerals except amorphous silica, input surface areas were estimated from the geometry of the modeled fracture (around 130 m^2/m^3 medium). For amorphous silica, a large surface area was estimated (10^7 cm^2/g) from Parks (1990, Fig. 16). Such a large value takes into account the very small size of amorphous silica particles in solution. Silica concentrations of 705 and 710 ppm were used, within the range of observed values (Figure 8.8-4).

Figure 8.8—4 Evolution of silica concentrations in the injected water.

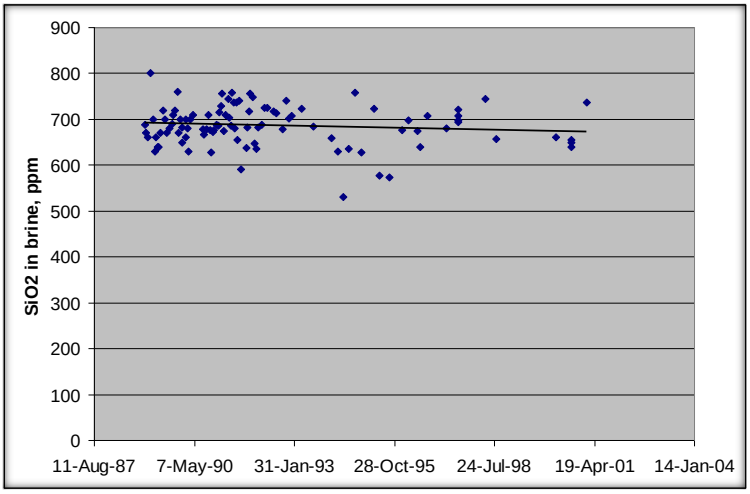

Parameters ϕ_c and n in Eq. (F. 8) in Appendix F were calibrated by comparing simulated injection indexes with measured data. The injection index is defined as

$$II = \frac{Flowrate}{P_b - P_i} \tag{8.1}$$

where, P_b is the borehole pressure and P_i is the initial reservoir pressure (116 bar). A total of 18 simulations were performed using the silica concentrations and values of parameters ϕ_c and n as listed in Table 8.8-2. The simulated time of injection was approximately 12 years, corresponding to the time from the initial acidization of the well in January, 1989, to the time of the well workover in January, 2001.

Table 8.8—2 List of simulations using different injection silica concentrations and values of parameters ϕ_c and n.

Silica concentration (ppm)	ϕ_c(%)	n	Simulation number
705	0.88	9	1
		11	2
		13	3
	0.90	7	4
		9	5
		11	6
	0.92	6	7
		8	8
		10	9
	0.94	3	10
		5	11
		6	12
710	0.90	3	13
		4	14
		5	15
	0.92	2	16
		3	17
		4	18

8.8.3 Results and discussion

The injection indexes can be reproduced by different sets of parameter combinations in the porosity-permeability relationship, Eq. (F.8) in Appendix F. For an injection silica concentration of 705 ppm, reasonable fits are obtained for the following combinations of ϕ_c and n values: (1) ϕ_c = 0.88% and n = 13, (2) ϕ_c = 0.9% and n = 11, (3) ϕ_c = 0.92% and n = 10, and (4) ϕ_c = 0.94% and n = 6. Here results obtained with only two sets of ϕ_c and n values are presented in Figure 8.8-5. More results can be found in Xu et al. (2004b). A smaller critical porosity ϕ_c requires a larger power term n. For a silica concentration of 710 ppm, the matching parameter combinations are (1) ϕ_c = 0.9% and n = 5, and (2) ϕ_c = 0.92% and n = 4. The simulated results show that small decreases in porosity result in steep reductions in permeability. This is consistent with a permeability experiment of Moore et al. (1983) in which a heated aqueous fluid was passed down a temperature gradient through Westerly Granite. The experiment showed a reduction in permeability of 96% with an 8% reduction of the initial porosity over a two-week period.

Figure 8.8—5 **Simulated injection indexes using an injection silica concentration of 705 ppm, together with measured data.**

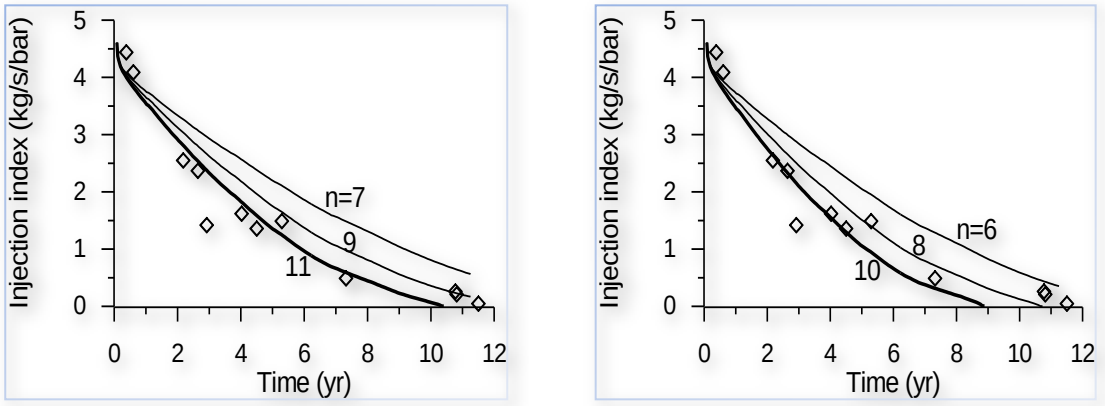

(a) ϕc = 0.90% **(b) ϕc = 0.92%**

An injection silica concentration of 705 ppm results in a total amorphous silica precipitation of 5.9 m^3 in the reservoir formation, while a silica concentration of 710 ppm results in 19.5 m^3. The estimated amount of amorphous silica in the formation dissolved by acid is about 1.4 m^3. Therefore, an injection silica concentration of 705 ppm could be a reasonable number for capturing total silica precipitation.

Further review of Figure 8.8-5 shows that the simulated injection indexes reach zero at earlier times than observed. Figure 8.8-3 indicates that after January 1996 (seven years after the simulation start) temperatures increase significantly above 160°C. We then performed an additional simulation using an injection temperature of 161°C for the later time period. Other parameters for the additional simulation are an injection silica concentration of 705 ppm, ϕ_c = 0.92% and n = 10. Results of the additional simulation are presented in Figure 8.8-6, showing that the match of injection indexes to observations for the later period was improved. The higher temperature results in some early precipitated silica dissolving at later time. At the end of the simulation, a total of 2 m^3 of amorphous silica remains in the formation, similar to the actual amount of 1.4 m^3 estimated to have been dissolved by acid.

Figure 8.8—6 **Simulated injection indexes using an injection temperature of 161°C for the later time period, together with measured data (silica concentration = 705 ppm, ϕ_c = 0.92%, and n = 10).**

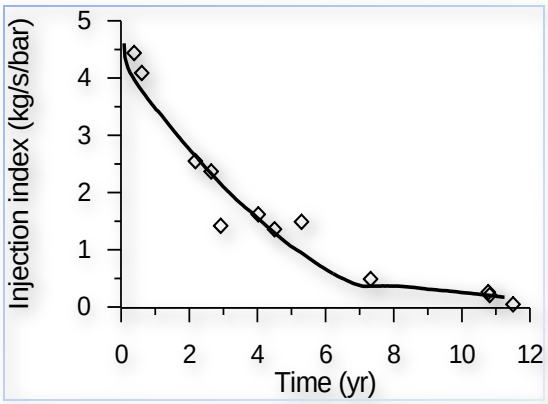

Significant reductions in porosity and permeability occur within a 10 m radius of the well (Figure 8.8-7). The pattern of permeability change on a logarithmic scale is similar to porosity change on a linear scale. The porosity reduction is mainly due to precipitation of amorphous silica (Figure 8.8-8). Some low-albite precipitation and minor illite precipitation and calcite dissolution occur in the simulations.

Figure 8.8—7 **Computed distribution of porosity and permeability along the well radius.**

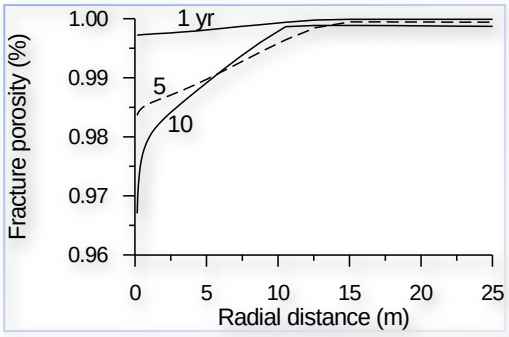

(a) Porosity

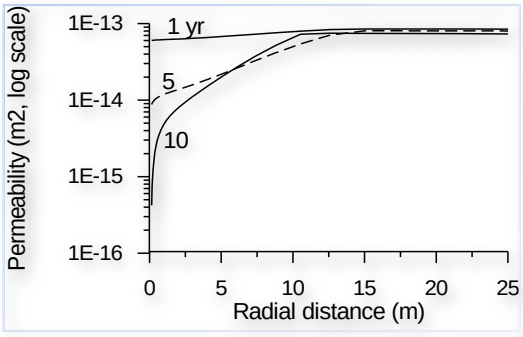

(b) Permeability

Figure 8.8—8 Predicted amorphous silica precipitation along the well radius.

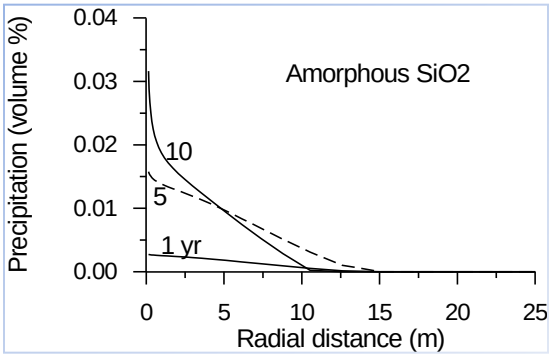

For only one simulation corresponding to Figure 8.8-6, input and output files are provided with the distribution files. To shorten the simulation time for benchmarking purposes, the time in the PARAM input block of flow.inp is specified as 3.5478e+07 s (1/10 of the entire simulation time and slightly longer than 1 year). Users can reset this variable to their desired time.

Other simulations can be achieved by modifying the ϕ_c and n values in file chemical.inp (under key word 'Permeability-Porosity Zones'). As mentioned before, only the fracture network is considered in the simulation. To allow for chemical reaction with the rock, 50% porosity was assigned to the blocks (with 50% pore volume and 50% rock volume). Therefore, an intrinsic porosity of 0.46 (in file chemical.inp) corresponds to bulk $\phi_c = 0.46 \times 2\% = 0.92\%$.

After the first phase of simulations of injectivity loss due to silica scaling, a simulation of acidizing for the injectivity recovery was performed. For the actual acidizing, a 5 wt% (about 2.5 mol/kg) HF acid was injected for five hours at an average rate of 18.2 kg/s. In the recovery simulation, a HF concentration of 1.25 mol/kg was used to account for some dilution by wellbore and formation waters. The predicted amount of amorphous silica dissolved by acid was also consistent with the estimated amount. Detailed results are given in Xu et al. (2004b).

8.8.4 Summary

A review of historical injection records, fluid chemistry data, and analyses of scale materials suggest silica scaling at Nag-67 occurred mainly in the rock formation immediately adjacent to the wellbore. Silica scaling (precipitation) decreases porosity, and in turn permeability and injectivity. A reactive transport numerical model, including the porosity-permeability relationship of Verma and Pruess (1988) was used to simulate injection loss and recovery. The porosity-permeability relationship involves two parameters: a "critical" porosity ϕ_c (which is the value of porosity at which permeability goes to zero) and a power term n (Eq. F.8). A number of simulations were performed using different combinations of values of ϕ_c and n under two different injection silica concentrations.

Significant precipitation of amorphous silica, and reductions of porosity and permeability occur within a 10 m radius from the well. The pattern of log10 scale of permeability is similar to linear scale of porosity. The simulated injection indexes were compared to measured data for each simulation. A good match was obtained using different parameter combinations; a smaller critical porosity ϕ_c requires a larger power term n. The porosity-permeability relationship is well suited for capturing the steep loss of injectivity at Nag-67. A steep reduction in permeability with a small decrease in porosity is consistent with a published permeability experiment. Taking an injection silica concentration of 705 ppm, within the range of observed values, results in a total amorphous silica precipitation of 2 m^3 in the reservoir formation, close to the amount of 1.4 m^3 estimated from the quantity of acid used to recover injectivity.

8.9 Problem 9 – Denitrification and Sulfate Reduction

8.9.1 Problem statement

To test the applicability of TOUGHREACT to reactive transport of denitrification and sulfate reduction, the column experiments of von Gunten and Zobrist (1993) were modeled. The experimental data were first used by Zysset et al. (1994) for their macroscopic model involving the transport of dissolved substances in groundwater-biofilm systems. Later, Doussan et al. (1997) used the same experimental data set for their model testing. They treated the diffusion dominated microscopic transport processes within the biofilm by using a mass-transfer coefficient in the macroscopic transport equations. These experiments were designed to simulate infiltration of an organically polluted river into an aquifer. Thus, synthetic river water, including an organic substrate (lactate) and electron acceptors of oxygen, nitrate and sulfate, were injected into columns filled with river sediments. Results of two column experiments were reported (von Gunten and Zobrist, 1993). The two columns have the same size of diameter 5 cm and length 29 cm. The model aquifer was a sand fraction (0.125 - 0.25 mm) from a fluvio glacial deposit. The sand contains only a small amount of organic material (<0.1%). The columns were kept at ambient temperature. Column 1 was inoculated at the inflow with an aqueous extract from a humus soil. Column 2 was inoculated with 1 g of material from the first 1-2 cm of Column 1. In the first column, only nitrate is added to the solution as an electron acceptor. In the second column, oxygen, nitrate, and sulfate are used as electron acceptors. The TOUGHREACT simulation results for experiments of two columns have been presented in Xu (2008).

8.9.2 Biodegradation kinetics and parameters

As described by the previous investigators, three major microbially-mediated reactions are involved in the experiments. Three electron acceptors are reduced, while dissolved organic matter (DOC) using lactate ($C_3H_5O_3^-$) in the experiment, are oxidized as follows:

$$3O_2(aq) + C_3H_5O_3^- \rightarrow 3HCO_3^- + 2H^+ \quad \textbf{(8.9.1)}$$

$$12NO_3^- + 5C_3H_5O_3^- + 2H^+ \rightarrow 15HCO_3^- + 6N_2(aq) + 6H_2O \quad \textbf{(8.9.2)}$$

$$3SO_4^{2-} + 4C_3H_5O_3^- \rightarrow 4C_2H_3O_2^- + 4HCO_3^- + 3HS^- + H^+ \quad \textbf{(8.9.3)}$$

The bacterial growth rates due to three different electron acceptors are given in Equations (8.9.4), (8.9.5) and (8.9.6), respectively. Denitrification is inhibited by oxygen, and sulfate reduction is inhibited by both oxygen and nitrate. The rate parameters for Equations (8.9.4) through (8.9.6) are given in Table 8.9-1.

$$r_b^{O_2} = k_b^{O_2} X_b \left(\frac{C_{DOC}}{K_{DOC}^{O_2} + C_{DOC}} \right) \left(\frac{C_{O_2}}{K_{O_2} + C_{O_2}} \right) \quad \textbf{(8.9.4)}$$

$$r_b^{NO_3} = k_b^{NO_3} X_b \left(\frac{C_{DOC}}{K_{DOC}^{NO_3} + C_{DOC}} \right) \left(\frac{C_{NO_3}}{K_{NO_3} + C_{NO_3}} \right) \left(\frac{I_{O_2 \rightarrow NO_3}}{I_{O_2 \rightarrow NO_3} + C_{O_2}} \right) \quad \textbf{(8.9.5)}$$

$$r_b^{SO_4} = k_b^{SO_4} X_b \left(\frac{C_{DOC}}{K_{DOC}^{SO_4} + C_{DOC}} \right) \left(\frac{C_{SO_4}}{K_{SO_4} + C_{SO_4}} \right) \left(\frac{I_{O_2 \rightarrow SO_4}}{I_{O_2 \rightarrow SO_4} + C_{O_2}} \right) \left(\frac{I_{NO_3 \rightarrow SO_4}}{I_{NO_3 \rightarrow SO_4} + C_{NO_3}} \right) \quad \textbf{(8.9.6)}$$

The overall biomass growth rate is expressed as

$$r_b = r_b^{O_2} + r_b^{NO_3} + r_b^{SO_4} - bX_b \quad \textbf{(8.9.7)}$$

where X_b is biomass concentration (mg/l), b is decay constant, and a value of 5.787×10^{-7} 1/s was used according to Doussan et al. (1997).

Table 8.9—1 List of biodegradation rate parameters used in Equations (8.9.4) through (8.9.6) (according to Doussan et al., 1997).

	O_2	NO_3	SO_4
Maximum specific growth constant *k* (1/s)	1.1574×10^{-4}	1.1667×10^{-5}	3.01×10^{-6}
Half-saturation constant of electron acceptors (mg/l)	0.77	7	5.35
Half-saturation constant of electron donor (mg/1)	3	3	3
Inhibition constants (mg/1)	$O_2 \rightarrow NO_3$ 10^{-3}		O_2 , $NO_3 \rightarrow SO_4$ 2×10^{-3}

In this example, biomass is assumed not subject to transport. Most of the bacteria are fixed on the solid phase within geologic media. A general multi-region model for hydrological transport interacting with microbiological and geochemical processes was used (Figure 8.9-1). The model consists of: (1) a mobile region (a fraction of the porosity), (2) an immobile region (another fraction of the porosity), and (3) a solid particle region where mineral dissolution/ precipitation and surface reactions may occur. Here the immobile region contains stagnant water and biomass. Currently, TOUGHREACT does not consider the dynamic changes in the volume of immobile region. The dynamic changes in porosity and volume will be implemented in the future. In principle, the multi-region model is similar to the model of "multiple interacting continua" (MINC) for resolving "global" fluid and heat flow and diffusion of chemicals in fractured rock and their interaction with the "local" exchange between fracture and matrix rock (Pruess and Narasimhan, 1985). Details on the multi-region model can be found in Xu (2008).

Figure 8.9—1 Schematic representation of a multi-region model for resolving local diffusive transport.

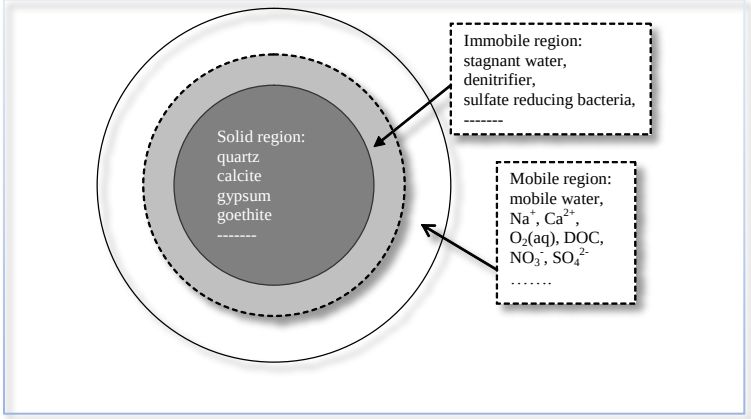

8.9.3 Denitrification

In the first column, only nitrate is added to the solution as an electron acceptor. As mentioned above, Doussan et al. (1997) modeled the reactive transport of denitrification in Column 1. They treated the diffusion-dominated microscopic transport processes within the biofilm by a mass-transfer coefficient, which was calibrated by the experimental data. Maximum specific growth rates and half-saturation constants were also calibrated. These calibrated parameters were also used for their Column 2 simulation. These parameter estimates were obtained with biomass growth. A yield coefficient of 0.4 was used in their simulations.

The experiments were started by inoculating the water in the columns with a small amount of bacteria, but no biomass concentration is reported in von Gunten and Zobrist (1993). Here a starting biomass concentration of 0.15 mg/l calibrated by Zysset et al. (1994) was used. Initial concentrations for all other species are set equal to a very small value of 10^{-10} mg/l (practically zero, because TOUGHREACT uses log10 calculations for a better

convergence). Constant concentrations at the boundary were used in the simulation, which are given in Table 8.9-2. A diffusion coefficient of 1×10^{-9} m^2/s was used.

Table 8.9—2 Boundary conditions used in the column experiments. Values are experimental data taken from Doussan et al. (1997).

	Column 1	Column 2
Injection flow rate (Darcy velocity, m/day)	1.8	0.37
O_2 (mg/l)		7
NO_3 (mg/l)	34.1	18.6
SO_4 (mg/l)		21.5
DOC (mg/l)	43.2	43.2

The physical parameters used for the three regions are given in Table 8.9-3. For the first trial run, 15% of the bulk porosity (0.4) was assumed for the immobile region. In the multi-region simulations, a porosity of 1 was assigned for the mobile region and a porosity of 0.5 was assigned for the immobile region consisting of stagnant water and biomass. Changes in porosity caused by bacterial growth are not currently considered. A 0.05 porosity was assumed for the solid particle region. In Section 8.9.5, a mineral composition is assigned for the solid particle region to illustrate the coupling of microbially-mediated redox reactions with mineral dissolution and precipitation. The distance (Table 8.9-3, $d = d_1 + d_2$) between the mobile and immobile regions is assumed to be 2×10^{-5} m, a fraction of the sand particle sizes range from 1.252×10^{-4} to 2.52×10^{-4} m (von Gunten and Zobrist, 1993). The interfacial area (A) was calibrated by matching the measured nitrate concentrations. The d between the immobile and solid regions (3×10^{-5} m) was set slightly larger than the mobile-immobile regions. The same A was used for immobile and solid regions. In fact, diffusive flux between regions is proportional to $D_0\tau A/d$, where D_0 is diffusion coefficient (10^{-9} m^2/s) and τ is tortuosity. The τ between two regions is calculated according to values in two regions (see Table 8.9-3) by $\tau = (d_1\tau_1+d_2\tau_2)/(d_1+d_2)$. Values of d, D_0, τ, and A all affect the diffusive flux. Therefore, errors in d, D_0, and τ will be passed along to A, because only the interfacial area is calibrated. The other conditions and parameters are unchanged from the previous 1-D porous medium simulation.

Table 8.9—3 List of physical parameters used for the three regions.

Parameter	Hydro-Region	Bio-Region	Chem-Region
Volume fraction of the medium	0.34	0.06 (15% of the bulk porosity)	0.60
Porosity	1.0	0.5	0.05
Distance (in m)	d_1	d_2 d_1	d_2
	10^{-5}	10^{-5} 10^{-5}	2×10^{-5}
Tortuosity	0.5	0.3	0.1
	0.4	0.1667	

The concentration profile of nitrate at different times obtained with the multi-region model is presented in Figure 8.9-2. Starting from a 15% immobile region, the 7-day curve agrees well the observed data. However, the 14-day curve is above the corresponding data (less reactive), but improved from the porous model. This may result from bacterial growth increasing volume of the immobile region. Currently, we simply let the run stop at 7 days and then restart by increasing the immobile region to 25% of the bulk porosity. The diffusion length was kept the same. Dynamic changes of the diffusion length together with immobile region volume and the interfacial area will be addressed in the future. The 14-day curve of 25% immobile region captures the observed data (Figure 8.9-2). Only one data point at (x = 0.0167) was off the curve, possibly because of other reasons (such as measurement errors). The simulated concentrations of dissolved organic carbon (DOC) and biomass obtained are presented in Figure 8.9-3. DOC decreases slowly here and is not a limiting factor for the bacterial growth. The growth is very slow until 7 days; then it accelerates dramatically.

The matches were adjusted with the interfacial area A between mobile and immobile regions. The calibrated values are 38 m^2 per cubic bulk medium for the initial period, 75 m^2 for the late period. The match and parameter calibration suggest that TOUGHREACT can not only be a useful interpretative tool for biogeochemical experiments, but also can produce insight into processes and parameters of microscopic diffusion and their interplay with biogeochemical reactions.

Figure 8.9—2 **Nitrate concentrations obtained with the multi-region model after 7 and 14 days, together with measured data.**

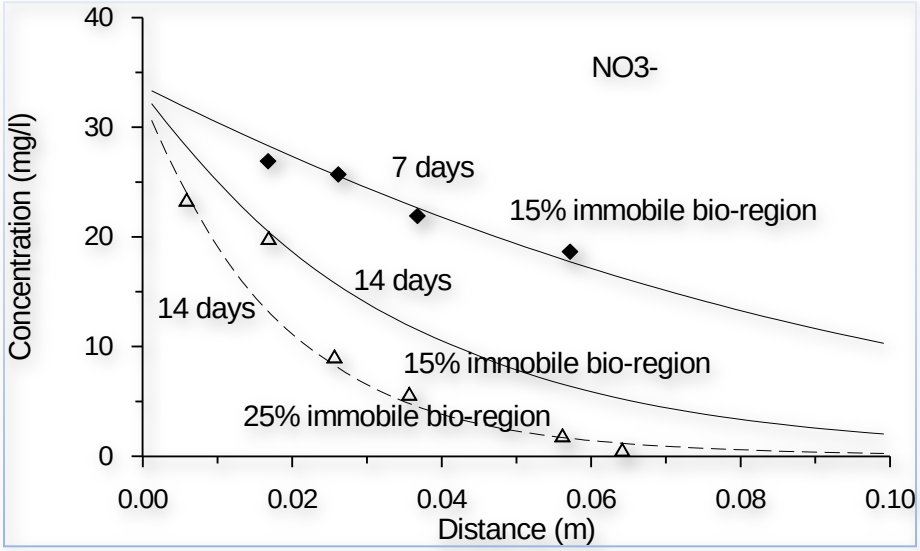

Figure 8.9—3 **Concentrations of dissolved organic carbon (DOC) and biomass obtained with the multi-region model after 7 and 14 days.**

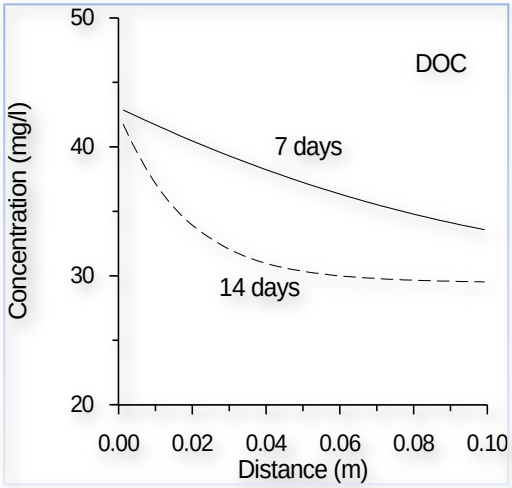

(a) DOC

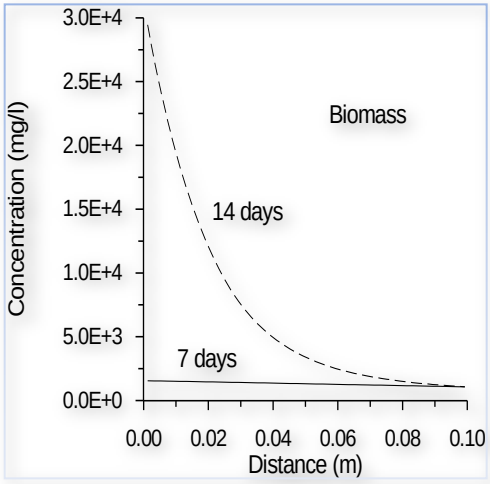

(a) Biomass

The EOS9 flow module is used for this denitrification problem. The flow and solute transport input files are similar to the previous examples. Here we only present the chemical input file in Figure 8.9-4. The complete input and output files are provided with the distribution files.

Figure 8.9—4 Chemical input file (chemical.inp) for Problem 9.

```
# Title
'Column a of Nitrate problem in Doussan et al., 1997, in Contam. Hydrology'
# '-------------------------------------------------------------------------------'
# 'DEFINITION OF THE GEOCHEMICAL SYSTEM'
# 'PRIMARY AQUEOUS SPECIES'  NoTransport
'h2o'                       0
'h+'                        0
'no3-'                      0
'DOC'                       0     ! Dissolved organic matter
'biomass'                   1     ! Biomass,         not subject to transport
'*'                         0
# 'AQUEOUS KINETICS'
  2                         ! Total number of kinetic aqueous reactions
  1                         ! Denitration, NO3-
       4   -6.195 'no3-' -2.5 'DOC'  1.0 'biomass'   -1.665e-5 'h+'  ! Consumption:
negative; production positive
       1      1              ! rate model index, No.mechanism
          1.6667E-5          ! rate constant (mass/L/s, maximum specific growth rate
          1   'biomass' 2  1.0                          ! Product    term,   2 means
concentration
          2   'DOC'   2  3.0    'no3-' 2  7.0           ! Monod      terms
          0                                            ! Inhibition terms
  2                           ! Biomass decay
       1     1.0 'biomass'    ! Consumption: negative; production positive
       1     1                ! rate model index; No.mechanism
         -5.787d-07           ! rate constant (decay constant, -b here)
          1   'biomass' 2  1.0                          ! Product    term,
          0                                            ! Monod      terms
          0                                            ! Inhibition terms
'*'
# 'AQUEOUS COMPLEXES'
'oh-'
'*'
# 'MINERALS'
'*'
# 'GASES'
'*'
# 'SURFACE COMPLEXES'
'*'
# 'species with Kd and decay    decay constant(1/s)'
'*'
# 'EXCHANGEABLE CATIONS'
'*'
# '-------------------------------------------------------------------------------'
# 'INITIAL AND BOUNDARY WATER TYPES'
3   1       ! niwtype, nbwtype = number of initial and boundary waters
# Index  Speciation T(C)  P(bar)
1          20.0            1.0
# '        icon        guess         ctot         '
'h2o'        1        1.000d+00      1.000d+00  '  '  0.
'h+'         3        1.0d-7         1.0d-7     '  '  0.         ! mol/l
'no3-'       1        1.0d-10        1.0d-10    '  '  0.         ! mg/l
'DOC'        1        1.0d-10        1.0d-10    '  '  0.         ! mg/l
'biomass'    1        1.5d-80        1.5d-80    '  '  0.         ! mg/l
'*'
# Index  Speciation T(C)  P(bar)
2          20.0            1.0
# '        icon        guess         ctot         '
'h2o'        1        1.000d+00      1.000d+00   '  '  0.
'h+'         3        1.0d-7         1.0d-7      '  '  0.      ! mol/l
'no3-'       1        1.0d-10        1.0d-10     '  '  0.      ! mg/l
'DOC'        1        1.0d-10        1.0d-10     '  '  0.      ! mg/l
'biomass'    1        1.0d-0         1.0d-0      '  '  0.      ! mg/l
'*'
# Index  Speciation T(C)  P(bar)
3          20.0            1.0
# '        icon        guess         ctot         '
```

```
'h2o'        1        1.000d+00      1.000d+00    '  '  0.
'h+'         3        1.0d-7         1.0d-7       '  '  0.      ! mol/l
'no3-'       1        1.0d-10        1.0d-10      '  '  0.      ! mg/l
'DOC'        1        1.0d-10        1.0d-10      '  '  0.      ! mg/l
'biomass'    1        1.5d-80        1.5d-80      '  '  0.      ! mg/l
'*'
# Index  Speciation T(C)  P(bar)
1          20.0            1.0
# '        icon        guess          ctot          '
'h2o'        1        1.000d+00      1.000d+00    '  '  0.
'h+'         3        1.0d-7         1.0d-7       '  '  0.
'no3-'       1        34.1           34.1         '  '  0.
'DOC'        1        43.2           43.2         '  '  0.
'biomass'    1        1.5d-80        1.5d-80      '  '  0.
'*'
# '-------------------------------------------------------------------------------'
# 'INITIAL MINERAL ZONES'
'*'
# '-------------------------------------------------------------------------------'
# 'INITIAL gas ZONES'
'*'
# '-------------------------------------------------------------------------------'
# 'Permeability-Porosity Zones'
'*'
# '-------------------------------------------------------------------------------'
# 'INITIAL SURFACE ADSORPTION ZONES'
'*'
# '---------------------------------------if Sden=0 Kd store retardation factor'
# 'INITIAL LINEAR EQUILIBRIUM Kd ZONE'
'*'
# '---------------------------------------if Sden=0 Kd store retardation factor'
# 'INITIAL ZONES OF CATION EXCHANGE'
'*'
# '-------------------------------------------------------------------------------'
# 'end'
```

8.9.4 Sulfate reduction

The evolution of sulfate in the Column 2 experiment of von Gunten and Zobrist (1993) was simulated together with that of oxygen and nitrate. Organic matter is successively oxidized by oxygen, nitrate, and sulfate. Denitrification is inhibited by oxygen, whereas sulfate reduction is inhibited by both oxygen and nitrate. The multi-region model used 25% of the bulk porosity (0.4) for the immobile region throughout the simulation. The increased immobile volume was attributed to (1) a longer simulation time (35 over 14 days) and (2) more electron acceptors (three over one). An interfacial area of 75 m^2 per cubic meter bulk medium, calibrated from the simulation of 7 to 14 day of Column 1 was used for the simulation of Column 2. The two columns have different injection flow rates (1.83 m/day for Column 1, and 0.37 m/day for Column 2). All other physical parameters were assumed to be the same as Column 1, because the sediment material is the same in both columns. Simulated concentrations of sulfate captured the measured data well (Figure 8.9-5). According to von Gunten and Zobrist (1993), the spatial resolution of the experiments did not allow for clear separation of oxygen respiration from denitrification. Virtually complete nitrate reduction took place within the first several centimeters of the flow distance. The simulation results are consistent with the nitrate observations.

Figure 8.9—5 **The simulated concentration profiles (lines) of sulfate, nitrate, and oxygen at steady-state (35 days), together with measured data of sulfate along Column 2.**

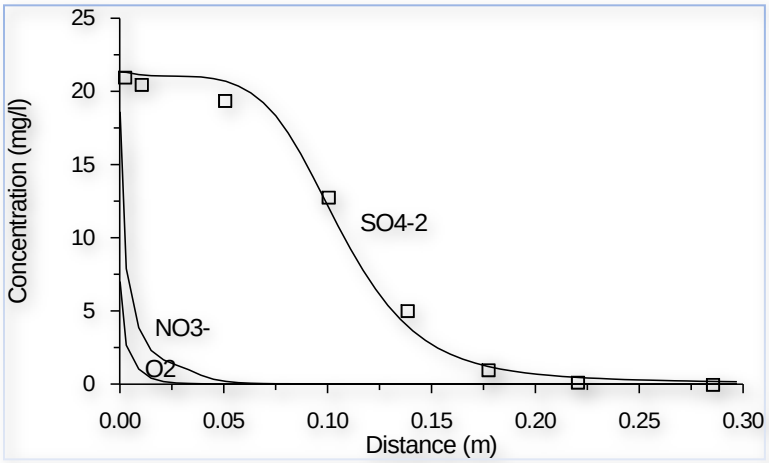

8.9.5 Interacting with the solid particle

To illustrate the possible participation of minerals in the solid particle region, and the interplay between biodegradation and geochemical reactions, two reactive minerals gypsum and goethite were assumed to be initially present in the region. SO_4 dissolved from gypsum diffuses to the immobile region and then is reduced to HS. In the solid region, Fe generated from goethite dissolution and HS diffused back from the immobile region may precipitate as pyrite. Ca from gypsum and HCO_3 from organic matter biodegradation may form calcite. The later two minerals were specified as potential secondary minerals. The parameters used for the rate law Equation (B.12) in Appendix B are presented in Table 8.9-4, only neutral mechanism was considered. Rate constants for goethite and pyrite were increased by 5 orders of magnitude from the values in Palandri and Kharaka (2004), who compiled and fitted many of the experimental data reported by a large number of investigators. The rate increase was for explicitly accounting for bacterial catalysis. The dissolution-rate constants for gypsum and calcite were assigned to be two times those of goethite and pyrite. The assigned geochemical reaction rates could be comparable to sulfate bio-reduction. Note that kinetic parameters, volume fractions and reactive surfaces in Table 8.9-4 may not reflect the field conditions, but the purpose of considering mineral dissolution and precipitation is to demonstrate the TOUGHREACT capabilities for geochemical processes. It should also be mentioned that typically the abundant iron in sediments is present as Fe(III) and it inhibits sulfate reduction. This inhibition effects is not considered here. However, in the pH range of natural waters, Fe(III) is extremely insoluble and dissolved iron exists mainly as Fe(II) (von Gunten and Zobrist, 1993).

Table 8.9—4 List of parameters for calculating kinetic rate of dissolution and precipitation of minerals.

Mineral	Chemical formula	Volume fraction (%)	Specific surface area (cm^2/g)	k ($mol/m^2/s$)
Gypsum	$CaSO_4 \bullet 2H_2O$	4	9.8	5.0×10^{-7}
Goethite	FeOOH	2	9.8	2.5×10^{-7}
Pyrite	FeS_2	0	9.8	2.5×10^{-7}
Calcite	$CaCO_3$	0	9.8	5.0×10^{-7}

The biogeochemical simulation of the multi-region model was based on sulfate reduction of Column 2, using 25% of the bulk porosity for the immobile region and an interfacial area of 75 m^2 per cubic meter medium. An arbitrary increased initial biomass concentration of 60 mg/l was used to allow for significant biodegradation from the start. Initial concentrations for all other species are set equal to a very small value. Only DOC is assumed to be available in the injection water, with a concentration of 10 mg/l. The only electron acceptor SO_4 results from the leaching of the materials in the solid region (gypsum dissolution).

Simulation results are presented in Figures 8.9-6 and 8.9-7. SO_4 concentrations increase along the distance (Figure 8.9-6a) because of gypsum dissolution (Figure 8.9-7b; Ca concentrations take on the same pattern). Significant SO_4 concentration gradients occurs between solid and immobile regions because of (1) consumption by sulfate reduction in the immobile region and (2) larger d of solid-immobile (3×10^{-5} over 2×10^{-5} m) and smaller τ (see Table 8.9-3). SO_4 concentration in the immobile region is slightly higher than that in the mobile region. HS concentrations are higher in the immobile region due to sulfate reduction there (Figure 8.9-6b), but its concentrations are reduced in the solid region resulting from the sink of pyrite precipitation (Figure 8.9-7d). HCO_3 concentrations increase (Figure 8.9-6c) and DOC decrease (Figure 8.9-6d) along the distance because of biodegradation. The difference of the latter two species among the three regions is very small.

Bacterial growth rates over the distance (Figure 8.9-7a) increase close to the inlet, because of the increase in SO_4 concentration, but later downstream decreases due to the low DOC concentrations. Biomass concentrations increase almost linearly with time. Returning to the solid region, pyrite precipitation pattern is similar to that of goethite dissolution. The former volume is slightly larger than the latter because of the slightly larger mole volume (23.94 over 20.82 cm^3/mol). Calcite was not found in the simulation for the shorter column distance, but it could form along flow path if the distance was long enough, because the HCO_3 concentrations steadily increase (Figure 8.9-6c). Gypsum dissolution promotes bio-reduction of sulfate. Then the bio-generation of HS reacts with Fe from goethite dissolution, resulting in pyrite precipitation. Geochemical processes in the solid region and micro-biological processes in the immobile region influence each other via micro-diffusion.

Figure 8.9—6 **Simulated concentrations of dissolved components in the three regions after 13 days for the biogeochemical simulation.**

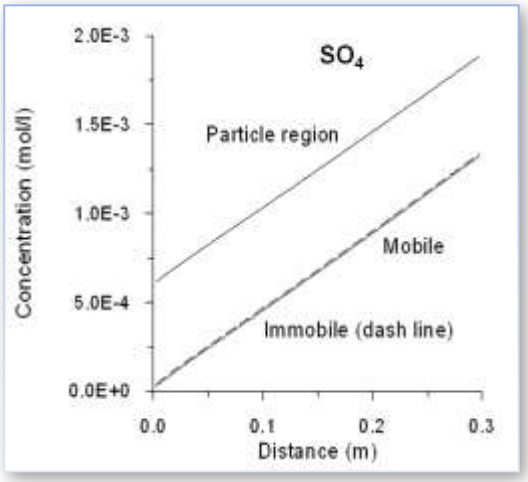

(a) SO4

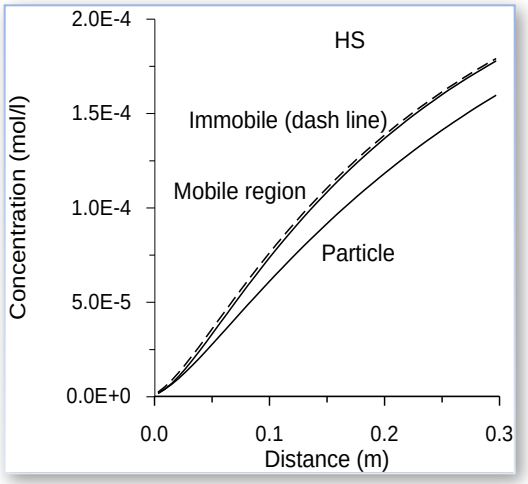

(b) HS

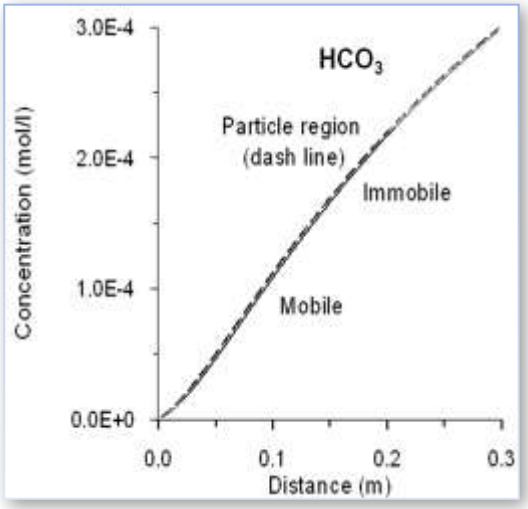

(c) HCO3

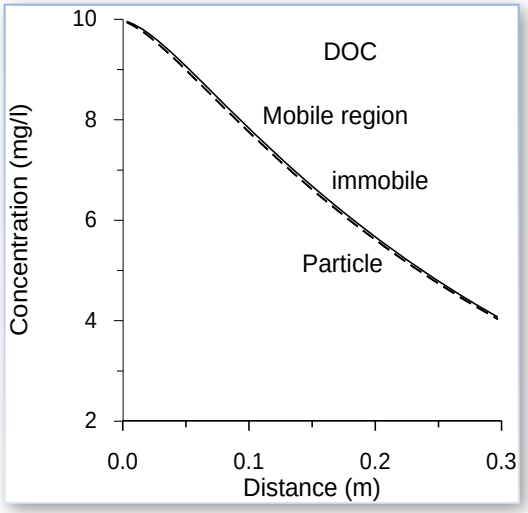

(d) DOC

Figure 8.9—7 **Simulated biomass concentrations in the immobile region (a) and mineral dissolution and precipitation in the solid region (b, c, and d) at different times.**

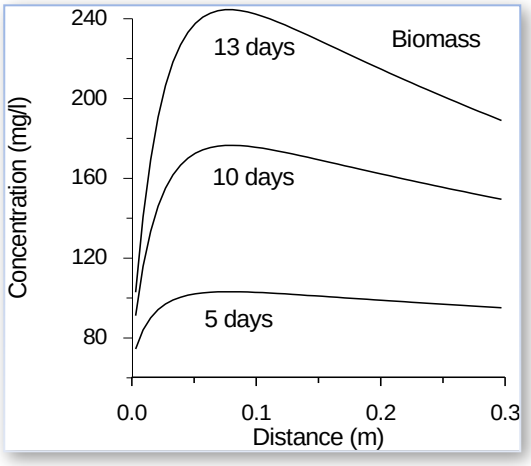

Biomass

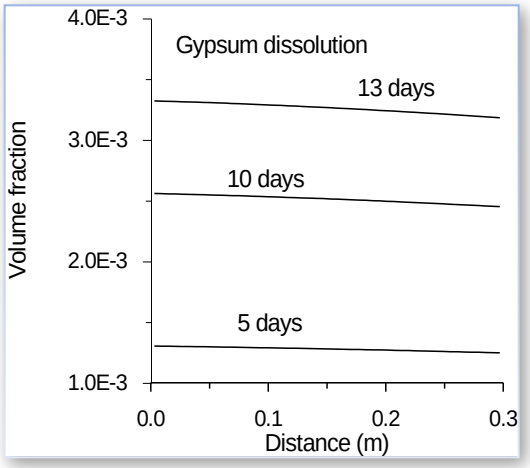

Gypsum

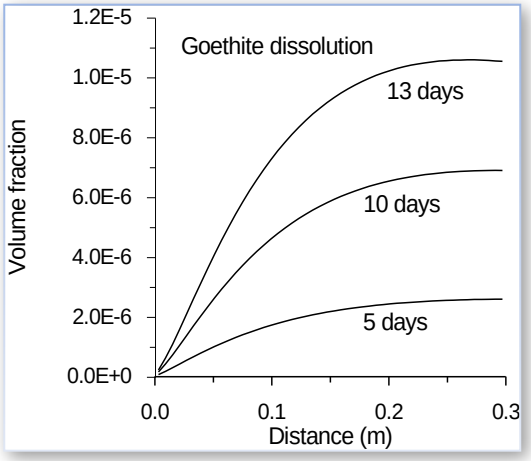

Goethite

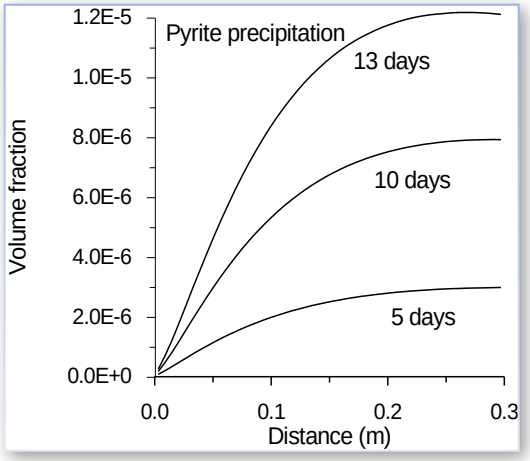

Pyrite

8.9.6 Summary

The applicability of this enhanced multi-region model for reactive transport of denitrification and sulfate reduction was evaluated by comparison with column experiments and model calibration. The matches with measured nitrate and sulfate concentrations were adjusted with the interfacial area between mobile and immobile regions. The values of 38 m^2 per cubic bulk medium for the initial period and 75 m^2 for the late period were calibrated. The match and parameter calibration suggest that TOUGHREACT can not only be a useful interpretative tool for biogeochemical experiments, but also can produce insight into the processes and parameters of microscopic diffusion and their interplay with biogeochemical reactions.

The interacting of an immobile region with solid particles consisting initially of reactive-minerals gypsum and goethite, was modeled. Gypsum dissolution promotes bio-reduction of sulfate, after which the bio-generation of HS reacts with Fe from goethite dissolution, resulting in pyrite precipitation. It has been shown that geochemical processes in the solid region and micro-biological processes in the immobile region influence each other via micro-diffusion.

The resulting biogeochemical-transport-simulation capabilities may be useful for many subsurface problems, including acidic mine drainage remediation, organic matter decomposition, oil and gas maturation, sulfite reduction in oil fields, and effective environmental remediation of groundwater contamination. However, evaluation of the model against experimental data at larger than a column, and in multi-dimensional flow fields, is recommended before to field-scale problems.

8.10 Problem 10 – Biogeochemical Cycling of Heavy Metals in Lake Sediments

This example builds on the work presented by Sengor et al. (2007a, b) on modeling the diffusive transport of heavy metals (Zn, Pb, Cu) in the sediments of Lake Coeur d'Alene, Idaho. Details on the conceptual model and implemented biogeochemical reaction network are given in Sengor et al. (2007a) and summarized below.

The sediments of Lake Coeur d'Alene have been heavily impacted by mining activities and, as a result, contain elevated concentrations of iron and heavy metals. These sediments contain significant amounts of iron hydroxides, primarily as ferrihydrite (Toevs et al., 2006; Moberly et al. 2009), together with quartz and siderite as major minerals. The microbial reductive dissolution of iron hydroxides in the sediments is thought to lead to the release of metals sorbed onto these mineral phases, generating benthic fluxes of metals from the sediments to the lake water (Balistrieri, 1998; Kuwabara et al., 2003). Deeper into the sediments, metals mobilized by reductive dissolution become immobilized by reaction with biogenic sulfide to form sulfide minerals. These coupled processes are simulated for a 1D sediment column under redox disequilibrium conditions (Figure 8.10-1).

Figure 8.10—1 Conceptual 1D diffusive biogeochemical model (Sengor et al., 2007a)

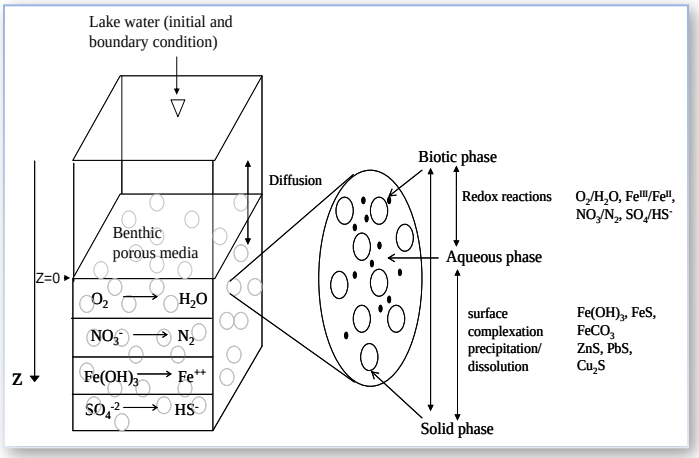

The model setup and input data are essentially unchanged from the model presented earlier (Sengor et al. 2007a), which was built using PHREEQC (Parkhurst and Appelo, 1999). The model incorporates a multicomponent biotic reaction network with multiple terminal electron acceptors (TEA) (Table 8.10-1), diffusive transport, mineral precipitation and dissolution, and surface complexation. The switch from one TEA to the next is implemented using inhibition factors (K^{in} in Table 8.10-1) in the manner proposed by Van Cappellen and Gaillard (1996). We have added to the original 1-D model the effect of sedimentation, approximated by advecting sediment solids and pore water downward at a rate decreasing with depth to mimic compaction. In addition to species originally considered for sorption onto Fe hydroxides (Zn^{2+}, Cu^{2+}, Cu^{+}, Pb^{2+}, H^{+}, Ca^{2+}, Mg^{2+}, SO_4^{2-}; Dzombak and Morel, 1990), Fe^{2+} surface complexation (Liger et al., 1999) was also added to the original model. Note that rate laws for the various biotic reactions (Table 8.10-1) are multiplied by a thermodynamic affinity term ($1 - Q/K$, where Q and K are the ion activity product and the equilibrium constant, respectively, of the reaction) that effectively shuts down the reaction if/when equilibrium is reached (at which point $Q = K$).

Table 8.10—1 Microbial reactions and rate laws (from Sengor et al., 2007a). See Table 8.10-2 for parameter values.

Microbially mediated reactions:

$CH_3COO^- + 2O_2 \rightarrow 2CO_3^{-2} + 3H^+$	R_{O2}
$CH_3COO^- + 1.6NO_3^- \rightarrow 2CO_3^{-2} + 0.8N_2 + 1.4H^+ + 0.8H_2O$	R_{NO3}
$CH_3COO^- + 8Fe^{+3} + 4H_2O \rightarrow 8Fe^{+2} + 2CO_3^{-2} + 11H^+$	R_{Fe+3}
$CH_3COO^- + SO_4^{-2} \rightarrow 2CO_3^{-2} + HS^- + 2H^+$	R_{SO4-2}

Kinetic rate laws:

$$R_{O2} = V_m^{O2} \frac{[O_2]}{[O_2] + K_s^{O2}}$$

$$R_{NO3} = V_m^{NO3} \frac{[NO_3]}{[NO_3] + K_s^{NO3}} \frac{K_{O2}^{in}}{K_{O2}^{in} + [O_2]}$$

$$R_{Fe+3}^{(*)} = V_m^{Fe} \frac{K_{O2}^{in}}{K_{O2}^{in} + [O_2]} \frac{K_{NO3}^{in}}{K_{NO3}^{in} + [NO_3]}$$

$$R_{SO4-2} = V_m^{SO4} \frac{[SO_4^{2}]}{[SO_4^{2}] + K_s^{SO4}} \frac{K_{O2}^{in}}{K_{O2}^{in} + [O_2]} \frac{K_{NO3}^{in}}{K_{NO3}^{in} + [NO_3]} \frac{K_{Fe}^{in}}{K_{Fe}^{in} + [Fe^{+3}]}$$

V_m^i	Maximum substrate utilization rate constant
K_s^i	Half saturation constant
K_i^{in}	Inhibition constants
(*)	Assumes unlimited Fe^{+3} supply from abundant solid Fe hydroxides

Table 8.10—2 **Values of parameters in Table 8.10-1 (from Sengor et al., 2007a, except for V_m^{Fe}). The value of V_m^{Fe} was recalibrated to take into account the effect Fe(II) sorption onto ferrihydrite, which was ignored in the original model.**

Parameter (units)	Model Value
V_m^{O2} (s^{-1})	5×10^{-9}
V_m^{NO3} (s^{-1})	2×10^{-10}
V_m^{Fe} (s^{-1})	15×10^{-12}
V_m^{SO4} (s^{-1})	3×10^{-9}
K_s^{O2} (molal)	2.41×10^{-5}
K_s^{NO3} (molal)	1.13×10^{-4}
K_s^{SO4} (molal)	1×10^{-3}
K_{O2}^{in} (molal)	1.61×10^{-8}
K_{NO3}^{in} (molal)	1×10^{-7}
K_{Fe}^{in} (molal)	1×10^{-8}

The top model boundary is located at the lake water-sediment interface. It is set at a fixed composition equal to the (measured) composition of lake water equilibrated with sorption sites on ferrihydrite. Transport is entirely diffusive, with a closed bottom model boundary. The simulated 1D sediment column is 45 cm long, with a grid spacing of 0.5 cm for the first top 8 cells, then increasing to 1 cm through the remainder of the column. The sedimentation rate is set at 2 cm/yr at the top of the column (Horowitz et al., 1995), and linearly decreasing to zero at the base of the column. The diffusion coefficient is low (~4×10^{-6} cm^2/s), reflecting very fine-grained sediments (Ballistrieri, 1998). Simulations are carried out for a period of about 5 years, after which nearly steady conditions prevail.

The same aqueous reaction network is modeled as in Sengor et al. (2007a) (Tables 8.10-1 and 8.10-2). Higher in the sediment column, iron-reducing bacteria reduce iron hydroxides:

$$8Fe(OH)_{3(s)} + CH_3COO^- + 15H^+ \rightarrow 8Fe^{2+} + 2HCO_3^- + 20H_2O \qquad (8.10.1)$$

This reaction leads to the release of sorbed metals (Zn, Cu, Pb). At depth, sulfate reducing bacteria produce sulfide, which can react with Fe(II) and other metals to form precipitates:

$$Fe^{2+} + CH_3COO^- + SO_4^{2-} \rightarrow FeS_{(s)} + 2HCO_3^- + H^+ \qquad (8.10.2)$$

Reactions (8.10.1) and (8.10.2) represent overall reactions that proceed though the coupling of the reaction network (Table 8.10-1) with ferrihydrite (modeled as $Fe(OH)_3$) and mackinawite (FeS, disordered) reacting at equilibrium. Sphalerite (ZnS), galena (PbS) and chalcocite (Cu_2S) are included as "proxy" phases precipitating under kinetic constraints to provide a sink for heavy metals. Siderite ($FeCO_3$) is also included as a phase reacting under kinetic constraints. The only minerals initially present in the modeled column consist of ferrihydrite and siderite, which are observed throughout the lake sediments in significant amounts (Toevs et al., 2006), likely from both detrital and diagenetic origins (Table 8.10-3).

Simulations are started with (oxic) lake water (Table 8.10-4) initially throughout the column. Redox stratification eventually develops through the microbial reaction network (Table 8.10-1), from oxic lake-water conditions at the top of the column to sulfate-reducing conditions at the bottom of the column. Kinetic reaction parameters are initially obtained from the literature, then are adjusted as necessary to best match the model results to field data (Winowiecki, 2002) (Figure 8.10-2). Note that the electron donor is taken as acetate, which is reported in pore water at ~150 µM and is assumed un-limiting.

Table 8.10—3 Minerals included in the simulation, and reaction constraints.

Mineral	Initial Amount (% Volume)	Constraint on reaction	$k \times A$ (mol s^{-1} kg^{-1}_{water})
Ferrihydrite	1.4	Equilibrium	None
FeS	none	Equilibrium	None
Siderite	10	$R_{FeCO3} = kA(Q/K-1)$	5×10^{-14}
Sphalerite[1]	none	$R_{ZnS} = kA[Zn^{+2}][H_2S](Q/K-1)^{0.01}$	2.7×10^{-3}
Galena[1]	none	$R_{PbS} = kA[Pb^{+2}][H_2S](Q/K-1)^{0.01}$	2.7×10^{-3}
Chalcocite[1]	none	$R_{Cu2S} = kA[Cu^{+}][H_2S](Q/K-1)^{0.01}$	2.7×10^{-3}

For each mineral, *k* and *A* represent the rate constant and reactive surface area, respectively, and *Q* and *K* represent the activity product and solubility product, respectively. Values of $k \times A$ were roughly calibrated, and intentionally kept low for heavy metal sulfides, which are only used here as "proxies" for precipitation in various sulfide forms. The form of the rate law for sulfides is after Rickard (1995), except for the $(1- Q/K)$ term, which was added to ensure the rate convergence to zero at equilibrium. The small exponent on this term is meant to keep it near 1 except at equilibrium when this term drops to 0.

Table 8.10—4 Input water composition (oxic lake water, from Sengor et al., 2007a).

Components	Concentration	Units
pH (25°C)	7.2	
Cl	1.95×10^{-5}	molal
$CO_{3(tot)}$	3.54×10^{-4}	molal
SO_4	5.83×10^{-5}	molal
Ca	1.37×10^{-4}	molal
Mg	8.64×10^{-5}	molal
Na	1.00×10^{-4}	molal
K	1.28×10^{-5}	molal
NO_3	8.00×10^{-5}	molal
$O_{2(aq)}$	4.25×10^{-4}	molal
Fe	3.11×10^{-9}	molal
Pb	5.31×10^{-8}	molal
Zn	8.72×10^{-6}	molal
Cu	1.18×10^{-8}	molal

Modeled concentrations trends for key species are generally consistent with measured data (Figure 8.10-2). The behavior of heavy metals is driven by desorption at shallow depth, accompanied by the microbial reductive

dissolution of ferrihydrite, and precipitation with biogenic sulfide deeper into the sediment column. In the present case, the precipitation rates of heavy metal sulfides are kept relatively low and roughly adjusted to yield metal concentrations within the range of observed concentrations. A delicate balance is predicted between the competition of FeS and $FeCO_3$ precipitation for Fe(II), and the competition of soluble (bi)sulfide complexes and sulfide mineral precipitation for biogenic sulfide. Results compare well with the original PHREEQC model developed by Sengor et al. (2007a), with small differences resulting from processes added to the original model, namely Fe(II) sorption onto ferrihydrite and sedimentation, and differences in the affinity terms on the kinetic rate laws of minerals (Table 8.10-3). This example provides a typical application of TOUGHREACT V2.0 to a complex reaction network in a shallow, low-temperature environmental system at redox disequilibrium.

Figure 8.10—2 **Concentrations of key parameters, redox species, and metals with depth from the top of the sediment column. Lines show computed values, symbols (Summer 2001: triangle symbols; Fall 2001: square symbols) are measured values by Winowiecki (2002), except for Cu (average over interval shown, from Sengor et al. 2007a).**

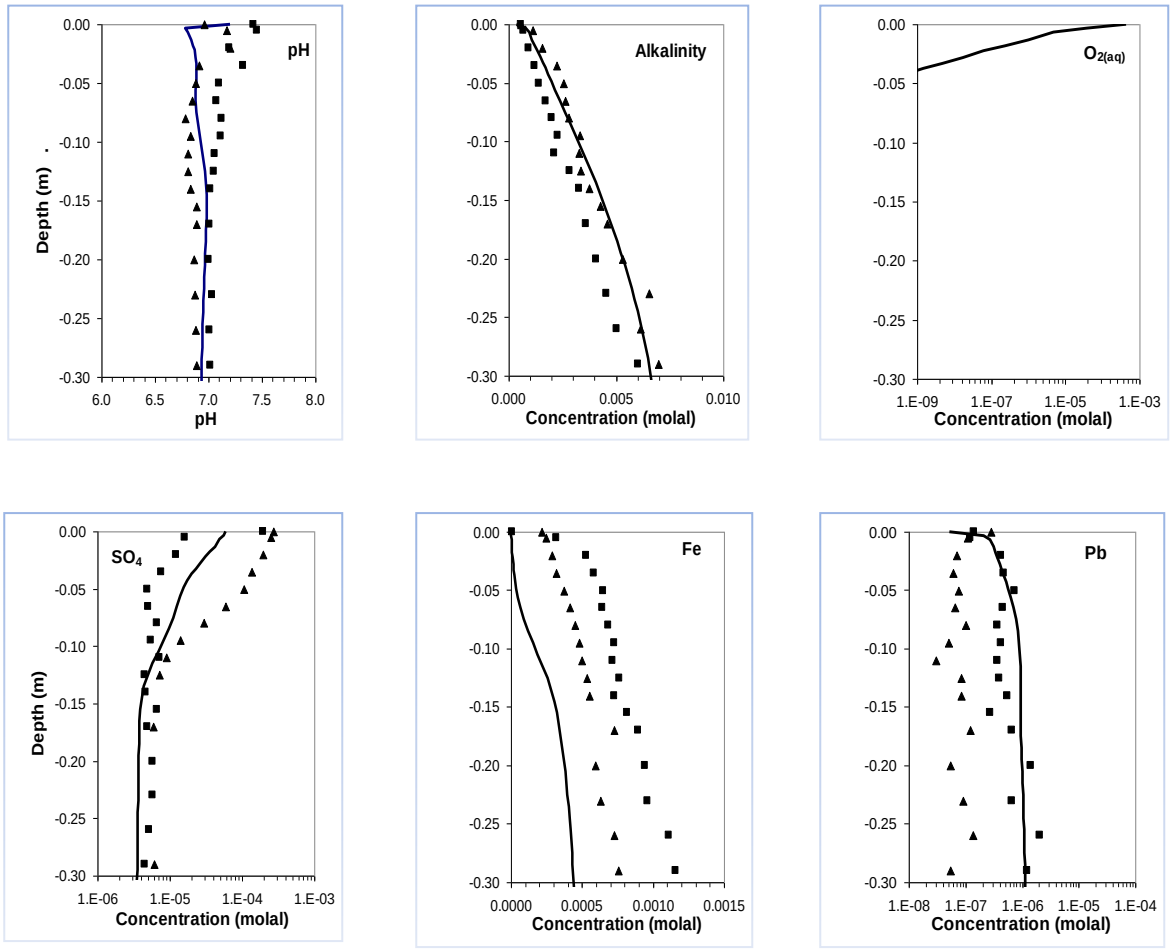

Figure 8.10—3 **Computed change in abundance of Fe minerals from the top of the sediment column. The reductive dissolution of ferrihydrite leads to an increase in Fe(II) (Figure 8.10-2) and subsequent FeS and siderite precipitation.**

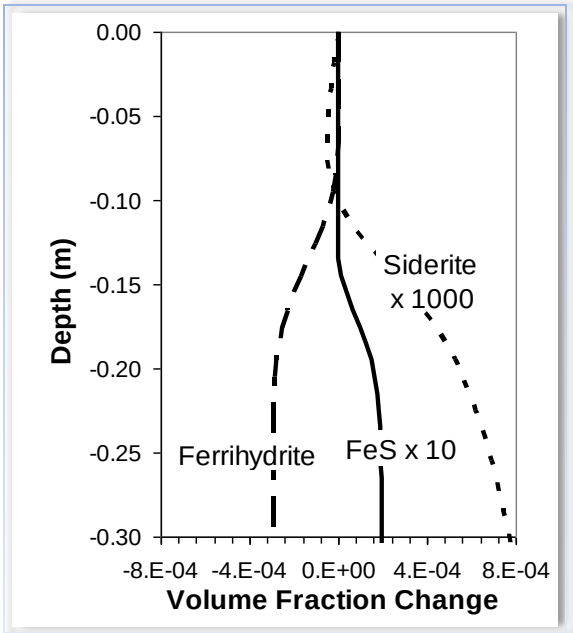

The EOS1 flow module is used for this metal cycling problem. The flow is similar to the previous examples. Here we present the solute and chemical input files in Figures 8.10-4 and 8.10-5, respectively. The complete input and output files are given in the distribution provided with the distribution files.

Figure 8.10—4 **Solute input file (solute.inp) for Problem 10.**

```
# Title
'LCdA 1D mesh1 '
# ISPIA INIBOUND ISOLVC NGAMM NGAS1 ichdump kcpl Ico2h2o  nu
    0    1       5       0    1       2     2    0       0
# SL1MIN        rcour     STIMAX    CNFACT(=1 fully implicit)
   1.00e-2   0.000    22.0        1.0
# Read input and output file names:
thermok3.01.dat                ! thermodynamic database
iter.dat                       ! iteration information
tec_conc.dat                   ! aqueous concentrations in tecplot form
tec_min.dat                    ! mineral data  in tecplot form
tec_gas.dat                    ! gas data  in tecplot form
time.dat                       ! concentrations at specific elements over time
# ITIME     WUPC    DFFUN     DFFUNG
 1.0       1.0  4.27d-10   1.0d-05
# MAXITPTR  TOLTR    MAXITPCH  TOLCH    MAXITPAD  TOLAD      TOLDC    TOLDR
   1     0.100E-05    500   0.100E-05   30      0.100E-05  0.00E-00 0.00E-00
# NWTI NWNOD NWCOM NWMIN NWAQ NWADS NWEXC iconflag(=1:mol/l) minflag(=1:Vf)
200    2     19    6    36   17    0        0                  1
# Nodes for which to output data in time file (15a5):
A21 1BA1 1
# Primary (total) aqueous species for which to output concentrations
3 4 5 6 7 8 9 10 11 12 13 14 15 16 17 18 19 20 21
# Minerals for which to output data in time and plot files:
1 2 3 4 5 6
# Individual species for which to output concentrations in time and plot files:
```

```
8 15 16 18 31 32 33 34 35 36 46 47 48 67 70 75 93 94 95 96 104 105 107 108 109 112 113 114
115 116 117 118 119 20 21 6
# Adsorption species for which to output concentrations in time and plot files:
1 2 3 4 5 6 7 8 9 10 11 12 13 14 15 16 17
# Exchange species for which to output concentrations in time and plot files:

# IZIWDF IZBWDF IZMIDF IZGSDF IZADDF IZEXDF IZPPDF IZKDDF (default)
    1    0        1    0        1      0      0     0
# ELEM NSEQ NADD IZIW IZBW IZMI IZGS IZAD IZEX izpp IZKD (chemical zones)

# this "end" record is needed now
end
```

Figure 8.10—5 Chemical input file (chemical.inp) for the metal cycling problem.

```
# Title
LCdA 1D mesh1
# ---------------------------------------------------------------------------
# DEFINITION OF THE GEOCHEMICAL SYSTEM
# PRIMARY AQUEOUS SPECIES
'h2o'           0
'h+'            0
'hco3-'         0
'ca+2'          0
'cl-'           0
'cu+'         0
'fe+3'          0
'fe+2'          0
'k+'            0
'mg+2'          0
'no3-'              0
'na+'           0
'n2(aq)'        0
'o2(aq)'        0
'pb+2'          0
'hs-'           0
'so4-2'         0
'zn+2'          0
'Ac-'           0
'hfo_soh'       2  'ferrihydrite' 4.428E-07 3
'hfo_woh'       2  'ferrihydrite' 1.780E-05 3
'*'
# AQUEOUS KINETICS
 4                ! total number of kinetic aqueous reactions
  1   !Oxygen TEA
       4   -1.0000 'Ac-' -2.0000 'O2(aq)'  2.0000 'HCO3-'  1.000 'H+'  0.0 0.0 0.0
       1      1                    !kinetic model index,  No.mechanism
          5.0d-09                  !forward rate constant (mol/kg,s)
          0                        !species in product term
          1  'O2(aq)' 1  2.41d-5    !species in monod terms,
          0                        !species in inhibition terms,
  2   !NO3 TEA
       6   -1.0000 'Ac-' -1.6000 'NO3-' -0.6000 'H+' 2.0000 'HCO3-' 0.8 'N2(aq)'  0.8 'H2O'
       1      1                    !kinetic model index,  No.mechanism
          2.0d-10                  !forward rate constant (mol/kg,s)
          0                        !species in product term
          1  'NO3-'   1  1.13d-4    !species in monod terms,
          1  'O2(aq)' 1  1.61d-8    !species in inhibition terms,
  3   !FeIII TEA
       6   -1.0000 'Ac-' -8.000 'Fe+++' -4.000 'H2O' 8.000 'Fe++' 2.0000 'HCO3-'  9.000
'H+'
       1      1                    !kinetic model index,  No.mechanism
          3.0d-12                  !forward rate constant (mol/kg,s)
          0                        !species in product term
          0                        !species in monod terms,
          2  'O2(aq)' 1  1.61d-8 'NO3-' 1  1.d-7   !species in inhibition terms
  4
       4   -1.0000 'Ac-'  -1.0000 'SO4--'  2.0000 'HCO3-'  1.000 'HS-'
```

```
       1      1                    !kinetic model index,  No.mechanism
          3.0d-09                  !forward rate constant (mol/kg,s)
          0                        !species in product term
          1 'SO4--'   1  1.e-3     !species in monod terms,
          3 'O2(aq)'  1  1.61e-8 'NO3-' 1  1.d-7  'Fe+++' 1  1.d-8
'*'
# AQUEOUS COMPLEXES
'*'
# MINERALS         ! equilibrium mineral goes first
'ferrihydrite' 0  0  0   0
0. 0. 0.
'FeS_m' 0  0  0   0
0. 0. 0.
'siderite'   1 3 0  0
1.00e-15 0 1.0 1.0 48.1  0.0 0.0 0.0                 !lowered to get FeS ppt
1.00e-15 0 1.0 1.0 48.1  0.0 0.0 0.0  1.e-6   0      !lowered to get FeS ppt
0.0 0.0 0.0
'chalcocite'  1    3   0    0
              1.e-15     0   1.0  1.0  50.    0.0  0.0  0.0
              0.E-00     2   0.01 1.0  0.0    0.0  0.0  0.0  1.e-6  0
                         1
                         1.e-4    50.   3  'h+' 1. 'hs-' 1. 'cu+' 2.
0.0 0.0 0.0
'galena1'      1    3   0    0
              1.e-15     0   1.0  1.0  50.    0.0  0.0  0.0
              0.E-00     2  0.01  1.0  0.0    0.0  0.0  0.0  1.e-6  0
                         1
                         1.e-4    50.   3  'h+' 1. 'hs-' 1. 'pb+2' 1.
0.0 0.0 0.0
'sphalerite'  1    3   0    0
              1.e-15     0   1.0  1.0  50.    0.0  0.0  0.0
              0.E-00     2   0.01 1.0  0.0    0.0  0.0  0.0  1.e-6  0
                         1
                         1.e-4    50.   3  'h+' 1. 'hs-' 1. 'zn+2' 1.
0.0 0.0 0.0
'*'               0      0    0            0
# GASES
'CO2(g)'
'*'
# SURFACE COMPLEXES
'*'
# species with Kd and decay    decay constant(1/s)
'*'                      0.0      0.0      0.0
# EXCHANGEABLE CATIONS
'*'
# ------------------------------------------------------------------------------
# INITIAL AND BOUDARY WATER TYPES
1   0   ! niwtype, nbwtype = number of initial and boundary waters
# Index  Speciation T(C)  P(bar)
1            25.0         1.0
#       icon     guess     ctot             constrain
'h2o'     1   0.1000E+01 0.1000E+01          '*'     0.0
'h+'      3   3.981E-08  6.30957E-08         '*'     0.0
'hco3-'   1   3.877e-04  3.535e-04           '*'     0.0
'ca+2'    1   6.239e-04  1.372e-04           '*'     0.0
'cl-'     1   7.899e-05  1.946e-05           '*'     0.0
'cu+'   1   1.180e-08  1.180e-08           '*'     0.0
'fe+3'    2   1.650e-05  3.009e-09 'Ferrihydrite'     0.0
'fe+2'    1   1.183e-05  2.034e-19           '*'     0.0
'k+'      1   1.586e-04  1.279e-05           '*'     0.0
'mg+2'    1   3.004e-04  8.641e-05           '*'     0.0
'no3-'        1   8.000e-05  8.000e-05           '*'     0.0
'na+'     1   1.001e-04  1.000e-04           '*'     0.0
'n2(aq)'  1   9.150e-19  9.150e-19           '*'     0.0
'o2(aq)'  1   2.5351E-53 4.249e-04           '*'     0.0
'pb+2'    1   6.275e-07  5.309e-08           '*'     0.0
'hs-'     1   1.000e-42  2.207e-28           '*'     0.0
'so4-2'   1   6.142e-04  5.830e-05           '*'     0.0
'zn+2'    1   2.906e-05  8.717e-06           '*'     0.0
'Ac-'     1   7.e-3      7.e-3               '*'     0.0
'hfo_soh' 1   0.1E-07    1.0000              '*'     0.0
```

```
'hfo_woh' 1   0.1e-07    1.0000              '*'     0.0
'*'
# ------------------------------------------------------------------------------
# INITIAL MINERAL ZONES
 1                              ! nmtype= number of mineral zones
 1                            ! imtype
#  mineral         volume fraction
'ferrihydrite'   1.3915e-2    0
'FeS_m'          0.0      0.0
'siderite'       0.1      1
0.0           1107.    0        !area cm2/g assumes 10 micron spherical grains
'chalcocite'       0.0    1
0.0           470.     2        !area m2/3  *por*dens_w to = about 1 for rate law
'galena1'       0.0      1
0.0           470.     2        !area m2/3  *por*dens_w to = about 1 for rate law
'sphalerite'       0.0    1
0.0           470.     2        !area m2/3  *por*dens_w to = about 1 for rate law
'*'
# ------------------------------------------------------------------------------
# INITIAL gas ZONES
'*'
# ------------------------------------------------------------------------------
# Permeability-Porosity Zones
'*'
# ------------------------------------------------------------------------------
# INITIAL SURFACE ADSORPTION ZONES
1                !ndtype= number of sorption zones
# zone       ad.surf.(cm2/g)  total ad.sites (mol/m2)
1  1    ! zone index, equilibration flag
'hfo_soh'    0    2.049E+06
'hfo_woh'    0    2.049E+06
'*'
# ----------------------------------------if Sden=0 Kd store retardation factor
# INITIAL LINEAR EQUILIBRIUM Kd ZONE
'*'
# ------------------------------------------------------------------------------
# 'INITIAL ZONES OF CATION EXCHANGE'
'*'
# ------------------------------------------------------------------------------
# end
```

8.11 Problem 11 – Heater Test Problem (EOS4 or EOS3)

This test problem of a large-scale *in-situ* thermal test at Yucca Mountain (Nevada) provides a complex 2-D example of coupled thermal, hydrological, and chemical (THC) processes in unsaturated fractured rock. The model setup incorporates many aspects of the capabilities of both TOUGH2 and TOUGHREACT, including time-dependent heat generation, dual-permeability, vapor pressure lowering (EOS4), numerous aqueous, gaseous, and mineral species, CO_2 diffusion (P- and T-dependent), and coupling of permeability and capillary pressure to porosity changes.

8.11.1 Background

The Drift Scale Test (DST) is the second underground thermal test carried out in the Exploratory Studies Facility (ESF) at Yucca Mountain, Nevada. The purpose of the test was to evaluate the coupled thermal, hydrological, chemical, and mechanical processes that take place in unsaturated fractured tuff over a range of temperatures (approximately 25°C to 200°C). Briefly, the DST consists of an approximately 50 m long drift that is

5 m in diameter. Nine electrical floor canister heaters were placed in this drift (the Heated Drift) to simulate nuclear-waste-bearing containers. Electrical heaters were also placed in a series of horizontal boreholes (wing heaters) drilled perpendicular outward from the central axis of the Heated Drift. These heaters were emplaced to simulate the effect of adjacent emplacement drifts. The DST heaters were activated on December 3, 1997, with a planned period of 4 years of heating, followed by 4 years of cooling. After just over 4 years, the heaters were switched off on January 14, 2002, and since that time the test area has been slowly cooling.

The first predictive model for THC processes in the DST was begun just prior to the initiation of heating in late 1997 with the final predictive report completed several months after the test had begun (Sonnenthal et al. 1998; Xu et al., 2001). The 2-D numerical grid, and thermal and hydrological properties for the THC model were based on the original TH model developed for the DST (Birkholzer and Tsang, 1997; 1998). Model development, results, and data shown in this test problem are based on Spycher et al. (2003b), and Sonnenthal et al. (2005).

8.11.2 Conceptual model for THC processes

The evolution of the chemical regime in the unsaturated zone surrounding a heat source is closely related to the spatial distribution of temperature and the transport of water and vapor. An important aspect of the unsaturated fractured tuff at Yucca Mountain is that the highly permeable fractures are nearly dry, whereas the low permeability and porosity rock matrix has a water saturation of about 90 percent. Heating of the rock results in boiling of the matrix pore water, transport of water vapor into fractures, and condensation along fracture walls. The numerical model for reaction-transport processes in the fractured welded tuffs must account for the different rates of transport in fractures, compared to a much less permeable rock matrix. Transport rates greater than the rate of equilibration via diffusion leads to disequilibrium between waters in fractures and matrix. Because the system is unsaturated, and undergoes boiling, the transport of gaseous species, especially CO_2, is an important consideration. The model must also capture the differences in initial mineralogy in fractures and matrix and their evolution.

In order to handle separate yet interacting processes in fractures and matrix, the dual permeability method has been adopted, such that each grid block is divided into matrix and fracture continua, characterized by their own pressure, temperature, liquid saturation, water and gas chemistry, and mineralogy. In the dual-permeability model, the fracture continuum is considered as co-located but interacting with the matrix continuum, in terms of the flow of heat, water, and vapor through advection, diffusion, and conduction (for heat). The aqueous and gaseous species are transported via advection and molecular diffusion between the fractures and matrix. Each continuum has its own well-defined initial physical and chemical properties.

8.11.3 Drift Scale Test 2-D numerical grid

The two-dimensional dual-permeability numerical grid for the DST represents a vertical cross section through the Heated Drift at a distance approximately 30 m from the bulkhead, separating the Heated Drift from the Access Drift (Figure 8.11-.1a). The mesh consists of 4,490 grid blocks, including fracture and matrix (Figure 8.11-

1a and b). The top boundary is approximately 99 m above the drift center, with the bottom boundary at approximately 157 m below the center. The DST includes a plane of linear wing heaters on each side of the drift that are given small grid blocks in the model. Small grid blocks are also employed adjacent to the wing heaters and drift wall to capture the strong gradients in temperature and liquid saturation in these regions (Figure 8.11-1b). Radial mesh blocks in the drift interior were removed from the original mesh and replaced near the drift base by Cartesian grid blocks to represent the concrete invert (Figure 8.11-1b). The Heated Drift grid block is connected directly to the Heater Test Alcove grid block. The connection area and distance were adjusted so that heat loss from the drift resulted in roughly similar crown temperatures to the maximum observed values. In the approximate location of the observation drift, the grid block volumes were increased to a large value to represent connection to the atmosphere. The distances from the drift center grid block and the connecting elements were modified to represent the true distance, so that heat could be applied to the drift center to approximate the effect of the electrical canister heaters.

Figure 8.11—1 Three-dimensional schematic diagram of the DST showing perspective view of 2-D numerical mesh for DST THC model simulations (mesh extends in all directions from area shown).

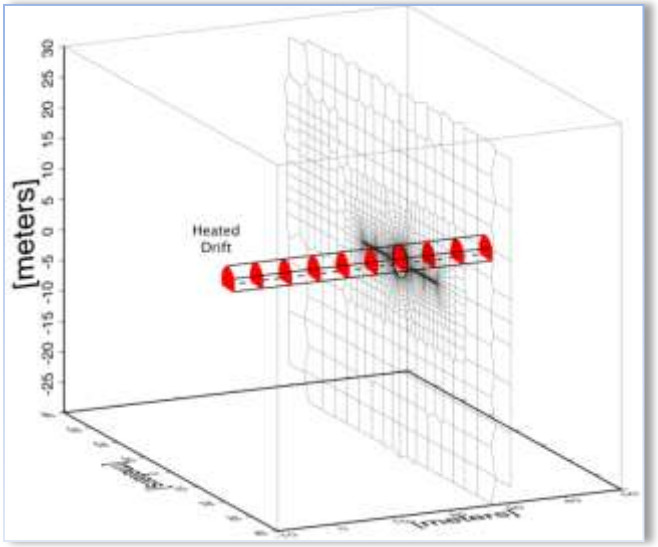

Figure 8.11—2 Enlarged view of the numerical mesh showing the locations of grid blocks representing the heated drift, wing heaters, and concrete invert.

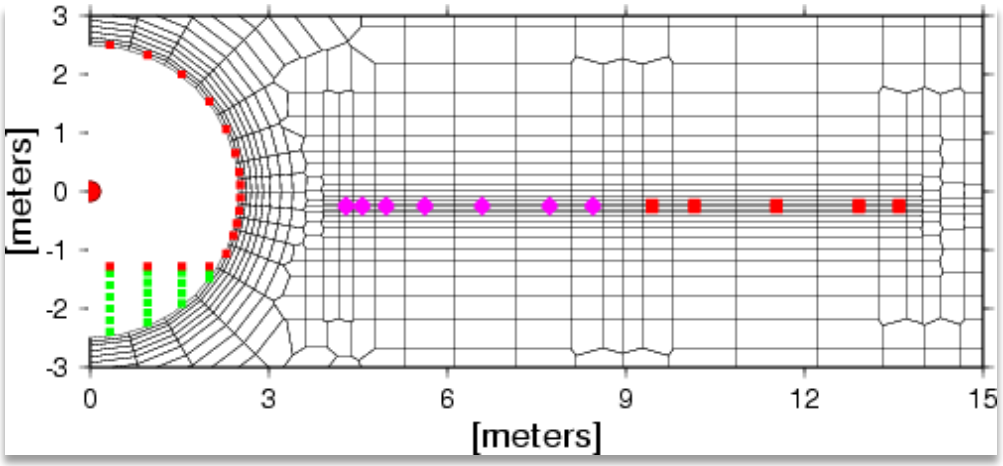

NOTE: Inner (violet diamonds closer to drift) and outer wing heater (red squares) indicate grid block coordinates. Heat was applied to the drift center. Green squares indicate grid block locations for the concrete invert.

In the Heated Drift, heat was applied solely to the drift-center grid block, which is connected to all surrounding grid blocks. The wing heaters are split into inner and outer zones, with more power applied to the outer zone to approximate the presence of an adjacent parallel drift. The positions of grid blocks representing heaters are shown in Figure 8.11-1b. The heating schedule was based on step-wise averages of the 10-day incremented power data. A 9-month initial period is set to the ambient temperature, corresponding approximately to the time that was required to set up the test. Intentional power reductions were directly accounted from the power data. Estimates were made of the duration of the longer (approximately greater than 1/2 day) temporary power outages. Table 8.11-1 gives the step-wise averaged power data implemented in the model simulations in the GENER file. Each time in Table 8.11-1 represents the initiation of a specific period of heating or power loss that continues until the succeeding time. The simulation can be run for the full period of heating plus a 4-year period of cooling (shown by the hypothetical end time at the base of Table 8.11-1). Depending on the speed of floating point calculations on a particular computer, the full simulation could take up to a few days or longer. The complexity of this heating schedule provides a good example of stepwise heat generation in TOUGH2/TOUGHREACT.

Table 8.11—1 Step-Wise Averaged Power Data

Date	Time (s)	Time (days)	Canister Power (watts)	WH (inner) Power (watts)	WH (outer) Power (watts)	Comments
3/5/97	0.00000E+00	0.00	0.0000	0.0000	0.0000	pre-test
12/3/97	2.35872E+07	273.00	1091.3740	1232.4007	1626.7690	heaters turned on
3/15/98	3.24000E+07	375.00	1091.3740	0.0000	0.0000	outage - right rib
3/16/98	3.25080E+07	376.25	1091.3740	1232.4007	1626.7690	
4/12/98	3.48192E+07	403.00	1077.9972	1198.5773	1582.1220	
8/10/98	4.51872E+07	523.00	1119.6842	1201.8035	1586.3807	
1/27/99	5.98752E+07	693.00	0.0000	0.0000	0.0000	power outage
1/27/99	5.99400E+07	693.75	1123.5789	1204.4465	1589.8693	
2/16/99	6.16032E+07	713.00	1102.5965	1189.0805	1569.5862	
5/27/99	7.02432E+07	813.00	0.0000	0.0000	0.0000	power outage
5/27/99	7.03080E+07	813.75	1102.5965	1189.0805	1569.5862	
5/29/99	7.04160E+07	815.00	0.0000	0.0000	0.0000	power outage
5/30/99	7.04808E+07	815.75	1087.8653	1155.5245	1525.2923	
6/18/99	7.21440E+07	835.00	0.0000	0.0000	0.0000	power outage
6/19/99	7.22088E+07	835.75	1087.8653	1155.5245	1525.2923	
7/9/99	7.39584E+07	856.00	0.0000	0.0000	0.0000	power outage
7/15/99	7.44768E+07	862.00	1087.8653	1155.5245	1525.2923	
8/27/99	7.81920E+07	905.00	0.0000	0.0000	0.0000	power outage
8/29/99	7.83216E+07	906.50	1087.8653	1155.5245	1525.2923	
11/22/99	8.57088E+07	992.00	1087.8653	0.0000	0.0000	outage - right rib
11/24/99	8.58816E+07	994.00	1087.8653	1155.5245	1525.2923	
2/11/00	9.27072E+07	1073.00	0.0000	0.0000	0.0000	power outage
2/11/00	9.27720E+07	1073.75	1078.7421	1184.6642	1563.7568	
3/2/00	9.44352E+07	1093.00	1029.1930	1115.3660	1472.2831	power reduction
3/12/00	9.52992E+07	1103.00	0.0000	0.0000	0.0000	power loss
3/13/00	9.54072E+07	1104.25	1029.1930	1115.3660	1472.2831	
5/2/00	9.97056E+07	1154.00	964.5263	1040.2813	1373.1713	power reduction
8/15/00	1.08778E+08	1259.00	917.3463	978.6397	1291.9364	power reduction
1/20/01	1.22429E+08	1417.00	0.0000	0.0000	0.0000	power outage
1/21/01	1.22515E+08	1418.00	917.3463	978.6397	1291.9364	
5/1/01	1.31155E+08	1518.00	875.5711	925.4672	1221.6168	power reduction
7/1/01	1.36426E+08	1579.00	0.0000	0.0000	0.0000	power outage
7/1/01	1.36490E+08	1579.75	875.5711	925.4672	1221.6168	
8/22/01	1.40918E+08	1631.00	826.8171	875.8317	1156.0979	power reduction
1/14/02	1.53446E+08	1776.00	0.0000	0.0000	0.0000	heaters turned off
1/14/06	2.79677E+08	3237.00	0.0000	0.0000	0.0000	cooling period end

8.11.4 Hydrological and thermal parameters

Values of hydrological and thermal input data are listed in Table 8.11-2. The fracture tortuosity (0.7) is based on models of in situ testing data. This value was further modified for fracture-fracture connections by multiplication of the tortuosity by the fracture porosity of the bulk rock. This operation yields a better approximation for the fracture-to-fracture interconnection area (only for calculation of diffusive fluxes; the entire grid block connection area is used for calculating advective fluxes, because the bulk fracture permeability is used for flow calculations). The capillary pressure in both fractures and matrix must reach some maximum, finite value upon complete dryout (zero liquid saturation). For fractures and matrix in the Tptpmn and Tptpll lithostratigraphic units (model units tsw34 and tsw35, respectively), the limit is set by the calculated slope of the Pcap versus liquid saturation curve at a liquid saturation value equal to Sr + ε. For these units, ε values for the matrix yield maximum Pcap values of 108 Pa (Table 8.11-2); for fractures, ε is set to 0.01 (maximum Pcap values around 103–104 Pa). These specific implementations of the van Genuchten equations are invoked by setting the MOPR(5) parameter to "2", in addition to the specific values given in the ROCKS block.

Table 8.11—2 Hydrological and thermal properties

Model Layer > Lithostratigraphic Unit >		tsw33 Tptpul	tsw34 Tptpmn	tsw35 Tptpll
MATRIX DATA				
permeability	km (m2)	6.57E-18	1.77E-19	4.48E-18
porosity	ϕ_m	0.1425	0.1287	0.1486
van Genuchten α	α_m (1/Pa)	6.17E-6	8.45E-6	1.08E-5
van Genuchten m (or λ)	m_m	0.283	0.317	0.216
residual saturation	Slr_m	0.12	0.19	0.12
satiated saturation	Sls_m	1.00	1.00	1.00
epsilon (for max Pcap)	ε	0.138	0.091	0.216
rock grain density	ρ_g (kg/m3)	2358	2466	2325
rock grain specific heat	Cp (J/kg-K)	985	985	985
dry conductivity	λdry (W/m-K)	1.164*	1.419*	1.278*
wet conductivity	λwet (W/m-K)	1.675*	2.074*	1.890*
tortuosity	τ	0.2	0.2	0.2
FRACTURE DATA[1]				
permeability	k_f (m^2)	7.80E-13	3.30E-13	9.10E-13
porosity	ϕ_f	5.8E-3	8.5E-3	9.6E-3
van Genuchten α	α_f (1/Pa)	1.59E-3	1.04E-4	1.02E-4
van Genuchten m (or λ)	m_f	0.633	0.633	0.633
residual saturation	S_{lrf}	0.01	0.01	0.01
satiated saturation	S_{lsf}	1.00	1.00	1.00
active fracture parameter	Gamma	0.60	0.57	0.57
Frequency	f (1/m)	0.81	4.32	3.16
fracture to matrix area	A (m^2/m^3)	4.44	13.54	9.68
Tortuosity	t	0.7	0.7	0.7
epsilon (for max P_{cap})	ε	0.01	0.01	0.01

NOTE: [1] Fracture thermal properties are derived using matrix properties.
* Bulk conductivities converted from grain conductivity values and lithophysal porosities, using $K_{bulk} = K_{grain} (1-\phi_{lith}) + \phi_{lith} K_{air}$, with K_{air} = 0.028 (W/m-K) (see Spycher et al., 2003b).

The thermal conductivities of fracture and matrix grid blocks are calculated assuming a linear interpolation between dry and wet conductivities as a function of liquid saturation. These are the thermal conductivities for the solid + fluid system. For fractures, thermal conductivities are multiplied by the fracture porosity to account for the correct fracture-to-fracture connection area in calculations of heat conduction (i.e., this is needed because full grid block areas are input into the model). Fracture thermal conductivities are also reduced by a factor of 10 to account for the limited spatial continuity and connectivity between fracture grid blocks. The volume of the fracture continuum is, however, only a small fraction of the matrix continuum. Therefore heat conduction occurs primarily through the matrix continuum and, as a result, the model is not sensitive to the amount of heat conduction in fractures.

8.11.5 Geochemical input data

Thermodynamic data and kinetic data are provided in the thermok1.01.dat and the chemical.inp files, respectively. Equilibrium and kinetic mineral-water reactions are treated in this test problem. Different representations for reactive surface areas of minerals in fractures and in the porous rock matrix are provided in the chemical.inp file. In most cases, the chemical and physical properties of minerals that form solid solutions are approximated by their individual endmember compositions and properties. An ideal solid-solution model was implemented for smectite (Na, Ca, and Mg endmembers), with each endmember's activity equaling its mole fraction. Treating the smectite as a solid solution, results in individual smectite endmembers either all dissolving or all precipitating, providing a better physical representation of dissolution/precipitation processes. Feldspar solid solutions are not considered because albite (Na-feldspar) and anorthite (Ca-feldspar) are generally strongly undersaturated in the simulations, and thus their dissolution rates are governed primarily by the kinetic rate constant rather than the saturation index. Coupling of permeability to mineral precipitation for fractures is given as a function of the hydraulic aperture and fracture porosity for each rock type (see Appendix F). For the rock matrix it is given as a relation to porosity, using a simplified form of the Kozeny-Carman equation. Coupling of capillary pressure to porosity and permeability is performed using Leverett scaling and “turned on” by setting the MOPR(6) parameter in the flow.inp file to “1”.

8.11.6 Initial and boundary conditions: Hydrological and thermal

The top and bottom boundaries were set to constant temperature, pressure, and liquid saturation, based on steady-state values obtained from simulations of a 1-D column extending from the land surface to the water table. The top boundary of the 2-D model extends 150 m above and below the drift center, but does not reach either the land surface or the water table. Under these conditions, the percolation flux at the top boundary is approximately 0.5 mm/yr. The bottom boundary condition is open to gas and to liquid flow. The side boundaries of the domain are located 81.5 m away from the drift center on each side (outside of the test influence area) and are no-flux for mass and heat. The air pressure and temperature in the observation drift are set to constant values. The Heated Drift wall

is open to advection and conduction of heat and mass (e.g., air, water vapor, and CO_2). The INCON file provides the steady-state thermohydrological conditions in EOS3 format. Vapor-pressure lowering (EOS4) is implemented by setting MOP(19) = 2, and the simulation can be run using either EOS module.

8.11.7 Initial and boundary conditions: Geochemical

Aqueous and gaseous species concentrations in the rock were initially set to uniform values, based on the measured pore water composition and calculated equilibrium values for CO_2 and some aqueous species. The Heater Alcove and Observation Drift CO_2 concentrations were fixed to approximately that of the atmosphere. The Heated Drift CO_2 concentration was initially set to the same value as that in the Observation Drift, but was allowed to exchange CO_2 with the Heater Test Alcove and with the surrounding rock. All initial geochemical conditions are provided in the chemical.inp and solute.inp files. Both the top and bottom boundary conditions are open to gas and aqueous species transport. The top and bottom boundaries were also set so that no mineral reactions take place (and therefore no changes in aqueous species concentrations occur as a result of mineral-water reactions). Their volumes were set to extremely large values, so that they act essentially as constant concentration boundaries. The side boundaries are no-flux for gas and aqueous-species transport.

8.11.8 Simulation parameters

The maximum simulation time for this test problem is set in the flow.inp file to 2.75 years (0.75 preheating period plus 2 years of heating), although the GENER file includes the full 8.65 year periods of preheating, heating, and cooling. The maximum time step is set to one day, so that errors due to the non-sequential iteration method, in particular related to gas phase CO_2 diffusion and rapid reaction rates, are reduced.

The corresponding input and some output files are given in the distribution provided with the distribution files. To shorten the simulation time for installation, the simulation time step variable, MCYC, in the PARAM input block of flow.inp is specified as 99. For the full simulation, users can reset MCYC to 9999. In TOUGHREACT, if MCYC = 9999, the simulation time is not controlled by MCYC, and is only controlled by TIMAX in Record PARAM.2 (see section 6.1). Parts of output files for fluid flow, aqueous chemical concentrations, and changes of mineral abundances are given in Figures 8.11-2, 8.11-3 and 8.11-4.

Figure 8.11—3 Part of file flow.out for Problem 11.

```
@@@@@@@@@@@@@@@@@@@@@@@@@@@@@@@@@@@@@@@@@@@@@@@@@@@@@@@@@@@@@@@@@@@@@@@@@@@@@@@@@@@@

  TOTAL TIME    KCYC    ITER  ITERC     KON     DX1M          DX2M          DX3M
 0.31557E+08     452       3   1759       2 0.110280E+03 0.234404E-01 0.559788E+02

@@@@@@@@@@@@@@@@@@@@@@@@@@@@@@@@@@@@@@@@@@@@@@@@@@@@@@@@@@@@@@@@@@@@@@@@@@@@@@@@@@@@

ELEM.  INDEX     P           T          SG          SL        XAIRG       XAIRL

f   5      1 0.88815E+05 0.87788E+02 0.98095E+00 0.19048E-01 0.37584E+00 0.39236E-05
m   5      2 0.91054E+05 0.87781E+02 0.26298E-01 0.97370E+00 0.39683E+00 0.42858E-05
f   6      3 0.88815E+05 0.86727E+02 0.98002E+00 0.19978E-01 0.40969E+00 0.43392E-05
m   6      4 0.90812E+05 0.86727E+02 0.25291E-01 0.97471E+00 0.42704E+00 0.46600E-05
f   7      5 0.88815E+05 0.85060E+02 0.97865E+00 0.21353E-01 0.45882E+00 0.49647E-05
m   7      6 0.90903E+05 0.85060E+02 0.24586E-01 0.97541E+00 0.47509E+00 0.53002E-05
f   8      7 0.88815E+05 0.83025E+02 0.97701E+00 0.22987E-01 0.51274E+00 0.56833E-05
m   8      8 0.91212E+05 0.83025E+02 0.24191E-01 0.97581E+00 0.52910E+00 0.60685E-05
f   9      9 0.88815E+05 0.81057E+02 0.97544E+00 0.24561E-01 0.55934E+00 0.63334E-05
m   9     10 0.91514E+05 0.81057E+02 0.23919E-01 0.97608E+00 0.57559E+00 0.67672E-05
f  10     11 0.88815E+05 0.79162E+02 0.97390E+00 0.26102E-01 0.59969E+00 0.69198E-05
m  10     12 0.91805E+05 0.79162E+02 0.23734E-01 0.97627E+00 0.61569E+00 0.74003E-05
f  11     13 0.88816E+05 0.76461E+02 0.97164E+00 0.28361E-01 0.65061E+00 0.76926E-05
m  11     14 0.92207E+05 0.76461E+02 0.23575E-01 0.97643E+00 0.66601E+00 0.82377E-05
f  12     15 0.88817E+05 0.73117E+02 0.96875E+00 0.31246E-01 0.70448E+00 0.85536E-05
m  12     16 0.92704E+05 0.73117E+02 0.23531E-01 0.97647E+00 0.71894E+00 0.91785E-05
```

Figure 8.11—4 Part of file tec_conc.dat for Problem 11, giving concentrations (mol/l) of aqueous components after t = 1 yr.

```
X      Z       pH       ca+2        mg+2        na+          cl-         sio2(aq)

1.999  -1.534  7.6709  0.7353E-03  0.3789E-03  0.3816E-02  0.3109E-02  0.2735E-02
1.999  -1.534  7.6208  0.7943E-03  0.4228E-03  0.4246E-02  0.3467E-02  0.3046E-02
2.039  -1.565  7.6563  0.7637E-03  0.4021E-03  0.4236E-02  0.3393E-02  0.3060E-02
2.039  -1.565  7.6085  0.7926E-03  0.4053E-03  0.4289E-02  0.3433E-02  0.3106E-02
2.102  -1.613  7.6365  0.7860E-03  0.3946E-03  0.4164E-02  0.3319E-02  0.2996E-02
2.102  -1.613  7.5909  0.8142E-03  0.3957E-03  0.4207E-02  0.3348E-02  0.3036E-02
2.182  -1.674  7.6122  0.8344E-03  0.4023E-03  0.4105E-02  0.3295E-02  0.2914E-02
2.182  -1.674  7.5686  0.8637E-03  0.4027E-03  0.4135E-02  0.3315E-02  0.2945E-02
2.261  -1.735  7.5902  0.8873E-03  0.4147E-03  0.4053E-02  0.3291E-02  0.2834E-02
2.261  -1.735  7.5484  0.9206E-03  0.4151E-03  0.4074E-02  0.3305E-02  0.2855E-02
2.340  -1.796  7.5727  0.9432E-03  0.4281E-03  0.4003E-02  0.3292E-02  0.2755E-02
2.340  -1.796  7.5309  0.9800E-03  0.4288E-03  0.4017E-02  0.3302E-02  0.2768E-02
2.459  -1.887  7.5522  0.1028E-02  0.4483E-03  0.3925E-02  0.3293E-02  0.2636E-02
2.459  -1.887  7.5098  0.1070E-02  0.4495E-03  0.3932E-02  0.3301E-02  0.2641E-02
2.618  -2.009  7.5330  0.1137E-02  0.4729E-03  0.3825E-02  0.3295E-02  0.2489E-02
2.618  -2.009  7.4900  0.1188E-02  0.4752E-03  0.3823E-02  0.3300E-02  0.2484E-02
2.777  -2.131  7.5212  0.1244E-02  0.4959E-03  0.3729E-02  0.3297E-02  0.2352E-02
2.777  -2.131  7.4777  0.1302E-02  0.4988E-03  0.3721E-02  0.3301E-02  0.2341E-02
2.975  -2.283  7.5144  0.1375E-02  0.5231E-03  0.3610E-02  0.3299E-02  0.2190E-02
2.975  -2.283  7.4712  0.1439E-02  0.5253E-03  0.3604E-02  0.3301E-02  0.2181E-02
3.213  -2.465  7.5161  0.1521E-02  0.5511E-03  0.3486E-02  0.3301E-02  0.2022E-02
3.213  -2.465  7.4751  0.1588E-02  0.5522E-03  0.3482E-02  0.3302E-02  0.2018E-02
3.768  -2.892  7.5501  0.1795E-02  0.5894E-03  0.3307E-02  0.3300E-02  0.1789E-02
3.768  -2.892  7.5216  0.1866E-02  0.5956E-03  0.3281E-02  0.3301E-02  0.1755E-02
```

Figure 8.11—5 Part of file tec_min.dat for Problem 11, giving changes in mineral abundances (in volume fraction, positive values indicate precipitation and negative dissolution) after t = 1 yr.

X	Z	gypsum	calcite	microcline	albite-low	anorthite
1.999	-1.534	0.0000E+00	0.2662E-04	-0.4580E-07	-0.4776E-06	-0.1750E-09
1.999	-1.534	0.0000E+00	0.7417E-05	-0.5739E-05	-0.2039E-04	-0.1816E-06
2.039	-1.565	0.0000E+00	0.3083E-04	-0.4868E-07	-0.4713E-06	-0.1691E-09
2.039	-1.565	0.0000E+00	0.7247E-05	-0.6391E-05	-0.1901E-04	-0.1703E-06
2.102	-1.613	0.0000E+00	0.3104E-04	-0.4912E-07	-0.4533E-06	-0.1592E-09
2.102	-1.613	0.0000E+00	0.7166E-05	-0.6191E-05	-0.1869E-04	-0.1536E-06
2.182	-1.674	0.0000E+00	0.2977E-04	-0.4846E-07	-0.4276E-06	-0.1471E-09
2.182	-1.674	0.0000E+00	0.6976E-05	-0.5700E-05	-0.1812E-04	-0.1354E-06
2.261	-1.735	0.0000E+00	0.2820E-04	-0.4752E-07	-0.4026E-06	-0.1360E-09
2.261	-1.735	0.0000E+00	0.6754E-05	-0.5208E-05	-0.1747E-04	-0.1200E-06
2.340	-1.796	0.0000E+00	0.2671E-04	-0.4654E-07	-0.3792E-06	-0.1260E-09
2.340	-1.796	0.0000E+00	0.6526E-05	-0.4747E-05	-0.1681E-04	-0.1070E-06
2.459	-1.887	0.0000E+00	0.2419E-04	-0.4497E-07	-0.3473E-06	-0.1129E-09
2.459	-1.887	0.0000E+00	0.6160E-05	-0.4098E-05	-0.1577E-04	-0.9102E-07
2.618	-2.009	0.0000E+00	0.2079E-04	-0.4301E-07	-0.3107E-06	-0.9848E-10
2.618	-2.009	0.0000E+00	0.5666E-05	-0.3333E-05	-0.1441E-04	-0.7491E-07
2.777	-2.131	0.0000E+00	0.1788E-04	-0.4134E-07	-0.2802E-06	-0.8689E-10
2.777	-2.131	0.0000E+00	0.5201E-05	-0.2691E-05	-0.1315E-04	-0.6304E-07
2.975	-2.283	0.0000E+00	0.1460E-04	-0.3951E-07	-0.2480E-06	-0.7507E-10
2.975	-2.283	0.0000E+00	0.4652E-05	-0.2025E-05	-0.1173E-04	-0.5227E-07
3.213	-2.465	0.0000E+00	0.1068E-04	-0.3739E-07	-0.2154E-06	-0.6369E-10
3.213	-2.465	0.0000E+00	0.4041E-05	-0.1372E-05	-0.1023E-04	-0.4330E-07
3.768	-2.892	0.0000E+00	0.6666E-06	-0.3324E-07	-0.1635E-06	-0.4646E-10
3.768	-2.892	0.0000E+00	0.2849E-05	-0.2941E-06	-0.7633E-05	-0.3160E-07

8.11.9 Model results and comparisons to measured data

Gas-Phase CO_2 Evolution

The concentration of CO_2 in the gas phase is a function of temperature, pressure, aqueous-phase chemistry, mineral-water reactions, and advective and diffusive transport. Simulation results are compared to concentrations measured in gas samples taken from boreholes during the heating phase of the DST. The modeled evolution of CO_2 has been validated by comparison to over 4 years of measurements from the Drift Scale Test. Simulated CO_2 concentrations in the fracture gas phase are shown after 3 years of heating in Figure 8.11-5. The results show the general outward migration of elevated CO_2 concentrations as the boiling front moves outward. The peak in CO_2 concentrations is centered at approximately the 60°C isotherm, and at higher temperatures the concentrations generally decline as a result of degassing and transport with water vapor to cooler regions.

Figure 8.11—6 **Modeled gas phase CO_2 concentrations in fractures after 3 years of heating. Note locations of numbered boreholes collared in the Observation Drift (circular region at left).**

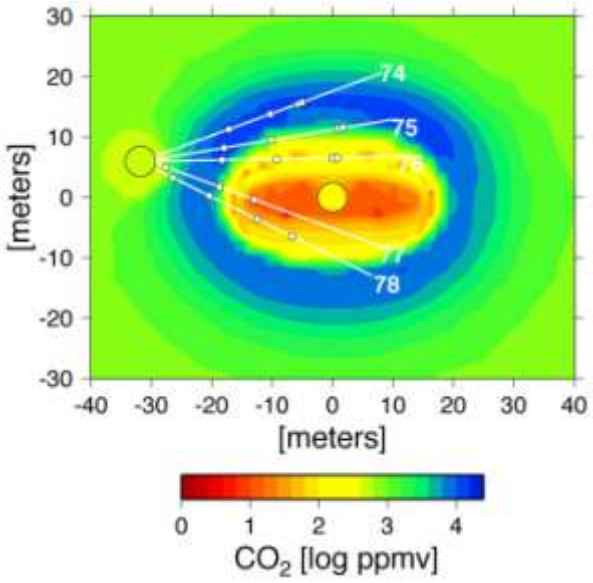

Comparisons of modeled CO_2 concentrations to measurements performed on gas samples from boreholes (shown in Figure 8.11-5) are presented in Figure 8.11-6. Samples were collected from zones a few meters (borehole interval 76-3) to about 15 meters away from the Heated Drift (borehole interval 74-3). Measured concentrations were corrected for water vapor condensation that took place as part of the procedure for gas sampling. Zones closest to the heaters (interval 76-3) exhibit narrower and earlier peaks in concentration compared to zones further out in the rock (interval 74-3). Simulated and measured concentrations are close in magnitude and in their trends. There is little difference between fracture and matrix concentrations, because of rapid equilibration by advection and diffusion of gas species and their local equilibration with pore water.

Figure 8.11—7 **Modeled CO_2 concentrations in fractures and matrix compared to measured values from boreholes (corrected for vapor condensation) (a) Borehole interval 74-3 (average of bounding grid blocks); (b) Borehole interval 75-3; (c) Borehole interval 76-3.**

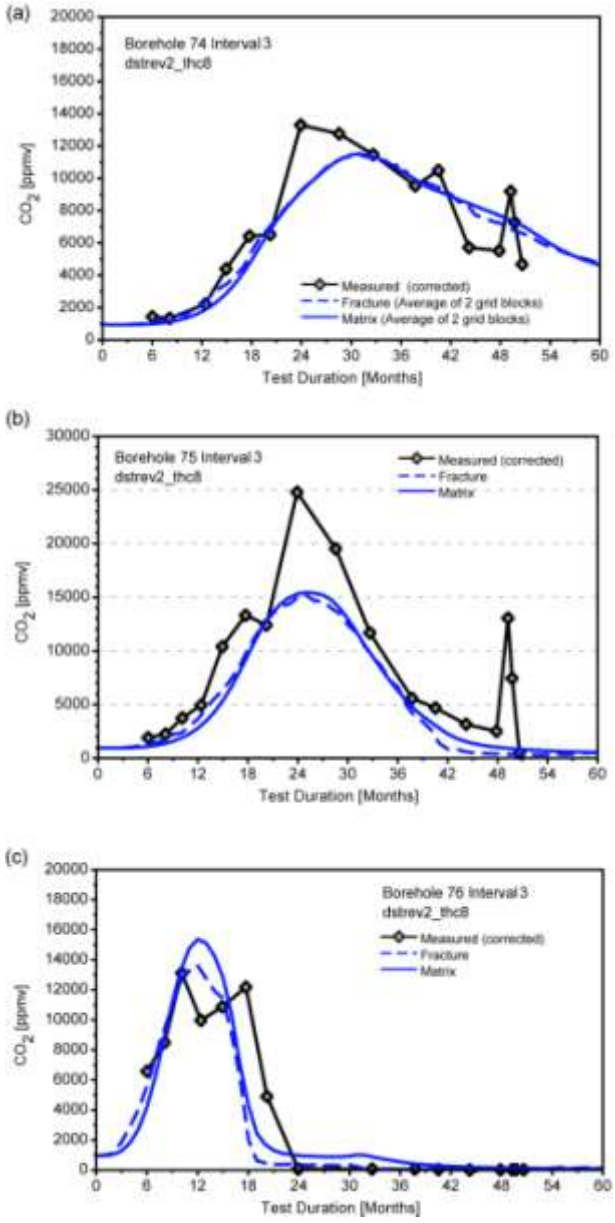

Aqueous species in waters collected in the DST exhibit small reductions in pH, from about pH 8 in the pore water to about 6-8 in condensate waters. The drop in pH is related to the local increases in CO_2 concentrations. Figure 8.11-7 shows an example of the initial drop in pH during vapor condensation, followed by increasing pH as the zone is further heated and CO_2 is diluted by water vapor.

Figure 8.11—8 Measured and modeled pH (in fractures) for samples collected from borehole interval 60-3, located below the heaters.

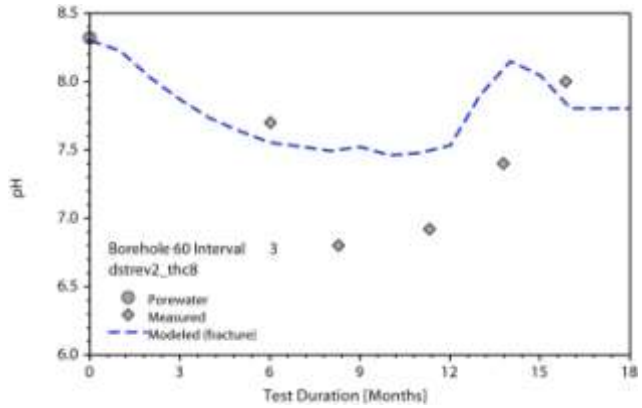

Simulated and measured concentrations of conservative species in the fractures, such as chloride, are much lower than in the initial matrix pore water, indicating that fracture-matrix interaction has been negligible. However, reactive species, such as silica and potassium show significant effects of reaction with fracture-lining silicate minerals.

Mineral Precipitation/Dissolution

Model predictions, followed by analyses of in-situ sidewall core samples, showed that amorphous silica, calcite and lesser amounts of gypsum are the dominant precipitating phases expected in the boiling regions. The greatest amount of mineral precipitation is predicted to be above the heaters where reflux of water condensed in fractures dissolves fracture-lining minerals and is boiled. Simulations and measurements of amorphous silica and calcite, along with locations of observed mineralization are shown in Figures 8.11-8 and 8.11-9. Amorphous silica forms only where strong evaporation by boiling takes place. Calcite also forms in the boiling zones, however calcite that is originally present in fractures dissolves in the lower pH waters that formed in condensation zones around the boiling zone and in the drainage zones below the heaters.

Figure 8.11—9 **Volume percent change in amorphous silica abundance in fractures. Filled circle indicates sidewall core sample locations where it was observed.**

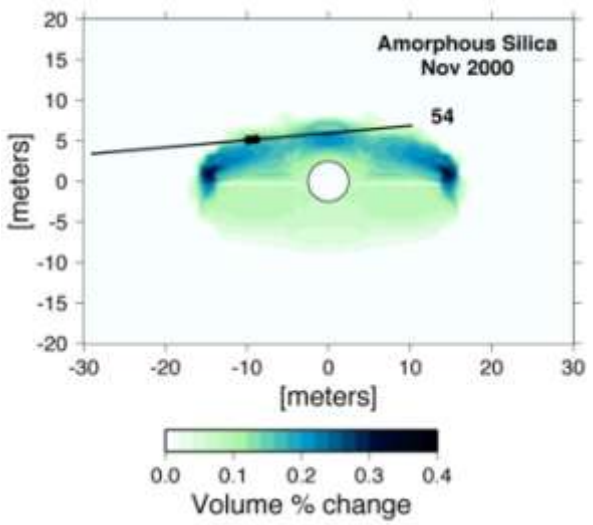

Figure 8.11—10 **Volume percent change in calcite abundance in fractures. Filled circle indicates sidewall core sample locations where it was observed.**

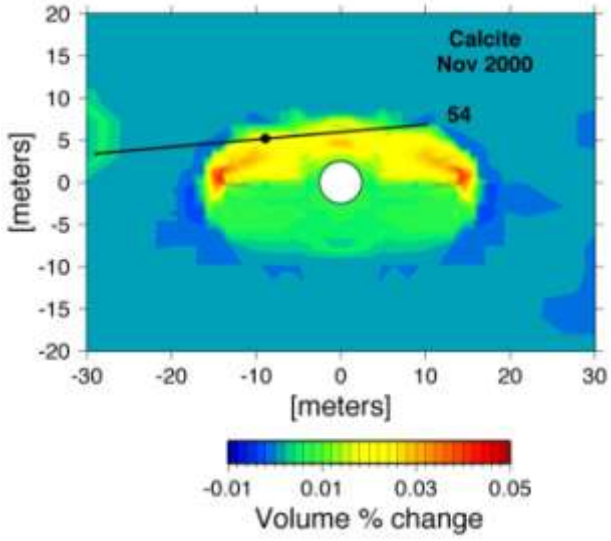

9 Concluding Remarks

TOUGHREACT is a comprehensive computer program for non-isothermal multiphase fluid flow and geochemical transport. The gas phase is considered active for multiphase fluid flow, species transport, and chemical reactions. The code is applicable to porous media as well as to fractured rocks. An integral finite difference (IFD) technique is employed for space discretization. The IFD methodology can deal with irregular grids, does not require reference to a global system of coordinates, and includes classical dual-continua, multiple interacting continua, and multi-region models for heterogeneous and fractured rocks. Non-isothermal effects are considered, including water-vapor phase change and air partitioning between the liquid and gas phases, temperature-dependence of thermophysical properties such as phase density and viscosity, and chemical properties such as thermodynamic and kinetic parameters. Chemical reactions considered under the local equilibrium assumption include aqueous complexation, acid-base, redox, gas dissolution/exsolution, cation exchange, and surface complexation. Mineral dissolution/precipitation can proceed either subject to local equilibrium or kinetic conditions.

TOUGHREACT is applicable to one-, two-, or three-dimensional geologic domains with physical and chemical heterogeneity, and can be applied to a wide range of subsurface conditions. Temperatures can range from 0 to 300 °C, limited at present by available geochemical databases such as EQ3/6 (Wolery, 1992). Pressures of 1 bar (atmospheric pressure) to several hundred bars (at several thousand meter depth) can be considered. Water saturation can range from completely dry to fully water saturated. The code can handle ionic strengths from dilute to saline waters with up to 6 mol/kg for an NaCl-dominant solution.

TOUGHREACT applications have been demonstrated for a variety of reactive fluid and geochemical transport systems, including (1) contaminant transport with linear Kd adsorption and decay, (2) natural groundwater quality evolution under ambient conditions, (3) assessment of nuclear waste disposal sites, (4**)** sedimentary diagenesis and CO_2 geological sequestration in deep saline formations, (5) mineral deposition such as supergene copper enrichment, (6) mineral alteration and silica scaling in hydrothermal systems under natural and production conditions, and (7) acidic mine drainage and groundwater contamination. Of course, many other potential geologic, experimental, and engineered systems could be analyzed using similar methodologies as given in these examples.

Acknowledgements. The documentation of Version 2 of TOUGHREACT was supported by the Zero Emission Research and Technology Project (ZERT) of the U.S. Department of Energy, under Contract No. DE-AC02-05CH11231. The development of TOUGHREACT was initiated with funding from the Laboratory Directed Research and Development Program of the Ernest Orlando Lawrence Berkeley National Laboratory. Subsequent development was supported by the Assistant Secretary for Energy Efficiency and Renewable Energy, Office of Geothermal Technologies; by the Director, Office of Science, Office of Basic Energy Sciences; by the Director, Office of Civilian Radioactive Waste Management; and by the Zero Emission Research and Technology project (ZERT), of the U.S. Department of Energy, under Contract No. DE-AC02-05CH11231. Work related to bentonite

alteration (Sample Problem 4) was supported by the National Co-operative for the Disposal of Radioactive Waste (NAGRA) of Switzerland.

10 References

Ague, J. J., and Brimhall, G. H., Geochemical modeling of steady state and chemical reaction during supergene enrichment of porphyry copper deposits: Economic Geology, v. 84, p. 506-528, 1989.

Ahlers, C. F., and Liu, H. H., Calibrated properties model, MDL-NBS-HS-000003 REV00., Yucca Mountain Project, Lawrence Berkeley National Laboratory, Berkeley, California, 2000.

Alpers, C. A., and Brimhall, G. H, Paleohydrologic evolution and geochemical dynamics of cumulative supergene metal enrichment at La Escondida, Atacama Desert, Northern Chile: *Economic Geology*, v. 84, p. 229-255, 1989.

Ananthaswamy, J., and G. J. Atkinson, Thermodynamics of concentrated electrolyte mixtures: 5. A Review of the thermodynamic properties of aqueous calcium chloride in the temperature range 273.15-373.15 K. *J. Chem. Eng. Data*, 30, 120, 1985.

Appelo, C. A. J., and Postma, D., *Geochemistry, groundwater and pollution*, Rotterdam, The Netherlands, Balkema, 536 pp., 1993.

Appelo, C. A. J., Cation and proton exchange, pH variations and carbonate reactions in a freshening aquifer, *Water Resour. Res*., v. 30(10), p. 2793-2805, 1994.

Apps, J. A., An approach to modeling of the chemistry of waste fluid disposal in deep saline aquifers, In Apps, J. A., and Tsang, C. F. (eds.), *Deep injection disposal of hazardous and industrial waste: Scientific and Engineering Aspects*, p. 465-488, Academic Press, San Diego, California, 1996.

Audigane, P., I. Gaus, I. Czernichowski-Lauriol, K. Pruess, and T. Xu, Two-dimensional reactive transport modeling of CO_2 injection in a saline aquifer at the Sleipner Site, *American Journal of Science*, v. 307, p. 974-1008. 2007.

Bachu, S., Gunter, W. D., and Perkins, E. H., Aquifer disposal of CO_2: hydrodynamic and mineral trapping, *Energy Convers. Mgmt.*, v. 35, p. 269-279, 1994.

Balistrieri, L.S., Preliminary estimates of benthic fluxes of dissolved metals in Coeur d'Alene Lake, Idaho 98-793. US Geological Survey, Seattle, WA, 1998.

Bear, J.: Dynamics of Fluids in Porous Media, Dover Publications, Inc., New York, 1972.

Birkholzer, J. T., and Tsang, Y. W., Pretest analysis of the thermal-hydrological conditions of the ESF Drift Scale Test, Yucca Mountain Project Level 4 Milestone SP9322M4, Lawrence Berkeley National Laboratory, Berkeley, California, 1997.

Birkholzer, J. T., and Tsang, Y. W., Interpretive analysis of the thermo-hydrological processes of the Drift Scale Test, In Drift Scale Test Progress Report, Chapter 6., Yucca Mountain Project Level 4 Milestone SP2930M4, Lawrence Berkeley National Laboratory, Berkeley, California, 1998.

Brimhall, G. H., Alpers, C. N., and Cunningham, A. B., Analysis of supergene ore-forming processes and ground water solute transport using mass balance principles: *Economic Geology*, v. 80, p. 1227-1256, 1985.

Brimhall, G. H., and Dietrich, W. E., Constitutive mass balance relations between chemical composition, volume, density, porosity, and strain in metasomatic hydrochemical systems: Results on weathering and pedogenesis, *Geochim. Cosmochim. Acta*, v. 51, p. 567-588, 1987.

Burnol A. and Claret, F., Using a generalized power law for simulating the feedback effct of dissolution/ precipitation on diffusive transfer in toughreact. Proceedings, TOUGH Symposium 2012, Lawrence Berkeley National Laboratory, Berkeley, California, September 17-19, 2012.

Carey, J. W., Chipera, S. J., Vaniman, D. T., Bish, D. L., Three-dimensional mineralogic model of Yucca Mountain,

Nevada, Rev 2.0., Los Alamos National Laboratory, Los Alamos, New Mexico, 1998.

Carlos, B. A., Chipera, S. J., Bish, D. L., Calcite and zeolite fracture coating in Topopah Spring Tuff along Drill Hole Wash, Yucca Mountain (Nevada), Proc. 6th Intl. Conf. High Level Rad. Waste Mgmt., p. 100-102, 1995.

Carroll, S., Mroczek, E., Alai, M., and Ebert, M., Amorphous Silica Precipitation (60 to 120°C): Comparison of Laboratory and Field Rates, *Geochim. Cosmochim. Acta*, v. 62, p. 1379–1396, 1998.

Chapelle, F. H., and Drummond, D. D., Hydrogeology, digital simulation, and geochemistry of the Aquia and Piney Point-Nanjemoy aquifer system in southern Maryland, *Rep. Invest. 38*, Md. Geol. Surv., Baltimore, Maryland, 1983.

Chapelle, F. H., and Knobel, L. L., Aqueous geochemistry and exchangeable cation composition of glauconite in the Aquia aquifer, Maryland, *Groundwater*, v. 21, p. 343-352, 1983.

Colin, E., Clarke, W., and Clew, D.N. Evaluation of the thermodynamic functions for aqueous sodium chloride from equilibrium and calorimetric measurements below 154°C. *J. Phys.Chem. Ref. Data* 14, 489-609, 1985.

Corey, A. T., The interrelation between gas and oil relative permeabilities, *Producers Monthly*, p. 38-41, 1954.

Dobson, P.F., T.J. Kneafsey, E.L. Sonnenthal, N.F. Spycher, and J.A. Apps, 2003. Experimental and numerical simulation of dissolution and precipitation: Implications for fracture sealing at Yucca Mountain, Nevada. Journal of Contaminant Hydrology. 62-63: 459-476.

Dobson, P. F., Salah, S., Spycher, N., and Sonnenthal, E. L., Simulation of water-rock interaction in the Yellowstone geothermal system using TOUGHREACT, *Geothermics*, v. 33, p. 493-502, 2004.

Domenico, P. A., and Schwartz, F. W., *Physical and Chemical Hydrogeology*, John Wiley and Sons, New York, 824 pp., 1990.

Doussan, C., Poitevin, G., Ledoux, E., and Detay, M., River bank filtration: modelling of the changes in water chemistry with emphasis on nitrogen species, Journal of Contaminant Hydrology, v. 25, p. 129-156, 1997.

Drever, J. I., Geochemistry of Natural Waters, 3rd Edition, Upper Saddle River, New Jersey: Prentice Hall, 436pp., 1997.

Drummond, J. M., Jr., Boiling and mixing of hydrothermal fluids: Chemical effects on mineral precipitation, Ph.D. thesis, The Pennsylvania State University, University Park, Pennsylvania, 1981.

Dzombak, D. A., and Morel, F. M. M., Surface complexation modeling: New York, Wiley Interscience, 431 pp., 1990.

Ehrlich R, Etris EL, Brumfield D, Yuan LP, Crabtree SJ. Petrography and reservoir physics III: physical models for permeability and formation factor. AAPG Bull 1991; 75(10):1579–92.

Engesgaard, P., and Kipp, K. L., A geochemical transport model for redox-controlled movement of mineral fronts in groundwater flow systems, A case of nitrate removal by oxidation of pyrite, *Water Resour. Res.*, v. 28, p. 2829-2843, 1992.

Ennis-King, J., and Paterson, L., Role of convective mixing of the long-term storage of carbon dioxide in deep saline formations, Paper SPE 84344, Presented at Society of Petroleum Engineers Annual Fall Technical Conference and Exhibition, Denver, CO, October 2003.

Fernández, R., Cuevas, J., Sánchez, L., de la Villa, R.V., Leguey, S., Reactivity of the cement-bentonite interface with alkaline solutions using transport cells, *Appl. Geochem.*, v. 21, p. 977–992, 2006.

Gaines, G.L. and Thomas, H.C., Adsorption studies on clay minerals. II. A formulation of thermodynamics of exchange adsorption. Journal of Chemical Physic, 21, 714-718, 1953.

Gapon, E.N., On the theory of exchange adsorption in soils. *J. Gen. Chem. USSR* 3: 144-152, 1933 (Chem. Abstr., 28: 4516, 1934)

García, J.E. Density of Aqueous Solutions of CO_2, Lawrence Berkeley National Laboratory Report LBNL-49023, Berkeley, CA, 2001.

Gérard, F., Xu, T., Brimhall, G., and Pruess, K., Modeling reactive chemical transport problems with the codes EQ3/6 and TRANQUI: Lawrence Berkeley Laboratory Report LBL-40505, Berkeley, California, 1997.

Gherardi, F., Xu, T., and Pruess, K., Numerical modeling of self-limiting and self-enhancing caprock alteration induced by CO_2 storage in a depleted gas reservoir. *Chemical Geology*, 244, (1–2), 103–129, 2007.

Gu, C., F. Maggi, W. J. Riley, G. M. Hornberger, T. Xu, C. M. Oldenburg, N. Spycher, N. L. Miller, R. T. Venterea, and C. I. Steefel, Aqueous and Gaseous Nitrogen Losses Induced by Fertilizer Application, J. Geophys. Res., doi:10.1029/2008JG000788, 2008.

Gunnarsson, I. and Arnórsson, S., Amorphous Silica Solubility and the Thermodynamic Properties of H_4SiO_4 in the Range of 0º to 350ºC at P_{sat}, *Geochim. Cosmochim. Acta*, v. 64, p. 2295-2307, 2000.

Gunter W. D., Perkins, E. H., and McCann, T. J., Aquifer disposal of CO_2-rich gases: Reaction design for added capacity. *Energy Convers. Mgmt.*, v. 34, p. 941-948, 1993.

Gunter W. D., Bachu, S., Law, D. H. S., Marwaha, V., Drysdale, D. L., MacDonald, D. E., and McCann, T. J., Technical and economic feasibility of CO_2 disposal in aquifers within the Alberta Sedimentary Basin, Canada, *Energy Convers. Mgmt.* v. 37, p. 1135-1142, 1996.

Gunter W. D., Wiwchar, B., and Perkins, E. H., Aquifer disposal of CO_2-rich greenhouse gases: extension of the time scale of experiment for CO_2-sequestering reactions by geochemical modeling, *Mineral. and Petrol.*, v. 59, p. 121-140, 1997.

Gwo, J. P., Jardine, P. M., Wilson, G. V., and Yeh, G. T., Using a multiregion model to study the effects of advective and diffusive mass transfer on local physical nonequilibrium and solute mobility in a structured soil, *Water Resour. Res.*, v. 32, p. 561-570, 1996.

Helgeson, H. C., Thermodynamics of hydrothermal systems at elevated temperatures and pressures. *Am.J.Sci.* 267, 729-804, 1969.

Helgeson, H. C., Kirkham, D. H., Flowers, D. C., Theoretical prediction of the thermodynamic behavior of aqueous electrolytes at high pressures and temperatures: IV. Calculation of activity coefficients, osmotic coefficients, and apparent molal and standard and relative partial molal properties to 600 C and 5 kb. *Am. J. Sci*., v. 281, p. 1249–1516, 1981.

Hellmann, R., Tisserand, D., Dissolution kinetics as a function of the Gibbs free energy of reaction: An experimental study based on albite feldspar. Geochimica et Cosmochimica Acta, 70, 364-383, 2006.

Hitchon, B. (ed.)., *Aquifer Disposal of Carbon Dioxide*, Geoscience Publishing, Ltd., Sherwood Park, Alberta, Canada, 1996.

Horowitz, A.J., Elrick, K.A., Robbins, J.A., and Cook, R.B., Effect of mining and related activities on sediment trace element geochemistry of Lake Coeur D'Alene, Idaho, USA Part II. Subsurface sediments: *Hydrol. Process.* 9, 35-54, 1995.

Javandel, J., Doughty, C., and Tsang, C. F., *Groundwater transport: Handbook of mathematical models*, American Geophysical Union, Washington D. C., pp. 228, 1984.

JNC, H12: Project to Establish the Scientific and Technical Basis for HLW Disposal in Japan, TN1410 2000-001, JNC, Tokai-mura, Japan, 2000.

Johnson, J. W., Oelkers, E. H., and Helgeson, H. C., SUPCRT92: A software package for calculating the standard molal thermodynamic properties of minerals, gases, aqueousspecies, and reactions from 1 to 5000 bars and 0 to 1000 degrees C: *Computers and Geosciences*, v. 18, p. 899–948, 1992.

Johnson. J. W., Nitao, J. J., Steefel, C. I., and Knaus, K. G., Reactive transport modeling of geologic CO_2 sequestration in saline aquifers: The influence of intra-aquifer shales and the relative effectiveness of structural, solubility, and mineral trapping during prograde and retrograde sequestration, In proceedings: First National Conference on Carbon Sequestration, Washington, DC, May 14-17, 2001.

Kuwabara, J.S., Carter, J.L., Topping, B.R., Fend, S.B., Importance of sediment–water interactions in Coeur d'Alene Lake, Idaho, USA: management implications. Environ. Manage. 32, 348–359, 2003.

Korbol, R., and Kaddour, A., Sleipner vest CO_2 disposal - injection of removed CO_2 into the Utsira Formation,

Energy Convers. Mgmt., v. 36(6-9), p. 509-512, 1995.

Langmuir, D., *Aqueous Environmental Geochemistry*, Prentice Hall, Upper Saddle River, New Jersey, 600pp, 1997.

Lagneau, V., Influence des processus géochimiques sur le transport en milieu poreux; Application au colmatage de barrières de confinement potentielles dans un stockage en formation géologique. Thèse, CEA, 2002.

Lasaga, A. C., Chemical kinetics of water-rock interactions, *J. Geophys. Res*., v. 89, p. 4009-4025, 1984.

Lasaga, A. C., Soler, J. M., Ganor, J., Burch, T. E., Nagy, K. L., Chemical weathering rate laws and global geochemical cycles. *Geochim. Cosmochim. Acta*, v. 58, p. 2361-2386, 1994.

Lasaga, A. C., *Kinetic Theory in the Earth Sciences*, Princeton University Press, Princeton, New Jersey, 811pp., 1998.

Lasaga, A.C., and A. Luttge. 2001. Variation of crystal dissolution rate based on a dissolution stepwave model. Science (Washington, DC) 291, 2400-2404.

Law, D.H.-S., Bachu S., Hydrogeological and numerical analysis of CO_2 disposal in deep aquifers in the Alberta sedimentary basin. *Energy Conversion and Management*, 37, (6–8), 1167–1174, 1996.

Lichtner, P. C., The quasi-stationary state approximation to coupled mass transport and fluid-rock interaction in a porous medium, *Geochim. Cosmochim. Acta*, v. 52, p. 143-165, 1988.

Lichtner, P. C., Continuum formulation of multicomponent-multiphase reactive transport, in Lichtner, P. C., Steefel, C. I., and Oelkers, E. H. (eds.), *Reactive transport in porous media*, Reviews in Mineralogy, Mineral Society of America, v. 34, p. 1-79, 1996.

Liger, E., Charlet L., Van Cappellen, P., Surface catalysis of U(VI) reduction by Fe(II). *Geochim. Cosmochim. Acta*, 63, 2939–2955, 1999.

Liu, H. H.; Doughty, C.; and Bodvarsson, G. S. An Active Fracture Model for Unsaturated Flow and Transport in Fractured Rocks. *Water Resour. Res*., v. 34, p. 2633-2646, 1998.

Lohuis, J. A. O., Carbon dioxide disposal and sustainable development in The Netherlands, *Energy Convers. Mgmt.*, v. 34(9-11), p. 815-821, 1993.

Maggi, F., C. Gu, W. J. Riley, G.M. Hornberger, R.T. Venterea, T. Xu, N. Spycher, C.I. Steefel, and N.L. Miller, Mechanistic modeling of biogeochemical nitrogen cycling: model development and application in an agricultural system, *J. Geophys. Res*. (Biogeosciences), J. Geophys. Res., 113, doi:10.1029/2007JG000578, 2008.

Marshall, B. D., Paces, J. B., Neymark, L. A., Whelan, J. F., and Peterman, Z. E., Secondary minerals record past percolation flux at Yucca Mountain, Nevada, In: Proceedings of the 8th International High-level Radioactive Waste Management Conference, May 11-14, Las Vegas, Nevada, USA, 1998.

Marshall, B. D., Neymark, L. A., Paces, J. B., Peterman, Z. E., Whelan, J. F., Seepage flux conceptualized from secondary calcite in lithophysal cavities in the Topopah Spring Tuff, Yucca Mountain, Nevada. The society for Mining, Metallurgy, and Exploration, Inc. Annual Meeting 2000, USGS, Denver, Colorado, 1999.

McPherson, B. J. O. L., and P. C. Lichtner, CO_2 sequestration in deep aquifers, In proceedings: First National Conference on Carbon Sequestration, Washington, DC, May 14-17, 2001.

Millington, R. J., and Quirk, J. P., Permeability of porous solids, Trans. Faraday Soc., v. 57, p. 1200-1207, 1961.

Moberly J.G., Borch T., Sani R.K, Spycher N.F., Sengor S., Ginn T.R., Peyton B., 2009. Heavy metal–mineral associations in Coeur d'Alene River sediments: a synchrotron-based analysis. *Water, Air, Soil Pollut.*, 201, 195–208.

Montazer, P. and Wilson, W. E., Conceptual hydrologic model of flow in the unsaturated zone, Yucca Mountain, Nevada, Water Resources Investigations Report 84-4355, USGS, Denver, Colorado, 1984.

Moore, D. E., Morrow, C. A., and Byerlee, J. D., Chemical reactions accompanying fluid flow through granite held in a temperature gardient. *Geochim. Cosmochim. Acta*, v. 47, p. 445-453, 1983.

Moridis, G., and Pruess, K., T2SOLV: An enhanced package of solvers for the TOUGH2 family of reservoir simulation codes, *Geothermics*, v. 27, p. 415-444, 1998.

Mote T. I., Brimhall, G. H., Tidy-Finch, E., Muller, G., and Carrasco, P., Application of mass-balance modeling of sources, pathways, and sinks of supergene enrichment to exploration and discovery of the Quebrada Turquesa Exotic Copper Orebody, El Salvador District, Chile, Economic Geology & the Bulletin of the Society of Economic Geologists, v. 96 (No. 2), p. 367-386, 2001.

Mukhopadhyay, S., Sonnenthal, E., and Spycher, N., Modeling of coupled heat transfer and reactive transport processes in porous media: Application to seepage studies at Yucca Mountain, Nevada. Journal of Porous Media, v. 12, p. 725-748, 2009.

Mualem, Y., A new model for predicting the hydraulic conductivity of unsaturated porous media, *Water Resour. Res*., v. 12, p. 513–522, 1976.

Nagy, K. L., Dissolution and precipitation kinetics of sheet silicates, *Chemical Weathering Rates of Silicate Minerals,* v. 31, p. 291–351, 1995.

NAGRA, Project Opalinus Clay: Safety Report. Demonstration of Disposal Feasibility (Entsorgungs-nachweis) for Spent Fuel, Vitrified High-Level Waste and Long-Lived Intermediate-Level Waste, NAGRA Technical Report NTB 02-05, NAGRA, Wettingen, Switzerland, 2002.

Narasimhan, T. N., and Witherspoon, P. A., An integrated finite difference method for analyzing fluid flow in porous media, *Water Resour. Res*., v. 12, p. 57–64, 1976.

Neymark, L. A., Amelin, Y. V., Paces, J. B., Peterman, Z. E., Whelan, J. F., Age constraints on fluid inclusions in calcite at Yucca Mountain, In: Proceedings of the 9th International High-level Radioactive Waste Management Conference, Las Vegas, Nevada, USA, April 29-May 3, 2001.

Nordstrom, D. K., and Muñoz, J. L., *Geochemical Thermodynamics*, The Benjamin/Cummings Pub. Co., Menlo Park, California, 477 pp., 1986.

Nordstrom, D. K., and Alpers, C. N., *The Environmental geochemistry of mineral deposits. Part A. Processes, methods and health Issues*. (Plumlee, G. S., Logsdon, M. J. (Eds)), Reviews in Economic Geology, v. 6**,** Society of Economic Geologists, 1997.

Oldenburg C. M., and Pruess, K., EOS7R: Radionuclide transport for TOUGH2, Lawrence Berkeley National Laboratory Report LBNL-34868, Berkeley, California, 1995.

Olson, G. J., Rate of pyrite bioleaching by *Thiobacillus ferrooxidans* - Results of an interlaboratory comparison, *Applied and Environmental Microbiology*, v. 57, p. 642-644, 1991.

Ontoy, Y., Molling, P. L., Xu, T., Spycher, N., Parini, M. and Pruess, K., Scaling of hot brine injection wells: supplementing field studies with reactive transport modeling. *In Proceedings of TOUGH Symposium 2003*, Lawrence Berkeley National Laboratory, Berkeley, California, May 12–14, 2003.

Paces, J. B., Marshall, B. D., Whelan, J. F., Neymark, L. A., Peterman, Z. E., Summary of subsurface calcite and opal deposits and estimates of the probable distribution and isotopic compositions of hydrogenic minerals along the East-West Cross Drift, Yucca Mountain, Nevada. U.S. Geol. Surv. Open File Rep., Denver, Colorado, 1998.

Paces, J. B., Neymark, L. A., Marshall, B. D., Whelan, J. F., Peterman, Z. E., Ages and origin of calcite and opal in the Exploratory Studies Facilities tunnel, Yucca Mountain, Nevada. U.S. Geol. Investigations Report, Denver, Colorado, 2001.

Palandri, J., and Kharaka, Y. K., A compilation of rate parameters of water-mineral interaction kinetics for application to geochemical modeling, US Geol. Surv. Open File Report 2004-1068, 64 pp., 2004.

Pape, H., Clauser C., and Iffland J., Permeability prediction based on fractural pore-space geometry, *Geophysics*, v. 64(5), p. 1447-1460, 1999.

Parks, G. A., Surface energy and absorption at mineral-water interfaces: an introduction, Review of Mineralogy, v. 23 (Miner.-Water Interface Geochem.), p. 133-75, 1990.

Parkhurst, D. L., Thorstenson, D. C., and Plummer, L. N., PHREEQE: A computer program for geochemical calculations, US Geol. Surv. Water Resour. Invest. 80-96, 174 pp., 1980.

Parkhurst, D.L., Appelo, C.A.J., 1999. User's Guide to PHREEQC (Version 2) – a computer program for speciation,

batch reaction, one-dimensional transport, and inverse geochemical calculations. U.S. Geol. Surv. Water-Resour. Investig. Rep. 99-4259, Denver, CO.

Perkins, E. H., and Gunter, W. D., Mineral Traps for Carbon Dioxide, in: Hitchon, B. (ed.), Aquifer Disposal of Carbon Dioxide, Geoscience Publishing, Ltd., Alberta, Canada, p. 93-113, 1996.

Pruess, K., and Karasaki, K., Proximity functions for modeling fluid and heat flow in reservoirs with stochastic fracture distributions, in Proceedings, Eighth workshop on geothermal reservoir engineering: p. 219-224, Stanford University, Stanford, California, 1982.

Pruess, K., and Narasimhan, T. N., A practical method for modeling fluid and heat flow in fractured porous media: *Society of Petroleum Engineers Journal*, v. 25, p. 14-26, 1985.

Pruess, K., TOUGH user's guide, Nuclear Regulatory Commission, report NUREG/CR-4645 (also Lawrence Berkeley Laboratory Report LBL-20700, Berkeley, California), 1987.

Pruess, K., TOUGH2: A general numerical simulator for multiphase fluid and heat flow, Lawrence Berkeley Laboratory Report LBL-29400, Berkeley, California, 1991.

Pruess, K., Oldenburg, C., and Moridis, G., TOUGH2 user's guide, Version 2.0, Lawrence Berkeley Laboratory Report LBL-43134, Berkeley, California, 1999.

Pruess, K., and García, J., Multiphase flow dynamics during CO_2 disposal into saline aquifers, Environmental Geology, v. 42, p. 282-295, 2002.

Pruess, K., Xu, T., Apps, J., and García, J., Numerical modeling of aquifer disposal of CO_2, Paper SPE-83695, SPE Journal, p. 49-60, 2003.

Pruess, K., ECO2N: A TOUGH2 Fluid Property Module for Mixtures of Water, NaCl, and CO_2, Lawrence Berkeley National Laboratory Report LBNL-57592, Berkeley, California, 2005.

Raffensperger, J. P., Numerical simulation of sedimentary basin-scale hydrochemical processes, In Advances in Porous Media, Corapcioglu, Y. C., (ed.), Amsterdam, The Netherlands, Elsevier Science, 440 pp., 1996.

Reed, M. H., Calculation of multicomponent chemical equilibria and reaction processes in systems involving minerals, gases and aqueous phase, *Geochim. Cosmochim. Acta*, v. 46, p. 513-528, 1982.

Reed M.H., 1998. Calculation of simultaneous chemical equilibria in aqueous-mineral-gas systems and its application to modeling hydrothermal processes. In: Techniques in Hydrothermal Ore Deposits Geology, Reviews in Economic Geology, Volume 10. Richards J, Larson P (eds), 109–124.

Richards, L. A., Capillary conduction of liquids through porous mediums, *Physics*, v. 1, p. 318-333, 1931.

Rickard, D., Kinetics of FeS precipitation: Par 1. Competing reaction mechanisms. Geochim. Cosmochim. Acta 59, 4367–4379, 1995.

Rimstidt, J. D. and Barnes, H. L., The kinetics of silica–water reactions, *Geochim. Cosmochim. Acta*, v. 44, p. 1683-1699, 1980.

Robinson, R. A., and Stokes, R. H., Electrolyte Solutions, the Measurement and Interpretation of Conductance, Chemical Potential and Diffusion in Solutions of Simple Electrolytes, 2nd Edition, London, England: Butterworths & Company, 1965.

Senger, R., T. Xu, P. Marschall, and S. Finsterle, Modeling approaches of two-phase flow phenomena associated with corrosion of SF/HLW canisters in a proposed repository in Opalinus clay, Switzerland, *Physics and Chemistry of the Earth*, v. 33, S317–S326, 2008.

Senger, R., Ewing, J., Evolution of temperature and water content in the bentonite buffer: Detailed modelling of two-phase flow processes associated with the early closure period – complementary simulations. Report NAB 08-53 for NAGRA, INTERA Inc., Austin, Texas 78758, 2008.

Sengör, S.S., Spycher N., Ginn T.R., Sani R.K., Peyton B., Biogeochemical reactive-diffusive transport of heavy metals in Lake Coeur d'Alene sediments, *Applied Geochemistry*, 22, 2569-2594, 2007a.

Sengör, S.S., Spycher, N.F., Ginn, T.R., Moberly, J., Peyton, B., & Sani, R.K., Reductive dissolution and metal

transport in Lake Coeur d'Alene sediments. In *Water-Rock Interaction, WRI-12* (Bullen T. and Wang Y., eds.), Taylor & Francis, New York, Vol. 2, 895-899, 2007b.

Shock, E. L., Helgeson, H. C., and Sverjensky, D. A., Calculation of the thermodynamic and transport properties of aqueous species at high pressures and temperatures: Standard partial molal properties of inorganic neutral species, *Geochim. Cosmochim. Acta*, v. 53 (9), p. 2157-2183, 1989.

Simunek, J., and Suares, D. L., Two-dimensional transport model for variably saturated porous media with major ion chemistry, *Water Resour. Res*., v. 30, p. 1115-1133, 1994.

Singer, P. C., and Stumm, W., Acid mine drainage - The rate determining step: Science, v. 167, p. 1121-1123, 1970.

Singleton, M.J., E.L. Sonnenthal, M.E. Conrad, D.J, DePaolo, and G.W. Gee, 2004. Multiphase reactive transport modeling of stable isotope fractionation in unsaturated zone pore water and vapor: Application to seasonal infiltration events at the Hanford Site, WA. Vadose Zone Journal, 3: 775-785.

Slider, H. C., Practical petroleum reservoir engineering methods, An Energy Conservation *Science*. Tulsa, Oklahoma, Petroleum Publishing Company, 1976.

Sonnenthal, E. and Ortoleva, P. J., Numerical simulations of overpressured compartments in sedimentary Basins, *Basin Compartments and Seals*. Ortoleva, P.J., ed., AAPG Memoir v. 61, p. 403-416, Tulsa, Oklahoma, American Association of Petroleum Geologists, 1994.

Sonnenthal, E. L., and Bodvarsson, G. S., Percolation flux estimates from geochemical and thermal modeling. Proceedings of the Eighth International Conference on High-Level Radioactive Waste Management, American Nuclear Society, p. 130-132, 1998.

Sonnenthal, E., Spycher, N., Apps, J. A., and Simmons, A., 1998, Thermo-hydro-chemical predictive analysis for the Drift-Scale Heater Test, Yucca Mountain Project Level 4 Milestone SPY289M4, Lawrence Berkeley National Laboratory, Berkeley, California, 1998.

Sonnenthal, E. L., Bodvarsson, G. S. Constraints on the hydrology of the unsaturated zone at Yucca Mountain, NV from three-dimensional models of chloride and strontium geochemistry. *J. Contam. Hydrol*., v. 38, p. 107-156, 1999.

Sonnenthal, E., A. Ito, N. Spycher, M. Yui, J. Apps, Y. Sugita, M. Conrad, and S. Kawakami, Approaches to modeling coupled thermal, hydrological, and chemical processes in the Drift Scale Heater Test at Yucca Mountain, *International Journal of Rock Mechanics and Mining Sciences*, v. 42, p. 698-719, 2005.

Sonnenthal, E. L., Spycher, N., Drift-Scale coupled processes (DST and THC seepage) models. AMR N0120/U0110 Rev.01, Yucca Mountain Project, Lawrence Berkeley National Laboratory, Berkeley, California, 2001.

Sonnenthal, E., N. Spycher, and T. Xu, 2003. Linking reaction, transport, and hydrological parameters in unsaturated fractured rock: TOUGHREACT implementation and application. Proceedings, TOUGH Symposium, 2003.

Sonnenthal, E., T. Xu, and G. Bodvarsson, Reply to "Commentary: Assessment of past infiltration fluxes through Yucca Mountain on the basis of the secondary mineral record – is it a viable methodology?", by Y.V. Dublyansky and S.Z. Smirnov, Journal of Contaminant Hydrology, v. 77, p. 225-231, 2005.

Spycher, N. F., and Reed, M. H., Fugacity coefficients of H_2, CO_2, CH_4, H_2O and of H_2O-CO_2-CH_4 mixtures: A virial equation treatment for moderate pressures and temperatures applicable to calculations of hydrothermal boiling, *Geochim. Cosmochim. Acta*, v. 52, p. 739-749, 1988.

Spycher N. F., Sonnenthal, E. L., and Apps, J. A., Fluid flow and reactive transport around potential nuclear waste emplacement tunnels at Yucca Mountain, Nevada, *J. Contam. Hydrol*., v.62-63, p. 653-673, 2003a.

Spycher, N., Sonnenthal, E. L., Dobson, P. F., Kneafsey, T., and Salah, S., Drift-scale coupled processes (DST and THC seepage) models, MDL-NBS-HS-000001 REV02, BSC: Las Vegas, NV, Report number LBID-2478, Lawrence Berkeley National Laboratory, Berkeley, California, 2003b.

Spycher, N., and Pruess, K., CO_2-H_2O mixtures in the geological sequestration of CO_2: II. Partitioning in chloride brines at 12–100°C and up to 600 bar, *Geochimica et Cosmochimica Acta*, v. 69, p. 3309-3320, 2005.

Spycher, N., Zhang, G., Sengor, S., Issarangkun, M., Barkouki, T., Ginn, T., Wu, Y., Smith, R., Hubbard, S., Fujita, Y., Sani, R., and Peyton, K., Application of TOUGHREACT V2.0 to environmental systems, In Proceedings of TOUGH Symposium 2009 Lawrence Berkeley National Laboratory, Berkeley, California, September 14-16, 2009.

Steefel, C. I., and van Cappellen, P., A new kinetic approach to modeling water-rock interaction: The role of nucleation, precursors and Ostwald ripening, *Geochim. Cosmochim. Acta*, v. 54, p. 2657-2677, 1990.

Steefel, C. I., and Lasaga, A. C., A coupled model for transport of multiple chemical species and kinetic precipitation/dissolution reactions with applications to reactive flow in single phase hydrothermal system, *Am. J. Sci.*, v. 294, p. 529-592, 1994.

Steefel, C. I., and MacQuarrie, K. T. B., Approaches to modeling of reactive transport in porous media, In Lichtner, P. C., Steefel, C. I., and Oelkers, E. H. (eds.), Reactive transport in porous media, Reviews in Mineralogy, Mineral Society of America, v. 34, p. 83-129, 1996.

Steefel, C. I., CRUNCH, Lawrence Livermore National Laboratory, pp. 76, 2001.

Stumm, W., and Morgan, J. J., Aquatic chemistry: *An Introduction Emphasizing Chemical Equilibria in Natural Waters*, John Wiley & Sons, New York, 780 pp., 1981.

Toevs, G.R., Morra, M.J., Polizzotto, M.L., Strawn, D.G., Bostick, B.C., Fendorf, S., Metal(loid) diagenesis in mine-impacted sediments of Lake Coeur d'Alene, Idaho. Environ. Sci. Technol. 40, 2537–2543, 2006.

Todaka, N., C. Akasaka, T. Xu and K. Pruess. Reactive geothermal transport simulation to study the formation mechanism of impermeable barrier between acidic and neutral fluid zones in the Onikobe geothermal field, Japan, J. Geophys. Res. Solid Earth, Vol. 109(B5):5209, doi: 10.1029/2003JB002792, 2004.

Van Cappellen, P., Gaillard, P., Biogeochemical dynamics in aquatic sediments. In: Lichtner, P.C., Steefel, C.I., Oelkers, E.H. (Eds.), Reactive Transport in Porous Media, vol. 34. Mineralogical Society of America, pp. 335–376 (Chapter 8), 1996.

Vanselow, A.P. 1932. Equilibria of the base-exchange reactions of bentonites, permutites, soil colloids, and zeolites. *Soil Sci.* 33: 95-113.

Van Genuchten, M. T., A closed-form equation for predicting the hydraulic conductivity of unsaturated soils, *Soil Sci. Soc. Am. J.*, v. 44, p. 892-898, 1980.

Vaniman, D. T., Chipera, S. J., Paleotransport of lanthanides and strontium recorded in calcite compositions from tuffs at Yucca Mountain, Nevada, USA. *Geochim. Cosmochim. Acta*, v.60(22), p.4417-4433, 1996.

Vaniman, D. T., Chipera, S. J., Bish, D. L., Carey, J. W., and Levy, S. S., Quantification of unsaturated-zone alteration and cation exchange in zeolitized tuffs at Yucca Mountain, Nevada, USA. *Geochim. Cosmochim. Acta*, v. 65(20), p. 3409-3433, 2001.

Vaughan, P. J., Analysis of permeability reduction during flow of heated, aqueous fluid through Westerly Granite, in C.F. Tsang (ed.), Coupled processes associated with nuclear waste repositories, pp. 529-539, Academic Press, New York, 1987.

Verma, A., and Pruess, K., Thermohydrological conditions and silica redistribution near high-level nuclear wastes emplaced in saturated geological formations, *J. Geophys. Res*., v. 93, p. 1159-1173, 1988.

Vinsome, P. K. W. and Westerveld, J., A simple method for predicting cap and base rock heat losses in thermal reservoir simulators, *J. Canadian Pet. Tech*., v. 19 (3), p. 87–90, 1980.

von Gunten, U. and Zobrist, J., Biogeochemical changes in groundwater infiltration systems: column studies, *Geochim. Cosmochim. Acta*, v. 57, p. 3895-3906, 1993.

Walter, A. L., Frind, E. O., Blowes, D. W., Ptacek, C. J., and Molson, J. W., Modeling of multicomponent reactive transport in groundwater: 1, Model development and evaluation, *Water Resour. Res*., v. 30, p. 3137-3148, 1994.

Weir, G. J., White, S. P., and Kissling, W. M., Reservoir Storage and Containment of Greenhouse Gases, in: K. Pruess (ed.), *Proceedings of the TOUGH Workshop '95*, Lawrence Berkeley National Laboratory Report LBL-37200, p. 233-238, Berkeley, CA, 1995.

White, S. P., Multiphase non-isothermal transport of systems of reacting chemicals, *Water Resour. Res*., v. 31, p.

1761-1772, 1995.

Winowiecki, L., 2002. Geochemical cycling of heavy metals in the sediment of Lake Coeur d'Alene, Idaho. Masters Thesis, University of Idaho, Moscow, Idaho.

Wolery, T. J., EQ3/6: Software package for geochemical modeling of aqueous systems: Package overview and installation guide (version 8.0), Lawrence Livermore National Laboratory Report UCRL-MA-110662 PT I, Livermore, California, 1992.

Wu, Y.-S., and Mishra, A.,K., Modifications and additions to the selected TOUGH2 modules. Lawrence Berkeley National Laboratory Report LBNL-41870, Berkeley, California, 58 pp., 1998.

Wu, Y.-S., Haukwa, C., and Mukhopadhay, S., TOUGH2 V1.4 and T2R3D V1.4: Verification and Validation Report, Rev.00, Revised 10/11/99, 1999. MOL.20000216.0111.

Xu, T., and Pruess, K., Coupled modeling of non-isothermal multiphase flow, solute transport and reactive chemistry in porous and fractured media: 1. Model development and validation, Lawrence Berkeley National Laboratory Report LBNL-42050, Berkeley, California, 38 pp., 1998.

Xu, T., Samper, J., Ayora, C., Manzano, M., and Custodio, E., Modeling of non-isothermal multi-component reactive transport in field-scale porous media flow system, *J. Hydrol*., v. 214, p. 144-164, 1999a.

Xu, T., Pruess, K., and Brimhall, G., An improved equilibrium-kinetics speciation algorithm for redox reactions in variably saturated flow systems, *Computers & Geosciences*, v. 25, p. 655-666, 1999b.

Xu, T., White, S. P., Pruess, K., Brimhall, G. H., and Apps, J., Modeling of pyrite oxidation in saturated and unsaturated subsurface flow systems, *Transport in Porous Media*, v. 39, p. 25-56, 2000.

Xu, T., and Pruess, K., On fluid flow and mineral alteration in fractured caprock of magmatic hydrothermal systems, *J. Geophys. Res*., v. 106, p. 2121-2138, 2001a.

Xu, T., and Pruess, K., Modeling multiphase fluid flow and reactive geochemical transport in variably saturated fractured rocks: 1. Methodology, *Am. J. Sci.*, v. 301, p. 16-33, 2001b.

Xu, T., Sonnenthal, E., Spycher, N., Pruess, K., Brimhall, G., Apps, J., Modeling multiphase fluid flow and reactive geochemical transport in variably saturated fractured rocks: 2. Applications to supergene copper enrichment and hydrothermal flows, *Am. J. Sci.*, v. 301, p. 34-59, 2001.

Xu, T., Sonnenthal, E., and Bodvarsson G., A reaction-transport model for calcite precipitation and evaluation of infiltration-percolation fluxes in unsaturated fractured rock, *J. Contam. Hydrol*., v. 64(1-2) p. 113 - 127, 2003a.

Xu, T., Apps, J. A., and Pruess, K., Reactive geochemical transport simulation to study mineral trapping for CO_2 disposal in deep arenaceous formations, *J. Geophys. Res*., v. 108 (B2), 2071, doi:10.1029/2002JB001979, 2003b.

Xu, T, Apps, J. A., and Pruess, K., Numerical simulation of CO_2 disposal by mineral trapping in deep aquifers, *Applied Geochemistry*, v. 19, p. 917-936, 2004a.

Xu, T., Ontoy, Y., Molling, P., Spycher, N., Parini, M., and Pruess, K., Reactive transport modeling of injection well scaling and acidizing at Tiwi Field Philippines, *Geothermics*, v. 33(4), p. 477-491, 2004b.

Xu, T., E.L. Sonnenthal, N. Spycher, and K. Pruess, TOUGHREACT - A simulation program for non-isothermal multiphase reactive geochemical transport in variably saturated geologic media: Applications to geothermal injectivity and CO_2 geological sequestration, *Computer & Geoscience*, v. 32/2 p. 145-165, 2006.

Xu, T., J. A. Apps, K. Pruess, and H. Yamamoto, Numerical modeling of injection and mineral trapping of CO_2 with H2S and SO2 in a sandstone formation, *Chemical Geology*, v. 242/3-4, p. 319-346, 2007.

Xu, T., Incorporation of aqueous reaction kinetics and biodegradation into TOUGHREACT: Application of a multi-region model to hydrobiogeochemical transport of denitrification and sulfate reduction, *Vadose Zone Journal*, v. 2008-7, p. 305-315, 2008.

Xu, T., R. Senger, and S. Finsterle, Corrosion-induced gas generation in a nuclear waste repository: Reactive geochemistry and multiphase flow effects, *Appl. Geochem.*, v. 23, 3423–3433, 2008.

Xu, T., Rose, P., Fayer, S., Pruess, On modeling of chemical stimulation of an enhanced geothermal system using a

high pH solution with chelating agent. *Geofluid*, v. 9, p. 167-177, 2009a.

Xu, T., Sonnenthal, E., Spycher, N., Zhang, G., Zheng, L., and Pruess, K., TOUGHREACT Version 2.0, In Proceedings of TOUGH Symposium 2009 Lawrence Berkeley National Laboratory, Berkeley, California, September 14-16, 2009b.

Xu, T., Spycher N., Sonnenthal E., Zhang G., Zheng L. and Pruess, K., TOUGHREACT Version 2.0: A simulator for subsurface reactive transport under non-isothermal multiphase flow conditions, Computers & Geosciences 37, 763–774, 2011.

Xu, T., Senger, R., and Finsterle, S., Bentonite alteration due to thermal-hydro-chemical processes during the early thermal period in a nuclear waste repository, Nuclear Technology, v.174, p. 438-451, 2011.

Yeh, G. T., and Tripathi, V. S., A model for simulating transport of reactive multispecies components: model development and demonstration, *Water Resour. Res*., v. 27, p. 3075-3094, 1991.

Zhang, W., Li, Y., Xu, T., Cheng, H., Zheng, Y., and Xiong, P., Long-term variations of CO_2 trapped in different mechanisms in deep saline formations: A case study of the Songliao Basin, China, *Greenhouse Gas Control Technologies*, v3(2), p. 161-180, 2009.

Zheng, L., Apps, J.A., Zhang, Y., Xu, T., and Birkholzer, J., On mobilization of lead and arsenic in groundwater in response to CO_2 leakage from deep geological storage, *Chemical Geology*, v. 268, p. 281-297, 2009.

Zysset, A., Stauffer, E., and Dracos, T., Modelling of reactive groundwater transport governed by biodegradation, *Water Resour. Res*., v. 30, p. 2423-2434, 1994.

Appendix A Mathematical Equations for Flow and Transport

All flow and transport equations have the same structure, and can be derived from the principle of mass (or energy) conservation. Table A-1 summarizes these equations and Table A-2 gives the meaning of symbols used. The models for fluid and heat flow are discussed in detail by Pruess (1987 and 1991) and Pruess et al. (1999). Aqueous species are subject to transport in the liquid phase and local chemical interaction with the solid and gaseous phases. Chemical transport equations are written in terms of total dissolved concentrations of chemical components comprised of concentrations of their basis species plus their associated aqueous secondary species (Yeh and Tripathi, 1991; Steefel and Lasaga, 1994; Walter et al., 1994). Advection and diffusion are considered for chemical transport, and diffusion coefficients are assumed to be the same for all aqueous species.

Table A—1 Governing equations for fluid and heat flow, and chemical transport. Symbol meanings are given in Table A-2. Take EOS3 and EOS4 flow modules as example. For EOS2 and ECO2N, component 'Air' in the table should be replaced with 'CO_2'. For EOS1, equation for air is not required. For EOS9, equations for air and heat are not required (only Richard's equation).

General governing equations: $$\frac{\partial M_\kappa}{\partial t} = -\nabla F_\kappa + q_\kappa$$

Water: $M_w = \phi(S_l\rho_l X_{wl} + S_g\rho_g X_{wg})$ $F_w = X_{wl}\rho_l \mathbf{u}_l + X_{wg}\rho_g \mathbf{u}_g$ $q_w = q_{wl} + q_{wg}$

Air: $M_c = \phi(S_l\rho_l X_{cl} + S_g\rho_g X_{cg})$ $F_c = X_{cl}\rho_l \mathbf{u}_l + X_{cg}\rho_g \mathbf{u}_g$ $q_c = q_{cl} + q_{cg} + q_{cr}$

Heat: $M_h = \phi(S_l\rho_l U_l + S_g\rho_g U_g) + (1-\phi)\rho_s U_s$ $F_h = \sum_{\beta=l,g} h_\beta \rho_\beta \mathbf{u}_\beta - \lambda\nabla T$ q_h

where $$\mathbf{u}_\beta = -k\frac{k_{r\beta}}{\mu_\beta}\left(\nabla P_\beta - \rho_\beta \mathbf{g}\right) \qquad \beta = l, g$$ **(Darcy's Law)**

Chemical components in the liquid phase ($j = 1,2,\ldots,N_l$):

$M_j = \phi S_l C_{jl}$ $F_j = \mathbf{u}_l C_{jl} - (\tau\phi S_l D_l)\nabla C_{jl}$ $q_j = q_{jl} + q_{js} + q_{jg}$

$\tau_\beta = \phi^{1/3} S_\beta^{7/3}$ **(Millington and Quirk, 1961)**

Table A—2 Symbols used in Table A-1.

C	component concentration, mol L^{-1}	ρ	density, kg m^{-3}
D	diffusion coefficient, m^2s^{-1}	μ	viscosity, kg $m^{-1}s^{-1}$
F	mass flux, kg $m^{-2}s^{-1}$ (*)	λ	heat conductivity, W $m^{-1}K^{-1}$
k	permeability, m^2		
k_r	relative permeability	Subscripts:	
g	gravitational acceleration, m s^{-2}	c	air
M	mass accumulation, kg m^{-3}	g	gas phase
N	number of chemical components	h	heat
p	pressure, Pa	j	aqueous chemical component
q	source/sink	l	liquid phase
S	saturation	r	reaction
T	temperature, °C	s	solid phase
U	internal energy, J kg^{-1}	w	water
u	Darcy velocity, m s^{-1}	κ	governing equation index
X	mass fraction	β	phase index
ϕ	porosity	τ	medium tortuosity

(*) For chemical transport and reaction calculations, molar units are used instead of kg.

The primary governing equations given in Table A-1 must be complemented with constitutive relationships that express all parameters as functions of thermophysical and chemical variables. The expressions for non-isothermal multiphase flow are given by Pruess et al. (1999). The expressions for chemical reactions are given in Appendix B.

Gas species diffusion coefficients are computed as a function of temperature, pressure, molecular weight, and molecular diameter. Assuming ideal gas behavior, the tracer diffusion coefficient of a gaseous species can be expressed as follows (Lasaga, 1998):

$$D = \frac{RT}{3\sqrt{2}\pi PN_A d_m^2}\sqrt{\frac{8RT}{\pi M}} \qquad \textbf{(A. 1)}$$

where:

D = diffusion coefficient (m^2/s)
R = molar gas constant (8.31451 $m^2kg\ s^{-2}mol^{-1}\ K^{-1}$)
T = temperature in Kelvin units
π = 3.1415926536
P = pressure (kg $m^{-1}\ s^{-2}$)
N_A = Avogadro's number (6.0221367×10^{23} molecules/mol)
D_m = molecular diameter (m)
M = molecular weight (kg/mol)

Appendix B Mathematical Formulation of Chemical Reactions

To represent a geochemical system, it is convenient to select a subset of N_C aqueous species as basis species (or component or primary species). All other species are called secondary species that include aqueous complexes, precipitated (mineral) and gaseous species (Reed, 1982; Yeh and Tripathi, 1991; Steefel and Lasaga, 1994). The number of secondary species must be equal to the number of independent reactions. Any of the secondary species can be represented as a linear combination of the set of basis species such as

$$S_i = \sum_{j=1}^{N_C} \nu_{ij} S_j \qquad i = 1,\ldots, N_R \tag{B.1}$$

where S represents chemical species, j is the basis species index, i is the secondary species index, N_R is the number of reactions (or secondary species), and ν_{ij} is the stoichiometric coefficient of j-th basis species in the i-th reaction.

B.1 Kinetic reactions among primary species

These type of reactions include aqueous and sorption reaction kinetics and biodegradation. A general-rate law is used,

$$r_i = \sum_{s=1}^{M} \left[\begin{array}{ll} k_{i,s} & \text{rate constant} \\ \times \prod_{j=1}^{N_l} \left(\gamma_j^{\nu_{i,j}} C_j^{\nu_{i,j}} \right) & \text{product terms} \\ \times \prod_{k=1}^{N_m} \dfrac{C_{i,k}}{K_{Mi,k} + C_{i,k}} & \text{Monod terms} \\ \times \prod_{p=1}^{N_p} \dfrac{I_{i,p}}{I_{i,p} + C_{i,p}} & \text{inhibition terms} \end{array} \right] \tag{B.2}$$

where r_i is the reaction rate of the i-th reaction, M is the number of mechanisms or pathways and s is the mechanism counter, k is a rate constant, (often denoted v_{max}, maximum specific growth constant for biodegradation), γ_j is the activity coefficient of species j, C_j is the concentration of species j (with biodegradation the product term is usually biomass concentration), $\nu_{i,j}$ is a stoichiometric coefficient, N_l is the number of reacting species in the forward rate term (called product terms), N_m is the number of Monod factors (Monod terms), $C_{i,k}$ is the concentration of the k-th Monod species, $C_{i,p}$ is the concentration of the p-th inhibiting species, $K_{Mi,k}$ is the k-th Monod half-saturation constant of the i-th species, N_P is the number of inhibition factors (inhibition terms), and $I_{i,p}$ is the p-th inhibition constant. Equation (B.2) accounts for multiple mechanisms and multiple products, Monod, and inhibition terms, which can cover many rate expressions (examples of rate expression are given in Samples 9 and 10).

B.2 Aqueous complexation

These reactions are assumed to be at local equilibrium. By making use of the mass action equation to the dissociation of the i-th aqueous complex (Equation B.1), concentrations of aqueous complexes can be expressed as functions of the concentrations of basis species:

$$c_i = K_i^{-1}\gamma_i^{-1}\prod_{j=1}^{N_c} c_j^{\nu_{ij}}\gamma_j^{\nu_{ij}} \tag{B.3}$$

where c_i is molal concentration of the i-th aqueous complex, and c_j is molal concentration of the j-th basis species, γ_i and γ_j are thermodynamic activity coefficients (details on calculation of activity coefficients are given in Appendix H), and K_i is the equilibrium constant.

B.3 Equilibrium mineral dissolution/precipitation

The mineral saturation ratio can be expressed as

$$\Omega_m = K_m^{-1}\prod_{j=1}^{N_C} c_j^{\nu_{mj}}\gamma_j^{\nu_{mj}} \qquad m = 1...N_P \tag{B.4}$$

where m is the equilibrium mineral index, and K_m is the corresponding equilibrium constant. At equilibrium, we have

$$SI_m = \log_{10}\Omega_m = 0 \tag{B.5}$$

where SI_m is called the mineral saturation index. The treatment for mineral solid solutions is given in Appendix I.

B.4 Kinetic mineral dissolution/precipitation

Kinetic rates could be functions of non-basis species as well. Usually the species appearing in rate laws happen to be basis species. In this model, we use a rate expression given by Lasaga et al. (1994):

$$r_n = f(c_1, c_2, ..., c_{N_C}) = \pm k_n A_n \left|1 - \Omega_n^{\theta}\right|^{\eta} \qquad n = 1...N_q \tag{B.6}$$

where positive values of r_n indicate dissolution, and negative values precipitation, k_n is the rate constant (moles per unit mineral surface area and unit time) which is temperature dependent, A_n is the specific reactive surface area per kg H_2O (details on A_n calculations are given in Appendix G), Ω_n is the kinetic mineral saturation ratio defined in (B.4). The parameters θ and η must be determined from experiments; usually, but not always, they are taken equal to one. The temperature dependence of the reaction rate constant can be expressed reasonably well via an Arrhenius

equation (Lasaga, 1984; Steefel and Lasaga, 1994). Because many rate constants are reported at 25°C, it is convenient to approximate rate constant dependency as a function of temperature, thus

$$k = k_{25} \exp\left[\frac{-E_a}{R}\left(\frac{1}{T} - \frac{1}{298.15}\right)\right] \quad \text{(B.7)}$$

where Ea is the activation energy, k25 is the rate constant at 25°C, R is gas constant, T is absolute temperature.

Carroll et al. (1998) noted that the rates of amorphous silica precipitation based on Rimstidt and Barnes (1980) are about three orders of magnitude lower than those observed in geothermal systems. Carroll et al. (1998) presented experimental data on amorphous silica precipitation for more complex geothermal fluids at higher degrees of supersaturation, and also for a near-saturation simple fluid chemistry. Under conditions far from equilibrium, the rate law for amorphous silica precipitation has been expressed as:

$$r = kA(\Omega)^{\theta} \quad \text{(B. 8)}$$

This rate does not tend to zero as Ω goes to one, and therefore, in TOUGHREACT, a modification was made to this law so that it tends to zero as Ω approaches one

$$r = kA\left[(\Omega)^{\theta} - \frac{1}{\Omega^{2\theta}}\right] \quad \text{(B. 9)}$$

The pH dependence of mineral precipitation and dissolution rates is calculated using the following expressions:

$$k_{adj} = k\,(10^{-pHc}/10^{-pH1})^{slope1} \qquad \text{if pHc < pH1} \quad \text{(B.10)}$$

$$k_{adj} = k\,(10^{-pHc}/10^{-pH2})^{-slope2} \qquad \text{if pHc > pH2} \quad \text{(B.11)}$$

where k_{adj} is the rate adjusted for pH, k is the original rate (Equation B.6), pH_c is the current (calculated) pH, *pH1* is the pH below which the rate is adjusted by *slope1* and *pH2* is the pH above which the rate is adjusted by *slope2*. Parameters *slope1* and *slope2* are the absolute values (both positive numbers) of the log(*k*) versus pH slopes below *pH1* and above *pH2*, respectively (Figure B.4-1). Between these two pH values, the rate is assumed to remain independent of pH.

Figure B.4—1 **Variation of reaction rate with pH. Slopes shown are for the dissolution of silicate and aluminosilicate minerals (After Drever, 1997).**

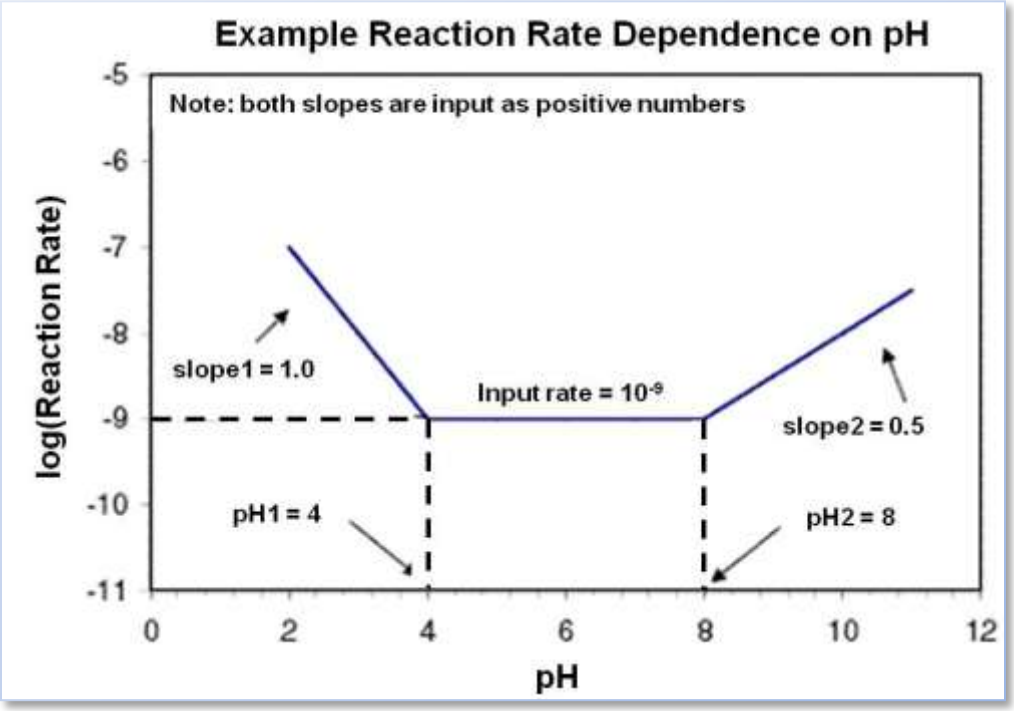

The kinetic rate constant (k) in Eqs. (B.6) and (B.7) only considers the most well-studied mechanism in pure H_2O (at neutral pH). Dissolution and precipitation of minerals are often catalyzed by H^+ (acid mechanism) and OH^- (base mechanism). For many minerals, the kinetic rate constant k includes each of these three mechanisms (Lasaga et al., 1994; Palandri and Kharaka, 2004), or

$$k = k_{25}^{nu}\exp\left[\frac{-E_a^{nu}}{R}\left(\frac{1}{T}-\frac{1}{298.15}\right)\right] + k_{25}^{H}\exp\left[\frac{-E_a^{H}}{R}\left(\frac{1}{T}-\frac{1}{298.15}\right)\right]a_H^{n_H} + k_{25}^{OH}\exp\left[\frac{-E_a^{OH}}{R}\left(\frac{1}{T}-\frac{1}{298.15}\right)\right]a_{OH}^{n_{OH}} \quad \text{(B.12)}$$

where superscripts or subscripts nu, H, and OH indicate neutral, acid and base mechanisms, respectively; a is the activity of the species; and n is power term (constant). Notice that parameters θ and η (see Eq. B.6) are assumed the same for each mechanism. The rate constant k can be also dependent on other species such as Al^{3+} and Fe^{3+}. Two or more species may be involved in one mechanism. A general form of species dependent rate constants (extension of Eq. B.12) is coded in TOUGHREACT, or,

$$k = k_{25}^{nu}\exp\left[\frac{-E_a^{nu}}{R}\left(\frac{1}{T}-\frac{1}{298.15}\right)\right] + \sum_i k_{25}^{i}\exp\left[\frac{-E_a^{i}}{R}\left(\frac{1}{T}-\frac{1}{298.15}\right)\right]\prod_j a_{ij}^{n_{ij}} \quad \text{(B.13)}$$

where superscripts or subscripts i is the additional mechanism index, and j is species index involved in one mechanism that can be primary or secondary species. TOUGHREACT considers up to five additional mechanisms and up to five species involved in each mechanism. An application of multiple mechanisms (Eq. B.13) can be found in the CO_2 disposal sample problem (Section 8.5).

The precipitation of a mineral can be suppressed up to a given, positive saturation index value, $\log(\Omega)_w$. Within this "supersaturation window", the mineral is not allowed to precipitate. The mineral precipitates if its saturation index $\log(\Omega) \geq \log(\Omega)_w$, and dissolves if $\log(\Omega) < 0$. The size of the window can be set to decrease exponentially with temperature as follows:

$$(\Omega)_{w,T} = \log(\Omega)_{w,T0} \exp(-4.61(T- T_0)/(T_1-T_0)) \quad \text{(B.14)}$$

where $\log(\Omega)_{w,T}$ is the window at the current temperature T and $\log(\Omega)_{w,T0}$ is the initial (input) window at temperature T_0. T_1 is the temperature at which the window is one-hundredth the size of the initial window (thus the temperature at which the effect of the window essentially disappears, see Figure B.4-2). Values of $\log(\Omega)_{w,T0}$, T_0, and T_1 are provided as input parameters.

Figure B.4—2 Supersaturation window dependence on temperature.

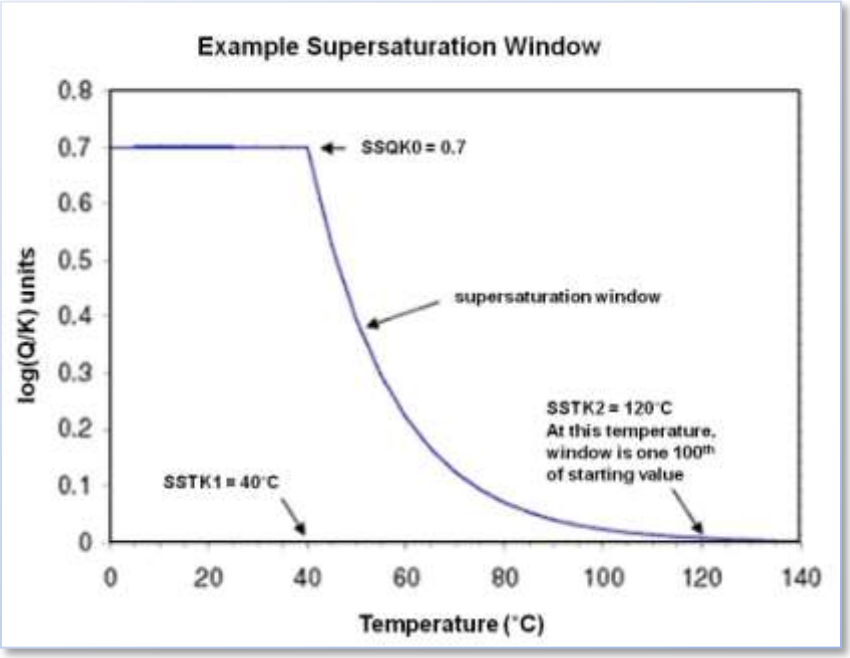

B.5 Gas dissolution/exsolution

Reactions involving aqueous and gaseous phases are usually assumed to be at equilibrium. According to the Mass-Action Law, one has:

$$P_f \Gamma_f K_f = \prod_{i=1}^{N_c} c_i^{\nu_{fi}} \gamma_i^{\nu_{fi}} \tag{B.15}$$

where subscript f is gas index, p is the partial pressure (in bar), Γ is the gas fugacity coefficient. For low pressures (in the range of atmospheric pressure), the gaseous phase is assumed to behave like an ideal mixture, and the fugacity coefficient Γ is assumed equal to one. At higher temperatures and pressures, such as boiling conditions in hydrothermal systems and CO_2 disposal in deep aquifers, the assumption of ideal gas and ideal mixing behavior is not valid, and the fugacity coefficients should be corrected according to temperatures and pressures (Spycher and Reed, 1988). For example, for H_2O-CO_2 mixtures in boiling conditions, we assume that H_2O and CO_2 are real gases, but their mixing is ideal. Following Spycher and Reed (1988), the fugacity coefficients is calculated from

$$\ln\Gamma = (\frac{a}{T^2} + \frac{b}{T} + c)P + (\frac{d}{T^2} + \frac{e}{T} + f)\frac{P^2}{2} \tag{B.16}$$

where P is the total gas pressure (vapor and CO_2), T is absolute temperature, and a, b, c, d, e, and f are constants fitted from experimental data. For P-T ranges, 50-350°C, up to 500 bars, the fitted constants for CO_2 have the following values: a = -1430.87, b = 3.598, c = -2.27376×10^{-3}, d = 3.47644, e = -1.04247×10^{-2}, and f = 8.36271×10^{-6}. Examples of equilibrium calculations between aqueous and gas phases show that ideal mixing of real gases is a reasonable approximation near the water saturation pressure curve (Spycher and Reed, 1988). Details on fugacity correction are given in Section H.4 of Appendix H.

For low ionic strength solution, the CO_2(aq) activity coefficient γ can be assumed equal to one. For a high ionic strength sodium chloride solution, γ should be corrected (salting out effect). Here we use an activity coefficient expression of Drummond (1981) for CO_2(aq):

$$\ln\gamma = (C + FT + \frac{G}{T})I - (E + HT)(\frac{I}{I+1}) \tag{B.17}$$

where T is the absolute temperature, I is ionic strength (or sodium chloride molality), C, F G, E, and H are constants (C=-1.0312, F=0.0012806, G=255.9, E=0.4445, and H=-0.001606). A similar expression is used in other geochemical modeling codes such as in EQ3/6 (Wolery, 1992). The ionic strength, I, is defined by

$$I = \frac{1}{2}\sum_i c_i z_i^2 \tag{B.18}$$

where the summation is over all aqueous species, and c_i and z_i are concentration (mol/kg H_2O) and electrical charge of species i.

B.6 Cation exchange

Cation exchange takes place when free cations in solution exchange with interlayer cations. This process can be described as an equilibrium reaction between an exchangeable cation and an exchange site. The equilibrium constant is usually known as the exchange coefficient because its value depends on the ionic strength of the solution. A general expression for cation exchange reactions according to the Gaines-Thomas convention is (Appelo and Postma, 1993):

$$\frac{1}{\nu_i} S_i + \frac{1}{\nu_j}\left(X_{\nu_j} - S_j\right) \Leftrightarrow \frac{1}{\nu_i}\left(X_{\nu_i} - S_i\right) + \frac{1}{\nu_j} S_j \tag{B.19}$$

where ν_i and ν_j are the stoichiometric coefficients (equal to their charges) of dissolved and interlayer cations, respectively; S_i and S_j denote dissolved cationic species and $\left(X_{\nu_i} - S_i\right)$ and $\left(X_{\nu_j} - S_j\right)$ represent exchange sites or exchange interlayer cations. Let's have an example:

$$Na^+ + 0.5Ca\text{-}X_2 = 0.5Ca^{2+} + Na\text{-}X \tag{B.19a}$$

$$Na^+ + K\text{-}X = K^+ + Na\text{-}X \tag{B.19b}$$

The equilibrium equation for cation exchange is obtained from the Mass Action Law:

$$K_{ij}^* = \frac{\bar{w}_i^{1/\nu_i} \cdot a_j^{1/\nu_j}}{\bar{w}_j^{1/\nu_j} \cdot a_i^{1/\nu_i}} \tag{B.20}$$

where K_{ij}^* is the exchange coefficient or selectivity, a_j is the activity of the j-th dissolved species and $\bar{w}_i$ is the activity of the i-th interlayer cation. For the example of (B.19a), we have:

$$K_{Na/Ca}^* = \frac{\bar{w}_{Na} \cdot a_{Ca}^{0.5}}{\bar{w}_{Ca}^{0.5} \cdot a_{Na}} \tag{B.20a}$$

Activities of dissolved cations are related to concentrations as given in Appendix H. Activities of interlayer cations are approximated by (1) their equivalent fractions of the number of exchange sites, which is commonly referred as the ***Gaines-Thomas*** convention (Appelo and Postma, 1993), after Gaines and Thomas (1953) who was among the first to give a rigorous definition of a thermodynamic standard state of interlayer cations; or (2) their molar fractions of the number of exchange sites, which follows ***Vanselow*** convention (Vanselow, 1932). Thus, the activity of the

interlayer cation $\overline{w}_i$ is assumed to be equal to its fraction β_i of equivalent (Gaines-Thomas convention) or mole (Vanselow convention), and is calculated as:

$$\overline{w}_i \cong \beta_i = \frac{w_i}{\sum_{i=1}^{N_w} w_i} \tag{B.21}$$

where w_i is the concentration of the i-th interlayer cation and N_w is the total number of such interlayer cations. The sum of concentrations of exchange sites or interlayer cations is the so-called cation exchange capacity (CEC). Substituting (B.21) into (B.20) yields the general equation for cation exchange:

$$K_{ij}^{*} = \frac{\beta_i^{1/\nu_i} \cdot \left(c_j \gamma_j\right)^{1/\nu_j}}{\beta_j^{1/\nu_j} \cdot \left(c_i \gamma_i\right)^{1/\nu_i}} \tag{B.22}$$

where the activity of each dissolved species a_i has been expressed as the product of its concentration c_i time its activity coefficients γ_i. The Na/Ca exchange example becomes

$$K_{Na/Ca}^{*} = \frac{\beta_{Na}^{1/1} \cdot \left(c_{Ca}\gamma_{Ca}\right)^{1/2}}{\beta_{Ca}^{1/2} \cdot \left(c_{Na}\gamma_{Na}\right)^{1/1}} \tag{B.22a}$$

From Eq. (B.22), β_j can be expressed as

$$\beta_j = \left(K_{ij}^{*}\right)^{-\nu_j} c_j \gamma_j \left(\frac{\beta_i}{c_i \gamma_i}\right)^{\nu_j/\nu_i} \qquad j = 1,2,\cdots,N_w \tag{B.23}$$

For Na/Ca exchange example, we have:

$$\beta_{Ca} = \left(K_{Na/Ca}^{*}\right)^{-2} c_{Ca}\gamma_{Ca}\left(\frac{\beta_{Na}}{c_{Na}\gamma_{Na}}\right)^{2/1} \tag{B.23a}$$

From the definition of Eq. (B.21), one has:

$$\sum_{j=1}^{N_w} \beta_j = 1 \tag{B.24}$$

Substituting Equation B.23 into B.24 results in:

$$\sum_{j=1}^{N_w}\left(K_{ij}^{*}\right)^{-\nu_j} c_j \gamma_j \left(\frac{\beta_i}{c_i \gamma_i}\right)^{\nu_j/\nu_i} = 1 \qquad \text{(B.25)}$$

which for given dissolved concentrations cj can be solved for the single unknown β_i. This equation is quadratic when cation exchange involves only homovalent and divalent cations. However, when cation exchange involves also trivalent cations a cubic equation is obtained. Once the equivalent fraction β_i is known the rest of exchange fractions can be calculated from Equation B.21. According to Equation B.21, the concentration of the i-th exchanged cation w_j (in moles per liter of fluid) can be obtained from

$$w_j = \beta_j \sum_{j=1}^{N_w} w_j \, \rho_s \frac{(1-\phi)}{100\phi z_j} \qquad \text{for } \textit{Gaines-Thomas} \text{ convention} \qquad \text{(B.26a)}$$

$$w_j = \beta_j \sum_{j=1}^{N_w} w_j \, \rho_s \frac{(1-\phi)}{100\phi} \qquad \text{for } \textit{Vanselow} \text{ convention} \qquad \text{(B.26b)}$$

For the commonly used Gaines-Thomas convention, $\sum_{j=1}^{N_w} w_j$ is also referred as CEC, the cation exchange capacity (usually measured as the number of milli equivalents of cations per 100 gram of solid), ϕ is the porosity, ρ_s is the density of the solids (kg of solids per dm^3 of solids), and z_j is the cation charge.

A third cation exchange convention implemented is ***Gapon*** convention (Gapon, 1933). In this convention, the activities of the adsorbed ions are expressed as a fraction of the number of exchange sites (X^-). When cation exchange involves homovalent and divalent cations, the reaction should be written as

$$Na^+ + Ca_{0.5}\text{-}X = 0.5Ca^{2+} + Na\text{-}X \qquad \text{(B.27)}$$

with

$$K_{Na/Ca}^{*} = \frac{[Na-X][Ca^{2+}]^{0.5}}{[Ca_{0.5}-X][Na^+]} = \frac{\beta_{Na}[Ca^{2+}]^{0.5}}{\beta_{Ca}[Na^+]} \qquad \text{(B.28)}$$

In this case, molar and equivalent fractions become identical since both are based on a single exchange site with charge -1.

Under variably water-saturated condition, exchangeable surface sites depend on water saturation. Assuming an ideal-wetting condition, using a correct with water saturation S_l, Eq. B.26a becomes (a similar form for B.26b):

$$w_j = \beta_j \sum_{j=1}^{N_w} w_j \, \rho_s \frac{(1-\phi)}{100\phi z_j S_l} \tag{B.29}$$

In Eq. B.29, as S_l goes to zero, the surface sites (concentration) would tend to infinity. Clearly, at a very low liquid saturation, the exchangeable (reactive or effective) sites of the soil contacted by water are likely much smaller than the total sites.

The dependence of the surface sites on water saturation is very complex in field-scale conditions. Two methods (models) have been implemented to address this phenomenon. The first method considers that the surface sites contacted by water diminish proportionately to the saturation (Model 1), or ideal-wetting condition. The second method considers multiplying a (correction) factor f that depends on liquid saturation, $f(S_l)$, or

$$w_j = \beta_j \sum_{j=1}^{N_w} w_j \, \rho_s \frac{(1-\phi)}{100\phi z_j S_l} f(S_l) \tag{B.30}$$

Values of the factor f range from zero to one, or $0 \le f \le 1$. One $f(S_l)$ function could be adopted from the reactive surface area calculations for dissolution and precipitation of minerals (Model 2; see Appendix K).

The above equations (B.19 to B.30) are formulated for a single-site exchange of cations. Multi-site exchanges are implemented. Each site is assumed to be independent. Eqs. B.19 to B.30 are applied for each site.

B.7 Surface Complexation

Surface Electric Potential Model

The sorption of solutes on solid surfaces can be described as a chemical reaction between the aqueous species and the specific surface sites (surface complexation). These surface reactions include proton exchange, cation binding and anion binding via ligand exchange at surface hydroxyl sites (represented here as XOH to avoid confusion with other chemical species). For example, the sorption of a metal could be represented as:

$$XOH + M^{z+} = XOM^{z+-1} + H^{+} \tag{B.31}$$

At equilibrium, the sorption reactions can be described by the mass law equation:

$$K_{app} = \frac{\left[XOM^{z_+^{-1}}\right] a_{H^+}}{[XOM]\, a_{M^{z+}}} \tag{B.32}$$

where K_{app} is referred to as the apparent equilibrium constant, because it includes surface charge effects and hence is dependent on the extent of surface ionization (Dzombak and Morel, 1990), *a* is the thermodynamic activity of the aqueous species, and the terms in brackets represent the concentration of surface complexes (mol/kg).

In aqueous complexation reactions, the electric charge is assumed to be homogeneous in the solution. However, surface reactions take place on a fixed charged surface creating an electrostatic field. An additional energetic term accounting for the work needed for the aqueous species to travel across the surface electric field is required:

$$\Delta G_{ads} = \Delta G_{intr} + \Delta G_{coul} = \Delta G_{intr} + (\Delta G_{\psi=0} - \Delta G_{\psi=\psi_0}) = \Delta G_{intr} - zF\psi_0 \quad \text{(B.33)}$$

where ΔG_{ads} is the free enthalpy change of the overall adsorption reaction, ΔG_{intr} and ΔG_{coul} are the free enthalpy change due to chemical bonding and to the electrostatic work, respectively, z is the charge of the surface species, F the Faraday's constant (96485 C/mol), and ψ_0 is the mean surface potential (V). Since

$$\Delta G = -RT\ln K, \quad \text{(B.34)}$$

Equation (B.33) can be rewritten as:

$$K_{app} = K_{int}\, e^{\frac{zF\psi_0}{RT}}, \quad \text{(B.35)}$$

where *R* is the gas constant (8.354 J/mol/K), *T* is the absolute temperature (K), and K_{int} is the intrinsic equilibrium constant which does not depend on the surface charge.

Diffuse Layer Model

The diffuse layer model has been described in great detail by Dzombak and Morel (1990) and was applied to adsorption of metals on iron oxide surfaces. In the diffuse layer model, the solid-water interface is composed of two layers: a layer of surface-bound complexes and a diffuse layer of counter ions in solution. The surface charge is calculated from the total surface species adsorbed on the layer:

$$\sigma_p = \frac{F}{A}\sum_{k=1}^{N_s} z_k y_k \quad \text{(B.36)}$$

According to the Gouy-Chapman theory, the surface charge density σ_p (c/m^2) is related to the potential at the surface (volt) by:

$$\sigma_d = (8RT\varepsilon\varepsilon_0 I \times 10^3)^{1/2} \sinh(zF\psi_0/2RT), \quad \text{(B.37)}$$

where R is the molar gas constant (8.354 J mol-1 K-1), T is the absolute temperature (K), is the relative dielectric constant of water (ε = 78.5 at 29oC), ε_0 is the permittivity of free space (8.754 10-12 C V-1 m-1 or 8.754 10-12 C2 J-1 m-1), and C is the molar electrolyte concentration (M). Equation (B.37) is only valid for a symmetrical electrolyte (Z=ionic charge). It is common to use the linearized version of Equation (B.37) for low values of the potential:

$$\sigma_p = \varepsilon\varepsilon_0\kappa\psi_0, \quad \text{(B.38)}$$

where 1/κ (m) is the double-layer thickness defined as:

$$\frac{1}{\kappa} = \left(\frac{\varepsilon\varepsilon_0 RT}{2F^2 \cdot 1000I}\right)^{1/2} \quad \text{(B.39)}$$

Equations (B.37) can be simplified by rewritten $(8RT\varepsilon\varepsilon_0 I \times 10^3)^{1/2}$ for 29°C:

$$\sigma_p = 0.1174 I^{1/2} \sinh(zF\psi_d/2RT) \quad \text{(B.40)}$$

Therefore, in the diffuse-layer model, the value of the capacitance *C* relating the surface charge and the potential can be calculated based on theoretical considerations (Equation B.38) instead of being an experimental fitting parameter.

Constant Capacitance Model

Similar to the diffused-layer, the constant capacitance model is based on the assumption that all the species are adsorbed in the same layer and a diffuse layer of counterions constitutes the transition to homogenous solution. However, differently from the diffuse-layer model, the relationship between the surface charge and the potential is assumed to be linear:

$$\sigma = C\psi \quad \text{(B.41)}$$

where *C* is a constant value to be obtained from fitting experimental data.

Mathematical Formulation of Adsorption Reactions

Lets us consider the following surface desorption reaction:

$$XOM^{z_+-1} = XOH + M^{z_+} - H^+$$

with the equilibrium constant of the reaction given as:

$$K_{\text{int}} = \frac{[XOH]a_M}{[XOM]a_{H^+}} e^{\left(\frac{-zF\psi_0}{RT}\right)} \tag{B.42}$$

Usually, the neutral surface complex *XOH* is included in the N_C aqueous primary species. The new unknown is the potential term

$$\tilde{\psi} = \frac{-F\psi_0}{RT} \tag{B.43}$$

The concentration of a surface complex, y_j, (mol/m^3), can be expressed in terms of the concentration of the primary species and the potential term:

$$y_j = K_j^{-1} \prod_{i=1}^{N_C} c_i^{\nu_{ji}^y} \gamma_i^{\nu_{ji}^y} e^{z_j \tilde{\psi}} \qquad j = 1 \ldots N_Y \tag{B.44}$$

where K_j is the intrinsic equilibrium constant of the desorption reaction.

In order to solve for the potential term, an additional equilibrium equation is needed. For the double diffuse layer model, we obtain Equation (B.45), if the Guoy-Chapman double-layer theory is used to relate surface charge and the potential (Equation (B.37)). If the linearized Equation (B.38) is used, we obtain Equation (B.46). If a constant capacity model is used, we obtain Equation (B.47).

$$(8RT\varepsilon\varepsilon_0 I \times 10^3)^{1/2} \sinh(-\tilde{\psi}/2) - \frac{F}{A} \sum_{k=1}^{N_s} z_k y_k = 0 \tag{B.45}$$

$$\frac{F^2}{A\varepsilon\varepsilon_0 \kappa RT} \sum_{k=1}^{N_s} z_k y_k + \tilde{\psi} = 0 \tag{B.46}$$

$$\frac{F^2}{ACRT} \sum_{k=1}^{N_s} z_k y_k + \tilde{\psi} = 0 \tag{B.47}$$

Appendix C Solution Method for Solute Transport Equations

Most chemical species are only subject to transport in the liquid phase. A few species can be transported in both liquid and gas phases such as O_2 and CO_2. We first derive the numerical formulation of reactive transport in the liquid phase. This will then be extended to transport in the gas phases for some gaseous species.

C.1 Transport in the Liquid Phase

In the sequential iteration approach (SIA), the mass transport equations and chemical reaction equations are considered as two relatively independent subsystems. They are solved separately in a sequential manner following an iterative procedure. If reactions taking place in the liquid phase are assumed to be at local equilibrium, mass transport equations can be written in terms of total dissolved component concentrations. By lumping all mass accumulation terms due to mass transfer between aqueous and solid phases including precipitated (kinetics and equilibrium), exchanged and sorbed species, and by using Equation (4.1) (in Chapter 4), we can write equations for multi-component chemical transport in the liquid phase as

$$\frac{\Delta t}{V_n}\sum_m A_{nm}\left[u_{nm}^{k+1}C_{nm}^{(j),k+1,s+1/2}+D_{nm}\frac{C_m^{(j),k+1,s+1/2}-C_n^{(j),k+1,s+1/2}}{d_{nm}}\right]= \Delta M_n^{(j),k+1}-q_n^{(j)k+1}\Delta t-R_n^{(j),k+1,s}\Delta t \qquad j=1,2,\ldots,N_C \tag{C.1}$$

where n labels the grid block, m label the adjacent grid blocks connected to n, j labels the chemical component, N_C is the total number of chemical components, l labels liquid phase (for simplicity, the liquid phase index l is neglected), k labels the number of the time step, s labels the number of the transport-chemistry iteration (details is given later), u_{nm} is the liquid volumetric flux or the Darcy velocity (m/s), D_{nm} is the effective diffusion coefficient (including effects of porosity, phase saturation, tortuosity and weighting factors between the two grid blocks), d_{nm} is the nodal distance, $R_n^{(j)k+1}$ are the overall chemical reaction source/sink terms.

The concentrations in the advective and diffusive flux terms of Equation (C.1) can be evaluated by

$$C_{nm}^{(j),k+1,s+1/2}=\theta\left[\varepsilon_{nm}C_n^{(j),k+1,s+1/2}+(1-\varepsilon_{nm})C_m^{(j),k+1,s+1/2}\right] (1-\theta)\left[\varepsilon_{nm}C_n^{(j),k}+(1-\varepsilon_{nm})C_m^{(j),k}\right] \tag{C.2}$$

$$C_n^{(j),k+1,s+1/2}=\theta C_n^{(j),k+1,s+1/2}+(1-\theta)C_n^{(j),k}$$

$$C_m^{(j),k+1,s+1/2}=\theta C_m^{(j),k+1,s+1/2}+(1-\theta)C_m^{(j),k}$$

where θ is the time weighting factor, with values in the range from 0 to 1; θ = 1 indicates a fully implicit calculation; and

$$\varepsilon_{nm} = \begin{cases} 0 & \text{if } u_{nm} \geq 0 \text{ inflow} \\ 1 & u_{nm} < 0 \text{ outflow} \end{cases}$$

Fully upstream weighting is used for advective flux calculations. The mass accumulation terms can be evaluated as

$$\Delta M_n^{(j),k+1} = S_{l,n}^{k+1} \phi_n^{k+1} C_n^{(j),k+1,s+1/2} - S_{l,n}^{k} \phi_n^{k} C_n^{(j),k} \tag{C.3}$$

By substituting Equations (C.2) and (C.3) into (C.1), and then rearranging them in terms of unknowns, $C^{(j),k+1,s+1/2}$ (total dissolved component concentrations), one has

$$\begin{aligned} &\left[S_{l,n}^{k+1} \phi_n^{k+1} + \frac{\theta \Delta t}{V_n} \sum_m A_{nm} \left(-u_{nm}^{k+1} \varepsilon_{nm} + \frac{D_{nm}}{d_{nm}} \right) \right] C_n^{(j),k+1,s+1/2} + \\ &\frac{\theta \Delta t}{V_n} \sum_m A_{nm} \left[u_{nm}^{k+1} (\varepsilon_{nm} - 1) - \frac{D_{nm}}{d_{nm}} \right] C_m^{(j),k+1,s+1/2} \quad = \\ &\frac{(1-\theta)\Delta t}{V_n} \sum_m A_{nm} \left(u_{nm}^{k+1} \varepsilon_{nm} - \frac{D_{nm}}{d_{nm}} \right) C_n^{(j),k} - \\ &\frac{(1-\theta)\Delta t}{V_n} \sum_m A_{nm} \left[u_{nm}^{k+1} (\varepsilon_{nm} - 1) + \frac{D_{nm}}{d_{nm}} \right] C_m^{(j),k} \\ &S_{l,n}^{k} \phi_n^{k} C_n^{(j),k} + q_n^{(j)k+1} \Delta t + R_n^{(j),k+1,s} \Delta t \qquad j = 1,2,..,N_C \end{aligned} \tag{C.4}$$

For the sequential iteration approach, the iteration index s is essential. A new transport-chemistry iteration consists of two parts, transport part denoted by, s+1/2, (it should be noted that ½ does not mean Δt/2), and chemistry part denoted by, s+1. Equation (C.4) for each chemical component j is linear if $R^{(j),s}$ is known, and has the same structure as the non-reacting (conservative) solute transport equation. The chemical reaction source/sink term $R^{(j),s}$ represents mass transfer of component j between aqueous and solid phases. The values of these source/sink terms at the new transport iteration, s+1/2, are evaluated at the previous chemistry iteration, s. The resulting new values of $C^{(j),s+1/2}$, obtained by solving transport Equations (C.1), are substituted into chemical reaction subroutines and one can compute new values of $R^{(j),s+1}$. Transport and chemical reaction equations are solved iteratively until the prescribed convergence criteria are satisfied. The essence of this sequential iteration approach is therefore the sequential solution of two independent sets of equations: the transport equations and the chemical equations. The transport equations are solved on a component-by-component basis, whereas the chemical equations are solved on a grid block by grid block basis. These two sets of equations are coupled by updating chemical source/sink terms.

For kinetic mineral dissolution-precipitation, the terms $R^{(j)}$ can be calculated directly from kinetic expressions. For equilibrium, these terms can be obtained indirectly from component mass balance equations. The solution of chemical equilibrium system and calculation of the source/sink terms $R^{(j)}$ are presented in Appendix D.

From the chemistry point of view, equilibrium mineral dissolution-precipitation does not appear in an explicit rate expression. To avoid confusion, we write the last term in Equation (C.4) as

$$R_n^{(j),k+1,s}\Delta t = -\Delta P_n^{(j),k+1,s} \tag{C.5}$$

where $\Delta P_n^{(j),k+1,s}$ means mass transfer of component j from the aqueous phase to the mineral phase at iteration s, grid block n and time step k+1 (or called mass accumulation in mineral phases; negative values indicate mass transfer from the mineral phase to the aqueous phase).

Returning to Equation (C.4), we can see that the coefficient matrix is the same for all chemical components as long as diffusion coefficients are the same for all aqueous species. The matrix depends on space and time discretization, and flow conditions. The equations for different components only differ in right-hand side terms.

The mathematical treatment of adding Kd linear adsorption and first-order decay effects in the model follows the work by Oldenburg and Pruess (1995, EOS7R), but no gas phase partitioning is considered. The mass accumulation term for any species (for simplification, the species index is not appeared in the following equations) with Kd adsorption on the solid matrix is

$$M = \phi S_l C + (1-\phi)\rho_s C K_d \tag{C.6}$$

where ϕ is porosity, S_l is the liquid saturation, C is the aqueous concentration (mol/l), ρ_s is the solid density (kg/dm^3), K_d is the distribution coefficient (l/kg = mass/kg solid divided by mass/l solution) and is species-dependent. The accumulation also term can be written in terms of a retardation factor

$$M = \phi S_l R C \tag{C.7}$$

and

$$R = 1 + \frac{(1-\phi)\rho_s}{\phi S_l} K_d \tag{C.8}$$

The input can be optionally by Kd and R, depending on user convenience and data availability.

The first-order decay of a species is handled by the discretized equation (Oldenburg and Pruess, 1995)

$$M_n^{k+1}(1+\lambda\Delta t) - M_n^k = \frac{\Delta t}{V_n}\left(\sum_m A_{nm} F_{nm}^{k+1} + V_n q_n^{k+1}\right) \tag{C.9}$$

where λ is decay constant (1/s) which is species-dependent, subscript n labels grid block, superscript k labels time step, subscript m labels the grid block connected to grid block n, Δt is time step size, M_n is the average mass per unit

volume, surface integrals are approximated as a discrete sum of averages over surface segments A_{nm}, F_{nm} is the average mass flux over the surface segment A_{nm} between volume elements V_n and V_m, and q is the average value of source/sink term per unit volume and unit time.

C.2 Transport in the Gas Phase

Gaseous species concentrations can be related to partial pressures by

$$C_g = \frac{10^2}{RT} P_g \tag{C.10}$$

where C_g are gaseous species concentrations (in mol/l), P_g is the gaseous species partial pressure (in bar), R is the gas constant (8.314 J mol^{-1} K^{-1}) and T is the absolute temperature. By following the same principle as used for transport in liquid phase and by considering Equation (C.10), the numerical formulation of gaseous transport in the gas phases can be expressed as

$$\left[\frac{10^2}{RT} S_{g,n}^{k+1}\phi_n^{k+1} + \frac{\Delta t}{V_n}\sum_m A_{nm}\frac{10^2}{RT}\left(-u_{g,nm}^{k+1}\varepsilon_{g,nm} + \frac{D_{g,nm}}{d_{nm}}\right)\right] P_{g,n}^{(j),k+1,s+1/2} +$$

$$\frac{\Delta t}{V_n}\sum_m A_{nm}\frac{10^2}{RT}\left[u_{g,nm}^{k+1}(\varepsilon_{g,nm}-1) - \frac{D_{g,nm}}{d_{nm}}\right] P_{g,m}^{(j),k+1,s+1/2} = \tag{C.11}$$

$$\frac{10^2}{RT} S_{g,n}^{k}\phi_n^{k} P_{g,n}^{(j),k} + q_n^{(j)k+1}\Delta t + R_n^{(j),k+1,s}\Delta t \qquad j = 1,2,...,N_g$$

where N_g is number of gaseous species. The structure of Equations (C.11) is the same as that of (C.4) for transport only in liquid phase. The same solution method can be applied for solving Equations (C.11).

Appendix D Solution Method for Mixed Equilibrium-Kinetics Chemical System

Aqueous complexation and gas dissolution/exsolution proceed according to local equilibrium, while mineral dissolution/precipitation are subject to equilibrium and/or kinetic conditions. Gas dissolution/exsolution is included in the model and treated in a similar way as equilibrium mineral dissolution/precipitation but fugacity correction. The formulation is based on mass balances in terms of basis species as used by Parkhurst el al. (1980) and Reed (1982) for the equilibrium chemical system. The kinetic rate expressions for mineral dissolution/precipitation are included in the equations along with the mass balances of basis species. At time zero (initial), the total concentrations of basis species j in the system are assumed to be known, and are given by

$$T_j^0 = c_j^0 + \sum_{k=1}^{N_x}\nu_{kj}c_k^0 + \sum_{m=1}^{N_p}\nu_{mj}c_m^0 + \sum_{n=1}^{N_q}\nu_{nj}c_n^0 + \sum_{z=1}^{N_z}\nu_{zj}c_z^0 + \sum_{s=1}^{N_s}\nu_{sj}c_s^0 \qquad j = 1...N_C \tag{D.1}$$

where superscript 0 represents time zero; c denotes concentration; subscripts j, k, m, n, z and s are the indices of the primary species, aqueous complexes, minerals at equilibrium, minerals under kinetic constraints, and exchanged and surface complexes, respectively; N_c, N_x, N_p, N_q, N_z and N_s are the number of corresponding species and minerals; and ν_{kj}, ν_{mj}, ν_{nj}, ν_{zj} and ν_{sj} are stoichiometric coefficients of the primary species in the aqueous complexes, equilibrium, kinetic minerals, and exchanged and surface complexes, respectively.

After a time step Δt, the total concentration of primary species j (T_j) is given by

$$T_j = c_j + \sum_{k=1}^{N_x} \nu_{kj} c_k + \sum_{m=1}^{N_p} \nu_{mj} c_m + \sum_{n=1}^{N_q} \nu_{nj} \left(c_n^0 - r_n \Delta t \right) + \sum_{z=1}^{N_z} \nu_{zj} c_z + \sum_{s=1}^{N_s} \nu_{sj} c_s \qquad j = 1 \ldots N_C \tag{D.2}$$

where r_n is the kinetic rate of mineral dissolution (negative for precipitation, units used here are mole per kilogram of water per time), for which a general multi-mechanism rate law can be used. Δt and T_j are related through generation of j among primary species as follows

$$T_j - T_j^0 = \sum_{l=1}^{N_a} \nu_{lj} r_l \Delta t \qquad j = 1, \ldots N_C \tag{D.3}$$

where *l* is the aqueous kinetic reaction (including biodegradation) index, N_a is total number of kinetic reactions among primary species, and r_l is the kinetic rate which is in terms of one mole of product species.

By substituting Equations (D.1) and (D.2) into Equation (D.3), and denoting residuals as F_j^c (which are zero in the limit of convergence), we have

$$\begin{aligned} F_j^c = {} & (c_j - c_j^0) && \text{primary species} \\ & + \sum_{k=1}^{N_x} \nu_{kj} (c_k - c_k^0) && \text{equilibrium aqueous complexes} \\ & + \sum_{z=1}^{N_z} \nu_{zj} (c_z - c_z^0) && \text{exchanged complexes} \\ & + \sum_{s=1}^{N_s} \nu_{sj} (c_s - c_s^0) && \text{surface complexes} \\ & + \sum_{m=1}^{N_p} \nu_{mj} (c_m - c_m^0) && \text{equilibrium minerals} \\ & - \sum_{n=1}^{N_q} \nu_{nj} r_n \Delta t && \text{kinetic minerals} \\ & - \sum_{l=1}^{N_a} \nu_{lj} r_l \Delta t && \text{kinetics among primary species} \\ = {} & 0 && j = 1 \ldots N_C \end{aligned} \tag{D.4}$$

According to mass-action equations, the concentrations of aqueous and exchanged complexes ck and cz can be expressed as functions of concentrations of the primary species cj. Kinetic rates rn and rl are functions of cj. The expression for rn is given in Eq. B.6 in Appendix B, and rl will be presented in Eq. B.2. Surface complexes are expressed as the product of primary species and an additional potential term Ψ. Additional equilibrium equations (Equation (B.42) or (B.43) depending on the surface complexation model have to be solved together with Equation (D.4). No explicit expressions relate equilibrium mineral concentrations cm to cj. Therefore, NP additional mass action equations (one per mineral) are needed, which are provided by Equation (B.5). At equilibrium we have the residual functions

$$F_m^p = SI_m = 0 \qquad m = 1, ..., N_P \tag{D.5}$$

where SI_m is the m-th equilibrium mineral saturation index which is a function of c_j (see Equations B.4 and B.5 in Appendix B). N_C equations in (D.4) and N_p in (D.5) constitute a complete set of equations needed for N_C+N_P primary variables, $(c_1, c_2, ..., c_{N_C}, c_1, c_2, ..., c_{N_p})$. Denoting the set of primary variables collectively as X_i (i=1, 2, ..., N_C+N_P), using Newton-Raphson iteration we have

$$\sum_{i=1}^{N_C+N_P} \frac{\partial F_j}{\partial X_i} \Delta X_i = -F_j \qquad j = 1, ..., N_C + N_P \tag{D.6}$$

where j is a row index and i is a column index (here j as a row index can be thought of as also representing an "extended" basis set including the equilibrium minerals). In matrix form Eqs. (D.6) reduce to

$$\mathbf{J}\Delta\mathbf{X} = -\mathbf{F} \tag{D.7}$$

where $\mathbf{J}$ is the so-called Jacobian matrix. The matrix elements are evaluated in Appendix E. The values of are used to update the primary variables:

$$X_i^{s+1} = X_i^s + \Delta X_i^s \tag{D.8}$$

where s labels iteration number. The $|\Delta X_i|$ are expected to decrease in successive iterations. The system of equations is considered satisfactorily solved when

$$\max_j \left(\frac{|F_j^c|}{T_j^0} \right) \le \tau \qquad j = 1, ..., N_C \tag{D.9}$$

where τ is specified tolerance limit. In order to avoid negative values for concentrations of the basis species, the relative change is restricted to one (called under-relaxation), or $\frac{|\Delta x_i|}{x_i} < 1 \quad i = 1...N_C + N_P + N_S$ ($i = 1...N_C$). As a consequence, although the iteration method becomes more robust, the rate of convergence may slow down in some cases. When a negative value of $X_i \ (i = N_C + 1, ..., N_C + N_p)$ is obtained, the corresponding mineral is considered exhausted and must be removed from the chemical system, and its corresponding equation disappears (Reed, 1982). In this case, the speciation in solution may change drastically. This might have a strong effect on kinetic rate laws. So when a change occurs in the mineral assemblage, one might have to limit the time step to retain accuracy in rate law integration. In addition, for a given time step the code checks that dissolution of a mineral cannot be greater than the amount present in the medium, in order to avoid "over-dissolution".

The solution of the reaction system requires knowing initial total concentrations of basis species j in the equilibrium system (aqueous and mineral), and the time step Δt_r. Adding kinetic mineral dissolution/precipitation processes does not require additional primary equations, because the reaction rate is a function of the concentrations of the basis species. Once the concentrations of the basis species are obtained, all other secondary variables can be computed in a straightforward manner.

Appendix E Evaluation of the Jacobian Matrix for the Chemical Equations

The final Jacobian matrix has *Nc+Np+* rows and *Nc+Np+* columns, as follows:

$$\begin{array}{c|ccc} & Nc & Np & N\psi \\ Nc & \frac{\partial F_j^c}{\partial c_i} & \frac{\partial F_j^c}{\partial p_i} & \frac{\partial F_j^c}{\partial \tilde{\psi}} \\ Np & \frac{\partial F_j^p}{\partial c_i} & \frac{\partial F_j^p}{\partial p_i} & \frac{\partial F_j^p}{\partial \tilde{\psi}} \\ N\psi & \frac{\partial F^{\tilde{\psi}}}{\partial c_i} & \frac{\partial F^{\tilde{\psi}}}{\partial p_i} & \frac{\partial F^{\tilde{\psi}}}{\partial \tilde{\psi}} \end{array} \qquad \text{(E.1)}$$

The entries of the Jacobian matrix are

$$J^{cc} = \frac{\partial F_j^c}{\partial c_i} = \delta_{ji} + \sum_{k=1}^{N_x} \nu_{kj} \nu_{ik} \frac{c_k}{c_i} + \sum_{n=1}^{Nq} \nu_{nj} \nu_{in} \frac{k_n A_n \Omega_n}{c_i} + \sum_{s=1}^{Ns} \nu_{sj} \nu_{is} \frac{c_s}{c_i} \qquad \text{(E.2)}$$

$$J^{cp} = \frac{\partial F_j^c}{\partial p_i} = \nu_{mj} \qquad \text{(E.3)}$$

$$J^{pc} = \frac{\partial F_j^p}{\partial c_i} = \frac{\nu_{mj}}{c_i} \tag{E.4}$$

$$J^{pp} = \frac{\partial F_j^p}{\partial p_i} = 0 \tag{E.5}$$

$$J^{c\tilde{\psi}} = \frac{\partial F_j^c}{\partial \tilde{\psi}} = \sum_{s=1}^{Ns} \nu_{sj} z_s c_s \tag{E.6}$$

$$J^{\tilde{\psi}c} = \frac{\partial F^{\tilde{\psi}}}{\partial c_i} = -\sum_{s=1}^{N_s} z_s \nu_{is} \frac{c_s}{c_i} \tag{E.7}$$

or

$$J^{\tilde{\psi}c} = \frac{\partial F^{\tilde{\psi}}}{\partial c_i} = \frac{F^2}{A\varepsilon\varepsilon_0\kappa RT} \sum_{s=1}^{N_s} z_s \nu_{is} \frac{c_s}{c_i} \tag{E.8}$$

or

$$J^{\tilde{\psi}c} = \frac{\partial F^{\tilde{\psi}}}{\partial c_i} = \frac{F^2}{ACRT} \sum_{s=1}^{N_s} z_s \nu_{is} \frac{c_s}{c_i} \tag{E.9}$$

$$J^{\tilde{\psi}\tilde{\psi}} = \frac{\partial F^{\tilde{\psi}}}{\partial \tilde{\psi}} = -\tfrac{1}{2}(8RT\varepsilon\varepsilon_0 I \times 10^3)^{1/2} \cosh(-\tilde{\psi}/2) - \frac{F}{A} \sum_{k=1}^{N_s} z_k z_k y_k \tag{E.10}$$

or

$$J^{\tilde{\psi}\tilde{\psi}} = \frac{\partial F^{\tilde{\psi}}}{\partial \tilde{\psi}} = \frac{F^2}{A\varepsilon\varepsilon_0\kappa RT} \sum_{s=1}^{N_s} z_s z_s c_s + 1 \tag{E.11}$$

or

$$J^{\tilde{\psi}\tilde{\psi}} = \frac{\partial F^{\tilde{\psi}}}{\partial \tilde{\psi}} = \frac{F^2}{ACRT} \sum_{s=1}^{N_s} z_s z_s c_s + 1 \tag{E.12}$$

Appendix F Effects of Mineral Precipitation/Dissolution on Hydrologic Properties

F.1 Porosity Changes

Porosity changes in matrix and fractures are directly tied to the volume changes as a result of mineral precipitation and dissolution. The molar volumes of minerals created by hydrolysis reactions (i.e., anhydrous phases, such as feldspars, reacting with aqueous fluids to form hydrous minerals such as zeolites or clays) are often larger than those of the primary reactant minerals; therefore, constant molar dissolution-precipitation reactions may lead to porosity reductions. Porosity changes are taken into account in the code as follows:

The porosity of the medium (fracture or matrix) is given by

$$\phi = 1 - \sum_{m=1}^{nm} fr_m - fr_u \tag{F.1}$$

where *nm* is the number of minerals, fr_m is the volume fraction of mineral *m* in the rock ($V_{mineral}/V_{medium}$, including porosity), and fr_u is the volume fraction of nonreactive rock. As the fr_m of each mineral changes, the porosity is recalculated at each time step. The porosity is not allowed to go below zero.

Several options are available in TOUGHREACT to compute permeability changes as a result of mineral precipitation and/or dissolution. Some options depend solely on porosity changes, whereas others employ options related to, for example, fracture aperture changes or pore throat diameter changes.

F.2 Fracture Permeability Changes

Option 3: Fracture permeability changes can be approximated using the porosity change and an assumption of plane parallel fractures of uniform aperture (cubic law; e.g., Steefel and Lasaga, 1994). The modified permeability, *k*, is then given by

$$k = k_i \left(\frac{\phi}{\phi_i} \right)^3 \tag{F.2}$$

where k_i and ϕ_i are the initial permeability and porosity, respectively. This law yields zero permeability only under the condition of zero fracture porosity.

Option 4: In most experimental and natural systems, permeability reductions to values near zero occur at porosities significantly greater than zero. This generally is the result of mineral precipitation in the narrower interconnecting apertures. The hydraulic aperture, as calculated from the fracture spacing and permeability (as determined through air-permeability measurements) assuming a cubic law relation, is a closer measure of the smaller apertures in the flow system. Using the hydraulic aperture, a much stronger relationship between permeability and porosity can be developed. This relationship can be approximated as follows:

The initial hydraulic aperture $b_{0,h}$ (m) is calculated using the following cubic law relation:

$$b_{0,h} = \left[12 k_0 s \right]^{1/3} \tag{F.3}$$

where k_0 is the initial fracture permeability (m^2) and *s* is the fracture spacing (m). The permeability (k') resulting from a change in the hydraulic aperture, is given by

$$k' = \frac{(b_{0,h} + \Delta b)^3}{12s} \tag{F.4}$$

where Δb is the aperture change resulting from mineral precipitation/dissolution.

The aperture change resulting from a calculated volume change can be approximated by assuming precipitation of a uniform layer over the entire geometric surface area of the fracture, assuming also that this area as well as the fracture spacing remains constant. The actual distribution of mineral alteration is much more heterogeneous and depends on many processes that are active at scales much smaller than the resolution of the model; however, the combined effect of the initial heterogeneities and localized precipitation processes can only be treated through model sensitivity studies and experiments.

For a dual permeability model, changes in the fracture porosity are calculated based on the porosity of the fracture medium, so that Δb can be approximated by

$$\Delta b = \frac{(\phi'_{fm} - \phi_{fm,0})}{\phi_{fm,0}} b_g \tag{F. 5}$$

Equations (F.3), (F.4), and (F.5) were implemented in TOUGHREACT with input parameters of b_g and s. An example of this type of porosity and permeability relationship is given in Sample Problem 4 (Section 8.11: Heater Test).

In this example problem, the initial aperture available for precipitation (b_g, the geometric, rather than the hydraulic, aperture) was estimated from the ratio of the initial fracture porosity ($\phi_{f,0}$) to the fracture surface area (A_f), as follows:

$$b_g = \phi_{f,0} \Big/ A_f \tag{F.6}$$

However, the user can, of course, use any methodology to calculate the geometric aperture.

F.3 Matrix Permeability Changes

Option 1: Matrix permeability changes are calculated from changes in porosity using ratios of permeabilities calculated from the Carman-Kozeny relation (Bear, 1972), and ignoring changes in grain size, tortuosity and specific surface area as follows:

$$k = k_i \frac{(1-\phi_i)^2}{(1-\phi)^2} \left(\frac{\phi}{\phi_i} \right)^3 \tag{F.7}$$

Option 2: Modified Hagen-Poiseulle Law. Studies on predicting the permeability of clastic rocks commonly found in sedimentary basins (e.g., sandstones and carbonate rocks) have shown that the permeability can be predicted using a form of the Hagen-Poiseulle equation and knowledge of the pore size distribution, pore throat size, and pore type (Ehrlich et al. 1991). In this study, pore throat sizes and distributions were obtained through a combination of mercury intrusion porosimetry, petrographic image analysis, and image processing.

Option 5: The simple cubic law (Eq. F.2) and the Kozeny-Carman (Eq. F.7) porosity-permeability equations may not reflect the complex relationship of porosity and permeability in geologic media that depends on an interplay of many factors, such as pore size distribution, pore shapes, and connectivity (Verma and Pruess, 1988). Laboratory experiments have shown that modest reductions in porosity from mineral precipitation can cause large reductions in permeability (Vaughan, 1987). Detailed analysis of a large set of field data also indicated a very strong dependence of permeability on small porosity changes (Pape et al., 1999). This is explained by the convergent-divergent nature of natural pore channels, where pore throats can become clogged by precipitation while disconnected void spaces remain in the pore bodies (Verma and Pruess, 1988). The permeability reduction effects depend not only on the overall reduction of porosity, but on the details of the pore space geometry and the distribution of precipitates within the pore space. These may be quite different for different media, which makes it difficult to achieve generally applicable predictions. To evaluate the effects of a more sensitive coupling of permeability to porosity, we also implemented a porosity-permeability relationship presented by Verma and Pruess (1988):

$$\frac{k}{k_i} = \left(\frac{\phi - \phi_c}{\phi_i - \phi_c} \right)^n \tag{F.8}$$

where ϕ_c is the value of "critical" porosity at which permeability goes to zero, and n is a power law exponent. Parameters ϕ_c and n are medium-dependent. An example of this porosity-permeability relationship is given in Sample problem 8 (Section 8.8: Injection well scaling).

F.4 Effects of Permeability and Porosity Changes on Capillary Pressures

Permeability and porosity changes will likely result in modifications to the unsaturated flow properties of the rock. Changes to unsaturated flow properties are approximated by modification of the calculated capillary pressure (*Pc*) using the Leverett scaling relation (Slider, 1976) to obtain a scaled *Pc´* as follows:

$$Pc' = Pc\sqrt{\frac{k_i \phi}{k \phi_i}} \tag{F.9}$$

Scaled capillary pressures are subject to the maximum capillary pressure prescribed in the capillary pressure function in the ROCKS or RPCAP blocks (see TOUGH2 V.2 users manual).

Appendix G Mineral Reactive Surface Areas

This appendix describes how input values of surface areas are used to calculate the reactive surface area needed for kinetic rate laws (e.g., in equations B.6 and B.9). The general methodology implemented into TOUGHREACT is presented first (Section G.1), followed by suggestions on how to calculate and input surface areas for fractures (Section G.2) and a porous rock matrix (Section G.3). Surface areas are input as variable AMIN on record Imin-6.1 (in file chemical.inp), using a choice of units defined by flag IMFLG on the same input record. Note that any approach may be used to calculate input surface areas as long as the correct units are entered for the specified value of IMFLG.

G.1 General Methodology

The following general relationship is implemented into TOUGHREACT to compute reactive surface areas of minerals:

$$A_r = (V_{frac} A_m + A_{prc}) / C_w \qquad \text{(G.1)}$$

with:

A_r	Effective reactive surface area of minerals in units of $m^2_{mineral}/kg_{water}$ for input into kinetic rate laws (e.g. equations B.6 and B.9)
Am	Surface area of minerals in units of $m^2_{mineral}/m^3_{mineral}$
Aprc	Precursor surface area (optional) in units of $m^2_{surface}/m^3_{medium}$
Vfrac	Mineral volume fraction in units of $m^3_{mineral}/m^3_{medium}$
Cw	Wetted-surface conversion factor in units of kg_{water}/m^3_{medium}

The values of A_m, V_{frac}, and C_w change in the course of a simulation as minerals dissolve and precipitate, and as the liquid saturation of the medium fluctuate. A_m is computed, in part, from input surface areas. A_{prc}, however, is an input parameter that remains constant in the course of a simulation. Various approaches are followed to compute A_m, V_{frac}, and C_w from input parameters and/or model assumptions, depending on whether a mineral is present or not, which type of surface area model is selected, which type of medium is considered (fractures or matrix), and which units are chosen to input surface areas. Approaches followed to compute these variables are described below.

Mineral volume fraction V_{frac}. For all minerals (initially present or not) included in a simulation, a minimum value of V_{frac} is calculated as

$$V^0_{frac} = maximum\ (\ \text{RNUCL}(1-\phi_{med});\ 10^{-10}\ ) \qquad \text{(G.2)}$$

where RNUCL in an assumed minimum volume fraction (in $m^3_{mineral}/m^3_{solids}$) (entered on record Miner-2.2 in file chemical.inp) and ϕ_{med} is the porosity of the medium. When a mineral is not initially present (i.e., case of a secondary phase that forms during a simulation), V_{frac} in Equation (G.1) always takes the value of V^0_{frac}. For

minerals that are present in the modeled system, V_{frac} is initially computed from input mineral volume fractions f_m (in $m^3_{mineral}/m^3_{solids}$) (VOL on record Imin-6 in file chemical.inp) and porosity of the medium (ϕ_{med}, read in flow.inp or INCON files) as:

$$V_{frac} = f_m\,(1-\phi_{med}) \tag{G.3}$$

The values of V_{frac} are then continuously updated from the computed amounts of minerals, as these dissolve and/or precipitate. Note that if, at any time, V_{frac} is less than V^0_{frac}, the value of V^0_{frac} is used instead of V_{frac} in equation (G.1).

Surface area A_m. Values of A_m are calculated as

$$A_m = A^0{}_m + A_{nucl} \tag{G.4}$$

A^0m is the input mineral surface area (AMIN, if IMFLG≠3, on record Imin-6.1 in chemical.inp). It is always internally converted to units of $m^2_{mineral}/m^3_{mineral}$. A_{nucl} is a surface area used to approximate nucleation effects (this is not a nucleation model!) By default, A_{nucl} is always set to zero if the value of RAD (on record Imin-6.1 in file chemical.inp) is set to zero. If RAD ≠0, a simple model is implemented to compute A_{nucl} as a function of mineral grain size, with RAD entered as the initial grain radius (in m). This is done by assuming simple cubic packing of spherical grains of radius r. This cubic arrangement of spheres yields, in a cube of side $4r$ and volume $(4r)^3$, a total of 8 spheres, each of radius r, volume $4/3\ \pi r^3$, and area $4\pi r^2$. Thus the surface area A_{nucl} (as the area of the spheres divided by the volume of the cube) is computed as

$$A_{nucl} = 0.5/r \tag{G.5}$$

For minerals not initially present, r is initially taken as the value of RAD (in m). Only on precipitation, the value of r is increased as the mineral forms, such that A_{nucl} decreases with increasing mineral amounts. This is accomplished by tying the increase of V_{frac} to r through a variable, n_{grain}, expressing the number of mineral grains per volume medium as follows

$$n_{grain} = 0.125\ V_{frac} / r^3 \tag{G.6}$$

Equation (G.6) is also derived assuming simple cubic packing of spherical grains. For minerals not initially present, the number of mineral grains is initially calculated using Equation (G.6) with $V_{frac} = V^0_{frac}$ and r = RAD. At subsequent time steps, as V_{frac} increases with mineral precipitation, n_{grain} is decreased proportionally to V_{frac}/ V^0_{frac} (an assumption) and the grain radius is recomputed by re-expressing Equation (G.6) to yield values of r:

$$r = \sqrt[3]{\frac{0.125 V_{frac}}{n_{grain}}} \tag{G.7}$$

As r grows and n_{grain} diminishes, A_{nucl} decreases to a point when $A_{nucl} << A^0_m$ and $A_m \approx A^0_m$ in Equations (G.4) and (G.1). On precipitation, because n_{grain} is forced to decrease, A_r also decreases as r grows, as long as $A_{nucl} > A^0_m$. In contrast, on dissolution, n_{grain} is kept constant (i.e., not recomputed), such that if $A_{nucl} > A^0_m$, A_r always keeps decreasing with decreasing r (as seen by substituting Equations G.3, G.4, and G.5 into Equation G.1).

Wetted-surface conversion factor C_w. This conversion factor (in units of kg_{water}/m^3_{medium}) usually takes the form

$$C_w = \rho_w \phi_{med} S_w \tag{G.8}$$

where ρ_w is the water density (kg/L), ϕ_{med} is the porosity of the medium, and S_w is liquid saturation. For a fully saturated system, $S_w = 1$. For an unsaturated system, $S_w < 1$. However, as S_w goes to zero, C_w goes to zero, and therefore the wetted reactive surface area A_r, which is proportional to $1/C_w$ (Equation G.1), tends to infinity. Clearly, at a very low liquid saturation, the surface area of the rock contacted by water is likely much smaller than the total area. Two methods are implemented to address this problem. The first method assumes that the wetted surface area diminishes proportionately to the liquid saturation. This behavior is achieved by multiplying the right side of Equation (G.1) by S_w. This cancels out S_w in Equation (G.8), such that the quantity C_w in Equation (G.1) becomes, in effect

$$C_w = \rho_w \phi_{med} \tag{G.9}$$

This method is implemented for both porous media and fractured systems. However, an other method is applied for fractured systems if the active-fracture model is enabled (which is done by specifying non-zero active-fracture parameters (CP(6), in the third record of the ROCKS block in file flowinp). This method employs the active-fracture-model of Liu et al. (1998) modified to consider water-rock reactions taking place below the residual saturation in fractures. The form of the active fracture parameter for reaction is given by the following set of equations:

$$S_{ar} = (S_w - S_m)/(1 - S_m) \tag{G.10}$$

$$a_{fmr} = S_{ar}^{(1+\gamma)} \tag{G.11}$$

where S_m is the minimum liquid saturation for which water-rock reactions are considered (input parameter SL1MIN on Record-3 in file solute.inp), S_{ar} is an effective saturation for reaction, and γ is the active fracture parameter. The factor that reduces the surface area contacted by water is given by a_{fmr}. Generally, S_m is set to a small value (e.g., 1×10^{-4}), to ensure that reactions take place until virtually no water is left (e.g., during dryout via ventilation or heating). Using this model, the quantity C_w is computed as

$$C_w = \rho_w \phi_{med} S_w / a_{fmr} \tag{G.12}$$

G.2 Estimation of Surface Areas for Fractures

In the dual permeability method, the porosity of the fracture medium could be taken as 1.0. However, for modeling of mineral dissolution and precipitation, there would then be no rock to dissolve. Therefore, a non-zero fracture-medium porosity (ϕ_{med}) must always be assumed for input into simulation (typically $0.5 < \phi_{med} < 0.9$; this porosity is not to be confused with the true fracture porosity ϕ_f). If the dissolution rates of minerals are small (which is the case for many minerals at temperatures below 100°C), only a small volume of rock adjoining the open space of the fracture needs to be considered as the starting rock fraction (i.e., ϕ_{med} can be large, as long as < 1).

Reactive surface areas of minerals on fracture walls can be calculated from the fracture-matrix interface area/volume ratio, the fracture porosity, and the derived mineral volume fractions. These areas can be calculated based on the fracture densities, fracture porosities, and mean fracture diameter. The wall of the fracture can be treated as a surface covered by mineral grains having the form of uniform hemispheres. The grain diameter and spatial density are not considered in this method, so that the area is actually only marginally greater than the fracture geometric surface area. Using this approach, the geometric surface area of the fracture wall can be approximated by:

$$A = \frac{\pi A_{f\text{-}m}}{2\phi_f} \qquad \text{(G.13)}$$

where A is the "reactive" surface area (in units of $m^2_{\text{reactive surface}}/m^3_{\text{fracture medium}}$), $A_{f\text{-}m}$ is the fracture-matrix interface area/volume ratio (in units of $m^2_{\text{reactive surface}}/m^3_{\text{total fracture+matrix medium}}$), and ϕ_f is the true fracture porosity of the rock. The factor of $\pi/2$ is a roughness factor equal to the actual surface area of solid grains on the fracture plane, divided by the fracture plane surface, given by cubic packing of spherical grains.

Surface areas calculated using Equation (G.13) are input as AMIN with IMFLG=3 on record Imin-6.1 in file chemical.inp. In this case, input AMIN values correspond to A_{prc} in Equation (G.1), and values of A^0_m in Equation (G.4) are internally set to zero (therefore $A_m = A_{nucl}$ in Equation G.1). In this scenario, A in Equation G.13 is assumed to be the same for all minerals.

An alternative is to consider mineral proportions in the surface coverage of fractures. Assuming that the fracture coverage for each mineral is proportional to the mineral volume fraction, $V_{frac,}$ the surface area for each mineral, A' (in units of $m^2_{\text{mineral}}/m^3_{\text{fracture medium}}$) can be calculated as

$$A' = A\, V_{frac} \qquad \text{(G.13)}$$

Values of A' calculated in this way are input as AMIN with IMFLG=2 on record Imin-6.1 in file chemical.inp. For minerals not initially present, V_{frac} in Equation (G.13) must be taken as V^0_{frac} (Equation G.2) for internal consistency. In this case, the input AMIN values correspond to A^0_m in Equation (G.1), and A_{prc} is this equation is internally set to zero.

G.3 Estimation of Surface Areas in the Rock Matrix (Porous Medium)

One method to calculate the reactive surface areas of minerals in a rock or granular material is to use a geometric area of a cubic array of truncated spheres to make up the framework of the rock (Sonnenthal and Ortoleva, 1994). Clay minerals can be considered as coatings of plate-like grains. The mineral surface areas of framework grains (truncated spheres) in contact with the open pore space can be calculated using an initial grain diameter, followed by successive truncation of the grains in the vertical direction until the porosity of this system is close to the measured porosity of the rock. The abundance of secondary phases (i.e., those that formed as alteration products or low-temperature coatings on the primary assemblage), such as clay minerals, can be used to reduce the free surface area of the framework grains. The surface areas of the secondary phases can be calculated based on their size and morphology.

A more approximate but very simple method is to consider geometric surface areas for either single sphere, simple cubic packing of untruncated spheres, or cubic-centered packing of untruncated spheres. The surface area is obtained by dividing the area of the spheres by the volume of the spheres (for the various packing arrangements) as shown below.

Single sphere – area $4\pi r^2$, volume $4/3\ \pi r^3$:

$$A = 3/r \tag{G.14}$$

Simple cubic packing – 8 spheres of total area $8x4\pi r^2$, in a cube of volume $(4r)^3$:

$$A = 0.5/r \tag{G.15}$$

Cubic-close packing – 4 spheres of total area $4\times4\pi r^2$, in a cube of volume $(2\sqrt{2}\ r)^3$:

$$A = \pi / (\sqrt{2}\ r) = 2.22/r \tag{G.16}$$

Note that differences in the constant terms in these equations are much smaller than the typical order-of-magnitude uncertainty of surface areas. If the grain radius r is in units of m, values of A calculated in this way are in units of $m^2_{mineral}/m^3_{mineral}$ and can be input directly as AMIN with flag IMFLG=1 in record Imin-6.1 (in file chemical.inp). Surface areas in units of cm^2/g can be calculated from

$$A' = 100\ A / \rho_m = 100\ A\ M_m / V_m \tag{G.17}$$

where ρ_m, M_m and V_m are the mineral density in g/cm^3, molecular weight in mol/g, and molar volume in cm^3/mol (M_m and V_m can be taken from record Mineral-1 in the thermodynamic database). In this case, A' is entered (in file chemical.inp) as AMIN with flag IMFLG=0 on record Imin-6.1.

Appendix H Calculation of Activity and Fugacity Coefficients

H.1 Extended Debye-Hückel Model for Ionic Species and Water

Activity coefficients of charged aqueous species and the water activity are computed using the extended Debye-Hückel model presented by Helgeson et al. (1981), often refered to as the HKF model (for Helgeson, Kirkham, and Flowers). We will use this accronym, below, to refer to the model, its authors, or their published paper.

The HKF model is applied making the assumption that the dominant cation and anion in solution are sodium and chloride, respectively, which entails limits on the model applicability. In addition, the Debye-Hückel model, even if extended, technically only applies to dilute solutions. For this reason, for applications at elevated ionic strengths (> ~1 molal), the model should be very carefully applied, with full knowledge its limitations, as discussed further below. Note that at ionic strength < ~1 molal, the HKF model yields results very close to the more commonly used "b-dot" extended Debye-Hückel model (Helgeson, 1969). Details on the formulation of activity coefficients for charged species, water activity, and the HKF model applicability are presented below in Sections H.1.1, H.1.2, and H.1.3, respectively.

H.1.1 Activity Coefficients of Charged Aqueous Species

The assumption is made that the dominant cation and anion in solution are sodium and chloride, respectively, so that HKF Equation (298) can be used directly, as follows:

$$\log(\gamma_j) = -\frac{A_\gamma z_j^2 I^{0.5}}{\Lambda} + \log(1 + 0.0180153 m^*) - \left[\omega_j b_{NaCl} + b_{Na^+,Cl^-} - 0.19(|z_j| - 1)\right] I \qquad \text{(H.1)}$$

and

$$\Lambda = 1 + \text{å}\, B_\gamma \bar{I}^{1/2} \qquad \text{(H.2)}$$

$$\omega_j = \eta \frac{z_j^2}{r_{e,j}} \qquad \text{(H.3)}$$

where the subscript j refers to each ion, γ is the activity coefficient of the ion, Debye-Huckel parameters b_{Na^+,Cl^-}, b_{NaCl}, Aγ and Bγ are given in HKF Tables 1, 29, and 30, Debye-Huckel parameter å is calculated as discussed below, z is the ion electric charge, I is taken as the true ionic strength of the solution, ω is the Born coefficient, η is a constant equal to 1.66027 (Å cal/mol), and $r_{e,j}$ is the effective ionic radius given in HKF Table 3 or estimated as shown on Table H.1-1 when not available.

Debye-Huckel parameters b_{Na^+,Cl^-}, b_{NaCl}, Aγ and Bγ were regressed as a function of temperature and the resulting functions and regression coefficients are currently built into TOUGHREACT. Values of å are calculated

by TOUGHREACT using effective ionic radii $r_{e,j}$. Making the assumption that NaCl is the dominant electrolyte, and using the ion charge to determine stoichiometry coefficients, HKF Equation (125) simplifies to (as implemented in models by Reed, 1982):

$$å_j = 2\,(r_{e,j} + 1.91\,|z_j|) / (|z_j| + 1) \quad \text{for anions} \tag{H.4}$$

$$å_j = 2\,(r_{e,j} + 1.81\,|z_j|) / (|z_j| + 1) \quad \text{for cations} \tag{H.5}$$

where the subscript j refers to each ion and other parameters are as defined above. The values of 1.91 and 1.81 in the above equations correspond to r_{e,Na^+} and r_{e,Cl^-}, respectively. Values of $r_{e,j}$ are input from the TOUGHREACT database and can be changed as deemed necessary in this database.

Table H.1—1 Estimated values of effective ionic radii ($r_{e,j}$) currently in the TOUGHREACT thermodynamic database for species that are not reported in HKF Table 3. When available, values from HKF Table 3 are used directly instead of those shown here.

Ion Charge	$r_{e,j}$	Source
-1	1.81	Cl- value
-2	3.00	Rounded average of CO3-- and SO4-- values
-3	4.2	Estimated from straight line fit with charge
+1	2.31	NH4+ value
+2	2.8	Rounded average for +2 species in HKF Table 3
+3	3.6	Rounded average for +3 species in HKF Table 3
+4	4.5	Estimated using HKF Equation 142 and average crystallographic radii of +4 species in CRC Handbook
< -3		Linear Extrapolation (charge × 4.2/3.0)
> +3		Linear Extrapolation (charge × 4.5/4.0)

H.1.2 Activity of Water

First, a simplification of HKF Equation (190) is used to compute the osmotic coefficient of the solution, Φ, as follows:

$$\Phi = -\frac{2.303}{m^*}\sum_j \left[m_{t,j} \left[\frac{A_\gamma\, z_j^2\, \bar{I}^{0.5}\, \sigma}{3} + \frac{\log(1+0.0180153 m^*)}{0.0180153 m^*} - 0.5\,(\omega_j b_{NaCl}\,\bar{I}) + (b_{Na^+,Cl^-} - 0.19(|z_j|-1))\,\frac{mchr}{2} \right] \right] \tag{H.6}$$

with

$$\sigma = \frac{3}{å\, B_\gamma^3 \bar{I}^{3/2}} \left[\Lambda - \frac{1}{\Lambda} - 2\ln(\Lambda) \right]$$

and with

$$\Lambda = 1 + \mathring{a}\, B_{\gamma}\, \bar{I}^{1/2} \qquad \text{and} \qquad \omega_j = \eta \frac{z_j^2}{r_{e,j}}$$

where the subscript *j* refers to each charged species in solution, m* is taken as the sum of the molalities of all species in solution, m_t is the total molality of each charged species, *mchr* is the sum of the molalities of all charged species, and $\bar{I}$ is taken as the stoichiometric ionic strength. Other parameters are as defined for Equation (H.1). The simplifications made in Equation (H.6) assume dominance of NaCl in solution, and are essentially the same as the simplifications made to derive Equation (H.1). Two differences are the use of the stoichiometric ionic strength instead of the true ionic strength, and the use of *mchr*/2 instead of true ionic strength. These modifications were made because they seemed to reproduce water activity data reported by Robinson and Stokes (1965) better than without these modifications. Once the osmotic coefficient is calculated, the water activity is then given by the HKF Equation (126), as:

$$\ln(a_w) = -\Phi\, m^* \frac{1}{55.51} \qquad \text{(H.7)}$$

H.1.3 Applicability of the HKF Extended Debye-Hückel Model

It is recommended that users understand the HKF model and its limitations before applying it at ionic strengths greater than about ~1 molal. The limits of applicability of this model depend, in part, on how well the assumption of NaCl-dominance in solution is satisfied. Also, consistency between the activity coefficient model and the types of ion pairs included in the thermodynamic database is critical. Good examples are the $NaCl^0$ and $CaCl_2^0$ (and $CaCl^+$) ion pairs. HKF fitted their Debye-Hückel parameters assuming that no significant formation of these ion pairs took place (i.e., the effect of these ion pairs are implicitly taken into account in the model parameters). Therefore, for applications at elevated ionic strengths (> ~1 molal), good results are obtained only after removing these ion pairs from the thermodynamic database.

With careful testing for each particular system, including determination of which ion pairs to include (or not) into the thermodynamic database, this model can be applied to ionic strengths up to about 2 molal, and possibly to up to 4 molal for simple salt systems. However, no general rule can be made as to the limits of applicability, except that we do not recommend using this model at ionic strengths greater than ~4 molal, especially at higher temperatures. It should be noted that for salt mixtures, the model limit should be evaluated by the user on a case-by-case basis, taking into consideration the overall reactive transport model uncertainty and the goals of the modeling work. As a general guideline, an ionic strength limit of 2 molal may be appropriate for many applications, and values greater than 4 molal should not be considered.

To evaluate the range of model applicability for single salt systems, speciation calculations (one grid block, no transport) were run for solutions of various single salts. Results were then compared with published experimental data (Robinson and Stokes 1965; Colin et al. 1985; and Ananthaswamy and Atkinson, 1985). Only electrolyte activity can be measured, from which mean activity coefficients can be derived (individual activity coefficients cannot be measured). For this reason, individual activity coefficients activities calculated with the HKF model need to be converted for comparisons to measured data (or vice versa). For an electrolyte k (e.g., NaCl) consisting of ionic species j (e.g., Na^+ and Cl^-), the mean activity coefficient, $\gamma_{k\pm}$, and electrolyte activity, a_k, can be related to the activity coefficients γ_j and activities a_j of individual ionic species using the following relationships (e.g., Robinson and Stokes, 1965, Equations 2.12, 2.8, and 2.13, respectively):

$$\gamma_{k\pm} = \left(\prod_j \gamma_j^{\upsilon_{j,k}} \right)^{1/\upsilon_k} \tag{H.8}$$

$$a_k = \prod_j (a_j)^{\upsilon_{j,k}} \tag{H.9}$$

$$a_k = \prod_j (\upsilon_{j,k}{}^{\upsilon_{j,k}})(m_k \gamma_{k\pm})^{\sum_j \upsilon_{i,k}} \tag{H.10}$$

where $\upsilon_{j,k}$ are stoichiometric coefficients of ionic species j in electrolyte k, and m_k is the electrolyte molality. For comparison with literature data, computed activity coefficients for individual ions (output in file *chdump.out*) were converted to mean activity coefficients using Equation (H.8). Activities for individual ions were also calculated from individual molalities (m_j) and activity coefficients (γ_j) (using the relationship $a_j = \gamma_j m_j$), then converted to mean activities using Equation (H.9). As necessary, Equation (H.10) was also used to convert mean activity coefficients from the literature data to mean activities. Finally, osmotic coefficients (Φ) from the literature were converted to water activities (a_{H2O}) using Equation (H.7). After these conversions, computed and measured data could be compared, with results summarized in Figures H.1-1 through H.1-5, and in Table H.1-2. As noted above, computations without including the secondary species $NaCl_{(aq)}$, $CaCl^+$, and $CaCl_{2(aq)}$ in the thermodynamic database provide best results, because the HKF model was developed assuming no explicit ion association for these salts. At elevated ionic strengths (> 1 molal), the model reproduces fairly well the mean activity coefficients of NaCl solutions up to at least 6M NaCl (ionic strength 6) (Figures H.1-1, H.1-3, and H.1-4). The reverse is true for species like $MgSO_4$ and Na_2SO_4, for which accurate activities cannot be computed without including the $MgSO_4$ and $NaSO_4^-$ species in the thermodynamic database, because the significant association of Mg and Na with SO_4 was considered in the HKF model. In this case, using dissociation constants from Shock et al. (1989) for these species, mean activities determined by Robinson and Stokes (1965) at 25°C can be reproduced fairly well up to 2M $MgSO_4$ (ionic strength = 8) and 1M Na_2SO_4 (ionic strength = 3) (Figure H.1-2). Activity coefficients and activities in $CaCl_2$ solutions are also reasonably reproduced up to about 1.5 m $CaCl_2$ (ionic strength = 4.5 molal) (Figures H.1-1, H.1-3, and H.1-5).

Figure H.1—1 **Mean-ion activity coefficients of NaCl and $CaCl_2$ at 25°C derived from individual activity coefficients calculated with Equation (H.1). Symbols represent data from measurements by Robinson and Stokes (1965).**

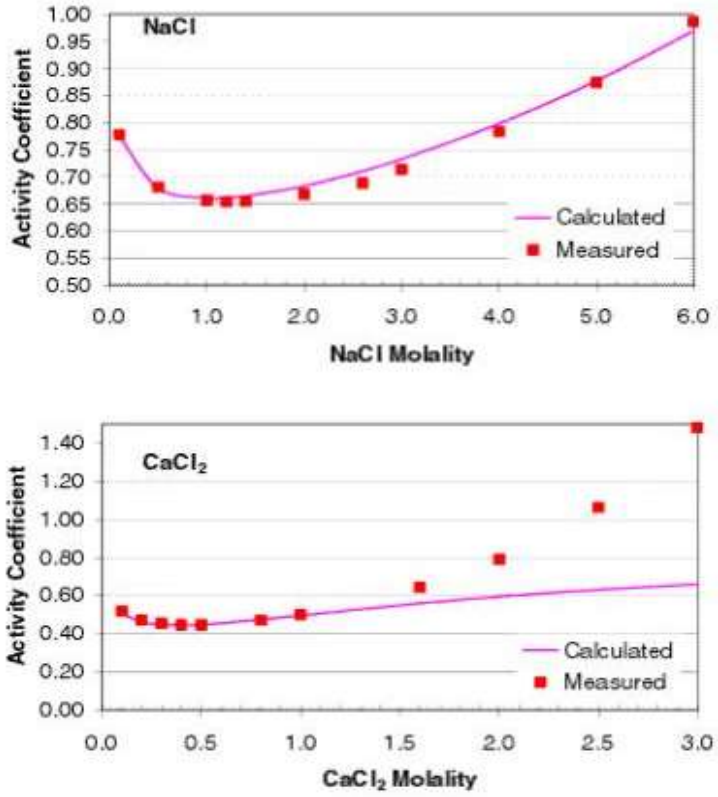

Figure H.1—2 **Activities of $MgSO_4$ and Na_2SO_4 at 25°C derived from individual activity coefficients calculated with Equation (H.1). Symbols represent data from measurements by Robinson and Stokes (1965). Actual activities, rather than activity coefficients, are compared here because significant ion association takes place.**

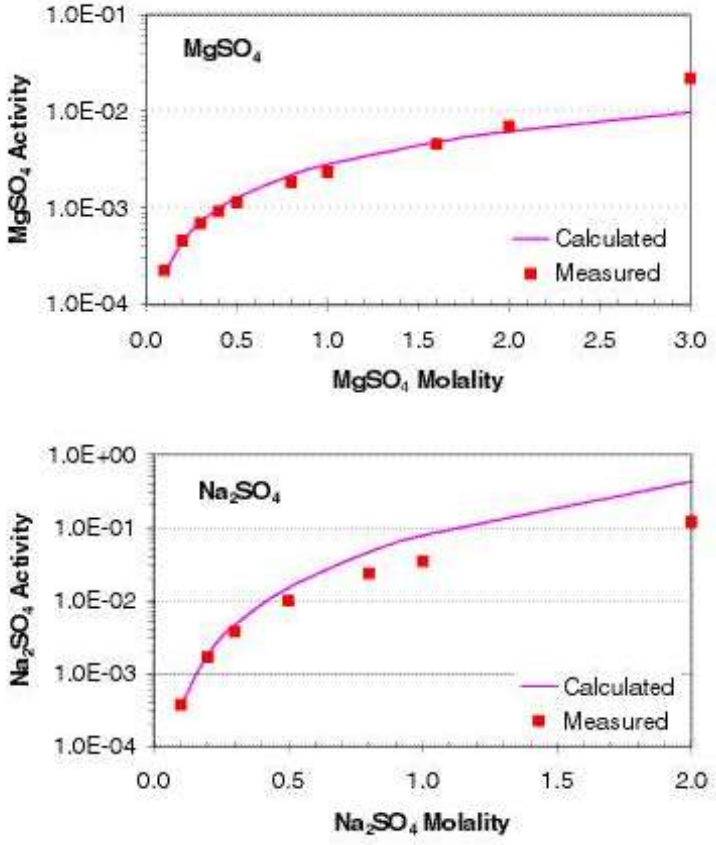

Figure H.1—3 **Activities of water in NaCl and $CaCl_2$ solutions at 25°C calculated with Equations (H.6) and (H.7). Symbols represent data from measurements by Robinson and Stokes (1965).**

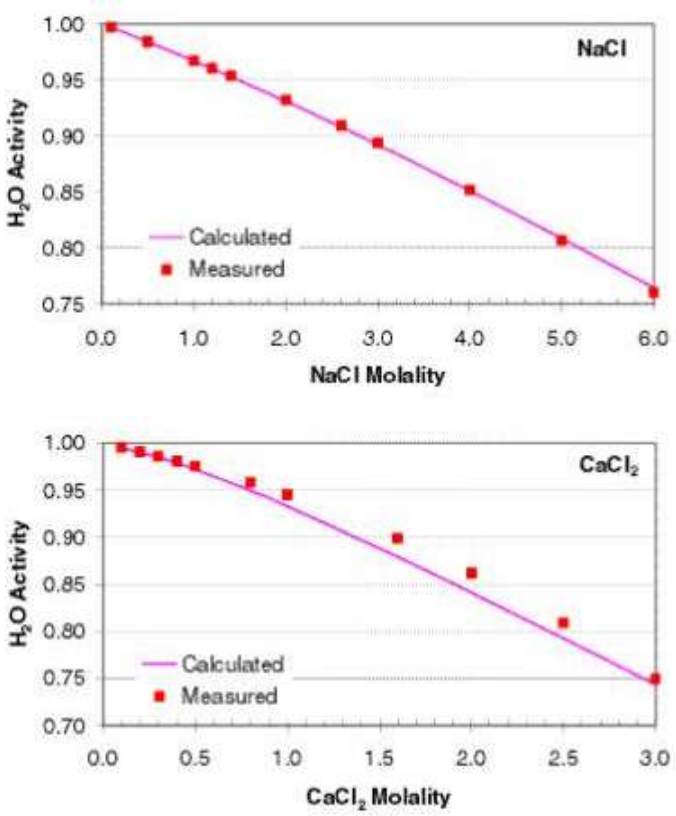

Figure H.1—4 **Comparison of measured (Colin et al. 1985) and computed activities for NaCl solutions. Note that the $NaCl_{(aq)}$ species is excluded from the simulation for consistency with the activity coefficient model.**

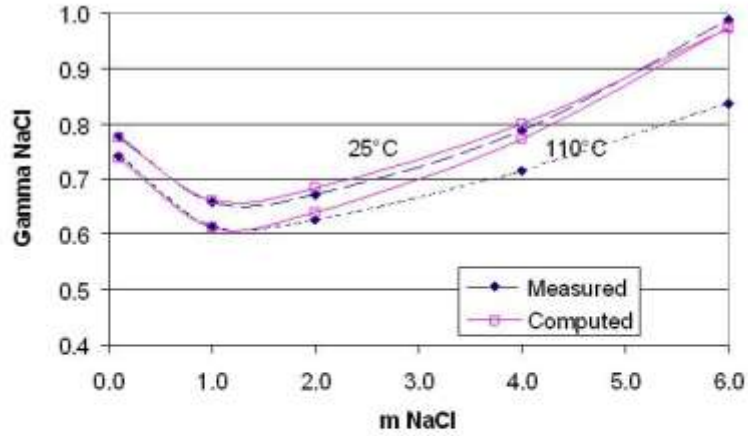

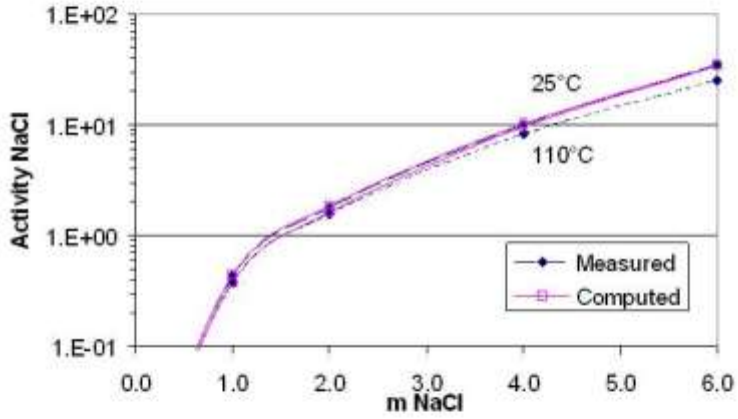

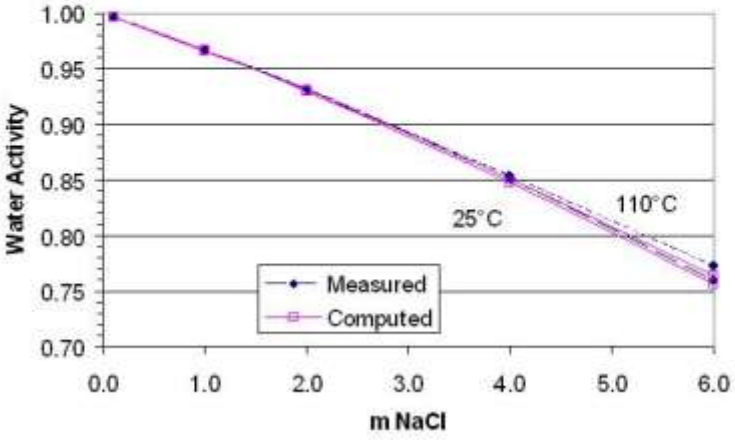

Figure H.1—5 **Comparison of measured (Ananthaswamy and Atkinson, 1985) and computed activities for $CaCl_2$ solutions. Note that the $CaCl_{2(aq)}$ and $CaCl^+$ species are excluded from the simulation for consistency with the activity coefficient model.**

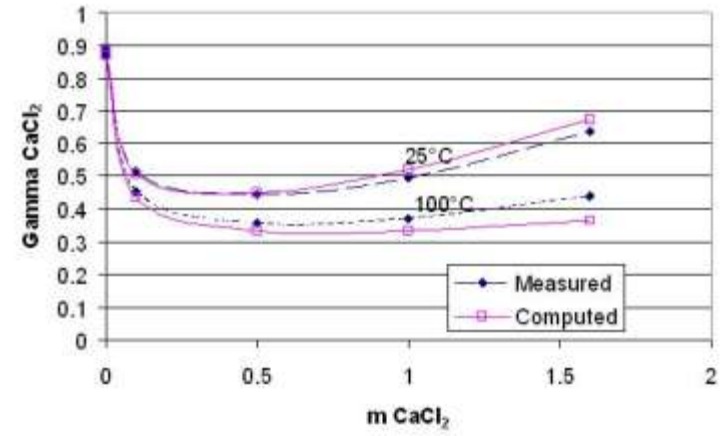

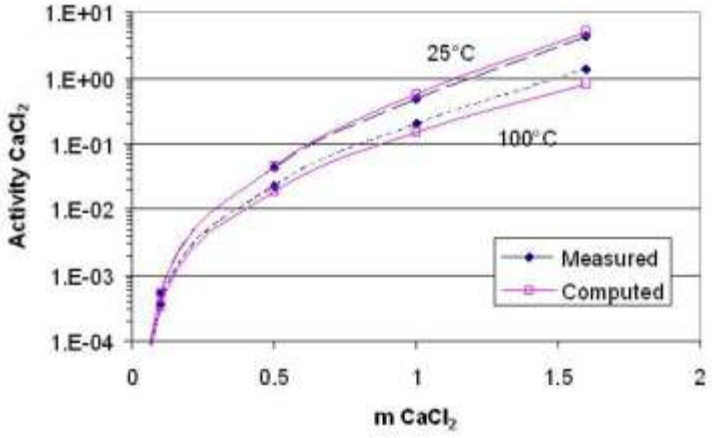

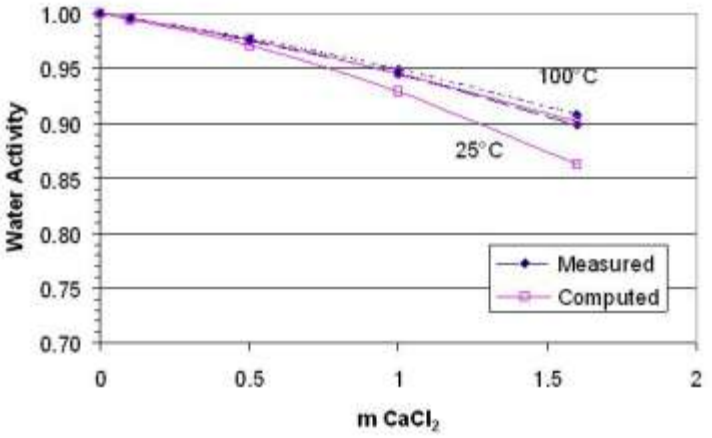

Table H.1—2 **Comparison of measured and computed activity data for NaCl and $CaCl_2$ solutions. Note that the $NaCl_{(aq)}$, $CaCl^+$, and $CaCl_{2(aq)}$ secondary species are excluded from the simulation for consistency with the activity coefficient model.**

			Mean activity coefficient			Mean activity			Water activity		
			$\gamma_{NaCl\pm}$	$\gamma_{NaCl\pm}$		a_{NaCl}	a_{NaCl}		a_{H2O}	a_{H2O}	
Temp (°C)	**m NaCl**	**Ionic Str.**	**Measured[1]**	**Computed**	**%Diff**	**Measured[1]**	**Computed**	**%Diff**	**Measured[1]**	**Computed**	**%Diff**
25	0.1	0.1	0.77753	0.775	-0.4	6.05E-03	6.00E-03	-0.7	0.9966	0.997	0.0
25	1	1	0.65805	0.661	0.5	4.33E-01	4.37E-01	0.9	0.9668	0.967	0.0
25	2	2	0.67131	0.684	1.8	1.80E+00	1.87E+00	3.7	0.9314	0.930	-0.1
25	4	4	0.78809	0.800	1.5	9.94E+00	1.02E+01	2.9	0.8512	0.851	0.0
25	6	6	0.98882	0.972	-1.7	3.52E+01	3.40E+01	-3.3	0.7601	0.764	0.5
110	0.1	0.1	0.74109	0.736	-0.7	5.49E-03	5.41E-03	-1.4	0.9967	0.997	0.0
110	1	1	0.61371	0.612	-0.2	3.77E-01	3.75E-01	-0.4	0.9670	0.967	0.0
110	2	2	0.62566	0.639	2.1	1.57E+00	1.63E+00	4.3	0.9317	0.930	-0.1
110	4	4	0.71514	0.772	7.9	8.18E+00	9.53E+00	17	0.8542	0.848	-0.8
110	6	6	0.83637	0.974	17	2.52E+01	3.42E+01	36	0.7727	0.756	-2.1
			Mean activity coefficient			**Mean activity**			**Water activity**		
			$\gamma_{CaCl2\pm}$	$\gamma_{CaCl2\pm}$		a_{CaCl2}	a_{CaCl2}		a_{H2O}	a_{H2O}	
Temp (°C)	**m $CaCl_2$**	**Ionic Str.**	**Measured[2]**	**Computed**	**%Diff**	**Measured[2]**	**Computed**	**%Diff**	**Measured[2]**	**Computed**	**%Diff**
25	0.001	0.003	0.8881	0.888	0.0	2.80E-09	2.80E-09	0.0	0.9999	1.000	0.0
25	0.1	0.3	0.5164	0.507	-1.8	5.51E-04	5.21E-04	-5.4	0.9954	0.995	0.0
25	0.5	1.5	0.4453	0.450	1.2	4.41E-02	4.57E-02	3.5	0.9756	0.971	-0.4
25	1	3	0.4959	0.522	5.3	4.88E-01	5.69E-01	17	0.9451	0.929	-1.7
25	1.6	4.8	0.6367	0.675	6.1	4.23E+00	5.04E+00	19	0.8989	0.863	-4.0
100	0.001	0.003	0.8695	0.869	-0.1	2.63E-09	2.62E-09	-0.2	0.9999	1.000	0.0
100	0.1	0.3	0.4530	0.438	-3.4	3.72E-04	3.35E-04	-9.9	0.9956	0.996	0.0
100	0.5	1.5	0.3568	0.334	-6.3	2.27E-02	1.87E-02	-18	0.9770	0.976	-0.1
100	1	3	0.3703	0.334	-9.7	2.03E-01	1.50E-01	-26	0.9493	0.946	-0.4
100	1.6	4.8	0.4381	0.366	-16	1.38E+00	8.04E-01	-42	0.9079	0.902	-0.7

[1]Data from, Colin et al., 1985; [2]Data from Ananthaswamy and Atkinson, 1985

H.2 Activity Coefficients of Neutral Aqueous Species

For dissolved gases with the following exact names in the thermodynamic database, activity coefficients are computed using an equation derived from correlations developed by Drummond (1981) for CO_2 gas dissolution in NaCl solutions up to 6 molal (see also Section B.4 in Appendix B):

'co2(aq)' or 'CO2(aq)'

'ch4(aq)' or 'CH4(aq)'

'h2(aq)' or 'H2(aq)'

'h2s(aq)' or 'H2S(aq)'

'o2(aq)' or 'O2(aq)'

'so2(aq)' or 'SO2(aq)'

$$\ln(\gamma) = (C + F\,T + G/T)\,I - (E + H\,T)\,I/(I + 1) \qquad \text{(H.11)}$$

where I and T are is the true ionic strength and absolute temperature, respectively, and C, E, F, G, and H are fit coefficients as follows:

C	-1.0312
E	0.4445
F	0.0012806
G	255.9
H	-0.001606

For other uncharged molecular species activity coefficients are set to one by default or can be optionally computed as (e.g. Langmuir 1997):

$$\log(\gamma_i) = K_i\,I \qquad \text{(H.12)}$$

where K_i are salting-out coefficients and I is the true ionic strength of the solution. Currently, values of K_i are assumed to be independent of temperature. These salting-out coefficients are input from the TOUGHREACT thermodynamic database (A0 in the primary and secondary species blocks, see Section 6.4), and default to zero (unit activity coefficients).

H.2.1 Fugacity Coefficients of Gases

When TOUGHREACT is compiled with the TOUGH2 module ECO2N, the fugacity coefficients of CO_2 are computed within the ECO2N module as a function of pressure, temperature, and composition, using the H_2O-CO_2 mutual solubility model of Spycher et al. (2005) for pure water and saline solutions (for temperature and pressure ranges of 10–110°C and 1–600 bar).

When TOUGHREACT is compiled with other EOS modules, or for initial speciation calculations, fugacity coefficients of CO_2, H_2, and CH_4, are computed as a function of pressure and temperature only (ideal mixing of real gases) using the correlations of Spycher and Reed (1988) (for temperature and pressure ranges of ~50–300°C and 1–500 bar for CO_2; 0–1000°C and 1–3000 bar for H_2; and 25–300°C and 1–500 bar for CH_4). Fugacity coefficients of other gases (besides H_2O gas) are assumed equal to 1 (ideal gas behavior and ideal mixing). The calculation of fugacity coefficients can be turned on or off for various EOS modules (except ECO2N) by setting flag iFugaC to 0 (off) or 1 (on) in subroutine Gas_Fuga_Coe (in treact_v2.f).

The behavior of H_2O gas (ideal or non-ideal), and computation of H_2O gas fugacity, is always taken into account by the selected TOUGH2 EOS module compiled with TOUGHREACT.

Appendix I Treatment for Mineral Solid Solutions

Currently, the only solid solution model implemented in TOUGHREACT is an ideal solid solution model. This model is only available for minerals that react under kinetic constraints.

The condition of equilibrium for a solid solution is

$$\left(Q_{ss} \diagup K_{ss} a_{ss}\right) = 1 \tag{I.1}$$

where the subscript *ss* refers to the solid solution, and *Q* and K are the ion activity product and equilibrium constant for that solid solution, respectively, and a is the activity of the solid solution. By convention, $a_{ss} = 1$.

A similar expression can be written for the condition of equilibrium for each end-member of the solid solution:

$$\left(Q_i \diagup K_i a_i\right) = 1 \tag{I.2}$$

In this case, the subscript *i* refers to each end member, and $a_i \neq 1$.

In the case of an ideal solid solution, the activity of each endmember, ai, is assumed to equal its mole fraction xi in the solid solution. Making this assumption and combining Equations (I.1) and (I.2) (with ass = 1) yields:

$$\left(Q_i \diagup K_i x_i\right) = \left(Q_{ss} \diagup K_{ss}\right) \tag{I.3}$$

For a solid solution composed of *n* end-members, Equation (I.3) is consistent with the relation (e.g. Reed, 1982):

$$\left(Q_{ss} \diagup K_{ss}\right) = \sum_{i=1}^{n} \left(Q_i \diagup K_i\right) \tag{I.4}$$

Alternatively, combining Equations (I.3) and (I.4) yields, at equilibrium

$$x_i = \frac{\left(Q_i \diagup K_i\right)}{\sum_{i=1}^{n} \left(Q_i \diagup K_i\right)} \tag{I.5}$$

For a solid solution reacting under kinetic constraints we can then write a rate law similar to Equation (B.5) in Appendix B.

$$R_{ss} = k_{ss} A_{ss} \left[1 - \left(Q_{ss} \diagup K_{ss}\right) \right] \tag{I.6}$$

where *R*, *A*, and *k* stand for the reaction rate, surface area, and rate constant of the whole solid solution *ss*. To treat the solid solution as a function of only individual endmembers, *i*, we write:

$$R_{ss} = \sum_{i=1}^{n} \left(x_i R_i\right) \tag{I.7}$$

with x_i and R_i being the mole fraction and rate, respectively, for each endmember of the solid solution. The rate of each endmember can be expressed as

$$R_i = k_i A_{ss} \left[1 - \left(Q_i \diagup K_i a_i\right) \right] \tag{I.8}$$

where k_i is the rate constant of each endmember. Assuming ideal behavior ($a_i = x_i$) and substituting Equation (I.8) into Equation (I.7) we get:

$$R_{ss} = \sum_{i=1}^{n}(x_i R_i) = \sum_{i=1}^{n}\left(x_i k_i A_{ss}\left[1-\left(Q_i / K_i x_i \right) \right]\right) \tag{I.9}$$

which can be further expanded as

$$R_{ss} = \sum_{i=1}^{n}\left(k_i A_{ss}\left[x_i -\left(Q_i / K_i \right)+1-1 \right]\right) = \sum_{i=1}^{n}\left(k_i A_{ss}\left[1-\left(Q_i / K_i \right)\right]+k_i A_{ss}\left[x_i -1\right] \right) \tag{I.10}$$

Equation (I.10) leads to the final relationship

$$R_{ss} = \sum_{i=1}^{n}\left[R_i '+k_i A_{ss}(x_i -1) \right] \tag{I.11}$$

where R_i' is the rate of the endmember as a pure mineral (that is, with a_i =1 in Equation (I.8)).

This approach is implemented in TOUGHREACT by adding a term equal to $k_i A_{ss}(x_i - 1)$ to the rates R_i' computed for each individual mineral that is part of a solid solution. In doing so, Equation (I.11) is implicitly treated by the total effect of the precipitation or dissolution of all endmembers. For precipitation, mole fractions x_i are computed using Equation (I.5), which technically only applies at equilibrium. For dissolution, values of x_i are calculated from the actual abundances of each endmember present.

It should be noted that this method is currently valid only for rate expressions without exponents on the affinity term (i.e. with exponents *m* and *n* set to 1 in Equation B.5), and close to equilibrium for precipitation. This approach also implies that

$$k_{ss} = \sum_{i=1}^{n}(x_i k_i) \tag{I.12}$$

and that

$$A_{ss} = \sum_{i=1}^{n}(A_i) \tag{I.13}$$

where A_i is the surface area computed from the abundance of each endmember. Note that stoichiometric dissolution is obtained by using identical k_i values for all endmembers in a given solid solution.

Appendix J Implementation of the Hellmann and Tisserand (2006) Rate Law for Mineral Dissolution and Precipitation

J.1 Rate Expression

Hellmann and Tisserand (2006) published an improved rate equation for low albite dissolution in the aqueous phase;

$$r = kA\left(1 - e^{ng^m}\right) \tag{J.1}$$

where n and m are fitted parameters, and

$$g = \ln\frac{Q}{K} \tag{J.2}$$

They used an extensive and continuous set of experimental data relating the dissolution rate of low albite to the affinity of the reaction. The highly non-linear behavior of the rate equation precludes use of a classical TST rate law embodied in Eq. J.1, except when the affinity is less than ≈15 kJ/mol (Lasaga, 1998, p. 678 *ff*). Hellmann and Tisserand's equation better describes the dissolution rate of albite in the transition region between TST control and the generalized dissolution rate established far from equilibrium and independent of the affinity of reaction, a region characterized by most laboratory studies of aluminosilicate dissolution. Similar complex dissolution rate behavior has been observed for other minerals, e.g., gibbsite, labradorite and smectite (Lasaga and Luttge, 2001).

Although a theoretical basis exists for calculating the transition in dissolution rate between TST control, and control by etch pits for each mineral (Lasaga and Luttge, 2001), parameters are not available for many minerals. Hellmann and Tisserand (2006) reported the parameters n and m for albite, n = 9.75×10^{-5} and m = 3.74. We implemented this new rate law in TOUGHREACT, but it has not been well-tested. For some user's interest, we document the implementation below.

J.2 Implementation

Compared to TST rate law, only two records Miner-2 and Miner-2.1 in file chemical.inp needs to be modified as follows:

Miner-2

Variable: NAMIN, IKIN, IDISPRE, ISS, M1

Format: A, 4I (free format)

IKIN: =2 for this new rate law (=1 for TST rate law).

Other variables: are the same as the TST rate law

Miner-2.1

Variable: RKF, IDEP, CK1, CK2, EA, ACFDISS, BCFDISS, CCFDISS

Format: F, I, 6F (free format)

CK1 and CK2: the exponents n and m, respectively in Eq. (J.1) above.

Other variables: are the same as the TST rate law

An example for albite-low is given below:

```
'albite~low'          2      3     0    0
             2.7542e-13    2    9.75E-5  3.74 69.80  0.0  0.0  0.0
                        1
                        6.9183e-11   65.0    1   'h+'   0.457 ! acid mechnism
             1.0000e-12  0  9.75E-5  3.74  67.83  0.0  0.0  0.0   1.e-6   0
0.0   0.    000.00
```

Appendix K Treatment of Cation Exchange under Water Unsaturated Conditions

Two models are used for cation exchange under water unsaturated conditions. The first model assumes cation exchange sites (CEC) remind constant as water saturation changes. In fact, the number of available exchange sites decreases as water saturation decreases. TOUGHREACT provides another option, the second model. The variation of exchange sites is addressed by simply scaling CEC by a factor, which is function of water saturation. TOUGHREACT can use a function $f(S_l)$ proposed by Liu et al. (1998) and is based on the change in reactive surface area with a change in saturation for fracture networks (see Appendix G):

$$f(S_l) = S_l^{(1+\gamma)} \tag{K.1}$$

where γ is an empirical coefficient. Both these functional forms are constrained in the range $0 \le f(S_l) \le 1$, and approach 0 as S_l approaches 0, and approach 1 as S_l approaches 1. Saturation values approaching 0 are usually not encountered, and are limited by the residual saturation in the capillary pressure curve. TOUGHREACT is, however, a nonisothermal code, and for boiling conditions, rocks can completely dry out. During complete dryout, Equations (K.1) become undefined at $S_l = 0$, and a lower limit must be placed on S_l to prevent this. For application under this condition, Sonnenthal et al. (2005) defined an effective residual saturation for reaction (S_{ar}), which is used in Equation (K.1) instead of S_l, and is expressed as

$$S_{ar} = \frac{S_l - S_m}{1 - S_m} \tag{K.2}$$

where S_m is the minimum liquid saturation for which reactions are considered and is generally set to a small saturation (such as 1×10^{-4}), to ensure that reactions take place until virtually no water is left (e.g., during dryout). Clearly, at a very low liquid saturation, the reactive exchange contacted by water is likely much smaller than the total sites. The dependence of reactive surface sites on water saturation is very complex in field-scale conditions. Additional investigations are needed to define the functional form of this relation.

Appendix L Utility Programs for the Thermodynamic Database

L.1 Converting from other databases

Description

Program DBCONV2 reads the thermodynamic database of either EQ3/6 v7.2b (data0.dat; Wolery, 1992), PHREEQC (phreeqc.dat; Parkhurst and Appelo, 1999), or SOLVEQ/CHILLER (soltherm.xxx; Reed, 1982 and 1998) formats the data for input into TOUGHREACT. The source code (dbconv2.f) is provided with the distribution files. For the most part, the conversion requires only reformatting of the same data values. However, the program also regresses input equilibrium constant values as a function of temperature in the form: $\log(K)_T = a * \ln(Tk) + b + c*Tk + d/Tk + e/Tk^2$ where Tk is temperature in degrees K. The program also assigns values of effective ionic radii to aqueous species by reading these values in a special input file (rej.dat). Currently, this file contains effective ionic radii from Helgeson et al. (1981; AJS, 1249-1516, Table 3). Radii of species for which data listed in rej.dat are computed as a function of ionic charge as shown in Table H.1-1 in Appendix H.

Input and output files:

The program needs to read in two input files and generates four output files. The names of input and output files are entered interactively when running the program. File contents and default names are as follows:

data0.dat	Main input file - original EQ3/6, PHREEQC or SOLVEQ/CHILLER thermodynamic database (the converter automatically detects the original file format).
rej.dat	Input data file containing effective ionic radii from Helgeson et al. (1981, AJS, 1249-1516, Table 3). The species listed in this file must have the same spelling as the species in the input thermodynamic database. If no match is found, rej values are computed based on ionic charge (See Table H.1-1 in Appendix H).
mvm0.dat	Mineral densities, used to compute molar volumes if these data are not available in the input database. References for these data are listed at the top of this file.
dbconv2.out	Main output file - converted database (for the file format, see Section 6.4 of this manual).
dump_aux.out	Separate subset of main output file containing converted data for auxiliary species only. To complete the conversion of the database, this file is to be manually inserted in dbconv2.out at the location indicated in that file.
checkfit.out	Print-plot file to visually check the quality of the log(K) regression. A user should always look at this file before using the output data.

checkdat.out	Printout of species for which one or more regressed log(K) value exceeds 0.1 log(K) units (generally, but not necessarily, indicating some problems with the regression).

For EQ3/6 conversions, the input file must have the format of EQ3/6 thermodynamic databases, with the following successive blocks of data. All these blocks are required in the input file and these data blocks must occur in the same order as shown below, otherwise input errors will occur:

```
+---------
basis species

+---------
auxiliary species

+---------
aqueous species

+---------
solid species

+---------
gases

+---------
solid solutions
```

To convert EQ3/6 files, the program will work only with input log(K) grids composed of eight values, at the following temperatures: 0, 25, 60, 100, 150, 200, 250, and 300°C. A log(K) value of 500 is interpreted as "no available data" and regression of log(K) values is not performed if at least one of log(K) value is set to 500. With PHREEQC databases, log(K) values are extrapolated only between 0 and 60°C using the van't Hoff equation and given enthalpy values, unless log(K) regression entries (*-analytic*) are present in the file. With SOLVEQ/CHILLER databases, log(K) values are regressed between 25 and 350°C, although log(K) values in the converted database are shown only up to 300°C.

L.2 Switching Basis (Primary) Species

Description

The program KSWITCH reads TOUGHREACT thermodynamic database entries and creates another identical set of entries with one of the component species "switched" with a derived species. For example, use KSWITCH to replace Al+++ (as a basis species) with new component species such as AlO_2^-.

Input data files and formats

One input file is needed (with default name thermok.dat, but any name can be chosen and input interactively). This file contains component species data, reaction stoichiometries and log(K) data entries that must have the same format as the entries for aqueous species, gases, and minerals in the TOUGHREACT thermodynamic database, including the same structure as the thermodynamic database (with a top record specifying temperature values for the log(K) data, then component (basis) species, derived species, minerals, and gases separated by records starting with 'null'). The entire thermodynamic database, or a subset of it, can be used as an input file. Also, any number of headers can appear at the top of the file before the temperature header. The remaining input is done interactively with self-explanatory prompts that ask for the names of input and output files, the species to switch (use the exact same spelling as in the input file), and the molecular weight of the switched species. The latter is used only for inclusion in the new component species entry and is not used in calculations. Note that the new component species must always be a derived species that is present in the input file. Also, only one switch is allowed for each run. For multiple switches, run the program more than once, reading the output of each run as input for the following run.

L.3 Regression of log(K) Data

Description

Program KREG is used to regress log(K) data in the thermodynamic database of TOUGHREACT as a function of temperature, and to generate records for aqueous species, minerals, and/or gases including the log(K) regression coefficients formatted for input into this thermodynamic database.

Input data files and formats

The names of input and output files are entered interactively when running the program. One input file (default name: kreg.dat) is required, containing: the first record identical to the first record of the thermodynamic database indicates the temperatures for which log(K) data are given, followed by records identical to those in the thermodynamic database for derived aqueous species, minerals, and/or gases. (3 records per entry: the first for stoichiometry, second for individual log(K) values, and the third for regression coefficients. The regression coefficients can be left blank, but the name of the species, mineral, or gas preceding the regression coefficients must be present). The entire thermodynamic database, with component (primary) species removed, can also be used as an input file.

L.4 Checking Mass and Charge Balances

Description

Program THERMOCHK reads the thermodynamic database of TOUGHREACT and checks the mass and charge balances of all reactions entered in that database. It does so by adding the molecular weights multiplied by stoichiometric coefficients (mass balance) and adding ionic charges multiplied by stoichiometric coefficients

(charge balance) of each specified reaction. The program then flags non-zero charge balances and mass balances greater than 5×10^{-5} times the molecular weight of the species/mineral/gas to which the reaction pertains.

Input data files and formats

The program needs to read in two input files and generates two output files. The names of input and output files are entered interactively when running the program. File contents and default names are as follows:

thermok.dat (default)	Main input file (TOUGHREACT database to check)
molwt_aq.dat	Input file with molecular weights of aqueous species, used only if this information is not already provided in the thermok.dat input file (i.e., as in earlier versions of the database).
thermochk.out	Ouput file listing charge and mass balances for all reactions.
error.out	Output file listing only those species, minerals, and gases for which reactions have non-zero charge balances and mass balances exceeding 5×10^{-5} times the molecular weight of the species, mineral, or gas in question.

A

B

C

D

E

F

G

H

I

K

L

M

N

O

P

R

S

T

U

V